AREVA

BEA Research Reactor Package

Safety Analysis Report
Docket 71–9341

Revision 10
May 2016

AREVA

DOCKET 71–9341

BEA Research Reactor Package

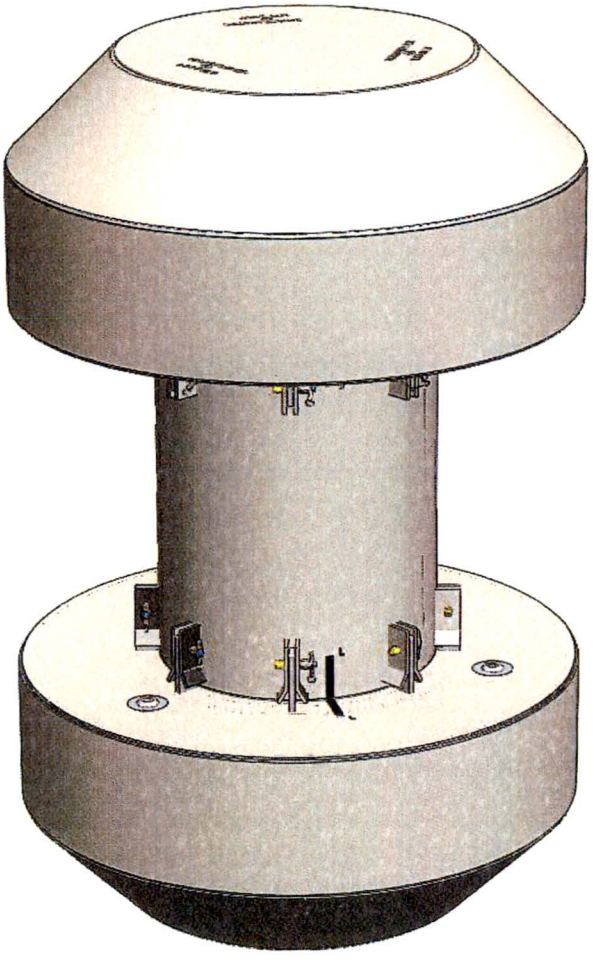

Safety Analysis Report

Revision 10

May 2016

AREVA Federal Services LLC

AREVA

Ref: AFS–16–0152

May 26, 2016

ATTN: Document Control Desk
Director, Spent Fuel Project Office
Office of Nuclear Material Safety and Safeguards
U. S. Nuclear Regulatory Commission
Washington, DC 20555–0001

SUBJECT: 1) BRR Package Amendment Request, Docket No. 71–9341, TAC No. L25031

2) Letter from Norma Garcia-Santos to Philip W. Noss of March 31, 2016, transmitting second NRC request for additional information (RAI)

AREVA Federal Services LLC (AFS) hereby submits Revision 10 of the Safety Analysis Report for the BRR Package, Docket No. 71–9341. This SAR revision includes changes made in response to the NRC RAI dated March 31, 2016.

Responses to each request for information are provided in Attachment A. The majority of the changes occur in the criticality analysis in Chapter 6 of the SAR. Minor changes were also made to Chapters 1, 2, and 7. The changes are summarized in Attachment B. All revisions made to the SAR are marked with a revision bar in the right margin. Note that pages not changed for Revision 10 will show Revision 8 or Revision 9 in the header.

Included with this letter is one paper copy of the SAR and one CD-R containing the PDF file "BRRC SAR, Complete, Rev. 10.pdf" (31,113 kb, 662 pages). The CD is contained within an envelope labeled, "BRR Package, Docket 71–9341 SAR Revision 10, Electronic Copy of Document". As a courtesy, two references are included on the CD that are mentioned in the response to RAI Sh-5-1_2:

- Dan Ilas, *Development of a SCALE Model for High Flux Isotope Reactor Cycle 400*, ORNL/TM-2011/367, Oak Ridge National Laboratory, February 2012.
- G. Radulescu, I. C. Gauld, and G. Ilas, *SCALE 5.1 Predictions of PWR Spent Nuclear Fuel Isotopic Compositions*, ORNL/TM-2010/44, Oak Ridge National Laboratory, March 2010.

To update a paper copy of the SAR, replace the cover sheet, Table of Contents, and Sections 1.2, 2.7, 6.1 through 6.6, and 7.1 in their entirety.

Should you have any questions regarding this submittal, please contact me at (253) 552–1321 or via E–mail (phil.noss@areva.com).

Very Truly Yours,
AREVA Federal Services LLC

Phil Noss

Phil Noss
Licensing Manager

NMSS20

cc: Ms. Norma Garcia-Santos, NRC (including one paper copy and one CD)
Mr. Douglas Morrell, DOE NEUP (including one paper copy and one CD)

ATTACHMENT A

AREVA Federal Services, LLC Responses to NRC Request for Additional Information Dated March 31, 2016

Docket No. 71-9341
Certificate of Compliance No. 71-9341
Model No. BEA Research Reactor (BRR) Package

The following material contains the response of AREVA Federal Services LLC (AFS) to the Request for Additional Information of the NRC dated 3/31/2016. Each response is preceded by the NRC question.

Sh-5-1$_2$. Pertinent to the increased quantity of plutonium in the fuel:

a. Justify the increase in the maximum quantity of plutonium for the Model No. BRR package to 6,500 Ci (from previous amount of 5,890 Ci) and demonstrate that this value bounds all fuel types to be transported in the Model No. BRR in terms of radiation source terms for the proposed shielding design.

b. Provide calculations used for determining the quantity of plutonium, including the source term, modeling assumptions, and name and version of the software.

c. Provide the benchmarking analyses performed for the code used to perform source calculations for the contents requested.

d. Revise the shielding calculation, if necessary, with the increased source term resulting from the increase of plutonium content in the fuel.

In Section 1.2.3 of the application, Revision 9, "Special Requirements for Plutonium," the applicant noted that the amount of plutonium was increased to 6,500 Ci without explaining and discussing the impact on the package external dose rates due to increasing the quantity of plutonium in the fuel.

This information is needed to determine compliance with 10 CFR 71.43, 71.47, and 71.51.

Response: The response to this question is as follows:

a. The plutonium activity is extracted from the same TRITON models used to generate the gamma and neutron source terms and is tabulated in Table 1.2-5 for each payload. During the first cycle of RAI responses, AFS obtained information that the PULSTAR reactor is being uprated from 1 MW to 2 MW. While the maximum fuel element burnup is the same, due to the higher power the maximum burnup could theoretically be achieved in half of the irradiation time. To reflect this change, the source terms for PULSTAR were regenerated and the plutonium content increased from 5,890 Ci to 6,500 Ci. The largest plutonium production is for the PULSTAR fuel element with 4% enrichment because low enrichments favor plutonium production. The shielding dose rate results for the various fuel element types are presented in Tables 5.4-3 through 5.4-9. Any plutonium present is included

in the source term and thus is included in the dose rate results. Section 1.2.3 has been revised to clearly indicate that the plutonium results are from the TRITON outputs.

b. SCALE6/TRITON is used to compute the source terms and plutonium production. The modeling assumptions are discussed in detail in Section 5.2, *Source Specification*. Detailed TRITON input data is also provided in Table 5.2-7 for TRIGA fuel, Table 5.2-10 for the plate fuels, and Table 5.2-14 for PULSTAR.

c. SCALE6/TRITON is state-of-the-art software provided by ORNL. While SCALE6/TRITON is more commonly used for commercial PWR and BWR analysis, it may be used for any fuel type. An extensive benchmark of SCALE5.1/TRITON for a number of PWR reactors is performed in ORNL/TM-2010/44, *SCALE5.1 Predictions of PWR Spent Nuclear Fuel Isotopic Compositions* (provided on the CD accompanying this submittal). Comparison between TRITON and experiments is generally good. These results would be directly applicable to the PULSTAR fuel, which is similar to PWR fuel.

   AFS contacted the SCALE development team for benchmarks more applicable to aluminum plate fuels and were told that TRITON has not been extensively benchmarked for aluminum plate fuel. ORNL did provide the document ORNL/TM-2011/367, *Development of a SCALE Model for High Flux Isotope Reactor Cycle 400* (provided on the CD accompanying this submittal), as the High Flux Isotope Reactor (HFIR) is also an HEU plate fuel design. While this document is concerned with the multiplication constant, core power distribution, and neutron flux rather than spent fuel isotopics, the document concludes that SCALE is an acceptable tool to analyze HIFR.

   Note that while TRITON has not been extensively benchmarked for aluminum plate fuels, the computed dose rates are significantly below the dose rate limits. The BRR package has been used to ship ATR, MITR-II, and MURR fuel for several years and measured dose rates have been acceptable and generally low, as predicted by the analysis, indicating the SCALE6/TRITON methodology is acceptable.

d. Since the source terms already include the plutonium source, no revision is required.

While not captured in Sh-5-1_2, during a phone conversation on April 7, the NRC requested information concerning the axial profile used in the analysis. The axial profile for the plate fuels is provided in Table 5.2-13 and is based data from the U-Mass reactor. This profile is used for the other plate fuels because the active fuel lengths of the various fuel types are the same and the axial profiles will be similar. This profile is also used for PULSTAR. Because the neutron source is computed with the 2D TRITON/NEWT sequence, the neutron source magnitude is increased by the factor 1.586 to account for the increase in the neutron source due to the axial power profile. This factor is derived in Table 5.2-13 (bottom row) and is included in the total neutron source magnitudes provided in Table 5.2-18 and Table 5.2-19.

Sh-5-2$_2$. Under normal conditions of transport and hypothetical accident conditions, clarify how the redesigned basket for loose fuel plates can maintain:

a. its integrity under normal conditions of transport and hypothetical accident conditions.
b. the external dose from the package within the regulatory limits.
c. the loose plates in a safe geometry.

In response to the staff RAI dated November 10, 2015, the applicant changed some assumptions in its safety analysis, such as:

- *changing the loose plate box material* from aluminum to stainless steel in order to maintain the geometry of the loose plate box under hypothetical accident condition.
- *requiring the insertion of aluminum dunnage* into the loose plate box beside the fuel plates to limit the potential for motion of the loose plate during transport (see Section 7.1.2.1 and 7.1.2.2 of the application).

From drawing No. 1910-01-01-SAR, the loose plates box does not have a lid. Although the applicant states that the package will be transported in a vertical position and dunnage will be used to prevent fuel plates from moving, the applicant has not demonstrated what component is used to hold the fuel plates in the loose plate box so that the fuel plates would not slide out of the basket under normal conditions of transport and hypothetical accident conditions.

The applicant needs to perform shielding analyses for the package consistent with the conditions of the geometry of the content and corresponding source distribution and demonstrate that the package meets the requirements of 10 CFR 71.43, 71.47, and 71.51. Under the head drop test, it is conceivable that the loose plates in a loose plate box without lid could slide out of the basket because there is no device to hold the fuel plates in the basket and there is a space between the fuel plates in the loose plate box and the package closure lid. Therefore, the applicant also needs to demonstrate that the package meets the requirements of 10 CFR 71.55(d)(2) and 71.55(e)(1) under the tests specified in 10 CFR 71.71(c)(7) and 71.73(c)(1).

This information is needed to determine compliance with 10 CFR 71.43, 71.47, 71.51, 71.55(d)(2), and 71.55(e)(1).

Response: Drawing 1910-01-01-SAR shows that the shield plug forms the top surface of the payload cavity, which defines the upper position limit for each of the baskets, as well as the fuel elements, loose plate box, and the loose plates. The loose plate box is designed to position the loose plates as close as practical to the top surface of the basket, and consequently there is relatively little clearance between the top of the loose fuel plates and the position limiting function of the shield plug. For this reason, the loose plates cannot move a significant distance in an axial direction, and cannot escape the confines of the loose plate box. Thus, no cover to the loose plate box is required. To assist in clarifying this matter, Figure 1.2-17 has been added to Chapter 1. This figure shows a cross sectional view of the cask cavity, the Square fuel basket, loose plate box, and loose plates.

In case the loose plate box is loaded with a partial load of loose plates, dunnage sheets must be used with the loose plates to restrict the unused space inside the box to a maximum of ¼ inches. The dunnage sheets are defined in detail in Section 7.1.2.1, *Wet Loading*, Step 12.b., and Section 7.1.2.2, *Dry Loading*, Step 12.b. These operational steps define the dunnage width, length, and minimum thickness. Further, a drawing of the dunnage sheets is given in Figure 7.1-1 (on the right side of the drawing). In this way, the possible movement of the loose fuel plates in all directions is limited.

Note that Figure 7.1-1 also shows a drawing of the spacer plates to be used with U-Florida fuel elements (on the left side of the drawing). Spacer plates must be used with each U-Florida element as required by Section 7.1.2.1, *Wet Loading*, Step 11.b., and Section 7.1.2.2, *Dry Loading*, Step 11.b. The spacer plates are completely defined by these procedural steps and by the figure. The text of the SAR has been revised to more carefully utilize the terms *spacer plate* (which pertains to U-Florida fuel elements only) and *dunnage sheet* (which pertains to loose fuel plates only) to ensure that these items cannot be confused.

To address the possibility that the loose plates could reconfigure structurally due to the HAC impact event, an analysis has been added to Section 2.7.1.8, *Fuel Impact Integrity*. This analysis shows that the stress in each fuel plate due to the worst-case HAC impact is well below the yield strength of the aluminum cladding at maximum temperature. Thus, the loose plates cannot move significantly nor reconfigure structurally under any conditions of transport, and all of the existing shielding and criticality model geometries are valid with respect to the location and integrity of the loose plates.

Cr-6-1$_2$. With respect to the dunnage to be used, provide the following:

a. a detailed drawing and specifications (i.e. materials of construction, dimensions, etc.) for the dunnage used to restrict the fuel plate from sliding out the loose plate baskets, and
b. a demonstration that the dunnage is effective for restricting the movement of the fuel plates in the box basket under normal and hypothetical accident conditions.

The applicant revised the design of the loose plate basket, in its response to the staff's RAI dated November 10, 2015, to use dunnage to restrict fuel movement out of the loose plate basket. However, the applicant did not provide any drawing and specifications for the dunnage to be used, nor a demonstration that the use of the dunnage is an effective mean for restricting the movement of the loose fuel plates. Regulations in 10 CFR Part 71 require that the geometric form of the content of a fissile package shall not substantially alter under normal conditions of transport [10 CFR 71.55(d)(2)] and that the package is subcritical with the fissile material in the most reactive credible configuration consistent with the damaged condition of the package and the chemical and physical form of the contents [10 CFR 71.55(e)(1)].

This information is needed in order for the staff to determine the package compliance with 10 CFR 71.55(d)(2), 71.71, and 71.73.

Response: See the response to RAI Sh-5-2_2 above. As noted in that response, the use of dunnage sheets as required by the relevant operational steps will ensure that the loose plates cannot move significantly nor reconfigure structurally under any conditions of transport, and the requirements of 10 CFR 71.55(d)(2) and 10 CFR 71.55(e)(1) are satisfied. With respect to the specific request of this RAI Cr-6-1_2:

a. The dunnage sheets used with loose plates and the spacer plates used with U-Florida fuel elements are defined in detail in Section 7.1.2.1, *Wet Loading*, and Section 7.1.2.2, *Dry Loading,* and in the drawing depicted in Figure 7.1-1.

b. The effectiveness of the dunnage is discussed in detail in the response to RAI Sh-5-2_2 above.

Cr-6-2_2. Demonstrate that the BRR package meets the regulatory requirements of 71.55(b) for all allowable contents requested in this amendment. This demonstration should include the number of plates at which the package reaches the maximum k_{eff}, for each fuel type with the appropriate criticality safety analyses.

In its response to RAIs Cr-6-1, Cr-6-2, and Cr-6-3, the applicant states that fewer than 31 plates may be loaded in a loose plate basket. One example is that the maximum number of plates per loose fuel basket is 17 for U-Florida fuel. However, the applicant did not provide:

- specific limitations on the number of plates that could be placed into a loose plate basket for each fuel type, or
- the criticality safety analysis for those various loading configurations with corresponding loading limits.

In addition, in its response to RAI Cr-6-3, the applicant states: "Note that the HAC single package analysis, which includes optimum moderation, bounds the requirements of 71.55(b)." The staff reviewed the assertion and found that the criticality safety analysis for a single package under HAC may not bound the requirements of 10 CFR 71.55(b) because: (1) the package is being loaded or unloaded in fresh water pool (wet loading) and therefore the number of plates increase or decreases during loading and unloading process, (2) the system is identified as under-moderated; therefore it will reach the optimal moderation as fuel plates are added or removed from the basket, and (3) the criticality safety analysis for the single package under HAC was performed with a fully loaded package and therefore may not bound the configurations with fewer fuel plates.

This information is needed in order for the staff to determine the package compliance with 10 CFR 71.55(b).

Response: Only 3 loose plate types are authorized for the loose plate box: U-Florida, U-Mass(Al), and Purdue. U-Florida bounds U-Mass(Al) and Purdue because U-Florida has 12.5 g U-235 per plate, while U-Mass(Al) and Purdue have only 9.3 g U-235 per plate. To simplify the analysis, only the U-Florida plate is modeled, which bounds U-Mass(Al) and Purdue. This is stated in Section 6.4.1.2, *HAC Single Package Configuration.*

The loose plate results with less than 31 fuel plates are provided in Table 6.4-7, Table 6.4-8, and Table 6.4-10. It is demonstrated that reactivity decreases when less than 31 plates are in the loose plate box. The system with 31 plates is undermoderated. Optimum moderation is achieved for a low number of plates (approximately 7 plates). *However, for the loose plate box, an undermoderated system with a large fissile mass is more reactive than an optimally moderated system with a small fissile mass.*

The criticality safety limitations are as follows:

- U-Florida loose plates: ≤ 31 per loose plate box
- U-Mass(Al) loose plates: ≤ 31 per loose plate box
- Purdue loose plates: ≤ 31 per loose plate box

For U-Florida, 31 plates will not fit in the loose plate box. However, 17 is not a criticality safety limit, it is a geometrical limit. The system is less reactive with 17 plates than with 31 plates, which is explicitly shown in Table 6.4-7.

Non-uniform pitches are also considered. Additional non-uniform pitch cases with 25 plates and 19 plates are added in Table 6.4-8 to demonstrate that 31 plates in a non-uniform pitch bounds all other configurations with less plates.

The following responses are in regard to the additional 71.55(b) comments. AFS agrees that the system with 31 plates is not "optimally moderated." A system with 31 plates has the maximum reactivity, but is not optimally moderated. However, moderation of the system with 31 plates is maximized to the extent possible using non-uniform pitches. (1) When the number of plates is increasing or decreasing it is bounded by 31 plates, as indicated in Table 6.4-7, Table 6.4-8, and Table 6.4-10. 31 plates bounds fewer plates. (2) The system with 31 plates is undermoderated. Loading fewer plates increases the moderation but decreases the reactivity due to less fissile mass. Optimal moderation is achieved for a small number of plates (~7), but the reactivity of such a system is low because the fissile mass is small. (3) It has been demonstrated with explicit MCNP models that loading less than 31 plates is less reactive that the maximum of 31 plates.

Cr-6-3$_2$. Demonstrate that the criticality safety calculations using MCNP models have properly converged for all requested loose plate contents and loading configurations.

The applicant used MCNP to perform criticality safety analysis for the BRR packages with various loose fuel basket and fuel loading patterns. In the safety analyses report the applicant states:

> "All moderated cases are run with a minimum of 2500 neutrons per generation for 250 generations, skipping the first 50."

Given the new design of the loose fuel plate baskets, including the addition of various spacers and dunnage, the staff needs assurance that the MCNP model using 250 generations would result in proper convergence of the calculations.

Based on papers published by the MCNP development experts (see Enclosure 2 for examples of these publications), convergence of k_{eff} for a system with large water gap between fuel or non-uniform distribution of fuel in water does not

assure the convergence of the calculation and the users should check the convergence of the calculations with Shannon Entropy to assure that the calculation has properly converged. The applicant needs to demonstrate that all criticality safety calculations using MCNP and the stated KCODE parameters have properly converged with both k_{eff} and Shannon Entropy indices.

This information is needed to determine compliance with 10 CFR 71.55.

Response: A check on Shannon entropy is not available for MCNP5.1.30, which is the version of MCNP used in the SAR. However, the loose plate box analysis is repeated for 1050 cycles, 5000 particles per cycle, skipping the first 50. Because the U-Florida analysis is similar to the loose plate box analysis, the U-Florida analysis is also repeated for 1050 cycles. The results are well converged and are essentially the same as before other than small Monte Carlo variations. The SAR has been updated for the new results.

OP-7-1. Revise the Operating Procedures to clearly state when spacers and/or dunnage are needed and provide specific instructions for use of these components.

The applicant revised the design of the loose plate basket in its response to the staff's RAI dated November 10, 2015 to use dunnage and spacers in the loose plate box to restrict the movement of fuel plates under normal conditions of transport and hypothetical accident conditions. The applicant also revised its Operating Procedures (OP) to include use of spacers. However, Step 12(b) of OP 7.1.2.1 and 7.1.2.2 state:

> "***Using aluminum dunnage as necessary***, minimize the free space between the flat face of the loose plates and the box opening."

This instruction seems to leave the users to determine if dunnage is necessary. However, the criticality safety analyses credited the dunnage as shown in Figures 6.4.7 to 6.4.11 of the application. This instruction could lead to a potential criticality safety accident as it stands because the instructions seem to indicate that the dunnage is an optional component of the packaging but it is in fact a component important to safety because the criticality safety of the package is dependent on the dunnage. The applicant also needs to revise the Operating Procedures to provide clear instructions for the use of dunnage.

This information is needed in order for the staff to determine the package compliance with 10 CFR 71.55 and 71.89.

Response: The text of Section 7.1.2.1, *Wet Loading*, and Section 7.1.2.2, *Dry Loading*, has been revised to prevent the confusion between *spacer plates*, which pertain only to U-Florida fuel elements, and *dunnage sheets*, which pertain only to loose plates. The use of spacer plates with U-Florida fuel elements has always been required by the procedure. These spacer plates (not dunnage) are the items shown and credited in Figure 6.4-7 through Figure 6.4-11 of the application. The SAR has been revised to also require the use of dunnage sheets to reduce the gap between the loose plates and the loose plate box to ¼ inches or less. (Note: dunnage sheets are not required if the gap is already equal to ¼ inches or less, without them. Thus, the words "as necessary" are still present, because

dunnage sheets may not be necessary to reduce the gap.) Since the dunnage sheets are not credited in the criticality analysis of loose plates, the dunnage sheets are not important to criticality safety. However, they are now required by the operating procedure in order to achieve strict compliance with 10 CFR 71.55(d)(2). Additional details are given in the response to RAI Sh-5-2_2.

ATTACHMENT B

BEA Research Reactor Package SAR, Rev. 10 Change List

Table of major changes for BRR Package Revision 10

Section or page no. of change	Material changed	Reason for change
1.2.2.5	Added reference to Figure 1.2-17	Update.
1.2.3	Updated discussion of plutonium	To strengthen the discussion of the plutonium source term.
Figure 1.2-17	Added figure	To help clarify the configuration of the loose plate box in the square fuel basket.
2.7.1.8	Added paragraph on loose plate structural integrity	Demonstrates that loose fuel plates in the loose plate box will not reconfigure in the HAC free drop.
Section 6.1.2	Summary information added on the loose plate box analysis	More clearly indicate the results and conclusions of the loose plate box analysis.
Table 6.1-1	Updated k_s values	Loose plate box analysis rerun with more cycles. RAI Cr-6-2_2 and Cr-6-3_2.
Page 6.3-3	Indicate the number of cycles run for each analysis type.	Revised for clarity.
Section 6.4.1.2	Loose plate box analysis rerun with more cycles. A sensitivity study is added to indicate the number of plates at which optimum moderation is achieved. Conclusions of the analysis more clearly defined.	RAI Cr-6-2_2 and Cr-6-3_2.
Section 6.4.1.2	U-Florida fuel analysis rerun with more cycles.	RAI Cr-6-3_2
Table 6.4-3	Loose plate results updated.	RAI Cr-6-2_2 and Cr-6-3_2.
Table 6.4-7	Loose plate results updated.	RAI Cr-6-2_2 and Cr-6-3_2.
Table 6.4-8	Loose plate results updated. Non-uniform pitches included in separate table. New non-uniform pitch cases added for 25 and 19 plates per box.	RAI Cr-6-2_2 and Cr-6-3_2.
Table 6.4-9	Loose plate results updated.	RAI Cr-6-2_2 and Cr-6-3_2.
Table 6.4-10	New loose plate results table added showing a decrease in reactivity if any plates are	RAI Cr-6-2_2

BEA Research Reactor Package SAR, Rev. 10 Change List

Section or page no. of change	Material changed	Reason for change
	removed.	
Table 6.4-12	U-Florida fuel analysis rerun with more cycles.	RAI Cr-6-3_2
Figure 6.4-3	New figure showing moderation curves for different numbers of fuel plates.	RAI Cr-6-2_2
Figure 6.4-7	New figure showing geometry corresponding to new loose plate box cases.	RAI Cr-6-2_2
Table 6.5-3	Loose plate results updated.	RAI Cr-6-2_2 and Cr-6-3_2.
Table 6.6-5	Loose plate results updated.	RAI Cr-6-2_2 and Cr-6-3_2.
7.1.2.1	Revise Steps 11.b. and 12.b	Step 11.b. adds detail to the description of the U-Florida spacer plate, and references Figure 7.1-1. Step 12.b. requires free space in the loose plate box to not exceed ¼ inches, adds detail to the description of the dunnage sheets, and references Figure 7.1-1.
7.1.2.2	Revise Steps 11.b. and 12.b	See discussion for Section 7.1.2.1.
Figure 7.1-1	Added drawing of U-Florida spacer plate and loose plate dunnage sheet	Update.

TABLE OF CONTENTS

1.2 Package Description

This section presents a basic description of the BRR package components and construction. General arrangement drawings are provided in Appendix 1.3.3, *Packaging General Arrangement Drawings*.

1.2.1 Packaging

The BRR package consists of a payload basket, a lead–shielded cask body, a separate, removable upper shield plug, a closure lid, twelve closure bolts, and upper and lower impact limiters containing polyurethane foam. Except for the closure bolts and impact limiter attachments, the package is of primarily welded construction, using Type 304 austenitic stainless steel. These components will now be discussed in detail.

1.2.1.1 Cask Body

The BRR cask body is a right circular cylinder 77.1 inches long and 38 inches in diameter (not including the impact limiter attachments and the thermal shield). It is composed of upper and lower massive end structures connected by inner and outer shells. Thick lead shielding is located between the two circular shells, in the lower end structure, and in the shield plug. The payload cavity has a diameter of 16 inches and a length of 54 inches.

The massive end structures may be cast from ASTM A351, Grade CF8A, or forged from ASTM A182, Type F304. The lower end structure contains a drain to allow removal of water from the payload cavity. The inner shell may be cast from ASTM A451, Grade CPF8A, or forged from ASTM A182, Type F304. The outer shell may be made from ASTM A240, Type 304 plate, or optionally cast from ASTM A451, Grade CPF8A or forged from ASTM A182, Type F304. The outer shell may have up to two, full penetration longitudinal seam welds. The inner shell is one inch thick, and is welded to each end structure using a full penetration weld. The outer shell is two inches thick, and is connected to each end structure using a full penetration weld. The weld of the outer shell to the upper end structure is made after lead pour.

The cask is lifted using four, 1–8 UNC threaded holes in the upper end structure, which may be optionally fitted with heavy duty thread inserts. See Zone D2 of sheet 3 of drawing 1910–01–01–SAR.

On the outside of the outer shell, in the region not covered by the impact limiters, is a thermal shield composed of an outer sheet of 12 gauge (0.105–inch thick) Type 304 stainless steel, separated from the outer shell by small strips of the same 12 gauge material.

A set of eight receptacles are attached to the outer shell at each end of the exposed region of the cask (total of 16 receptacles), that serve as impact limiter attachments (see Zone A4 of sheet 2 of drawing 1910–01–01–SAR). The receptacles consist of two closely spaced plates, 1/2–inches thick, that pass through the thermal shield and attach directly to the outer shell using a full penetration groove weld with a 1/2–inch fillet reinforcement on one side. Each impact limiter features eight, 3/4–inch thick blades that pass between the receptacle plates on the cask body. The attachment is completed by passing a one inch diameter, stainless steel ball lock pin through the three plates. The ball lock pins therefore act in double shear. Each impact limiter is retained by eight such attachments.

All lead shielding is made from ASTM B29, chemical lead, or optionally, from lead per Federal Specification QQ–L–171E, Grade A or C. The lead shield on the side of the cask body is cast–in–place through the upper end structure, and is nominally 8 inches thick. The shield at the

bottom is made from lead sheet material that is packed firmly into place, and is 7.7 inches thick. The bottom lead cavity is closed using a one inch thick plate secured with a full penetration groove weld, see Zone A6/7 of sheet 3 of drawing 1910–01–01–SAR.

The removable shield plug is located at the top of the payload cavity. The outer shell is made from Type 304 plate material of 1/2–inch, 3/8–inch, 1–inch, and 1½–inch thickness. See Zone D2 of sheet 4 of drawing 1910–01–01–SAR. The cavity is filled with lead sheet material that is packed firmly into place. The total thickness of the plug is 11.2 inches, and the lead thickness is 9.7 inches. The plug rests on a shoulder located approximately half way along the length of the plug. A corresponding shoulder is located in the upper end structure of the cask body to support the shield plug. A 3/4–inch diameter pipe passes through the plug to ensure proper draining and drying of the cask. The pipe is oriented approximately diagonally to prevent a deleterious shine path. The shield plug is lifted using a central, 1/2–13 UNC threaded hole.

The closure lid is made from 2–inch thick, ASTM A240, Type 304 stainless steel plate. It is attached to the cask using 12, 1–8 UNC bolts made of ASTM A320, Grade L43 material, with hardened steel washers. The bolts are plated with electroless nickel per MIL–DTL–26074 Rev. F Class 1 Grade B, and tightened to a torque of 220 ± 20 ft-lb. The mating holes in the cask body may be optionally fitted with heavy duty thread inserts. The mating surface of the lid features a step relief located at the bolt circle. This relief prevents any contact from occurring between the lid and the body outside of the bolt circle, thus preventing prying loads from being applied to the closure bolts. The closure lid includes two O–ring seals made from butyl rubber of 3/8–inch cross sectional diameter. The inner O–ring is the containment seal, and the outer is the test seal. The seals are retained in dovetail grooves in the lid. The O–ring material (including the sealing washers, see below) is made from Rainier Rubber R-0405–70, and subject to the tests given in Section 8.1.5.2.

The BRR package provides a single level of leaktight containment. The containment boundary of the BRR package consists of the following elements. Unless noted, all elements are made of ASTM Type 304 stainless steel in various product forms.

- The lower massive end structure (including the passage to the drain port)
- The inner cylindrical shell
- The upper massive end structure
- The containment elastomer O–ring seal (the inner seal in the closure lid)
- The closure lid
- The vent port in the closure lid including elastomer sealing washer
- The drain port in the lower end structure including elastomer sealing washer

The containment boundary is shown in Figure 1.2-16.

As noted above, the BRR package features two ports that are part of the containment boundary: a vent port in the closure lid, and a drain port in the lower end structure. Both ports are closed with threaded plugs made of ASTM B16 brass and sealed with butyl rubber sealing washers. A threaded brass cover is used to protect the port plugs. A seal test port is located between the containment O–ring seal and test O–ring seals, and is not part of containment.

1.2.1.2 Impact Limiters

Impact limiters are attached to each end of the BRR package, having essentially identical design, and are shown in drawing 1910–01–02–SAR. Each limiter is 78 inches in diameter and 34.6 inches long overall, with a conical section 15 inches long towards the outer end. The impact limiter design consists of Type 304 stainless steel shells and approximately 9 lb/ft^3 polyurethane foam. The external shells (except for the end plate) are 1/4 inches thick, and the internal shells (that interface with the cask body) are 1/2 inches thick. The outer end plate is 1/2 inches thick. The closure end impact limiter features three reinforced, 1/2–13UNC holes for lifting of the impact limiter only. An optional drain tube, aligned along the long axis of the cask, may be included in the lower impact limiter. The polyurethane foam is rigid, closed–cell, and is poured in place. On the side that mates with the cask, the annular sheet features three plastic melt–out plugs designed to relieve pressure in the HAC fire event. The attachment of the impact limiters to the cask body is described in Section 1.2.1.1, *Cask Body*.

1.2.1.3 Baskets

There are five baskets used with the BRR package, one for MURR, MITR-II, ATR, and TRIGA fuel types, and one for several fuel types each having a square or rectangular cross section and loose plates. The baskets are shown in drawing 1910–01–03–SAR. The baskets are made from welded construction using Type 304 stainless steel in plate, bar, pipe, and tubular forms. Each basket has a diameter of 15.63 inches and a length of 53.45 inches, and features a number of cavities that fit the size and shape of the fuel. The cavities are sized to minimize free play between the fuel and the basket, while ensuring free insertion and removal of the elements. The baskets are open on the top, and the fuel is located at the top end, nearest the shield plug. The baskets are designed to freely drain water when the cask is lifted out of the spent fuel pool.

1.2.1.3.1 MURR

The MURR basket consists of an outer rolled shell, an inner pipe, and thick radial plates that form eight pie–shaped cavities for the fuel in a circular array. The bottom of the fuel cavities is formed by a 3/8–inch thick plate that is welded to the inside of the shell. The lifting bar divides the interior of the inner tube in half and prevents loading any fuel within the inner tube. The MURR basket is shown in Figure 1.2-4.

1.2.1.3.2 MITR–II

The MITR-II basket consists of a cylindrical weldment supported by a 14 inch diameter pedestal. Twenty-nine (29) flat plates of variable thicknesses are machined and stacked to create eight (8) diamond shaped fuel cavities. Fuel cavities are arranged symmetrically about the center axis of the basket. The top plate of the weldment is machined to prevent the loading of fuel into the central cavity of the basket. The bottom plate of the weldment provides support for the fuel and allows for drainage of water from the fuel cavities. The MITR–II basket is shown in Figure 1.2-5.

1.2.1.3.3 ATR

The ATR basket consists of a rolled outer shell, an inner pipe, and radial plates that form eight pie–shaped cavities for the fuel in a circular array. Since the outer shell is somewhat smaller than the cask cavity, the ATR basket features four circular ribs having an outer diameter of 15.63 inches.

The bottom support plate is 1/2–inches thick. The lifting bar divides the interior of the inner tube in half and prevents loading any fuel within the inner tube. The ATR basket is shown in Figure 1.2-6.

1.2.1.3.4 TRIGA

The TRIGA basket consists of an array of 19 tubes having a 2–inch outer diameter and an 11–gauge wall thickness. The tubes are held in place by a top plate, a bottom support plate, and a central support plate. A 13–inch diameter, 1/4–inch thick circular shell forms the lower portion of the basket. The short spacer pedestal and the adjustable spacer pedestal are used to customize the fuel cavity for various TRIGA fuel lengths. The TRIGA basket is shown in Figure 1.2-7.

1.2.1.3.5 Square Fuel

The Square fuel basket is designed to house all of the fuel types listed in Section 1.2.2.5, *Square Fuel and Loose Plates*, which have a square or rectangular cross section, and three types of loose plates taken from those fuels. It consists of an array of eight square tubes having a wall thickness of 0.105 inches, held in position by three, ½-inch thick spacer plates. A 14-inch diameter, ¼-inch thick circular shell forms the lower portion of the basket. The tubes are arranged with six around the outer circumference and two in the middle. Loose plates are contained in a loose plate box. Spacer pedestals are used in each cavity, as required, to support the fuel elements at the top of the basket. The Square fuel basket is shown in Figure 1.2-8.

1.2.1.4 Gross Weight

The gross weight of the BRR package, including the cask, impact limiters, and maximum payload, is 32,000 lb. A summary of overall component weights is shown in Table 2.1-2 and discussed in Section 2.1.3, *Weights and Centers of Gravity.*

1.2.1.5 Neutron Moderation and Absorption

The BRR package maintains criticality control by means of limitation of the quantity of fissile material present and by maintaining a safe configuration of the material under all NCT and HAC. The design of the BRR package does not include any components whose principal purpose is the absorption of neutrons. A more detailed description of the package criticality control functions is given in Chapter 6, *Criticality Evaluation.*

1.2.1.6 Receptacles, Valves, Testing and Sampling Ports

The BRR package closure lid contains a vent port and a containment seal test port. A body drain port is located on the side of the lower end of the cask. There are no valves or receptacles used in the BRR package.

1.2.1.7 Heat Dissipation

The dissipation of heat from the BRR package is entirely passive. The impact limiters are painted white to reduce the absorption of solar heat. A thermal shield is used on the cask body to limit the temperature of the lead gamma shield in the HAC fire event. A more detailed description of the package thermal design is given in Chapter 3, *Thermal Evaluation.*

1.2.1.8 Lifting and Tie–down Devices

Other than the threaded holes in the top of the cask body, there are no lifting or tie–down devices that are a structural part of the BRR package. The package is secured to the transport vehicle using structures that interface with the surfaces of the upper and lower impact limiters. The package rests on a lower frame that is attached to the vehicle. An upper frame contacts the upper impact limiter and is attached to the vehicle using cables or the equivalent. There are no provisions to lift the package with the impact limiters installed.

1.2.1.9 Pressure Relief System

There is no pressure relief system in the BRR package.

1.2.1.10 Shielding

Biological shielding of gamma radiation is provided by a combination of lead and the thick steel shells of the BRR package. Hydrogenous neutron shielding is not necessary and none is included in the package design. Details of the gamma shielding are provided in Section 1.2.1.1, *Cask Body*. A full assessment of the shielding design is provided in Chapter 5, *Shielding Evaluation.*

1.2.2 Contents

The BRR package may contain up to 8 irradiated MURR, MITR-II, ATR, and Square fuel elements or loose plate boxes, and up to 19 irradiated TRIGA fuel elements. Only one fuel element is allowed per basket location. Loose plate boxes may be loaded in the same basket as fuel elements. Details for each fuel type are provided in the following paragraphs.

1.2.2.1 MURR

The MURR fuel element may be irradiated to a maximum burnup of 180 MWD (218,196 MWD/MTU, or a U-235 depletion of 30.9%). The minimum cooling time is 180 days after discharge from the core.

Each fresh MURR element contains 775.0 ± 7.8 g U–235, with an enrichment of 93 ± 1 wt.%. The weight percents of the remaining uranium isotopes are 1.2 wt.% U–234, 0.7 wt.% U–236, and 5.0 – 7.0 wt.% U–238. The MURR fuel element fissile material is uranium aluminide (UAl_x).

Each MURR fuel element contains 24 curved fuel plates. Fuel plate 1 has the smallest radius, while fuel plate 24 has the largest radius, as shown in Figure 1.2-9. The fuel "meat" is a mixture of uranium metal and aluminum, while the cladding and structural materials are an aluminum alloy. The fuel plates are rolled to shape and swaged into the two fuel element side plates. The fissile material (uranium aluminide) is nominally 0.02–in thick for all 24 plates. The minimum cladding thickness is 0.008-in. Fuel element side plates are fabricated of ASTM B 209, aluminum alloy 6061–T6 or 6061–T651 and are approximately 0.15–in thick. The averaged measured channel spacing between fuel plates, over the entire fuel element, is less than or equal to 0.088–in at the time of fabrication. The maximum local channel spacing at the time of fabrication is 0.090-in.

The MURR element overall length, including irradiation growth, is 32.75 inches. The bounding weight of one assembly is 15 lb. The maximum decay heat per fuel element is 158 W.

1.2.2.2 MITR–II

The MITR–II fuel element may be irradiated to a maximum burnup of 165 MWD (306,900 MWD/MTU, or a U–235 depletion of 43.9%). The minimum cooling time is 120 days after discharge from the core.

Each fresh MITR–II element contains 510.0 +3.0/-10.0 g U–235, with an enrichment of 93 ± 1 wt.%. The weight percents of the remaining uranium isotopes are 1.2 wt.% U–234, 0.7 wt.% U–236, and 5.0 – 7.0 wt.% U–238. Like the MURR fuel element, the MITR–II fuel element fissile material is uranium aluminide (UAl_x).

Each MITR–II fuel element contains 15 flat fuel plates, as shown in Figure 1.2-10. The fuel plates are fabricated and swaged into the two fuel element side plates. The fuel "meat" is a mixture of uranium metal and aluminum, while the cladding and structural materials are an aluminum alloy. The fissile material (uranium aluminide) is nominally 0.03–in thick and the cladding is nominally 0.025–in thick. The minimum cladding thickness, including the thermal groove, is 0.008-in. Fuel element side plates are fabricated of ASTM B 209, aluminum alloy 6061–T6 and are approximately 0.19–in thick. The averaged measured channel spacing between fuel plates, over the entire fuel element, is less than or equal to 0.082–in at the time of fabrication (excluding the thermal grooves). The maximum local channel spacing at the time of fabrication is 0.090-in (excluding the thermal grooves).

The MITR–II element overall length, including irradiation growth, is 26.52 inches. The bounding weight of one assembly is 10 lb. The maximum decay heat per assembly is 150 W.

1.2.2.3 ATR

The ATR fuel element may be irradiated to a maximum burnup of 480 MWD[1] (491,155 MWD/MTU, or a U–235 depletion of 58.6%). The minimum cooling time is 1,670 days (4.6 years) after discharge from the core.

There are two general classes of ATR fuel element, XA and YA. The XA fuel element has a fresh fuel loading of 1,075 ± 10 g U–235, with an enrichment of 93 ± 1 wt.%. The weight percents of the remaining uranium isotopes are 1.2 wt.% U–234 (max), 0.7 wt.% U–236 (max), and 5.0 – 7.0 wt.% U–238. Like the MURR and MITR–II fuel elements, the fuel element fissile material is uranium aluminide (UAl_x).

The XA fuel element is further subdivided into fuel element types 7F, 7NB, 7NBH. In the 7F fuel element, all 19 fuel plates are loaded with enriched uranium in an aluminum matrix with the eight outer plates (1 through 4 and 16 through 19) containing boron as a burnable poison. The fuel element with the greatest reactivity is the 7NB that contains no burnable poison. The 7NBH fuel element is similar to the 7NB fuel element except that it contains one or two borated plates. The YA fuel element is identical to the 7F fuel element except that plate 19 of the YA fuel element is an aluminum alloy plate containing neither uranium fuel nor boron burnable poison. The YA fuel element has a fresh fuel loading of 1,022.4 ± 10 g U–235. A second YA fuel element design (YA–M) has the side plate width reduced by 15 mils.

[1] The element burnup of 480 MWD should not be a limit for licensing purposes because the element burnup is typically not known in units of MWD. The final U-235 mass within an element is computed and recorded by ATR staff.

The ATR fuel elements contain 19 curved fuel plates. A section view of an ATR fuel element is given in Figure 1.2-11. Note that an intact ATR fuel element has end boxes (as shown on Figure 1.2-11), although these end boxes are removed prior to insertion in the BRR package. The fuel plates are rolled to shape and swaged into the two fuel element side plates. Fuel plate 1 has the smallest radius, while fuel plate 19 has the largest radius. The fissile material (uranium aluminide) is nominally 0.02–in thick for all 19 plates. The minimum cladding thickness is 0.018-in for plates 1 and 19, and 0.008-in for plates 2 through 18. Fuel element side plates are fabricated of ASTM B 209, aluminum alloy 6061–T6 or 6061–T651 and are approximately 0.19–in thick. The averaged measured channel spacing between fuel plates, over the entire fuel element, is less than or equal to 0.085–in at the time of fabrication. The maximum local channel spacing is 0.087-in at the time of fabrication.

The ATR element overall length, after removal of the end box structures, 51.0 inches max. The bounding weight of one assembly is 25 lb. The maximum decay heat per assembly is 30 W.

1.2.2.4 TRIGA

Many different types of TRIGA fuel elements have been fabricated over the past several decades. TRIGA fuel elements utilize a zirconium hydride fuel matrix. Twenty-six (26) different TRIGA element types are evaluated. These element types are identified by their General Atomics catalog number. TRIGA elements fall into five general categories:

- Standard (100 series)
- Instrumented (200 series). Instrumented rods contain thermocouples used to measure temperature during reactor operation. The fueled region is essentially the same as a standard rod, although instrumented rods may be longer.
- Fueled Follower Control Rods (FFCR) (300 series). FFCR rods contain boron carbide neutron absorber outside the active fuel region.
- Cluster rods (400 series). Typically three or four cluster rods are used to build a cluster assembly. For transportation in the BRR package, the cluster rods are disassembled from the cluster assembly.
- Instrumented cluster rods (500 series). Instrumented rods contain thermocouples used to measure temperature during reactor operation. The fueled region is essentially the same as a standard cluster rod, although instrumented cluster rods may be longer.

Basic fresh fuel data used to describe the various TRIGA fuel elements are summarized in Table 1.2-1. A basic TRIGA fuel element is depicted in Figure 1.2-12. The maximum length of an element, including irradiation growth, is 45.50 inches. Non–instrumented fuel elements are somewhat shorter. For all fuel elements, spacers are utilized within the TRIGA baskets.

The maximum burnup and minimum required cooling time after reactor discharge for the various element types is summarized in Table 1.2-2. The burnup and cooling time combinations are selected to limit the decay heat to 20 W. When using this table to qualify fuel for shipment, the actual burnup value shall be rounded up to the next higher burnup value shown in the table.

Table 1.2-2 is developed based on an in-core residence time of 4 years. It is expected that such a short residence time would result in bounding cooling times in most situations, as TRIGA fuel typically has an in-core residence time of at least 10 years. However, for fuel with an in-core residence time less than 4 years, the decay heat shall be independently confirmed to be $\leq$ 20 W.

The bounding weight of any TRIGA fuel element is 10 lb.

1.2.2.5 Square Fuel and Loose Plates

The Square fuel basket is used to transport fuel that has a nominal square or rectangular geometry, including plate fuel, the loose plate box, and PULSTAR fuel. The heat load of the Square fuel basket is limited to 30 watts per compartment.

The Square plate fuels (i.e., all square fuels except PULSTAR) include Rhode Island Nuclear Science Center (RINSC), University of Massachusetts at Lowell (U-Mass), Ohio State University (Ohio State), Missouri University of Science and Technology (Missouri S&T), University of Florida (U-Florida), and Purdue University (Purdue). The plate fuels are 20% enriched. Fuel data for the square plate fuels is summarized in Table 1.2-3.

With the exception of U-Mass, the plate fuels have a uranium silicide (U_3O_2) fuel matrix mixed with aluminum. U-Mass has two fuel element types currently in use, uranium silicide and uranium aluminide (UAl_x). The U-Mass (aluminide) fuel originally was manufactured for the Worcester Polytechnic Institute (WPI) reactor.

Each RINSC fuel element contains 22 flat fuel plates fitted within aluminum side plates, and the maximum allowable channel spacing between fuel plates is less than or equal to 0.099 inches at the time of fabrication. The maximum burnup is limited to 52.5 MWD, and the minimum cooling time is 120 days after discharge from the core. RINSC fuel is illustrated in Figure 1.2-13, and is illustrative of the other square fuels that have swaged plate designs using side combs.

Each U-Mass (aluminide) fuel element contains 18 flat fuel plates fitted within aluminum side plates, and the maximum allowable channel spacing between fuel plates is less than or equal to 0.119 inches at the time of fabrication. The maximum burnup is limited to 9.7 MWD, and the minimum cooling time is 1,000 days after discharge from the core. This fuel was partially burned in the WPI reactor before being transferred to U-Mass for further irradiation. The burnup limit for this fuel element is the total combined burnup for the WPI and U-Mass reactors.

Each U-Mass (silicide) fuel element contains 16 flat fuel plates fitted within aluminum side plates, and the maximum allowable channel spacing between fuel plates is less than or equal to 0.122 inches at the time of fabrication. The maximum burnup is limited to 9.7 MWD, and the minimum cooling time is 1,000 days after discharge from the core.

Each Ohio State fuel element contains 16 flat fuel plates fitted within aluminum side plates, and the maximum allowable channel spacing between fuel plates is less than or equal to 0.127 inches at the time of fabrication. The maximum burnup is limited to 64 MWD, and the minimum cooling time is 120 days after discharge from the core.

Each Missouri S&T fuel element contains 18 curved fuel plates fitted within parallel aluminum side plates, and the maximum allowable channel spacing between fuel plates is less than or equal to 0.139 inches at the time of fabrication. The maximum burnup is limited to 74 MWD, and the minimum cooling time is 365 days after discharge from the core.

Each U-Florida fuel element contains 14 flat fuel plates that include spacers and combs and are screwed together at 4 corners (no side plates), and the maximum allowable channel spacing between fuel plates is less than or equal to 0.117 inches at the time of fabrication. The maximum burnup is limited to 87 MWD, and the minimum cooling time is 120 days after discharge from the core. The U-Florida screw-assembly design is illustrated in Figure 1.2-14.

Each Purdue fuel element contains of a maximum of 14 flat fuel plates loaded into a grooved fuel box and contained with a screwed on lifting bar at top, and the maximum allowable channel spacing between fuel plates is less than or equal to 0.175 inches at the time of fabrication. The maximum burnup is limited to 0.57 MWD, and the minimum cooling time is 120 days after discharge from the core.

A loose plate box is used to transport up to 31 loose plates per box. Loose plates are limited to U-Mass (aluminide), U-Florida, and Purdue fuel plates. A depiction of the Square fuel basket, loose plate box, and loose plates inside a BRR package is shown in Figure 1.2-17.

The PULSTAR fuel element may be irradiated to a maximum burnup of 20,000 MWD/MTU. The minimum cooling time is 1.5 years after discharge from the core. PULSTAR fuel is similar to light water reactor fuel, as it has a UO_2 fuel matrix, zirconium alloy cladding, cylindrical fuel rods, and a nominal enrichment between 4 and 6%. PULSTAR fuel data is summarized in Table 1.2-4. The fuel is arranged in a 5 × 5 rectangular lattice, as shown in Figure 1.2-15. The active fuel region is contained within a zirconium alloy box, although the end fittings are aluminum alloy. Including a spacer pedestal, the weight of a PULSTAR element is 48 lb, which bounds the weight of all other fuels used in the Square fuel basket.

1.2.3 Special Requirements for Plutonium

The BRR package may contain plutonium in excess of 20 Ci as a consequence of irradiation of the reactor fuel. As such, the plutonium is in solid form within the fuel matrix. Table 1.2-5 summarizes the plutonium activity for each of the five basket types, both on a per-element and per-cask basis. The plutonium activities are extracted from the SCALE6/TRITON output files used to generate the gamma and neutron source terms. The source term development is described in detail in Section 5.2, *Source Specification.* The maximum quantity of plutonium for the BRR package is 6,500 Ci, which occurs for 4% enriched PULSTAR fuel. PULSTAR fuel has an approximately square outer dimension and is transported in the Square fuel basket.

1.2.4 Operational Features

The BRR package is of conventional design and is not complex to operate. Operational features are depicted on the drawings provided in Appendix 1.3.3, *Packaging General Arrangement Drawings*. Operating procedures and instructions for loading, unloading, and preparing an empty package for transport are provided in Chapter 7, *Package Operations*.

Table 1.2-1 – TRIGA Fresh Fuel Characteristics

ID	Type	Cladding	U (wt.% fuel)	Fuel Length (in)	U-235 (wt.% U)	U (g)	U-235 (g)	Fuel OD (in)	Rod OD (in)	Cladding Thickness (in)	H/Zr	Overall Length (in)	Er (wt.%)
101	Std.	Al	8.0	14	20	166	32	1.41	1.48	0.03	1.0	28.62	0
	Std.	Al	8.5	15	20	189	37	1.41	1.48	0.03	1.6	28.62	0
103	Std.	SS	8.5	15	20	197	39	1.44	1.48	0.02	1.6	29.15	0
105	Std.	SS	12	15	20	285	56	1.44	1.48	0.02	1.6	29.15	0
107	Std.	SS	12	15	20	271	53	1.40	1.48	0.02	1.6	30.14	0
109	Std.	SS	8.5	15	70	194	136	1.44	1.48	0.02	1.6	29.15	1.2
117	Std.	SS	20	15	20	503	99	1.44	1.48	0.02	1.6	29.93	0.5
119	Std.	SS	30	15	20	825	163	1.44	1.48	0.02	1.6	29.93	0.9
201	Ins.	Al	8.5	15	20	189	37	1.41	1.48	0.03	1.6	28.78	0
203	Ins.	SS	8.5	15	20	197	39	1.44	1.48	0.02	1.6	45.50	0
205	Ins.	SS	12	15	20	285	56	1.44	1.48	0.02	1.6	45.50	0
207	Ins.	SS	12	15	20	271	53	1.40	1.48	0.02	1.6	45.50	0
217	Ins.	SS	20	15	20	503	99	1.44	1.48	0.02	1.6	40.35	0.5
219	Ins.	SS	30	15	20	825	163	1.44	1.48	0.02	1.6	40.35	0.9
303	FFCR	SS	8.5	15	20	163	32	1.31	1.35	0.02	1.6	44.00	0
305	FFCR	SS	12	15	20	237	47	1.31	1.35	0.02	1.6	44.00	0
317	FFCR	SS	20	15	20	418	82	1.31	1.35	0.02	1.6	44.00	0.5
319	FFCR	SS	30	15	20	685	135	1.31	1.35	0.02	1.6	44.00	0.9

(continued)

Table 1.2-1 – TRIGA Fresh Fuel Characteristics (concluded)

ID	Type	Cladding	U (wt.% fuel)	Fuel Length (in)	U-235 (wt.% U)	U (g)	U-235 (g)	Fuel OD (in)	Rod OD (in)	Cladding Thickness (in)	H/Zr	Overall Length (in)	Er (wt.%)
403	Cluster	SS	8.5	15	20	166	33	1.37	1.41	0.02	1.6	30.38	0
405	Cluster	SS	12	15	20	243	48	1.37	1.41	0.02	1.6	30.38	0
417	Cluster	SS	20	15	20	427	85	1.37	1.41	0.02	1.6	30.38	0.5
419	Cluster	SS	30	15	20	710	141	1.37	1.41	0.02	1.6	30.38	0.9
503	Ins. cluster	SS	8.5	15	20	166	33	1.34	1.41	0.02	1.6	45.50	0
505	Ins. cluster	SS	12	15	20	243	48	1.34	1.41	0.02	1.6	45.50	0
517	Ins. cluster	SS	20	15	20	427	85	1.34	1.41	0.02	1.6	45.50	0.5
519	Ins. cluster	SS	30	15	20	710	141	1.34	1.41	0.02	1.6	45.50	0.9

Note: General Atomics catalog numbers are not necessarily unique. TRIGA elements with the same ID could have different fuel parameters. In this table, two variants of the Type 101 element are listed. Overall length includes 0.25 inches for irradiation growth.

Table 1.2-2 – TRIGA Fuel Qualification Table

Type	Maximum Burnup (MWD)	Minimum Cooling (days)	Type	Maximum Burnup (MWD)	Minimum Cooling (days)
101 (8.0%)	23	90	303	22	90
201/101 (8.5%)	26	90	305	32	90
109	88	350	317	58	210
	70	250		46	150
	52	170		34	90
	34	90	319	97	420
203/103	27	90		76	290
205/105	39	120		55	180
	33	90		34	90
207/107	38	120	503/403	23	90
	33	90	505/405	33	90
217/117	71	280	517/417	60	220
	52	180		47	150
	34	90		34	90
219/119	122	600	519/419	101	430
	91	370		79	290
	63	220		56	180
	34	90		34	90

Note: This table is developed based on an in-core residence time of 4 years to result in a decay heat ≤ 20 W. For fuel with an in-core residence time less than 4 years, the decay heat shall be independently confirmed to be ≤ 20 W.

Table 1.2-3 –Square Plate Fuel Characteristics

Parameter	RINSC	U-Mass (Al)	U-Mass (Si)	Ohio St	Miss. S&T	U-Florida	Purdue
U-235 loading (g)	275±7.7	167±3.3	200±5.6	200±5.6	225±6.3	175±4.9	129.92±2.52
Nominal U-235 Enrichment (%)	19.75	19.75	19.75	19.75	19.75	19.75	19.75
Fuel matrix	U_3Si_2+Al	UAl_x	U_3Si_2+Al	U_3Si_2+Al	U_3Si_2+Al	U_3Si_2+Al	U_3Si_2+Al
Maximum burnup (MWD)	52.5	9.7	9.7	64.0	74.0	87.0	0.57
Minimum decay time (D)	120	1,000	1,000	120	365	120	120
Nominal fuel meat width (in.)	2.395	2.320	2.395	2.395	2.395	2.395	2.395
Nominal fuel meat thickness (in.)	0.02	0.03	0.02	0.02	0.02	0.02	0.02
Nominal fuel plate thickness (in.)	0.05	0.06	0.05	0.05	0.05	0.05	0.05
Nominal active fuel length (in.)	23.25	23.25	23.25	23.25	23.25	23.25	23.25
Number of fuel plates	22	18	16	16	18	14	14
Maximum channel spacing (in.)	0.099	0.119	0.122	0.127	0.139	0.117	0.175
Weight (lb)	14	12	12	12	14	10	10
Maximum cross section (in.)	3.097×3.097	3.097×3.097	3.097×3.097	3.05×3.05	3.036×3.212	2.9×2.424	3.011×3.011
Maximum overall length (in.)④	39.75	39.75	39.75	35.25	34.50	27.38	32.49
Loose plate④	no	①	no	no	no	②	③

Notes:

1. U-Mass (Al) loose plates have a U-235 loading of 9.28 ± 0.18g and dimensions of 2.78 inches wide by 24.88 inches long.
2. U-Florida loose plates have a U-235 loading of 12.5 ± 0.35g and dimensions of 2.85 inches wide by 25.88 inches long.
3. Purdue loose plates have a U-235 loading of 9.28 ± 0.18g and dimensions of 2.85 inches wide by 25.88 inches long.
4. Maximum length includes 0.25 inches for irradiation growth.

Table 1.2-4 –PULSTAR Fuel Characteristics

Parameter	Value
Nominal U-235 Enrichment (%)	4.0/6.0
Fuel matrix	UO_2
Maximum burnup (MWD/MTU)	20,000
Decay time (years)	1.5
Maximum fuel pellet diameter (in.)	0.423
Minimum cladding thickness (in.)	0.0185
Cladding material	Ziconium alloy
Maximum cladding OD (in.)	0.474
Maximum active fuel length (in.)	24.1
Fuel rod pitch X (in.)	0.607
Fuel rod pitch Y (in.)	0.525
Box outer dimensions (in.)	3.15 x 2.74
Box thickness (in.)	0.06
Box material	Ziconium alloy
Maximum overall length (in.)①	38.23

Notes:

1. Maximum length includes 0.25 inches for irradiation growth.

Table 1.2-5 – Plutonium Activity

Plutonium Activity per Fuel Element (Ci)					
Isotope	**MURR**	**MITR–II**	**ATR**	**TRIGA**	**Square①**
Pu–238	1.63E+00	5.16E+00	8.38E+00	1.35E+01	1.32E+01
Pu–239	1.03E-01	9.80E-02	1.90E-01	4.91E-01	5.16E+00
Pu–240	4.91E-02	5.81E-02	1.38E-01	5.36E-01	3.46E+00
Pu–241	1.19E+01	2.61E+01	4.60E+01	2.27E+02	7.90E+02
Pu–242	3.66E-05	1.35E-04	4.93E-04	4.15E-03	4.48E-03
Total	1.37E+01	3.14E+01	5.48E+01	2.42E+02	8.12E+02
Plutonium Activity per BRR Package (Ci)					
Isotope	**MURR**	**MITR–II**	**ATR**	**TRIGA**	**Square①**
Pu–238	1.30E+01	4.13E+01	6.70E+01	2.57E+02	1.06E+02
Pu–239	8.26E-01	7.84E-01	1.52E+00	9.32E+00	4.13E+01
Pu–240	3.93E-01	4.65E-01	1.10E+00	1.02E+01	2.77E+01
Pu–241	9.56E+01	2.09E+02	3.68E+02	4.32E+03	6.32E+03
Pu–242	2.93E-04	1.08E-03	3.95E-03	7.88E-02	3.59E-02
Total	1.10E+02	2.51E+02	4.38E+02	4.60E+03	6.50E+03

①Fuels transported in the Square fuel basket include RINSC, U-Mass, Ohio State, Missouri S&T, U-Florida, Purdue, and PULSTAR. The limiting plutonium activity occurs for PULSTAR.

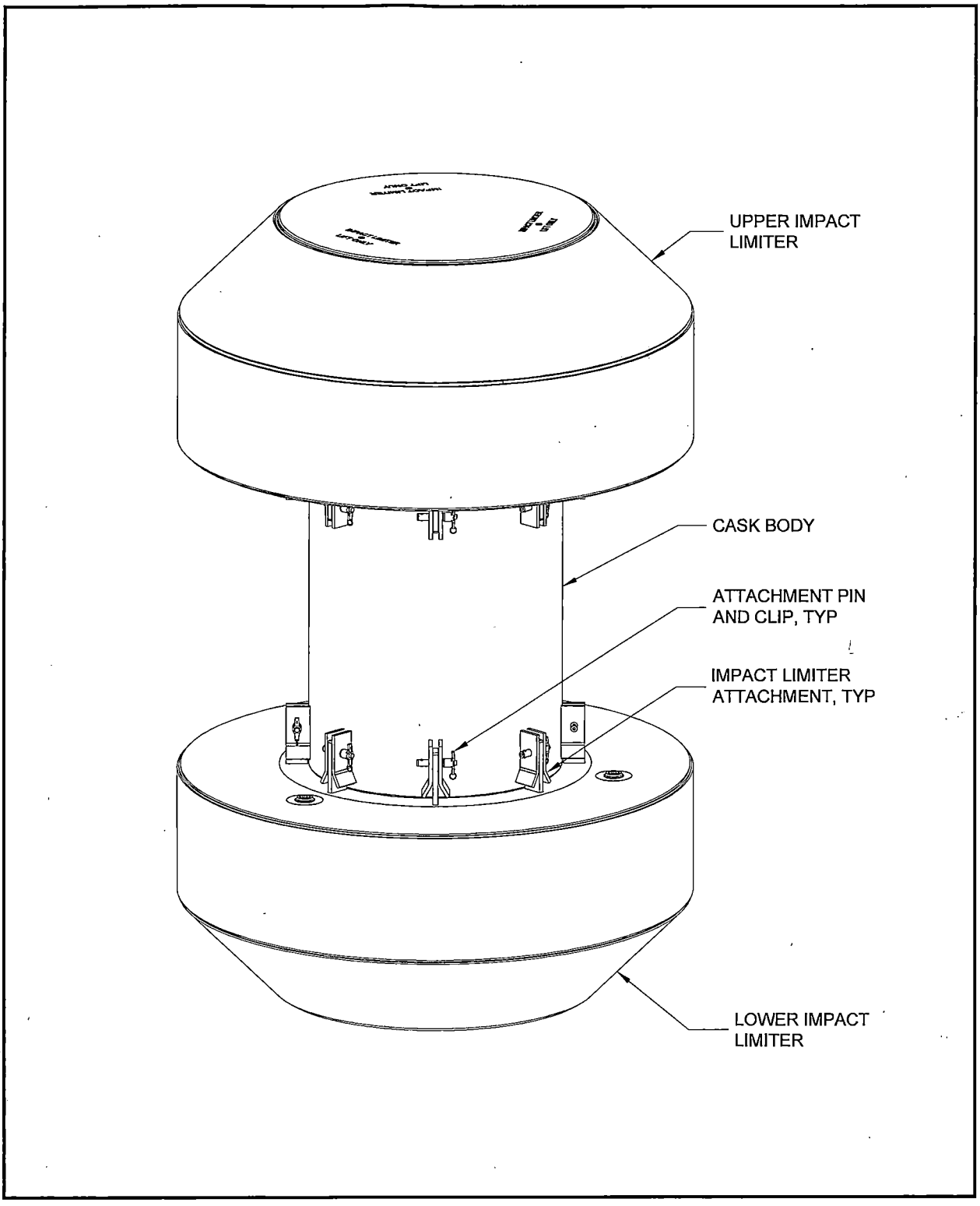

Figure 1.2-1 – BRR Packaging Components

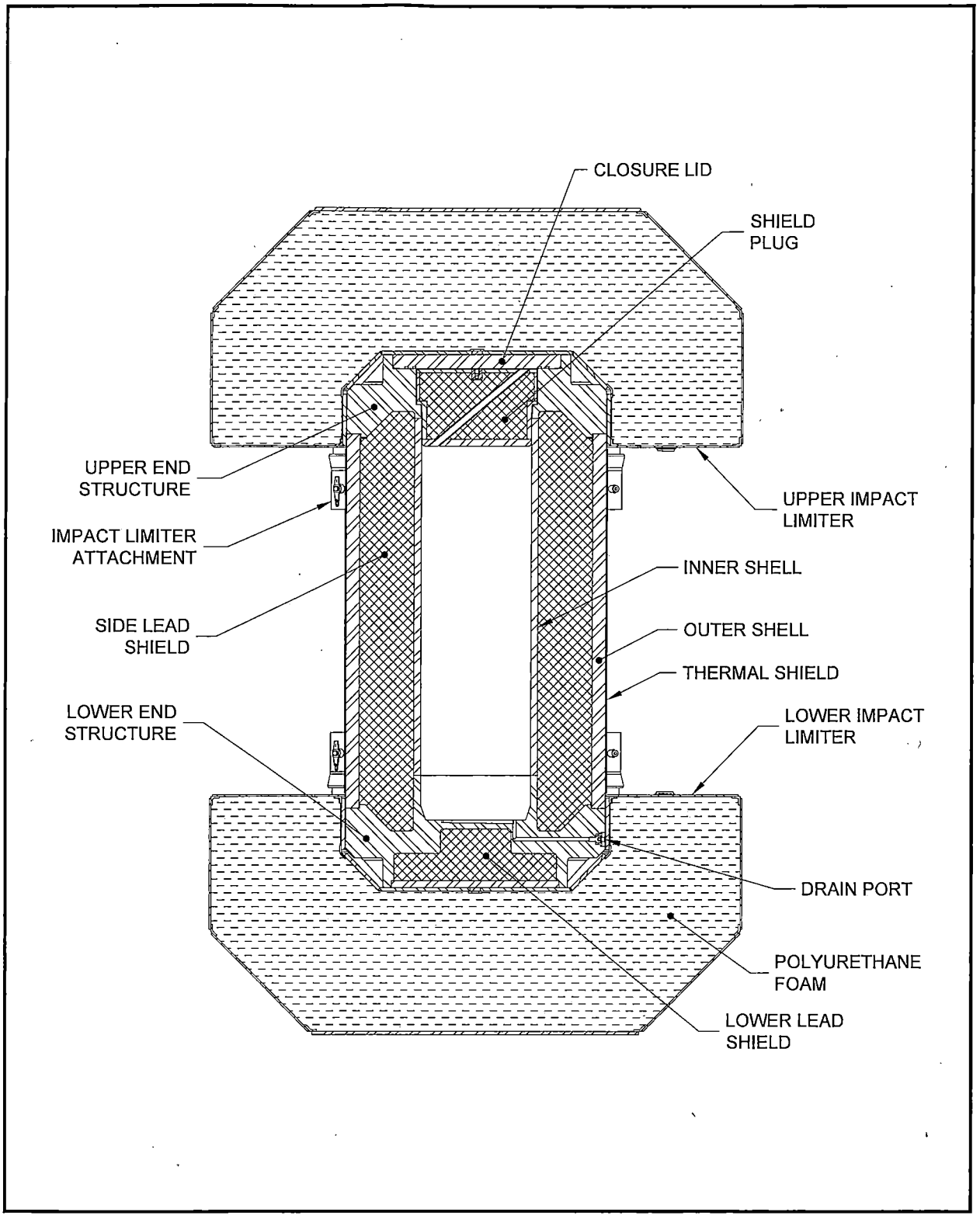

Figure 1.2-2 – BRR Package Cross Section

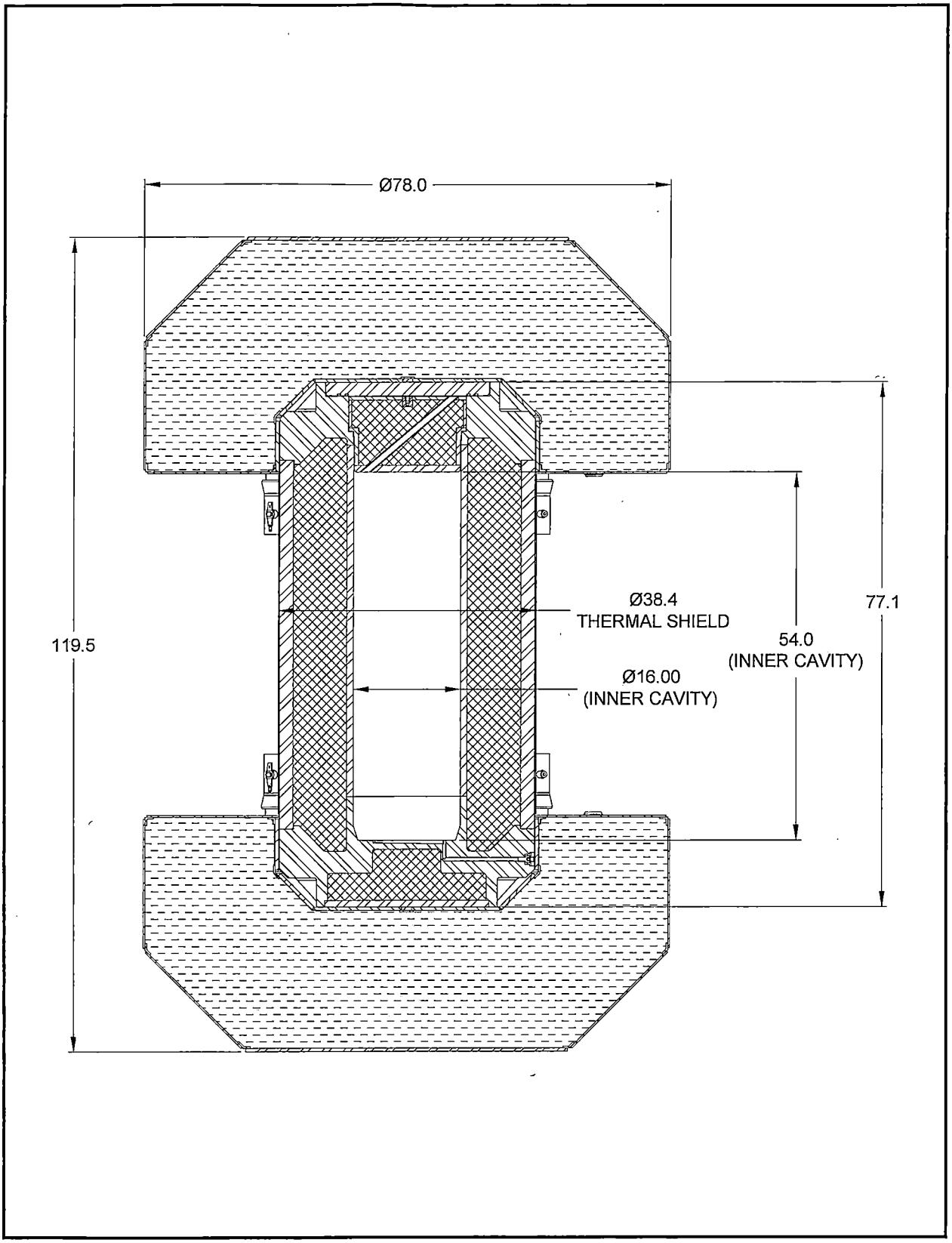

Figure 1.2-3 – BRR Package Dimensions

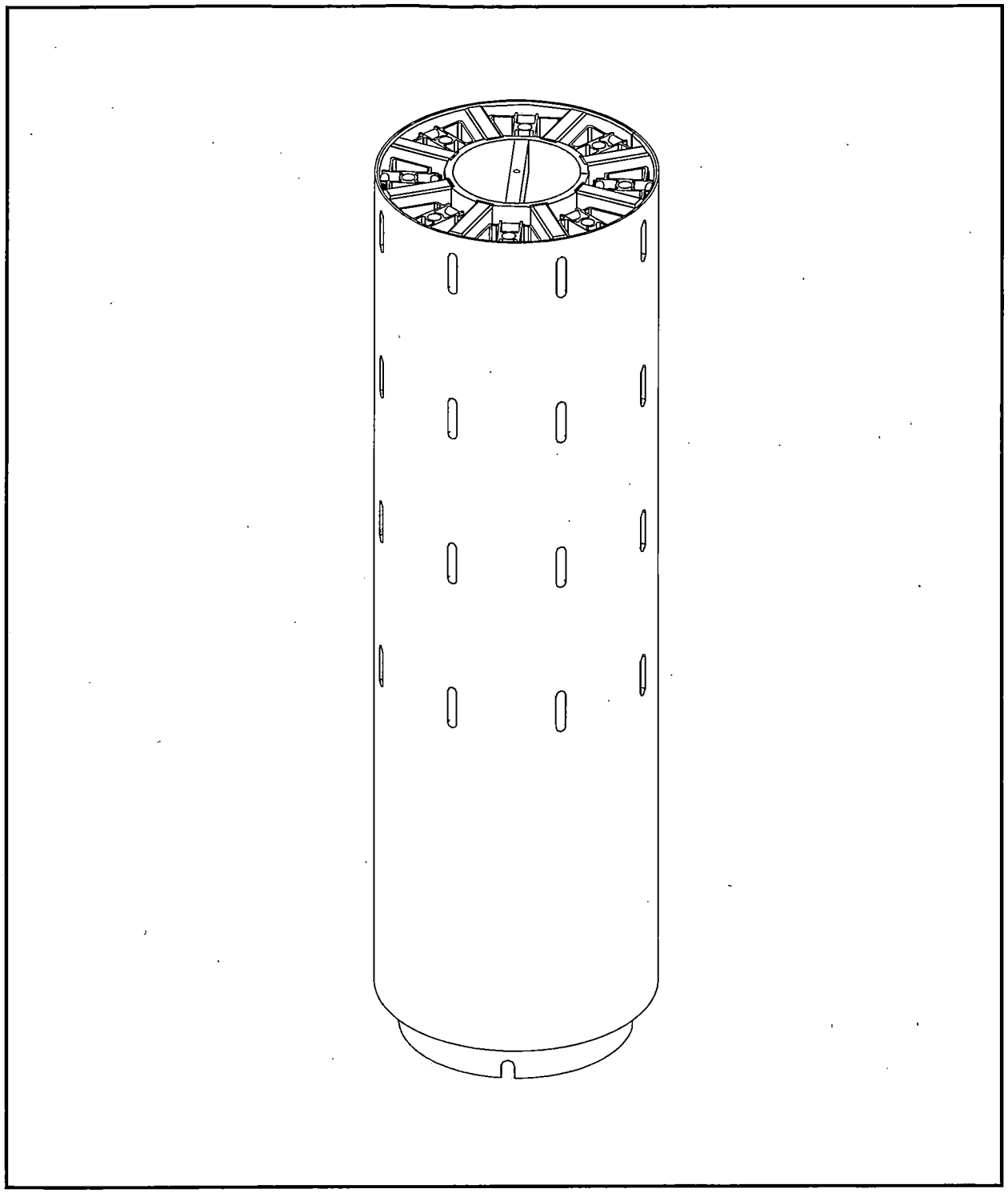

Figure 1.2-4 – MURR Fuel Basket

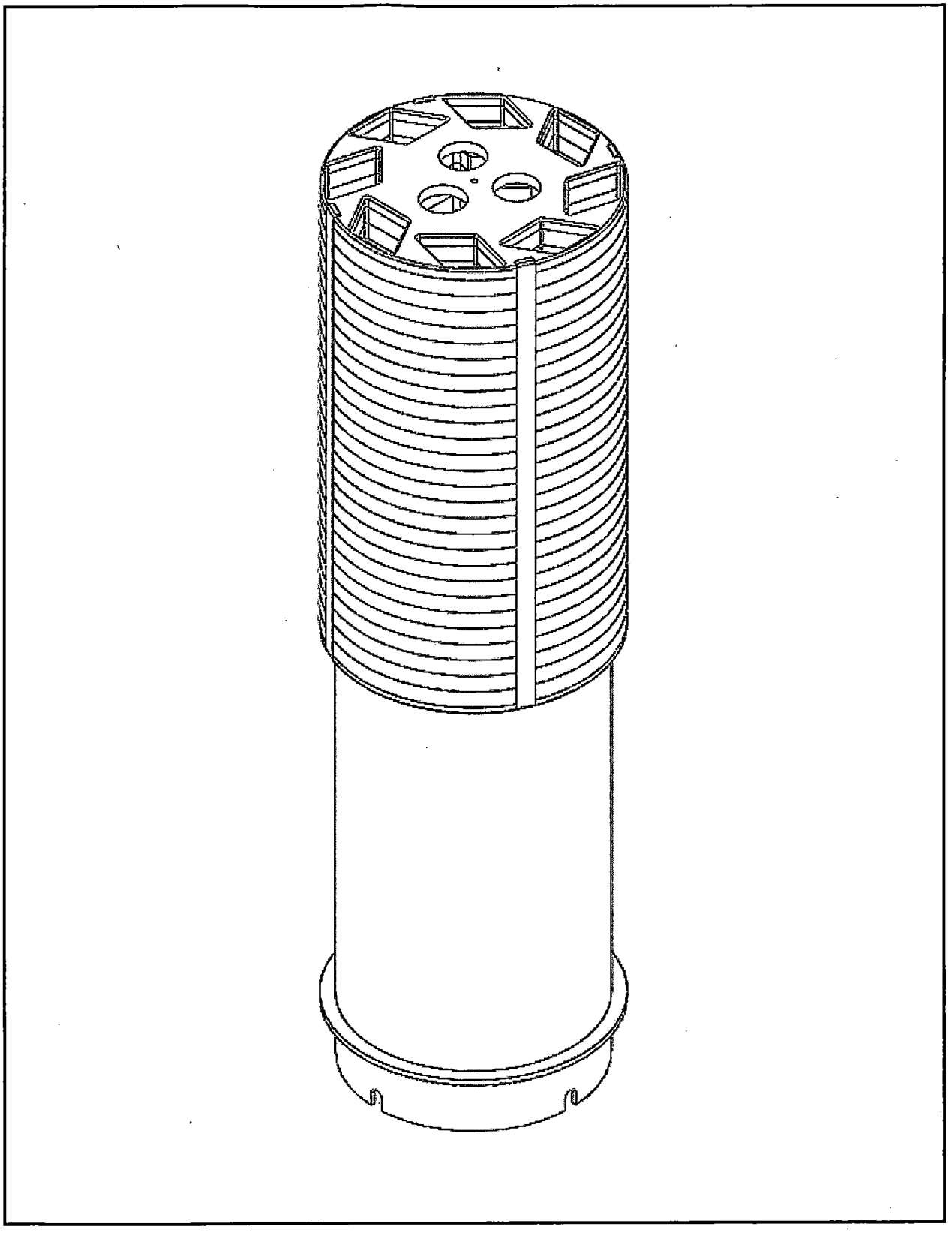

Figure 1.2-5 – MITR–II Fuel Basket

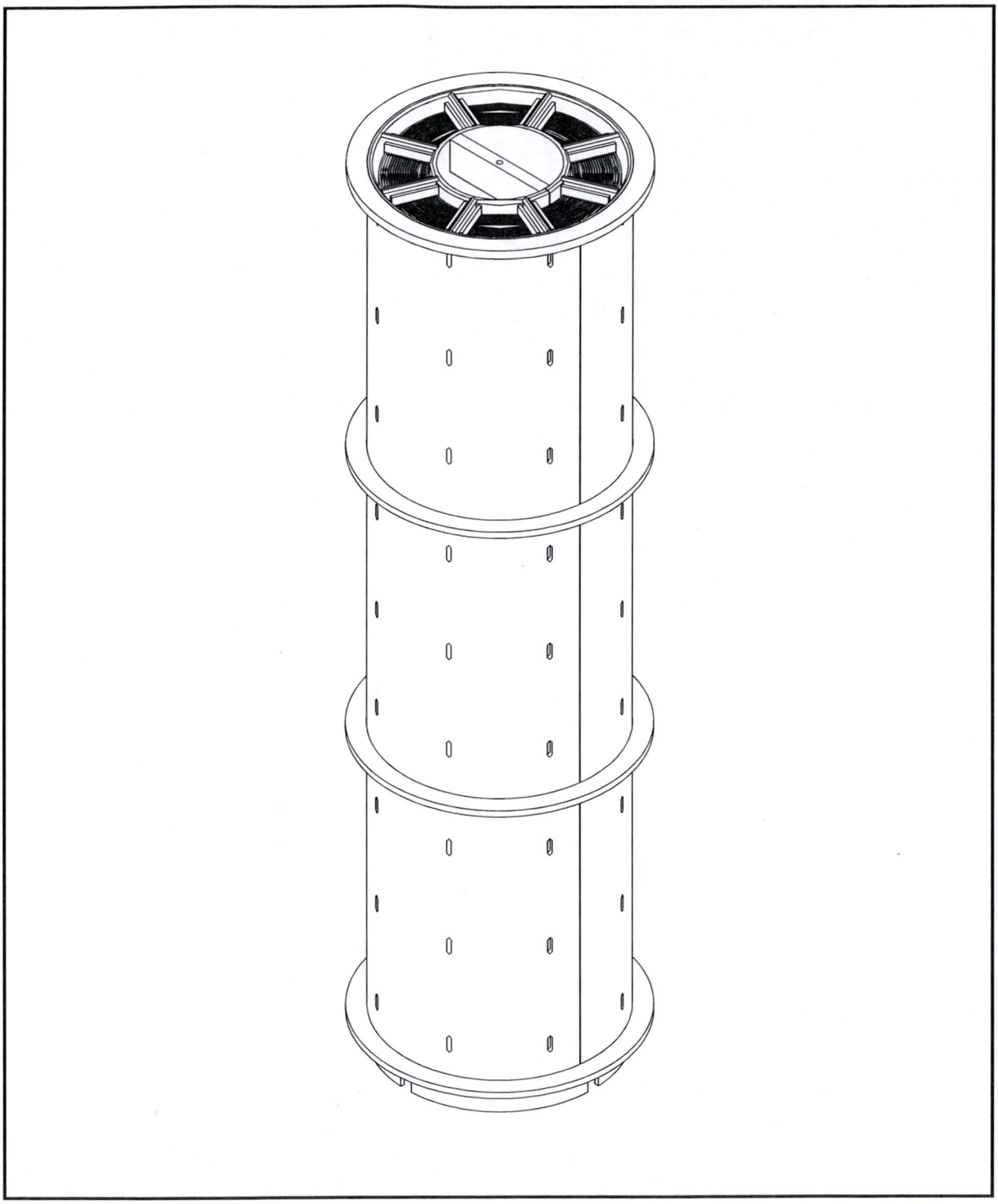

Figure 1.2-6 –ATR Fuel Basket

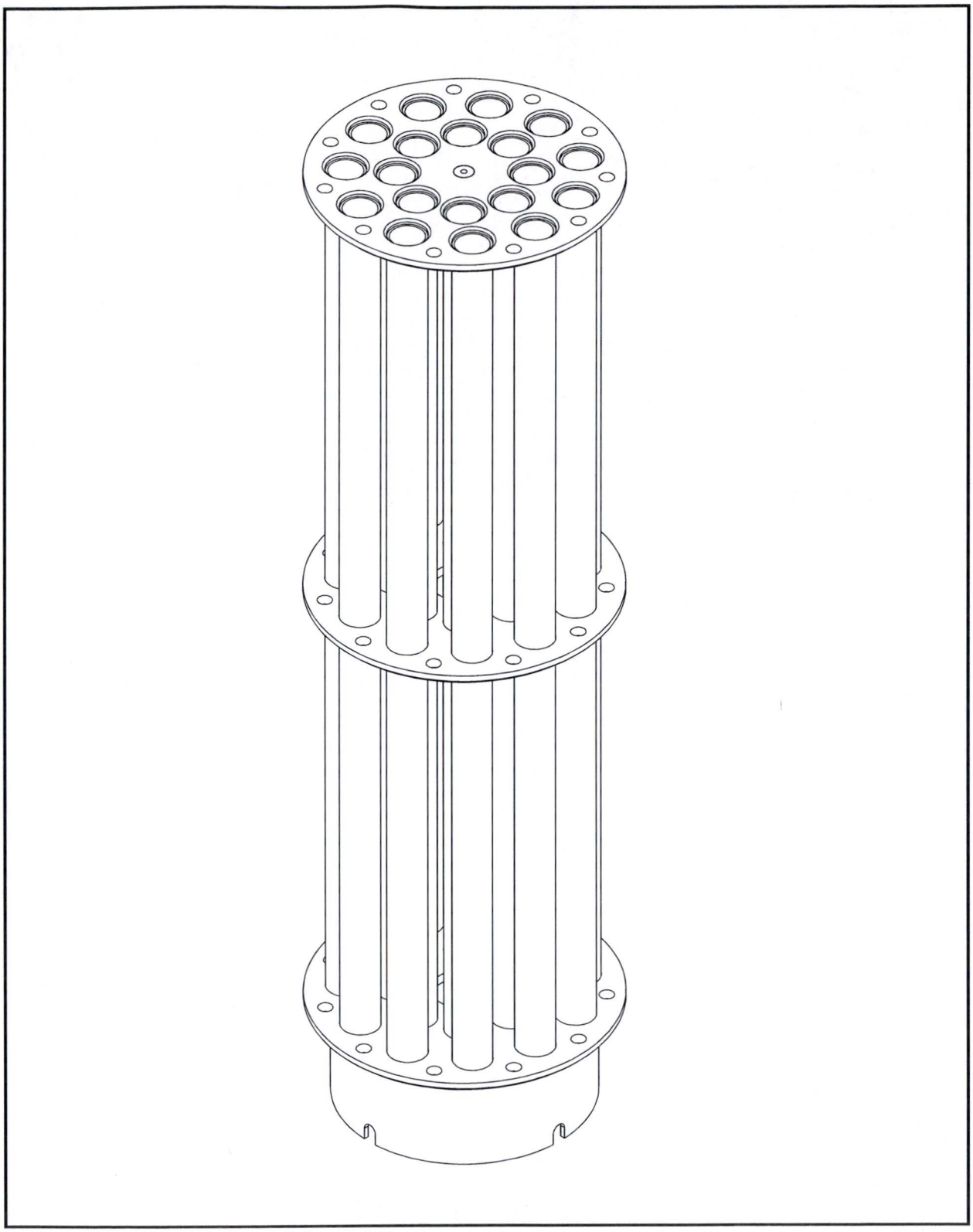

Figure 1.2-7 – TRIGA Fuel Basket

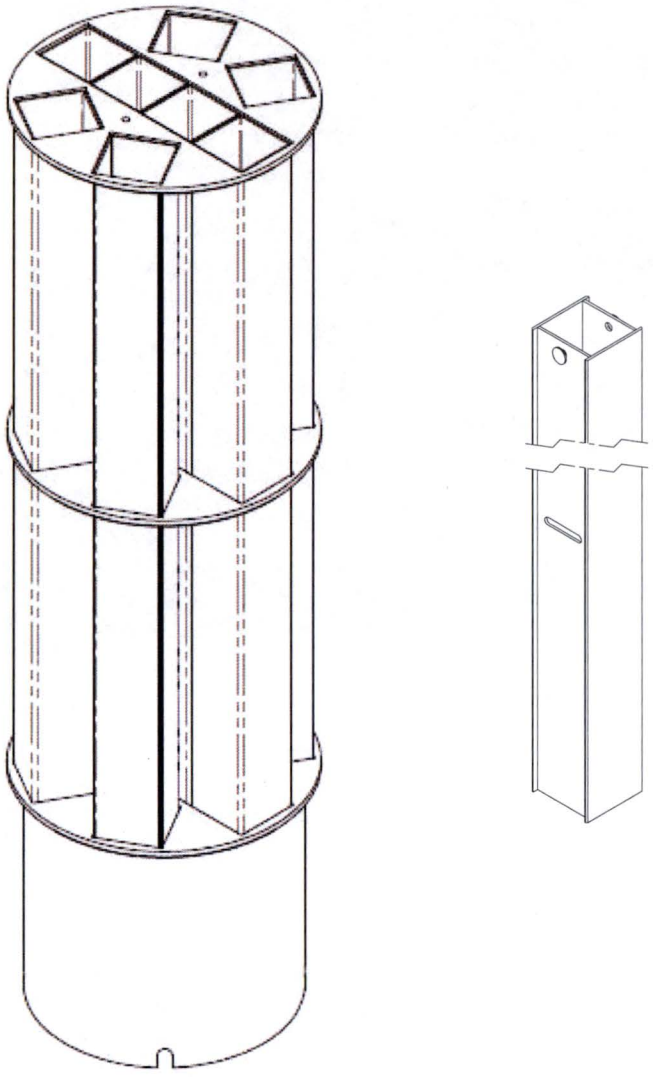

Figure 1.2-8 – Square Fuel Basket and Loose Plate Box

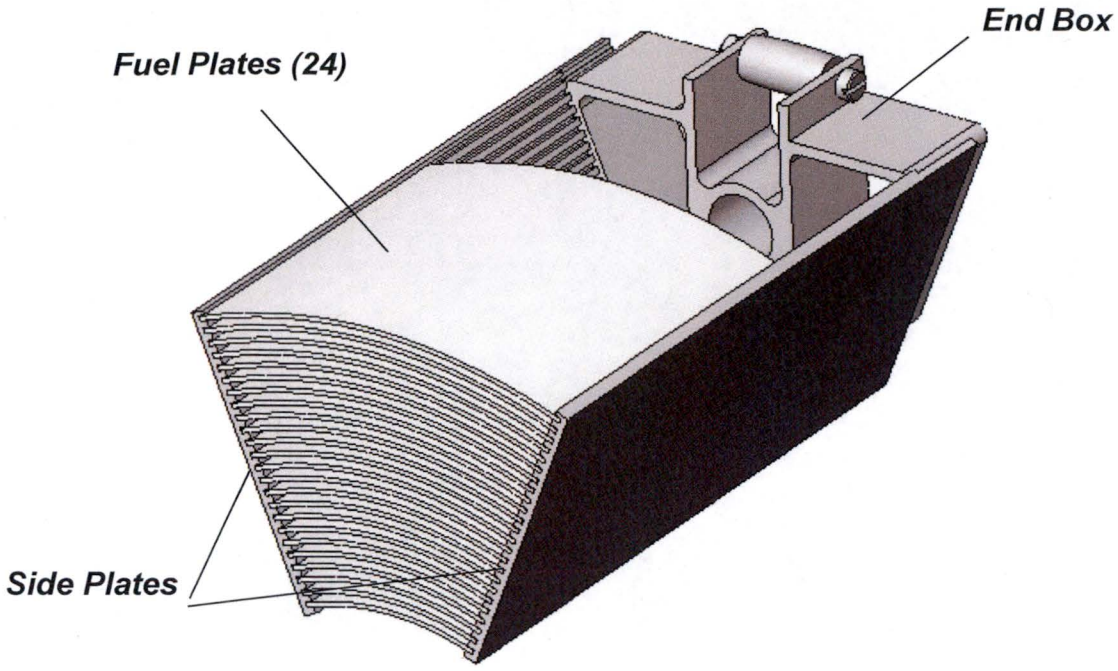

Figure 1.2-9 – MURR Fuel Element – Section View

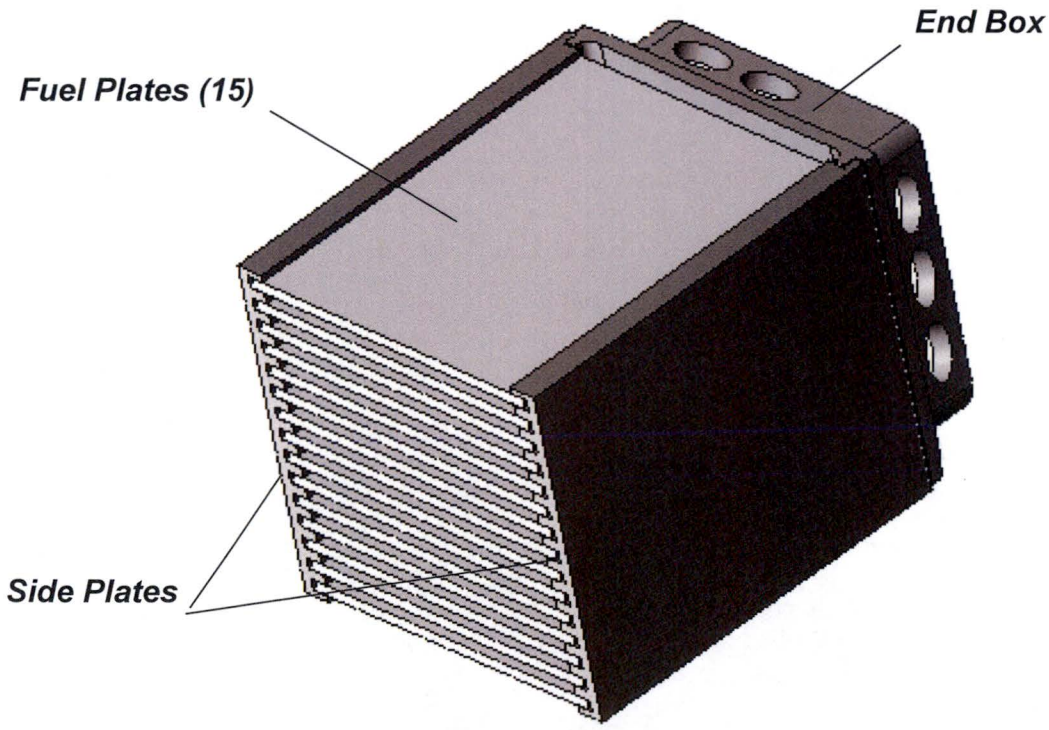

Figure 1.2-10 – MITR–II Fuel Element – Section View

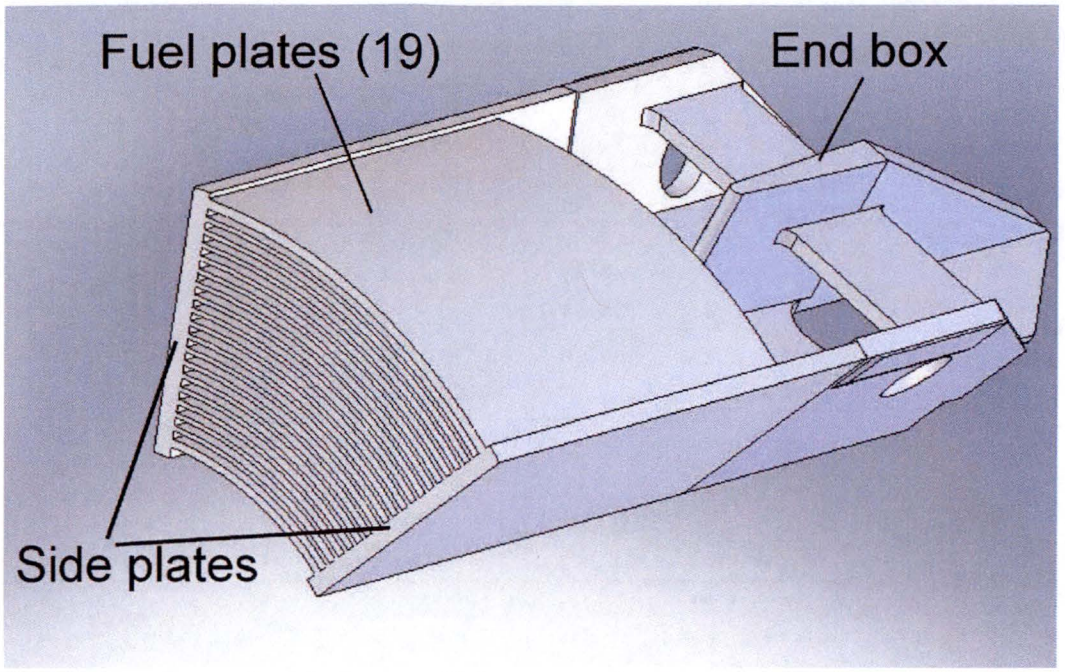

Note: The end box shown in this figure will be removed prior to insertion in the BRR package.

Figure 1.2-11 – ATR Fuel Element – Section View

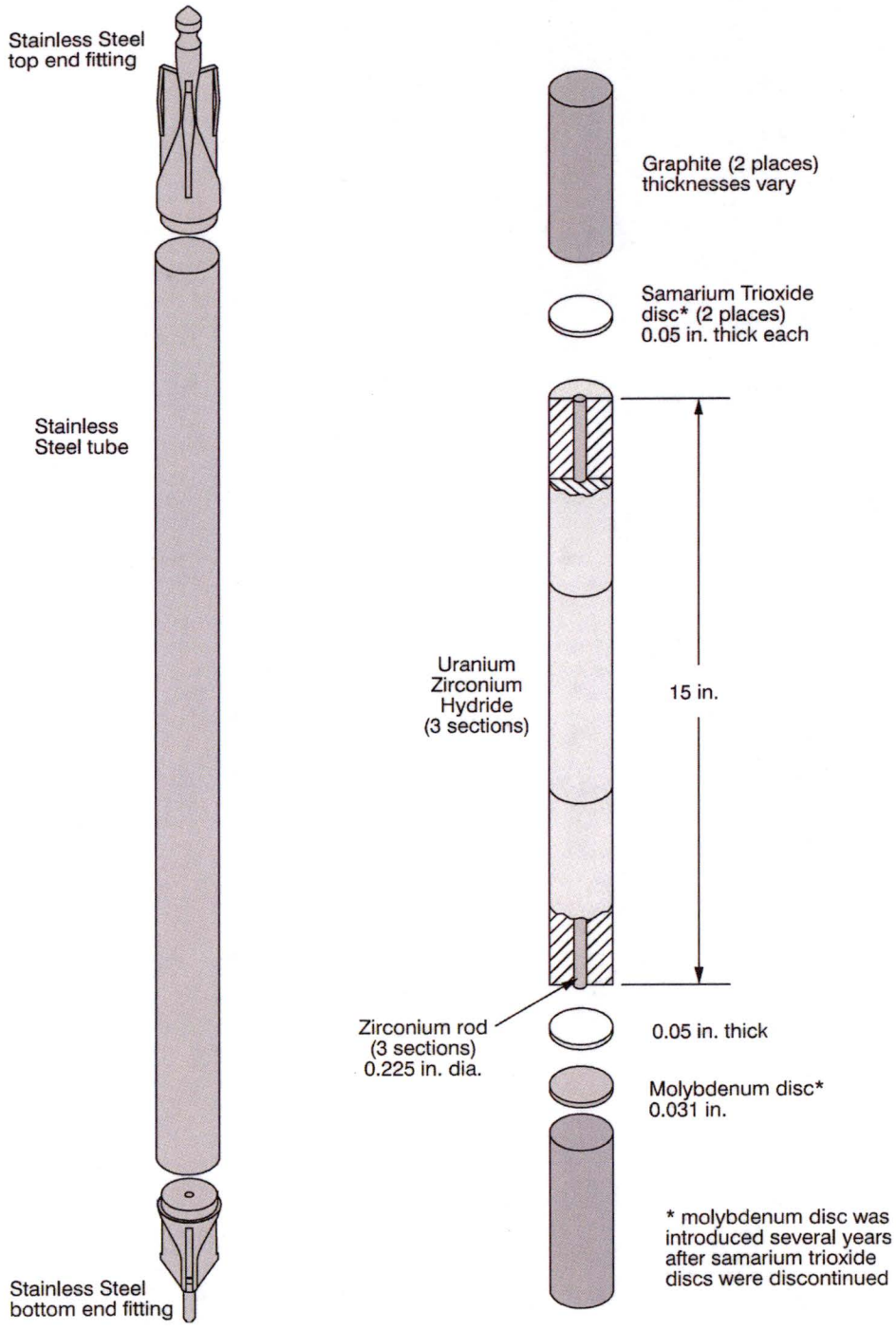

Figure 1.2-12 – TRIGA Fuel Element (Stainless Steel Clad)

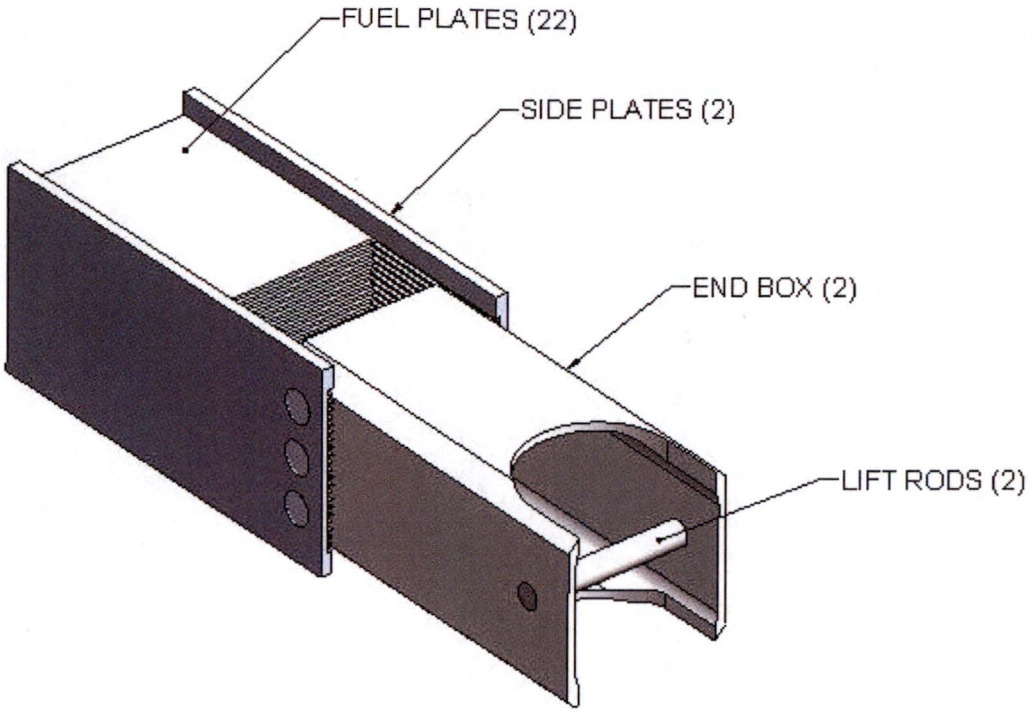

(Representative of Square or Rectangular, Swaged Plate Designs)

Figure 1.2-13 – Rhode Island Nuclear Science Center Fuel Element

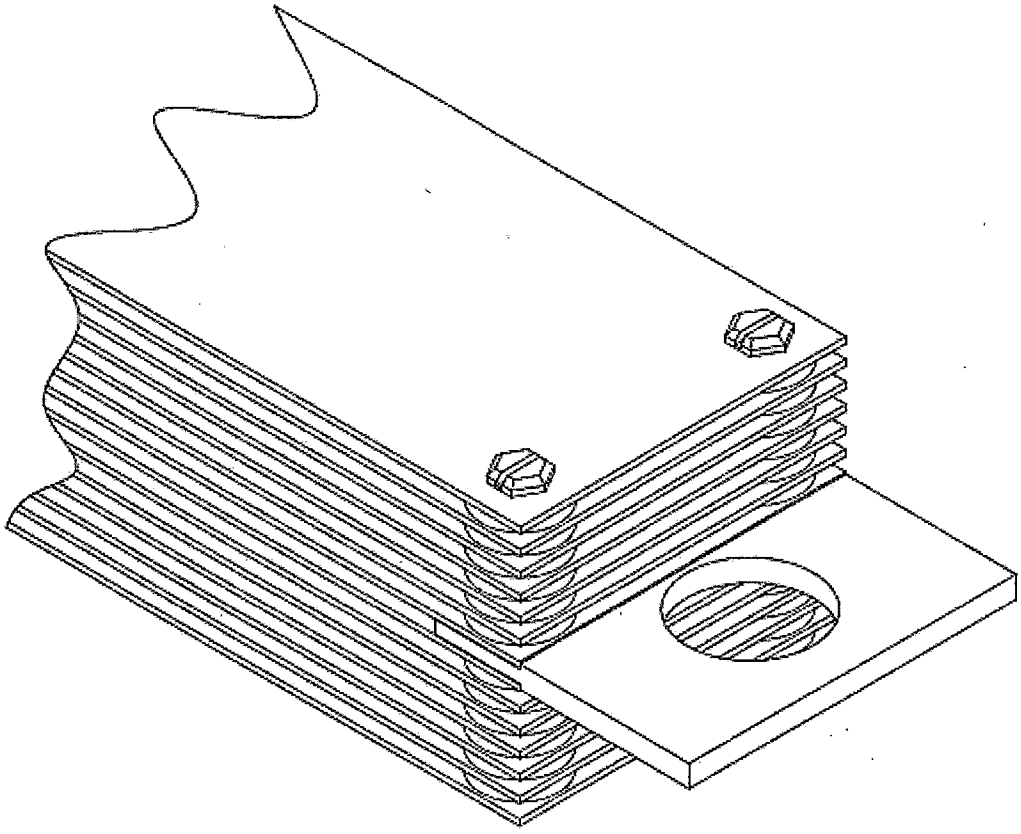

Figure 1.2-14 – University of Florida Fuel Element

Security-Related Information Figure Withheld Under 10 CFR 2.390.

Figure 1.2-15 – PULSTAR Fuel Element

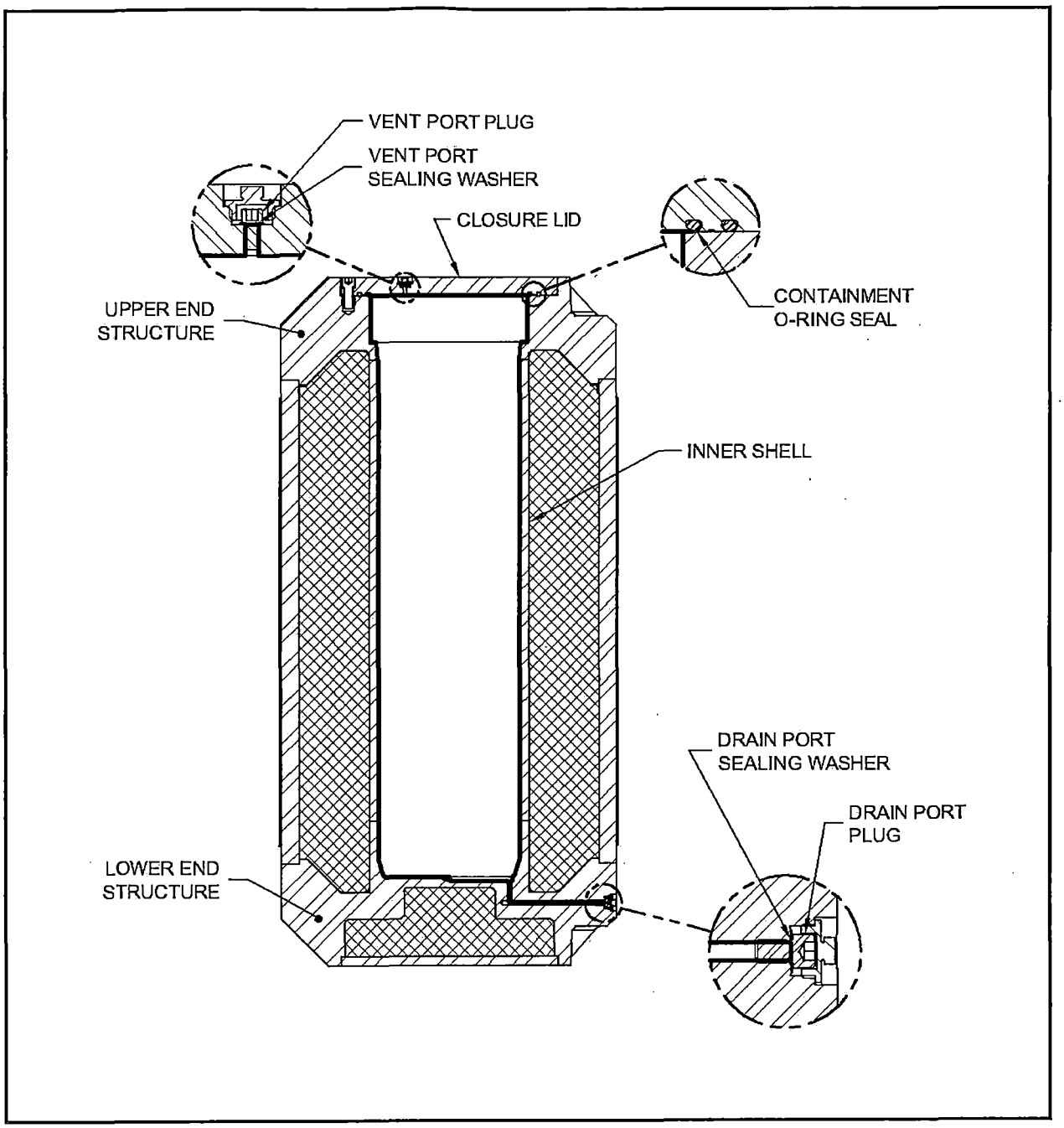

Figure 1.2-16 – BRR Package Containment Boundary

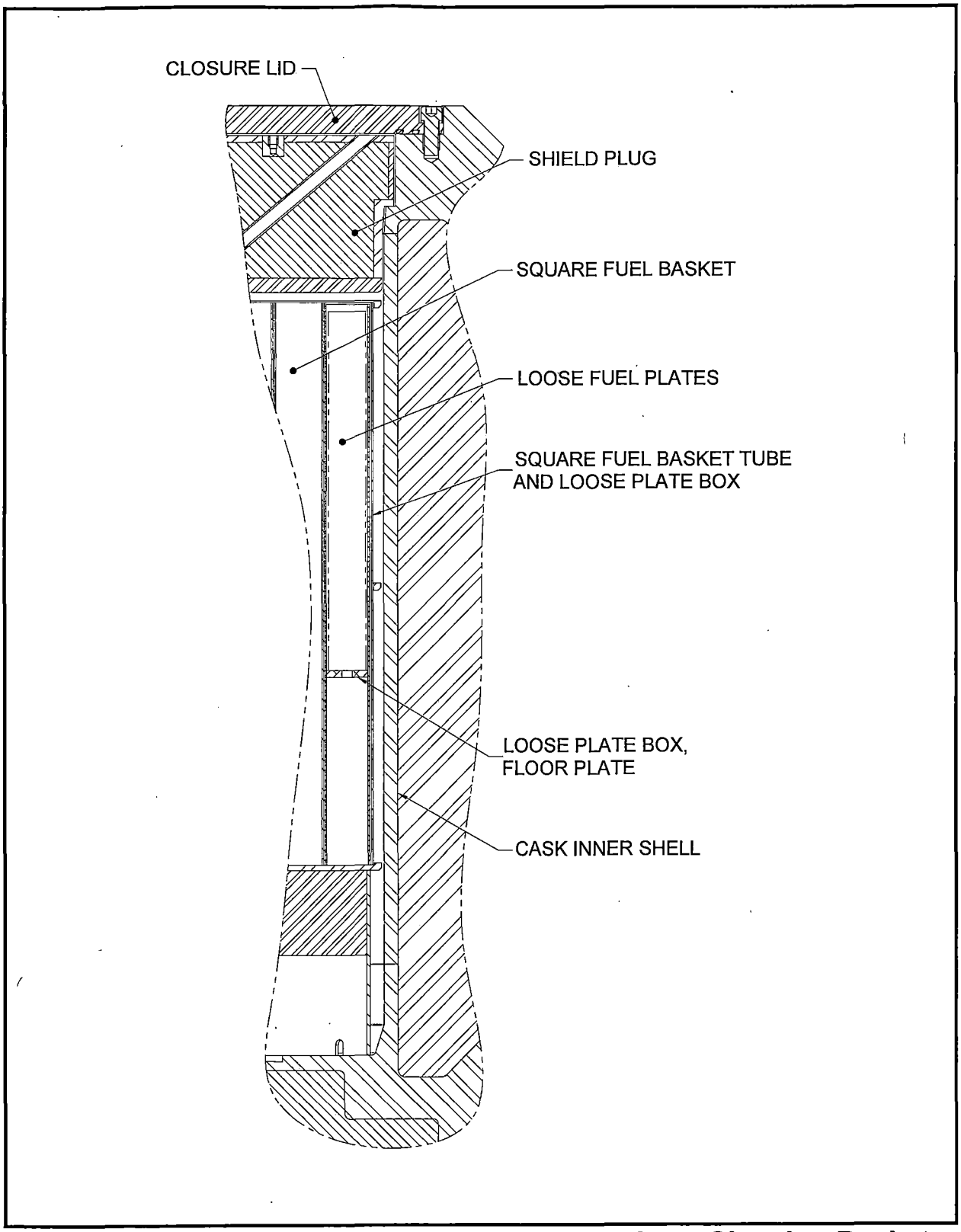

Figure 1.2-17 – Cross Section View of BRR Package Showing Basket, Loose Plate Box, and Loose Plates

2.7 Hypothetical Accident Conditions

When subjected to the hypothetical accident conditions (HAC) as specified in 10 CFR §71.73 [1], the BRR package meets the performance requirements specified in Subpart E of 10 CFR 71. This is demonstrated in the following subsections, where each accident condition is addressed and the cask shown to meet the applicable design criteria. The method of demonstration is primarily by analysis. The loads specified in 10 CFR §71.73 are applied sequentially, per Regulatory Guide 7.8 [3]. Resulting stresses are maintained below the limits established by Regulatory Guide 7.6 [2]. Dynamic testing of impact limiter performance is discussed in Section 2.12.3, *Certification Test Results*. A summary of cumulative damage is provided in Section 2.7.8, *Summary of Damage*.

2.7.1 Free Drop

Subpart F of 10 CFR 71 requires that a 30 ft free drop be considered. The free drop is to occur onto a flat, essentially unyielding, horizontal surface, and the cask is to strike the surface in an orientation for which maximum damage is expected. Several impact orientations and bounding ambient environments are considered. In order to minimize the number of specific analyses that must be performed, the worst case maximum cold drop impact loads are conservatively applied to the cask using material properties and allowables corresponding to maximum (warm) Normal Conditions of Transport (NCT) temperatures.

2.7.1.1 Impact Forces and Deformations

In Section 2.1.2.2, *Other Structures*, the design criteria of the impact limiters of the BRR Package includes the requirement to limit the free drop impact such that cask component stress and deflection criteria are met. The impact and deformation response of the impact limiters is evaluated and discussed in Appendix 2.12.5, *Impact Limiter Performance Evaluation.* This appendix also includes a comparison of the analysis results to the results obtained from the half-scale certification testing of the impact limiters. The tests are described in Appendix 2.12.2, *Certification Test Plan*, and in Appendix 2.12.3, *Certification Test Results*. The analysis results contributed to informing the choice of physical test orientations. The half-scale test impacts (tests D1, D2R, and D3) were all lower than predicted. The maximum predicted impact in full-scale is 86.8g for the secondary impact in the 15° oblique slapdown orientation. All of the calculations in this section utilize a bounding HAC impact of 120g, which is nearly 40% higher than the maximum result obtained from either test or analysis. Although no NCT tests were performed, the same conservative prediction techniques were used to set the bounding NCT impact at 40g, as described in Appendix 2.12.5, *Impact Limiter Performance Evaluation.*

The second design criterion of the impact limiters is to prevent "hard" contact of a rigid part of the cask with the ground due to excessive deformation of the foam. Since all of the certification testing was performed at the cold condition in order to obtain the maximum impact, the maximum crush deformation, which occurs at the maximum NCT hot temperature, could not be obtained directly from the testing. However, as the crush distances obtained from the half-scale test were found to be below the predicted cold case values, it is conservative not to adjust the predicted hot case crush distances downward. The maximum predicted hot case crush distance occurs in the 15° oblique secondary impact event, and amounts to 15.9 inches, or 83.2% of the available crush distance. Not only is the majority of the foam in the limiter at a lower value of

strain than this maximum value, the value is well within the range in which strain energy absorption is effective. The bounding bulk average foam temperature used for the analysis of 150 °F conservatively bounds the temperature predicted in the thermal analysis.

The final requirement is that the impact limiter structures and attachments to the cask maintain sufficient integrity subsequent to the HAC free drop and puncture drop events so that the containment O–ring seal is protected from excessive temperature in the subsequent HAC fire event. As documented in Appendix 2.12.3, *Certification Test Results*, while the original design did not meet this requirement, the final design of the attachment structures did meet it, as demonstrated by half-scale test. Section 2.7.1.7, *Impact Limiter Attachments*, shows that the final design is stronger than the successfully tested design. In addition, the worst–case damage to the impact limiter shells as a result of the puncture tests is fully accounted for in the thermal model, as discussed in Chapter 3, *Thermal Evaluation.*

For these reasons, the performance of the impact limiters is considered acceptable.

2.7.1.2 End Drop

The HAC end orientation free drop is evaluated using a combination of computer and manual calculations using an acceleration of 120g as discussed in Section 2.7.1.1, *Impact Forces and Deformations*. Stresses in the cask body are evaluated using the finite element model described in Appendix 2.12.4, *Stress Analysis Finite Element Models*. Both bottom down and top down impact orientations are considered. Including manual calculations, eight analyses of the HAC end drop are performed:

- Cask body stress
- Closure bolt stress
- Closure lid stress
- Lower closure plate weld stress
- Shield plug shell stress
- Buckling evaluation
- Lead slump evaluation
- Fuel basket stress is discussed in Section 2.7.1.5, *Basket Stress Analysis*.

Cask body stress. From Section 2.12.4.4.5, *Case No. 5, HAC Bottom-down End Drop*, the maximum stress intensity resulting from the bottom-down impact of 120g is 45,681 psi, located at the outside surface of the bottom end structure, as shown in Figure 2.12.4-10. The stress is linearized through the lower massive end structure cross section, Figure 2.12.4-11, and the maximum primary membrane stress is 22,680 psi. From Table 2.1-1, the limit on primary membrane stress is the lesser of $2.4S_m$ and $0.7S_u$, which for Type 304 cast or forged material (see Table 2.2-2) is $0.7S_u = 44{,}835$ psi at 250 °F. The margin of safety is:

$$MS = \frac{44{,}835}{22{,}680} - 1 = +0.98$$

The maximum membrane plus bending stress through the lower massive end structure cross section is 43,080 psi. The allowable membrane plus bending stress, from Table 2.1-1, is the

lesser of $3.6S_m$ or S_u, which for Type 304 cast or forged material is S_u = 64,050 psi at 250 °F. The margin of safety is:

$$MS = \frac{64{,}050}{43{,}080} - 1 = +0.49$$

From Section 2.12.4.4.8, *Case No. 8, HAC Top-down End Drop*, the maximum stress intensity resulting from the bottom-down impact of 120g is 40,140 psi, located at the top of the inner shell, as shown in Figure 2.12.4-15. The stress is linearized through the inner shell cross section, Figure 2.12.4-16, and the maximum primary membrane stress is 22,720 psi. From Table 2.1-1, the limit on primary membrane stress is the lesser of $2.4S_m$ and $0.7S_u$, which for Type 304 cast or forged material (see Table 2.2-2) is $0.7S_u$ = 44,835 psi at 250 °F. The margin of safety is:

$$MS = \frac{44{,}835}{22{,}720} - 1 = +0.97$$

The maximum membrane plus bending stress through the inner shell cross section is 33,400 psi. The allowable membrane plus bending stress, from Table 2.1-1, is the lesser of $3.6S_m$ or S_u, which for Type 304 cast or forged material is S_u = 64,050 psi at 250 °F. The margin of safety is:

$$MS = \frac{64{,}050}{33{,}400} - 1 = +0.92$$

As shown, all cask body margins of safety for the HAC end free drop condition are positive.

Closure bolt stress. In the top–down orientation, the non–prying closure bolt load is calculated according to Section 4.6 of [10] using:

$$Fa = \frac{1.34\sin(xi)(DLF)(ai)(Wl + Wc)}{Nb} = 28{,}140 \text{ lb}$$

where the impact angle, xi = 90° for the end drop impact, the dynamic load factor, DLF = 1.05 as discussed below, the impact magnitude, ai = 120g for the HAC impact, the weight of the lid, Wl = 280 lb, and the weight of the contents, Wc = 1,720 lb[1] from Table 2.1-2, and the quantity of bolts, Nb = 12. Note that no support for the lid is assumed from the inner surface of the impact limiter.

The sum of all applied loads (the HAC free drop load of 28,140 lb plus the load due to the design pressure, equal to 789 lb as determined in Section 2.6.1.5, *Closure Bolts*) is equal to 28,140 + 789 = 28,929 lb. This value exceeds the preload of 19,200 lb. The average tensile stress is:

$$Sba = 1.2732\frac{Fa}{Dba^2} = 47{,}779 \text{ psi}$$

where the value of Dba was computed as 0.878 inches in Section 2.6.1.5, *Closure Bolts*. From Table 2.1-1, the allowable average tensile stress intensity for HAC is the lesser of $0.7S_u$ or S_y, which for the ASTM A320 L43 bolting material is $0.7S_u$ = 87,500 psi at 250 °F. The margin of safety is:

$$MS = \frac{87{,}500}{47{,}779} - 1 = +0.83$$

[1] This weight consists of the shield plug plus the heaviest basket/fuel combination.

The dynamic load factor (DLF) used in this section and in Section 2.6.7.1, *NCT End Free Drop*, is calculated using NUREG/CR–3966 [26] (this quantity is called the DAF in that document). In Section 2.2.3 of [26], an estimated impact pulse duration is developed assuming a constant impact acceleration:

$$t_1 = \frac{Mv_o}{F_{max}}$$

This equation, however, underestimates the duration of a varying pulse such as a sinusoidal pulse, which is the closest shape to an actual, measured pulse. For a sinusoidal pulse, from Newton's Second Law:

$$F = Ma = MA\sin\omega t$$

The area under the pulse is the total change in velocity. Since the impact velocity is v_0, and the package comes to a complete stop during impact, the change in velocity is simply v_0. This can be written:

$$v_o = A\int_0^{\pi/\omega}\sin\omega t dt = -\frac{A}{\omega}\cos\omega t\Big|_0^{\pi/\omega} = \frac{2A}{\omega}$$

From this,

$$\omega = \frac{2A}{v_o}$$

Since the pseudo–frequency of the pulse is a full sine wave (two pulse lengths), the pulse length is equal to:

$$t_1 = \frac{T_1}{2} = \frac{1/f}{2} = \frac{2\pi/\omega}{2} = \frac{\pi}{\omega}$$

Substituting from above,

$$t_{1\text{-HAC}} = \frac{\pi v_o}{2A} = \frac{828.6}{A}$$

where v_0 is the impact speed for a 30–foot free drop of 527.5 in/s. Parameter A is the acceleration, in/s^2. For the bounding impact acceleration of 120g, equivalent to A = 46,368 in/s^2, the pulse length of the sinusoidal impact time history is $t_{1\text{-HAC}}$ = 0.018 s, which compares well with the duration of the end drop impact pulse accelerometer traces shown in Section 2.12.3.7, *Accelerometer Plots*.

For the NCT impact, the impact velocity for the two foot free drop is 136.2 in/s, and the bounding impact is 40g. The corresponding impact pulse length is:

$$t_{1\text{-NCT}} = \frac{\pi v_o}{2A} = 0.014\text{ s}$$

The frequency of the closure lid is found using [25], Table 36, Case 11a. The lowest mode frequency for a flat circular plate, assuming a simply supported edge, is found from:

$$f = \frac{K_n}{2\pi}\sqrt{\frac{Dg}{wr^4}} = 650\text{ Hz}$$

where $K_1 = 4.99$, $g = 386.4$ in/s^2, and the lid bolt radius, $r = 11.38$ inches. Since from Table 2.1-2, the weight of the lid, $W = 280$ lb and the area, $A_{lid} = \pi r^2 = 406.9$ in^2, the weight per unit area, $w = W/A_{lid} = 0.688$ psi. Parameter D is found from:

$$D = \frac{Et^3}{12(1-\upsilon^2)} = 20.0(10^6)\,\text{in} - \text{lb}$$

where $E = 27.3(10^6)$ psi for Type 304 steel at 250 °F, $\nu = 0.3$, and the thickness, $t = 2.0$ inches. The period of the lid is equal to 1/f, or $T = 1/650 = 0.00154$ s. The amplification factor for a half sine wave is given in Figure 2-15 of [26]. The abscissa of the figure is the ratio t_1/T. The smallest value of the ratio occurs in the NCT impact, where $t_{1\text{-NCT}} = 0.014$ s:

$$\frac{t_{1-\text{NCT}}}{T} = 9.09$$

This value exceeds the range shown in the figure. The corresponding ratio for HAC, where t_1 equals 0.018 s, is even larger. As the curve is clearly tending toward unity, it is concluded that the DLF may be conservatively bounded by a value of 1.05 for both NCT and HAC.

Closure lid stress. In the top–down drop orientation, the closure lid supports both the contents weight and its self–weight against the impact load of 120g. The lid is a solid, 2–inch thick plate made of Type 304 stainless steel. The outer diameter of the lid will be taken as the bolt circle, since that is the location of the step (see Section 2.6.1.5, *Closure Bolts*, for a discussion of the lid step). The bolt circle diameter is 22.75 inches. The self–weight of the lid is 280 lb, and the maximum contents weight is 1,720 lb (including the shield plug and the maximum basket/fuel weight), from Table 2.1-2. The total weight is 1,720 + 280 = 2,000 lb. For an impact of 120g, the total force applied to the lid is 2,000 × 120 = 240,000 lb. From above, the area of the lid, $A_{lid} = 406.9$ in^2.

The lid will be considered as uniformly loaded. This is somewhat conservative, since the shield plug is very stiff, and will consequently shift some of the load toward the edges of the lid, lessening the bending stress. In addition, the internal design pressure is 25 psig. The uniform load is:

$$q = \frac{240{,}000}{A_{lid}} + 25 = 614.8\ \text{psi}$$

From [25], Table 24, Case 10a for a simply supported, uniformly loaded plate, the bending moment is:

$$M = \frac{qa^2(3+\upsilon)}{16}\text{DLF} = 17{,}243\ \text{in} - \text{lb/in}$$

where the radius, $a = 22.75/2 = 11.38$ inches, $\nu = 0.3$, and the dynamic load factor, DLF = 1.05 as discussed above. The stress is:

$$\sigma = \frac{6M}{t^2} = 25{,}865\ \text{psi}$$

where the plate thickness, $t = 2.0$ inches. The allowable membrane plus bending stress, from Table 2.1-1, is the lesser of $3.6S_m$ or S_u, which, from Table 2.2-1, is equal to 68,600 psi for ASTM A240, Type 304 at 250 °F. The margin of safety is:

$$MS = \frac{68{,}600}{25{,}865} - 1 = +1.65$$

Thus, the allowable stress is satisfied for the closure lid in the HAC end drop.

As noted in Section 2.1.2.1, *Containment and Criticality Control Structures*, a stress intensity in the cask closure region (such as the closure lid) which could affect compression of the containment O-ring seal is limited to the lesser of the Table 2.1-1 allowable, or the yield strength. For ASTM A240, Type 304 at 250 °F, the yield strength from Table 2.6-1 is 23,700 psi. The calculated value of stress exceeds the yield stress by approximately 5%. However, as noted above, the calculation is conservative, and the impact magnitude of 120g is very conservative. As found in Table 2.12.5-11, the actual calculated end drop impact is 74.4g, which bounds an even lower actual impact recorded in the certification testing. Therefore it is evident that the actual stress in the closure lid is well below the yield stress of the lid material.

Lower closure plate weld stress. In the bottom–down drop orientation, the lower closure plate supports both the lower lead shield hydrostatic pressure and its self–weight against the impact load of 120g. The closure plate is a solid, 1–inch thick plate made of Type 304 stainless steel. The outer diameter of the plate is d = 24.5 inches and connected by a full penetration weld to the adjacent massive end structure. The area of the closure plate is:

$$A_{cp} = \frac{\pi}{4} d^2 = 471.4 \text{ in}^2$$

The self–weight of the closure plate is:

$$W_{cp} = A_{cp} \rho_{ss} = 136.7 \text{ lb}$$

where the density of steel is $\rho_{ss} = 0.29$ lb/in^3. The weight of the lower lead is modeled as two separate hydrostatic loads based the inner and outer lead depths above the upper surface of the closure plate (see Section 2.12.4.2.2, *Free Drop Impact Loads*). The maximum hydrostatic pressure will be conservatively applied to the entire plate. The hydrostatic force is:

$$F = \rho \cdot h \cdot A_{cp} = 1{,}488.2 \text{ lb}$$

where the maximum depth of the lead column, h = 7.7 inches and the density of lead is 0.41. The total weight is 1,488.2 lb + 136.7 lb = 1,624.9 lb. For an impact of 120g, the total force applied to the closure plate is 1,624.9 × 120 = 194,988 lb.

Conservatively the closure plate will be considered as uniformly loaded. The uniform load is:

$$q = \frac{194{,}988}{A_{cp}} = 413.6 \text{ psi}$$

From [25], Table 24, Case 10b for a fixed edge, uniformly loaded plate, the maximum bending moment at the edge of the plate is:

$$M = \frac{qa^2}{8} DLF = 8{,}146 \text{ in} - \text{lb/in}$$

where the radius, a = 24.5/2 = 12.25 inches and the dynamic load factor, DLF = 1.05 as discussed above. The stress is:

$$\sigma = \frac{6M}{t^2} = 48{,}876 \text{ psi}$$

where the plate thickness, t = 1.0 inches. The shear stress at the fixed end of the closure plate is:

$$\tau = \frac{194{,}988}{24.5\pi t} \text{DLF} = 2{,}660 \text{ psi}$$

The maximum stress intensity is determined by combining the component stresses using Mohr's circle as follows:

$$\text{SI} = \sqrt{\sigma^2 + 4\tau^2} = 49{,}165 \text{ psi}$$

The allowable membrane plus bending stress found above is equal to 68,600 psi for ASTM A240, Type 304 at 250 °F. The margin of safety is:

$$\text{MS} = \frac{68{,}600}{49{,}165} - 1 = +0.40$$

Thus, the allowable stress is satisfied for the closure plate in the HAC end drop.

Shield plug shell stress. In a bottom–down end drop, the shield plug lead will be supported by the lower plate of the shield plug shell. The one–inch thick plate is 15.8 inches in diameter and connected by a complete joint penetration weld to the adjacent cylindrical shell. The weight of the lead in the shield plug, plus the self–weight of the lower steel plate, will be conservatively bounded by utilizing the weight of the full shield plug, from Table 2.1-2, of 950 lb. To simplify the calculation, the lead will be treated very conservatively as a liquid. The entire weight of 950 lb will therefore be applied as a pressure to the plate inner surface.

The area of the plate is:

$$A_p = \frac{\pi}{4} 15.8^2 = 196.1 \text{ in}^2$$

For the end drop impact of 120g, the total loading per unit area of the plate is:

$$q = \frac{950 \times 120}{A_p} = 581.3 \text{ psi}$$

It will be further conservatively assumed that the plate has a simply supported edge. From [25], Table 24, Case 10a, the maximum moment at the center of the plate is:

$$M_c = \frac{qa^2(3+\upsilon)}{16} \text{DLF} = 7{,}856.7 \text{ in} - \text{lb/in}$$

where the plate radius, a = 15.8/2 = 7.9 inches and the DLF is defined as equal to 1.05 above. The maximum stress is:

$$\sigma_c = \frac{6M_c}{t^2} = 47{,}140 \text{ psi}$$

where the thickness, t = 1 inch. The allowable membrane plus bending stress found above is equal to 68,600 psi for ASTM A240, Type 304 at 250 °F. The margin of safety is:

$$MS = \frac{68{,}600}{47{,}140} - 1 = +0.46$$

The side wall and weld are checked by establishing moment equilibrium between the bottom plate and cylindrical shell, solving for the common moment, and calculating the stress. The direct tension stress is also added.

The slope at the outer edge of the bottom plate is the sum of the slope of a simply supported plate with a pressure load q, and the slope from a restoring moment, M_o, applied in the opposite direction by the cylindrical shell. The pressure load causes the plate to deflect downward, and the moment causes it to deflect upward. The slope due to the pressure load, θ_d (see [25], Table 24, Case 10a) is:

$$\theta_d = \frac{qa^3}{8D_p(1+\upsilon)}$$

The slope due to the moment load (see [25], Table 24, Case 13a, for $r_o = a$) is:

$$\theta_m = K_\theta \frac{M_o a}{D_p}$$

The parameter D_p is:

$$D_p = \frac{Et_p^3}{12(1-\upsilon^2)} = 2.5(10^6)\,\text{in} - \text{lb}$$

where $E = 27.3(10^6)$ psi, $\nu = 0.3$, and the plate thickness, $t_p = 1.0$ inches. The sum of these two slopes is:

$$\theta_d + \theta_m = 0.0098 - 2.338(10^{-6})M_o$$

where the lead hydrostatic pressure, $q = 581.3$ psi, the radius to the meridion of the cylindrical shell, $a = 7.6$ inches, and $K_\theta = -0.76923$.

The corresponding slope of a cylindrical shell under the action of an end moment is found from [25], Table 29, Case 3, as:

$$\theta_w = \frac{M_o}{D_w \lambda}\frac{C_{12}}{C_{11}}$$

Note that the notation for the slope has substituted θ for ψ for consistency. In addition, the sign value of the slope has been redefined to be opposite to that given in the introduction to Table 29 [25], thus, the negative sign has been omitted from the equation. The parameter λ is:

$$\lambda = \left[\frac{3(1-\upsilon^2)}{R^2 t_w^2}\right]^{1/4} = 0.602$$

where $R = a = 7.6$ inches, and the thickness of the cylindrical wall, $t_w = 0.6$ inches. The parameter D_w is:

$$D_w = \frac{Et_w^3}{12(1-\upsilon^2)} = 5.4(10^5)\,\text{in} - \text{lb}$$

Since the length of the lower cylindrical shell is L = 5 inches, the parameter λL is 3.01 inches. Parameters C_{12} and C_{11} are essentially identical, so their ratio is unity. The slope of the shell can now be evaluated as:

$$\theta_w = \frac{M_o}{D_w \lambda}\frac{C_{12}}{C_{11}} = 3.076\left(10^{-6}\right)M_o$$

Setting $\theta_w = \theta_d + \theta_m$,

$$3.076\left(10^{-6}\right)M_o = 0.0098 - 2.338\left(10^{-6}\right)M_o$$

Solving, M_o = 1,810.1 in–lb/in. The stress in the cylindrical shell is:

$$\sigma_m = \frac{6M_o}{t_w^2}\text{DLF} = 31{,}677 \text{ psi}$$

To this stress, the direct tension stress is added. The area of the weld to the cylindrical shell is:

$$A_s = \frac{\pi}{4}\left(OD^2 - ID^2\right) = 28.65 \text{ in}^2$$

where the shell outer diameter, OD = 15.8 inches and the inner diameter, ID = 14.6 inches. The direct stress is therefore:

$$\sigma_D = \frac{950 \times 120}{A_s}\text{DLF} = 4{,}178 \text{ psi}$$

The stress sum in the weld is:

$$\sigma_{Sum} = \sigma_m + \sigma_D = 35{,}855 \text{ psi}$$

For a full penetration weld, the allowable stress is the same as determined above. The margin of safety is:

$$MS = \frac{68{,}600}{35{,}855} - 1 = +0.91$$

Thus, the allowable stress is satisfied for the shield plug lower plate stress and lower plate weld stress in the HAC end drop.

Buckling evaluation. In the end drop orientation, the outer shell will carry most of the axial loads due to its much greater stiffness compared to the inner shell. Therefore, end drop buckling analysis may be conservatively performed by considering only the outer shell. The outer shell, which is cooler than the inner shell, is subject to tensile thermal stress, but for the buckling evaluation, the thermal stress on the outer shell is conservatively neglected. Since the inner shell is neglected, lead shrinkage pressure, which only affects the inner shell, is not considered. The maximum cold HAC impact of 120g is conservatively applied along with the bounding hot temperature case of 250 °F.

The only applied stress is axial, and assumes a bottom–down end drop configuration, for which the weight supported by the outer shell is larger than for the top–down case. The total weight supported by the outer shell is the sum of the total cask body (25,400 lb), less the side lead and bottom lead (see below), the closure lid (280 lb), the shield plug (950 lb), and the upper impact limiter (2,300 lb). Weight values are taken from Table 2.1-2.

The weights for the side and bottom lead are calculated using a lead density of 0.41 lb/in^3. The side lead has an outer diameter of 34.0 inches (outer shell ID), an inner diameter of 18.0 inches

(inner shell OD), and a lower–bound length (cylindrical length only) of 55.0 inches. The conservatively underestimated weight of the side lead is:

$$W_{PbS} = \frac{\pi}{4}\left(34.0^2 - 18.0^2\right)(55.0)(0.41) = 14{,}735 \text{ lb}$$

The bottom lead has a large diameter of 23.7 inches and a length of 4.2 inches, and a small diameter of 10.3 inches and a length of 3.5 inches. The weight of the bottom lead is:

$$W_{PbB} = \frac{\pi}{4}\left[\left(23.7^2\right)(4.2) + \left(10.3^2\right)(3.5)\right](0.41) = 879 \text{ lb}$$

Conservatively, the bottom lead weight will be underestimated by 100 lb, so that W_{PbB} = 779 lb. The total weight supported by the outer shell is therefore:

$$W_{tot} = 25{,}400 - 14{,}735 - 779 + 280 + 950 + 2{,}300 = 13{,}416 \text{ lb}$$

The weight used is conservative, since it underestimates the removed weight of the side lead and bottom lead, and includes the lower end structure as part of the cask body weight, even though it is not supported by the outer shell. The cross sectional area of the outer shell is:

$$A_{OS} = \frac{\pi}{4}\left(38.0^2 - 34.0^2\right) = 226.2 \text{ in}^2$$

The axial stress is:

$$\sigma_\phi = \frac{W_{tot}}{A_{OS}}(120) = 7{,}117 \text{ psi}$$

No other stresses are applied in the end drop. Shell dimensions are taken from Table 2.7-1. The factor of safety is equal to 1.34, consistent with Code Case N–284–2 for HAC. The results are shown in Table 2.7-2. As shown, all interaction parameters, including the maximum value of 0.4024 are less than unity, as required. Therefore, buckling of the cask shells in the HAC free drop will not occur.

Lead Slump. In the end drop, impact forces act on the lead gamma shield which could cause a reconfiguration of the lead in the direction of impact. As shown in the evaluation of the cask body stress above, the steel shells which enclose the lead will not significantly deform, but the lead could experience flow strains causing a gap to appear at the upper surface of the lead. In the following analysis, the lead is conservatively treated as a fluid, having no resistance to flow from impact forces. The lead will therefore occupy the lower portion of the volume available within the lead cavity. The difference between the cavity volume and the lead volume defines the maximum possible gap at the top of the lead. Of note, since the shield plug and bottom lead shield are installed manually, using small scraps and lead wool hammered into place to fill all cavities, lead slump cannot occur. The following analysis applies only to the side cavity in which lead is poured in the molten state.

The amount of lead installed in the side cavity of the BRR cask body is assumed to correspond to the volume of the cavity at the point of solidification of the lead of 620 °F. At this point, there is no difference between the volume of the cavity and the volume of the lead. As the cask cools to the minimum HAC temperature of -20 °F, the lead will shrink more than the cavity due to the greater thermal expansion coefficient of lead than steel, generating a volume difference. Assuming the lead behaves as a fluid in the end drop concentrates this volume difference at one

end or the other of the cask cavity, which constitutes the lead slump gap. This gap is further evaluated in Chapter 5, *Shielding Evaluation.*

To simplify calculations, the side lead shield is assumed to have a fully rectangular cross section, i.e., the lead cavity is assumed to have square corners at the full length. This simplification does not have a significant affect on the calculation. The lead cavity at the assumed fabrication temperature of 70 °F has an inner diameter of 18 inches (the inner shell OD), an outer diameter of 34 inches (the outer shell ID), and a length of 60.9 inches. The volume therefore is:

$$V_{CAV-RT} = \frac{\pi}{4}\left(34^2 - 18^2\right)60.9 = 39{,}795 \text{ in}^3$$

It will be convenient to define a volumetric expansion relation. Note that, for a general case:

$$V_C = L_C^3$$

$$L_H = L_C(1 + \alpha\Delta T)$$

where V_C and L_C are the original (cold state) volume and length, respectively, L_H is the expanded (hot) length, and α and ΔT are the thermal expansion coefficient and the change in temperature, respectively. Since the expanded (hot) volume is:

$$V_H = L_H^3 = L_C^3(1 + \alpha\Delta T)^3,$$

Then:

$$V_H = V_C(1 + \alpha\Delta T)^3$$

From Table 2.2-4, the thermal expansion coefficient of steel between 70 °F and 620 °F is α_{s620} = 9.84(10^{-6})in/in/°F. The lead cavity and lead volumes at the lead solidification temperature are then:

$$V_{CAV620} = V_{L620} = V_{CAV-RT}(1 + \alpha_{s620}\Delta T_{70-620})^3 = 40{,}445 \text{ in}^3$$

Next, calculate the volume of the lead at 70 °F and at -20 °F. This must be done in two steps because the thermal expansion coefficients are referenced to 70 °F. The thermal expansion of lead between 620 °F and 70 °F is α_{L620} = 20.4(10^{-6})in/in/°F, and between 70 °F and -20 °F is $\alpha_{L\text{-}20}$ = 15.7(10^{-6})in/in/°F, as shown in Table 2.2-4.

$$V_{L-RT} = V_{L620}(1 - \alpha_{L620}\Delta T_{620-70})^3 = 39{,}099 \text{ in}^3$$

$$V_{L-20} = V_{L-RT}(1 - \alpha_{L-20}\Delta T_{70--20})^3 = 38{,}933 \text{ in}^3$$

The volume of the cavity at -20 °F, utilizing the thermal expansion coefficient between 70 °F and -20 °F of $\alpha_{s\text{-}20}$ = 8.2(10^{-6})in/in/°F, is:

$$V_{CAV-20} = V_{CAV-RT}(1 - \alpha_{s-20}\Delta T_{70--20})^3 = 39{,}707 \text{ in}^3$$

The difference in volume between the cavity and the lead at the HAC free drop temperature of -20 °F is:

$$\Delta V_{-20} = V_{CAV-20} - V_{L-20} = 774 \text{ in}^3$$

The volume of the cavity per inch of length is:

$$\Delta V_{/in} = \frac{\pi}{4}\left(34^2 - 18^2\right) = 653 \text{ in}^3/\text{in}$$

The lead slump dimension (the gap between the top of the lead cavity and the top of the lead) therefore has a bounding value of:

$$x_{slump} = \frac{\Delta V_{-20}}{\Delta V_{/in}} = 1.185 \text{ in}$$

This value is conservative since it takes no credit for any resistance to flow of the lead material. The effect of this gap is evaluated in Chapter 5, *Shielding Evaluation.*

2.7.1.3 Side Drop

The HAC side orientation free drop is evaluated using the finite element model described in Appendix 2.12.4, *Stress Analysis Finite Element Models*, and an acceleration of 120g as discussed in Section 2.7.1.1, *Impact Forces and Deformations.*

From Section 2.12.4.4.11, *Case No. 11, HAC Side Drop*, the maximum stress intensity resulting from the side drop impact of 120g is located at the bottom outside edge of the lower lead cavity as shown in Figure 2.12.4-21. The stress is linearized through the lower closure plate cross section, Figure 2.12.4-22, and the maximum primary membrane stress is 16,330 psi. From Table 2.1-1, the limit on primary membrane stress is the lesser of $2.4S_m$ and $0.7S_u$, which for Type 304 cast or forged material is $0.7S_u$ = 44,835 psi at 250 °F. The margin of safety is:

$$MS = \frac{44{,}835}{16{,}330} - 1 = +1.75$$

The maximum membrane plus bending stress resulting through the lower closure plate cross section is 51,990 psi. The allowable membrane plus bending stress, from Table 2.1-1, is the lesser of $3.6S_m$ or S_u, which for Type 304 cast or forged material is S_u = 64,050 psi at 250 °F. The margin of safety is:

$$MS = \frac{64{,}050}{51{,}990} - 1 = +0.23$$

As shown, all cask body margins of safety for the HAC side drop condition are positive.

2.7.1.4 Oblique Drop

For the HAC free drop, the BRR package can strike the ground in any primary orientation. As shown in the following discussion, the cask stresses for all oblique drop orientations are conservatively bounded by the side drop (horizontal) orientation when performed using an impact of 120g. This evaluation is based on the axial, shear, and moment forces in the cask shells as derived in NUREG/CR–3966 [26]. It is shown that, for the specific impact forces developed in the HAC oblique free drops, the cask shell stress intensity is governed by the side drop case.

In Section 2.2 of [26], the maximum axial force, R, shear force, V, and bending moment, M, in the cask shells are given for the primary oblique impact as:

$$R_p = F_p \sin(\theta)$$

$$V_p = F_p \cos(\theta)$$

$$M_p = (4/27)\, F_p L \cos(\theta)$$

where the subscript p indicates the primary impact event, L is the overall length of the cask, θ is the primary impact angle with respect to the horizontal, and F_p is the maximum primary impact limiter force. For the subsequent secondary (slapdown) impact, the maximum values of the above parameters are:

$$R_s = 0$$

$$V_s = F_s$$

$$M_s = (4/27)\, F_s L$$

where the subscript s indicates the secondary impact event, and F_s is the maximum secondary impact limiter force. In the horizontal side drop impact, the maximum values of the above parameters are:

$$R_h = 0$$

$$V_h = F_h$$

$$M_h = (1/4)\, F_h L$$

where the subscript h indicates the horizontal case, and F_h is the maximum impact limiter force in the side drop. The cask shell stresses resulting from these applied forces and moments can be calculated as follows:

$$\sigma_a = \frac{R_i}{A}$$

$$\tau = \frac{V_i}{A}$$

$$\sigma_b = \frac{M_i c}{I}$$

where σ_a is the axial stress, τ the shear stress, and σ_b the bending stress in the cask shells, and where A is the cross sectional area of the cask shells, and I is the moment of inertia. The maximum stress intensity in the cask shells is determined by combining the component stresses using Mohr's circle as follows:

$$SI = \frac{\sigma_a + \sigma_b}{2} \pm \sqrt{\left(\frac{\sigma_a + \sigma_b}{2}\right)^2 + \tau^2}$$

For purposes of comparison, it is only necessary to consider one shell, for example, the inner shell. The cross sectional area of the inner shell is

$$A = (\pi/4)\left(d_o^2 - d_i^2\right) = 53.4 \text{ in}^2$$

and the moment of inertia is

$$I = (\pi/64)\left(d_o^4 - d_i^4\right) = 1{,}936 \text{ in}^4$$

where d_o = 18.0 inches and d_i = 16.0 inches. The parameter c = 18.0/2 = 9.0 inches, and the length between the center of the cylindrical portion of each impact limiter is L = 70 inches.

The maximum force on each impact limiter in the HAC 30 ft, horizontal side drop for the bounding impact value of g_h = 120g and an overall cask weight of W = 32,000 lb is:

$$F_h = \frac{Wg_h}{2} = 1.920(10^6)\,lb$$

The worst case oblique free drop is the shallow–angle side slapdown orientation at a primary impact angle of 15°, as discussed in Appendix 2.12.5, *Impact Limiter Performance Evaluation.* The primary and secondary impact limiter forces are found using the calculated maximum deformation at cold conditions and the force-deflection curves corresponding to the impact orientation. From Table 2.12.5-11, the maximum primary deformation for the 15° impact case is 10.7 inches, and from Table 2.12.5-12, the maximum secondary deformation is 12.1 inches. From Figure 2.12.5-4 (primary impact at 15°), the maximum crush force at the primary deformation of 10.7 inches is bounded by a value of 1,049,000 lb, and from Figure 2.12.5-3 (secondary impact, taken at 0°), the maximum crush force at the secondary deformation of 12.1 inches is bounded by a value of 1,220,000 lb.

The resulting cask shell forces and maximum combined stress intensities are shown in Table 2.7-3. Since only the inner shell properties are used, the stress intensity is relative, and is used for comparison between the different cases only. The stress values in the table therefore do not represent actual inner shell stress intensity. As shown, the stress intensity is greatest in the horizontal side drop case at the bounding value of 120g. Since, according to Section 2.7.1.1, *Impact Forces and Deformations*, the actual impacts are lower than the calculated values, the difference between the actual loading in the oblique impacts and the bounding side drop is even greater. Therefore, the side drop stress analyses, detailed in Section 2.7.1.3, *Side Drop*, are enveloping for all oblique drop orientations.

2.7.1.5 Fuel Basket Stress Analysis

Each of the five fuel baskets and the loose plate box is evaluated for structural integrity in the governing free drop orientations of end and side. The maximum cold impact acceleration of 120g is used, but conservatively the material allowable stresses are evaluated at the maximum NCT temperature of 400 °F. Allowable stresses are taken from Table 2.1-1. Each basket is analyzed for several modes of failure which are applicable to its design, including bending, weld shear, and buckling. Bounding weights for the baskets and fuel are given in Table 2.1-3.

The smallest margin of safety of any of these evaluations is +0.12, for the shear load on the TRIGA basket spacer pedestal screw. All of the evaluations and corresponding margins of safety are summarized in Table 2.7-4. The analysis details are provided in Appendix 2.12.8, *Fuel Basket Stress Analysis*. Therefore, the BRR package fuel baskets are adequate to support the fuel in all HAC free drops.

In the HAC side drop impact orientation, the fuel baskets apply a load to the inside of the inner shell. The heaviest basket is for MURR fuel, but this basket has no ribs and the load is well distributed. The next-heaviest basket, for ATR fuel (650 lb), has four ribs. The top rib is a 0.5-inch thick plate with a 0.19-inch chamfer, for a land width of 0.31 inches. The middle two ribs are made from 0.38-inch thick plate with 0.19-inch chamfers, for a land width of 0.19 inches each. The lowest rib is made from 0.50-inch thick plate with a 0.13-inch step and a 0.19-inch chamfer, for a land width of 0.18 inches. The diameter of each rib is 15.63 inches. The projected bearing area of the ribs against the inner shell is:

$$A = 15.63(0.31 + 0.19 + 0.19 + 0.18) = 13.60\,in^2$$

The side load, using the bounding side drop impact of 120g, is:

$$P = 650(120) = 78{,}000 \text{ lb}$$

The bearing stress is:

$$\sigma = \frac{P}{A} = 5{,}735 \text{ psi}$$

The MITR-II basket, with a loaded weight of 640 lb, is nearly the same weight as the ATR. But, as in the case of the MURR basket, the weight of the basket is well distributed to the interior wall of the cask; primarily over the area of the massive weldment with the minor addition of the pedestal support ring.

The TRIGA and Square fuel baskets are lighter than the other three baskets and not bounding. At the bounding fuel basket temperature of 400 °F, the minimum yield strength of the inner shell material, from Table 2.2-2, is 20,700 psi. Since this stress is over three times larger than the bearing stress, bearing yield of the basket ribs or of the inner shell will not occur.

2.7.1.6 Fuel Impact Deformation

During the end drop, the fuel elements may experience a separate, internal impact with the cask or basket structures. This impact could occur if, during the period of package free fall, the fuel was in contact with the upper end of its cavity, which would be possible due to the zero–g environment of free fall. When the package strikes the ground, the velocity of the cask would begin to decrease, but the fuel would continue to fall freely until impact with the lower end occurred. When the gap between the fuel and the cask was traversed, the fuel would hit the cavity end. The fuel would have the full free drop velocity, v_o, but the cask cavity would be traveling in the same direction with a lower velocity. See Figure 2.7-1.

To simplify calculations, it will be conservatively assumed that, at the moment of impact with the fuel, the cask inner contact surface is motionless and unyielding. Further, it will be assumed that the deceleration of the package during the period of fuel traversing the gap is constant and equal to the maximum bounding deceleration of 120g. The fuel will therefore experience an equivalent free drop. This analysis will determine the magnitude of the free drop impact and determine the effect on the fuel elements.

At the moment of impact with the ground, both the cask and fuel have a velocity of v_o. The cask immediately begins to decelerate according to:

$$v(t) = at + v_o$$

The distance the cask travels until the moment of impact with the fuel is:

$$x_c = a\int_0^T t\,dt = \frac{1}{2}at^2 + v_o t\Big|_0^T = \frac{1}{2}aT^2 + v_o T$$

where T is the time of fuel impact, and $x_c = 0$ at $t = 0$ (the time of package impact). Note that during time T, the fuel has traveled the distance the cask has traveled, plus the initial gap between the fuel and cask. Alternately, it can be stated that the fuel has traveled $v_o T$, since its velocity is unchanged during this interval. Therefore:

$$x_c + GAP = v_o T, \quad \text{or}$$
$$x_c = v_o T - GAP$$

Substituting this into the formula for x_c above,

$$x_c = \frac{1}{2} a T^2 + v_o T = v_o T - GAP$$

Simplifying,

$$T = \left(\frac{-2GAP}{a} \right)^{1/2}$$

Since the difference in velocity between the fuel and the cask at time T is equal to the decay in velocity over the interval, equal to (aT), the difference can be written as:

$$\Delta v = aT = a\left(\frac{-2GAP}{a} \right)^{1/2} = (-2aGAP)^{1/2}$$

(Note that since the acceleration is negative (deceleration), the quantity under the square root will be positive.) The energy associated with a change in velocity, Δv, is equivalent to the energy of a free drop height, h. Since:

$$h = \frac{\Delta v^2}{2g_g}$$

then the equivalent free drop height of the fuel element in the BRR package impact is:

$$h = \bar{g} GAP$$

where g_g is the acceleration due to gravity, and the deceleration in g–units, $\bar{g} = a/g_g = 120g$. The energy to be dissipated during the impact of the fuel is equal to Wh, or:

$$E = W\bar{g}GAP$$

where W is the weight of a fuel element. If this energy is absorbed in the fuel structure by volumetric plastic flow, the energy absorbed is related to the volume of flow according to:

$$E = V\sigma_f$$

where σ_f is the flow stress of the material, equal to the average of the yield and ultimate tensile strengths. Solving this for the volume,

$$V = \frac{W\bar{g}GAP}{\sigma_f}$$

Since the material flow is assumed to occur on the fuel cross section, the deformation length is equal to the volume divided by the cross–sectional area of the fuel element, $L = V/A_{xc}$, or:

$$L = \frac{W\bar{g}GAP}{\sigma_f A_{xc}}$$

This formula will be evaluated for the bounding fuel case. The fuel is made from 6061–T6 aluminum material. From the ASME B&PV Code, Section II, Part D, Table Y–1, the yield strength at a temperature of 400 °F is equal to 13.3 ksi. Since this material does not appear in

Table U, an ultimate tensile strength at temperature is not readily available. Conservatively, the yield strength will be used for the flow strength as defined above. Therefore, σ_f = 13,300 psi.

The total gap value, GAP, consists of a) the free space between the fuel element and the basket cavity length, plus b) the difference between the cask cavity and the basket length. Parameter a), denoted as L_{FB}, is calculated by subtracting the fuel length from the basket cavity length, and is listed in Table 2.7-5. Parameter b) is found by subtracting the basket length (equal to 53.45 inches in all cases) from the cask cavity length of 54.0 inches, and is equal to 0.55 inches. The total fuel gap is therefore:

$$GAP = L_{FB} + 0.55$$

Due primarily to its larger gap and weight, the ATR fuel is the governing case. The maximum deformation length of any fuel element is therefore:

$$L = \left(\frac{W}{A_{xc}}\right)\frac{\bar{g}GAP}{\sigma_f} = 0.096 \text{ inches}$$

The fuel bounding weights, cross–sectional areas, and W/A_{xc} ratios are presented in Table 2.7-5. The bounding fuel weights are taken from Section 1.2.2, *Contents*. The areas are calculated from CAD drawings of the fuel active region cross section, and do not consider the end structures. The end structures are considered sacrificial since a) they do not contain any fissile material and b) the criticality analysis discussed in Section 6.3.1 does not model the end structures, and determines the most reactive axial position of the active length of the fuel as if the end structures were absent. Since the fuel end structures do not serve a safety function, they are ignored in the axial deformation analysis.

This maximum deformation length, which is just below $1/10^{th}$ of an inch, is negligible from a structural, shielding, or criticality perspective. Therefore fuel behavior in the HAC end drop is acceptable.

2.7.1.7 Impact Limiter Attachments

As reported in Appendix 2.12.3, *Certification Test Results*, the initial design of the impact limiter attachments was not adequate, since they did not securely retain the primary impact limiter in the 15° oblique slapdown free drop impact. The redesigned attachments are shown in the drawings in Appendix 1.3.3, *Packaging General Arrangement Drawings*. One half-scale certification test limiter was refurbished, as far as possible, to incorporate the revised design and retested to confirm its adequacy. The attachment load path of the refurbished test article, when converted to full-scale, was conservatively less strong than the revised design, as shown by the comparison shown in Table 2.7-6. Note: in the table, the blade is the attachment component integral to the impact limiter, and the receptacle is the pair of plates, attached to the cask, that accept the blade.

As detailed in Section 2.12.3.6, *Confirmatory Test of Attachments*, the 15° oblique slapdown free drop was repeated, followed by a puncture test. The attachments that experienced the greatest loads from the puncture test were the same ones that experienced the greatest loads in the free drop test. The result was that the impact limiter was securely retained on the test cask. The only measurable change to the refurbished attachment hardware was a negligible elongation of one of the blade holes by 0.07 inches (full-scale). Other than that slight deformation, there were no signs of distress or impending failure in any other feature located in the attachment load path. Of note, no other free drop or puncture drop test orientation caused any significant damage to the

original, smaller design of the attachments. Therefore the impact limiter attachments are adequate to securely retain the impact limiter in the worst-case series of free drop and puncture events.

2.7.1.8 Fuel Impact Integrity

During the HAC impact, the fuel will experience forces which could affect their structural integrity. The following demonstration shows that all fuel, with the exception of U-Florida, retains its integrity following the governing impacts.

Plate Fuel

Plate fuels transported in the BRR package consist of MURR, MITR-II, ATR, RINSC, U-Mass, Ohio State, Missouri S&T, and Purdue. U-Florida plate fuel will be discussed separately. These fuel elements are represented in Figure 1.2-9, Figure 1.2-10, Figure 1.2-11, and Figure 1.2-13. As shown, the fuel elements include side plates (or "combs") which support the fuel plates along their long sides. The side plates extend for the full length of the fuel plates and are incorporated into end structures (at one or both ends), providing a rigid structure. The ATR fuel element was physically tested in the certification test of the ATR-FFSC package (NRC Docket 71-9329) without loss of structural integrity and with damage only to the element's end structures. The ATR-FFSC is a relatively light, rigid package without impact limiters, and thus the HAC free drop impact magnitude is much higher than that of the BRR package. For this reason, it may be concluded that the plate fuel elements will not lose structural integrity (i.e., remain a structural unit) in the governing HAC free drop. As discussed in [35], the corrosion sometimes found to be present on plate fuel elements after many years in storage is not structurally significant.

While the overall structural integrity of the plate fuels will not be affected by the HAC free drop, it is noted that in a side drop of the BRR package, the fuel plates could be loaded perpendicular to their plane. The stress generated in this scenario is well below the yield strength of the fuel plate cladding material, shown as follows. The discussion focuses on the governing flat plate.

To bound the behavior of all plates, the thickest plate from Table 5.2-10 (0.06 inches) will be loaded with the thickest and most dense meat (0.03 inches from Table 6.2-11 and 5.5 g/cm^3 from Table 6.2-12). The section properties, however, will be taken assuming the thinner plates from Table 5.2-10 (0.05 inches). The meat density is 5.5 g/cm^3 = 0.20 lb/in^3, and with a thickness of 0.03 inches, the mass of the meat in one square inch of plate is $m_m = 0.20 \times 0.03 = 0.006$ lb/in^2. The aluminum cladding (for mass purposes) is a total of 0.06 – 0.03 = 0.03 inches, having a mass per square inch of $m_c = 0.099 \times .03 = 0.003$ lb/in^2, where the density of aluminum is taken as 0.099 lb/in^3. The total weight per square inch is w = 0.009 lb/in^2. Since the fuel plates are supported along their long sides, their behavior can be modeled using a unit width beam, where the width dimension is parallel to the axis of the fuel element, and the length of the beam is the plate width, upper-bounded by the basket opening dimension of 3.4 inches. The uniform loading on the beam is the value of w = 0.009 lb/in, found above for one square inch of plate. Even though the fuel plates are typically swaged into the side plates, simple support at the comb side plate will be conservatively assumed. The section properties are based on the thinner fuel plates which are 0.05 inches thick, and conservatively neglecting the meat thickness of the thinner plates of 0.02 inches thick. The moment of inertia and the c-distance are:

$$I = \frac{1}{12}(0.05^3 - 0.02^3) = 9.75(10^{-6})\ in^3, c = \frac{0.05}{2} = 0.025\ in$$

For a bounding impact in the horizontal cask orientation of 120g, with a flat, horizontal fuel plate orientation, modeled as a simply supported beam L = 3.4 inches long, the moment and stress in the fuel plate are:

$$M = \frac{w(L^2)}{8}120 = 1.56\ in - lb,$$

$$\sigma = \frac{Mc}{I} = 4{,}000\ psi$$

From the ASME B&PV Code, Section II, Part D, Table Y-1, the yield strength of 6061 aluminum alloy at a temperature of 400 °F is 13,300 psi. The margin of safety on the permanent deformation of the plate fuel in the side drop is:

$$MS = \frac{13{,}300}{4{,}000} - 1 = +2.33$$

Thus, the fuel plates will not deform out-of-plane. Since the plates are restrained all along their length, they will furthermore not buckle from axial impact forces.

Loose plates in the loose plate box are not joined together, but the clearance between the loose plates and the box in a direction normal to the plane of the plates is limited to a maximum of ¼ inches per the procedure in Section 7.1.2.1, *Wet Loading*, and Section 7.1.2.1, *Dry Loading*. Since the loose fuel plates are closely confined in this way, any reconfiguration of the loose plates in the HAC impact event will be prevented. Note also that the axial stress in the aluminum cladding material is very low in the end drop impact. As shown above, the plates weigh no more than 0.009 lb/in^2. For bounding loose plate dimensions of 26 inches long and 3 inches wide, the weight of one plate is 26 × 3 × 0.009 = 0.7 lb, or a maximum of one pound. In a 120g end drop impact, the weight on the lower end of the plate is therefore bounded by 120 lb. As noted above, the non-fueled cladding thickness is 0.05 – 0.02 = 0.03 inches. The cross-sectional area, conservatively taking a plate width of only 2.5 inches is thus 0.03 × 2.5 = 0.075 in^2. The stress in the aluminum cladding in the end drop (where the impact load is parallel to the plane of the plates) is:

$$\sigma = \frac{120}{0.075} = 1{,}600\ psi$$

Since the same allowable applies from the previous stress analysis, the margin against yield of the loose plates is:

$$MS = \frac{13{,}300}{1{,}600} - 1 = +7.31$$

Since the loose plates are confined by the sides and bottom plate of the loose plate box and by the shield plug over the top of the box, the plates cannot come out of the box. Nor can the plates reconfigure within the box as just shown. A depiction of a partial cross section of the cask with the loose plate box and loose plate fuel is shown in Figure 1.2-17.

The U-Florida fuel element is different in that it does not have full length side plates, instead having a small number of discrete side combs. There are also small spacers made of aluminum, welded to the fuel plates near their center. Because the U-Florida fuel element lacks full side plates, both buckling and bending of the plates are possible in the HAC free drop impact. However, the four screws located at the four corners of the fuel element will not be subjected to

critical levels of tension or shear loading. This is because the U-Florida fuel element is confined by the square fuel basket tube and supported by a pedestal spacer on the bottom and the shield plug on the top. Thus, the fuel element will remain an integral unit. In addition, a solid spacer of 0.8-inch thickness will be used alongside the U-Florida element to reduce free space in the basket tube. But because the U-Florida fuel plates may not remain planar or equally spaced over their entire extent, the criticality safety evaluation of the U-Florida fuel assumes a worst-case plate spacing, as discussed in Section 6.4.1.2, *HAC Single Package Configuration.*

TRIGA Fuel

TRIGA fuel elements are loaded into the tubes of the TRIGA fuel basket, which are 1.76 inches inner diameter. As such, the maximum clearance to the minimum diameter TRIGA fuel element of 1.35 inches is 0.41 inches. Thus, the TRIGA fuel basket prevents buckling or lateral deformation in TRIGA fuel during the HAC free drop impact.

PULSTAR Fuel

PULSTAR fuel elements consist of an array of 25 fuel rods having a configuration very similar to commercial nuclear fuel, but only approximately 26 inches long. The fuel element is supported along its entire length in the square fuel basket. The rods are held in position at each end by thick aluminum spacer plates, and at three locations along their length, the rods are separated by orthogonally located tabs, attached to the cladding OD. The array is surrounded by a 0.06-inch thick, Zr-2 alloy outer box. All of the rods are in nominal contact with each other and with the outer box by means of the tabs. The tabs support the rods in all directions and thus, the maximum free length of any rod is equal to the maximum axial distance between the tabs, equal to L = 6.37 inches. Both bending and buckling in this span will be checked.

The cladding OD is 0.474 inches and the ID is 0.430 inches. Thus the moment of inertia of the cladding is:

$$I = \frac{\pi}{64}(0.474^4 - 0.430^4) = 8.0(10^{-4})\ in^4$$

The weight of one rod is 1.45 lb, or w = 0.0604 lb/in, using the active fuel length of 24 inches. A fixed-end, uniformly loaded beam is used to model a governing intermediate length of rod. For a 120g side drop impact, the maximum moment is:

$$M = \frac{w(L^2)}{12}120 = 24.51\ in - lb$$

The bending stress is:

$$\sigma = \frac{Mc}{I} = 7{,}261\ psi$$

where c = 0.474/2 = 0.237 inches. From [36], the yield strength of Zr-2 at 400 °F is bounded by a value of 25,000 psi. The margin of safety on yield in bending is:

$$MS = \frac{25{,}000}{7{,}261} - 1 = +2.44$$

Consequently the rods will not permanently deform due to lateral bending. The buckling of the fuel rods will be evaluated using [37], equation 18. The modulus of elasticity of the cladding, E_c = $12.0(10^6)$ psi from [36], $I_c = 8.0(10^{-4})$ in^4 as found above, ($W_c + W_f$) = the total weight of the

fuel rod of 1.45 lb, and the maximum unbraced length of the rods is l_c = 6.37 inches. The critical inertia magnitude, α_{cr}, is:

$$\alpha_{cr} = \frac{\pi^2}{l_c^2}\frac{E_c I_c}{(W_c + W_f)} = 1{,}610\ g$$

Since this value is much greater than 120g, the rods will not buckle. The margin of safety against buckling is:

$$MS = \frac{1{,}610}{120} - 1 = +12.4$$

Thus the PULSTAR fuel element will remain intact and undeformed in the bounding HAC free drop impact.

As stated in Section 7.1.2.1, *Wet Loading* and Section 7.1.2.2, *Dry Loading*, all fuel elements must be intact and undamaged prior to loading into the BRR package (note that ATR fuel elements may be trimmed per Section 1.2.2.3, *ATR*).

2.7.2 Crush

Since the weight of the BRR package exceeds 1,100 lb, the crush test specified in 10 CFR §71.73(c)(2) does not apply.

2.7.3 Puncture

The BRR package is evaluated for puncture resistance under HAC as defined in 10 CFR §71.73(c)(3). The puncture event is defined as a free drop from a height of 40 inches onto a vertical, cylindrical mild steel bar, 6 inches in diameter, in an orientation and in a location for which maximum damage is expected. Puncture performance of the BRR package is divided into two categories: puncture on the impact limiters, which was evaluated by half-scale certification test, and puncture of the package body, which is evaluated by analysis.

2.7.3.1 Puncture on the Impact Limiters

Appendix 2.12.2, *Certification Test Plan*, discusses the strategy used to evaluate the puncture performance of the impact limiters under the worst-case conditions, including the test objectives and success criteria. Section 2.12.2.4.1, *Test Sequence and Damage Accumulation*, identifies the five puncture tests that were performed on the half-scale certification test unit. The results of these tests is summarized below. Details are to be found in Appendix 2.12.3, *Certification Test Results*. The configuration of each test is shown schematically in Figure 2.12.3-2.

Test P1. This test was designed to show that the puncture bar would not penetrate beyond the impact limiter shell located on the flat bottom. This protects the closure lid from direct puncture bar loading, and prevents possible excessive loss of foam for protection in the HAC fire event. This test was performed subsequent to the end free drop test. The bar impacted the shell at an oblique angle through the cask c.g., which would enhance its ability to perforate the plate. The result shown in Figure 2.12.3-12 demonstrates that the impact limiter shell prevents perforation by the bar.

Test P2. This test was designed to show that the puncture bar would not create a significant exposure of foam adjacent to the cask (and containment seal) or dislodge the impact limiter from

the end of the cask. Although Figure 2.12.3-2 shows the impact occurring on the same side as the slapdown free drop primary damage, it was found that it would be much more challenging to impact the side opposite to this damage, since that is the azimuth location where the attachments experienced the greatest loading in the free drop. This test was successfully repeated (test P2C) after the redesign of the impact limiter attachments, and subsequent to the repeated 15° oblique slapdown free drop (test D2C). As shown in Figure 2.12.3-40, the impact with the bar did not perforate the shell or expose any foam, and the discussion in Section 2.12.3.6.4, *Examination of Attachments*, documents that the impact limiter was not dislodged by the impact.

Test P3. This test was designed to show that the puncture bar would not enter the impact limiter through a side impact on the limiter shell (in this case, the secondary slapdown damage area caused by the 15° oblique slapdown free drop) and rip open a large area that could compromise the performance in the subsequent HAC fire event. As shown in Figure 2.12.3-34, no perforation of the shell occurred.

Test P4. This test was designed to show that the puncture bar damage from impact on the c.g.-over-corner free drop damage would be acceptable. The bar impacted the thinner shell material (formerly the conical portion of the limiter shell, before the free drop deformation occurred), adjacent to the thicker bottom plate material. As shown in Figure 2.12.3-29, the exposure of foam from this test was modest, and is bounded by a large margin by the exposure of foam from test P5.

Test P5. This test was originally designed to apply an oblique impact on a damaged portion of the shell to determine that the exposure of foam would be acceptable. When it was determined that the limiter shell corner joint between the top flat annular portion and the cylindrical side had developed a crack in the secondary 15° oblique slapdown free drop, this test was used to accumulate the maximum amount of damage in that area. The orientation of the test is shown in Figure 2.12.3-30. The impact with the bar opened up the cracked region and peeled back part of the annular plate, exposing the underlying foam. The final configuration is shown in Figure 2.12.3-31 and Figure 2.12.3-32. Since this test is clearly governing above the other puncture tests regarding the HAC fire event, it is used in modeling the fire event as discussed in Section 3.4, *Thermal Evaluation for Hypothetical Accident Conditions*. It is worth noting that a design change was made subsequent to this test, aimed at preventing this breach of the joint from recurring. The design shown in Appendix 1.3.3, *Packaging General Arrangement Drawings*, includes the stronger joint. The details of the change are discussed in Section 2.12.3.3, *Test Unit Configuration*. However, as just noted, in spite of the design change, the result from the half-scale puncture test P5 was conservatively used for the HAC fire event analysis.

2.7.3.2 Puncture on the Cask Body

The puncture resistance of the outer surface of the cask body is evaluated using Nelms' Equation [27], which is used to determine the resistance to puncture of lead–backed stainless steel shells. For the NCT hot case temperature of 250 °F, the ultimate strength of the Type 304 outer shell (assuming the lower strength cast or forged option) is S_u = 64,050 psi from Table 2.2-2. The bounding weight of the BRR package, including impact limiters, is W = 32,000 lb. The required thickness of the outer shell to resist puncture is:

$$t = \left(\frac{W}{S_u}\right)^{0.71} = 0.61 \text{ inches}$$

The thickness of the outer shell is 2 inches. The margin of safety on the cask outer shell thickness is:

$$MS = \frac{2.0}{0.61} - 1 = +2.28$$

Therefore, puncture of the BRR package is not of concern.

2.7.4 Thermal

The BRR package is designed to withstand the HAC 30 minute fire specified in 10 CFR §71.73(c)(4). The thermal evaluation is presented in Section 3.4, *Thermal Evaluation under Hypothetical Accident Conditions*.

2.7.4.1 Summary of Pressures and Temperatures

As shown in Table 3.1-2, the maximum internal cask pressure as a result of the HAC fire event is 11.7 psig. This is significantly lower than the design pressure of 25 psig stated in Section 2.6.1.1, *Summary of Temperatures and Pressures*. Package component stresses were calculated for an internal pressure of 25 psig in Section 2.6.1.3, *Stress Calculations*, and are compared to allowable stress at the higher HAC temperature in Section 2.7.4.3, *Stress Calculations*.

From Table 3.1-1, as a result of the HAC fire event, the maximum temperature of any part of the cask (except closure bolts) may be bounded by a temperature of 710 °F. The maximum temperature of the closure bolts is considered to be the same as that of the closure lid, bounded by a temperature of 350 °F. Conservatively, all stainless steel components will be assumed to be made from cast or forged Type 304 material, which has a lower ultimate strength than plate material. From Table 2.2-2, S_u = 59,140 psi at 710 °F. The value of S_u for the closure bolts at 350 °F is equal to 125,000 psi, from Table 2.2-3.

2.7.4.2 Differential Thermal Expansion

Differential expansion under NCT is evaluated in Section 2.6.1.2.1, *Baskets*. In that case, the basket was given a uniform bounding temperature of 400 °F, and the thermal expansion of the cask was conservatively neglected. The resulting minimum axial clearance is shown as 0.16 inches, and the minimum diametral clearance is 0.10 inches. In the HAC fire event, from Table 3.1-1, the peak basket temperature is given as 437 °F. Since the basket temperature is locally only 37 °F hotter than the uniform NCT assumption, and in consideration of the significant thermal expansion of the cask cavity dimensions (for example, the inner shell peak temperature is 393 °F), the clearance between the basket and the cask will not be significantly affected by the cask temperatures resulting from the fire event.

Similarly, the fuel axial clearance was evaluated using a uniform bounding temperature of 400 °F in Section 2.6.1.2.2, *Fuel*, and found to have a minimum value of 0.08 inches. Given that the local peak fuel temperature, from Table 3.1-1 is only 451 °F, and that the NCT evaluation again neglected the thermal expansion of the cask components, the clearance between the fuel and the basket will not be significantly affected by the cask temperatures resulting from the fire event.

2.7.4.3 Stress Calculations

Cask stress due to the internal design pressure of 25 psig is presented in Section 2.6.1.3.1, *Stresses Due to Pressure Loading*, as equal to 1,002 psi. This corresponds to the stress in the

outer fiber of the closure lid, and is classified as a membrane plus bending stress. This stress clearly bounds the stress generated under an internal pressure in the HAC fire event of 8.8 psig, and the margin of safety may be conservatively calculated using this stress along with the lower fire case allowable stress determined in Section 2.7.4.1, *Summary of Temperatures and Pressures*. The margin of safety is:

$$MS = \frac{59{,}140}{1{,}002} - 1 = +58.0$$

The primary load on the closure bolts is governed by the preload force, calculated in Section 2.6.1.5, *Closure Bolts*, as equal to 19,200 lb. The stress is:

$$Sbs = 1.2732 \frac{19{,}200}{Dba^2} = 31{,}711 \text{ psi}$$

where the stress diameter, Dba = 0.878 inches from Section 2.6.1.5. From Table 2.1-1, the allowable average tensile stress intensity for HAC is the lesser of $0.7S_u$ or S_y, which for the ASTM A320 L43 bolting material is $0.7S_u$ = 87,500 psi at 350 °F. The margin of safety is:

$$MS = \frac{87{,}500}{31{,}711} - 1 = +1.76$$

Per Regulatory Guide 7.6, paragraph C.7, the extreme range of stress must be considered. Of all the various allowable stresses corresponding to the different conditions evaluated (including fabrication stresses and normal conditions of transport), the largest allowable stress is equal to the material ultimate strength, S_u. It is therefore conservative to assume that S_u bounds all stresses actually developed in the structure. For Type 304 stainless steel, S_u = 75,000 psi at 70 °F. The maximum possible stress intensity range is twice this value, or 150,000 psi. Applying a factor of four to account for possible stress concentrations at structural discontinuities gives a total elastic stress range of 600,000 psi. The alternating component is one-half of this value, or 300,000 psi. To account for temperature effects, this value of alternating stress is factored by the ratio of modulus of elasticity. This ratio is formed between the modulus of elasticity at room temperature (at which the test data applies directly) and the modulus of elasticity at the maximum temperature, conservatively bounded by a temperature of 710 °F for any structural part of the package. The adjusted stress is

$$S_{alt} = 300{,}000 \frac{E_{70°F}}{E_{710°F}} = 343{,}725 \text{ psi}$$

where $E_{70°F} = 28.3(10^6)$ psi and $E_{710°F} = 24.7(10^6)$ psi. Per Figure I-9.2.1 and Table I-9.1 of the ASME Code [9], the allowable value for S_{alt} at 10 cycles is 708,000 psi. The margin of safety is

$$MS = \frac{708{,}000}{343{,}725} - 1 = +1.06$$

Considering the significant conservatism used in the underlying assumptions (e.g., use of allowable stress rather than smaller actual stresses, assuming worst case stresses are fully reversing, use of the maximum factor of stress concentration), it is apparent that the actual margin of safety is larger than 1.06. Thus, the requirement of paragraph C.7 of Regulatory Guide 7.6 is met.

2.7.5 Immersion – Fissile

An immersion test for fissile material packages is required by 10 CFR §71.73(c)(5). The criticality evaluation presented in Chapter 6, *Criticality Evaluation*, assumes optimum hydrogenous moderation of the contents, thereby conservatively addressing the effects and consequences of water in–leakage.

2.7.6 Immersion – All Packages

An immersion test for all packages is required by 10 CFR §71.73(c)(6), in which a separate, undamaged specimen must be subjected an equivalent pressure of 21.7 psig. Since the BRR package is evaluated to the much greater hydrostatic pressure of the deep immersion test (see the next section), this test does not need to be evaluated.

2.7.7 Deep Water Immersion Test (for Type B Packages Containing More than 10^5 A_2)

For Type B packages containing an activity of more than 10^5 A_2, 10 CFR §71.61 requires that an undamaged containment system withstand an external pressure of p_o = 290 psig for a period of not less than one hour without collapse, buckling, or inleakage of water. This test will not have a significant effect on the BRR package. Although a temperature is not specified for this test, a lead shrinkage (fabrication) stress corresponding to a temperature of -40 °F, taken from Section 2.6.2, *Cold*, will be conservatively applied in addition to the specified hydrostatic pressure. The lead shrinkage pressure is p_c = 787 psi. Conservatively, the inner shell is evaluated neglecting the outer shell, even though the external pressure would be applied to the much stronger outer shell.

The internal pressure in the cask is assumed to be ambient, thus the net external pressure across the inner shell on its outer cylindrical surface is equal to a sum of the applied hydrostatic pressure of 290 psig and the lead shrinkage pressure of 787 psi, or a total of:

$$p_{cyl} = 290 + 787 = 1{,}077 \text{ psi}$$

The compressive hoop stress is:

$$\sigma_\theta = p_{cyl}\frac{r_{avg}}{t} = 9{,}155 \text{ psi}$$

where the mean inner shell radius, r_{avg} = 8.5 inches, and the thickness, t = one inch. The compressive axial stress, obtained by supporting the hydrostatic pressure load, p_o, from the entire cask end cross section over the inner shell cross section, is:

$$\sigma_\phi = \frac{p_o \pi r_{cask}^2}{2\pi r_{avg} t} = 6{,}289 \text{ psi}$$

where r_{cask} = 38.4/2 = 19.2 inches. Using Mohr's circle, the maximum shear stress is:

$$\sigma_{\phi\theta} = \frac{1}{2}(\sigma_\theta - \sigma_\phi) = 1{,}433 \text{ psi}$$

The possibility of buckling of the inner shell is evaluated using [13]. Consistent with Regulatory Guide 7.6, a factor of safety corresponding to ASME Code, Service Level D is employed. In this case, the applicable factor of safety is 1.34 for hypothetical accident conditions, as specified in [13].

The analysis used a modulus of elasticity of $28.3(10^6)$ psi, corresponding to 70 °F. Buckling analysis geometry and loading parameters are listed in Table 2.7-7 and results of the analysis in Table 2.7-8. As shown, all interaction parameters, including the maximum value of 0.4286, are less than unity, as required. Thus, the deep water immersion test is not of concern for the BRR package.

2.7.8 Summary of Damage

From the analyses presented, it is shown that the HAC sequence does not result in significant damage to the BRR package, and that all stress criteria established for HAC in Section 2.1.2, *Design Criteria*, are satisfied. The margins of safety resulting from the analyses performed in this section are shown in Table 2.7-9.

The BRR cask body and internal components were evaluated primarily by analysis, and the impact limiters and attachments were evaluated by test. The test results confirmed that the impact acceleration of 120g used in the analyses was bounding for all free drop orientations. The tests are summarized below.

The analysis of the cask body and internal components under free drop impact included the cask body structure, the closure lid, the closure bolts, and the shield plug shell. Bounding orientations of end and side drop were evaluated. A demonstration that the side drop governs over the worst-case slapdown is provided in Section 2.7.1.4, *Oblique Drop*. The cask body was analyzed using finite element analysis, in which the cask was loaded by self-weight and contents weight, and supported by the impact limiters. Conservatively, the lead shielding was considered to act as a fluid, having no structural strength. The minimum margin of safety from the finite element analysis, which corresponded to the side drop impact case, was +0.23. All of the manual evaluations resulted in larger margins of safety, as shown in Table 2.7-9. The end drop buckling analysis of the package shells, performed using ASME Code Case N-284-2, resulted in a maximum check value of 0.4024, which is well below the limit of unity, as required by the Code Case. An evaluation of lead slump in the end drop orientation was performed, and resulted in a bounding value of 1.185 inches. This value was used in the shielding evaluation documented in Chapter 5.0, *Shielding Evaluation*. An analysis of the fuel baskets, loose plate box, and spacer pedestals was performed as documented in Appendix 2.12.8, *Fuel Basket Stress Analysis*. Each basket was evaluated for governing modes of failure, with a minimum margin of safety of +0.12. A summary of the margins of safety for the fuel baskets is provided in Table 2.7-4. An analysis of fuel impact integrity is summarized in Table 2.7-4. An analysis of the puncture test on the cask body was performed using Nelms' equation, and resulted in a margin of safety of +2.28. Therefore, since all margins of safety are positive, the criteria of Section 2.1.2, *Design Criteria*, are satisfied for the BRR package.

The impact limiter design was tested using half-scale, prototypic certification test units and a dummy cask body. The impact limiters successfully performed their role in limiting the impact acceleration to a value considerably lower than the value of 120g used for stress analysis. In addition, the test showed that the calculated maximum strain in the energy-absorbing polyurethane foam of 83.2% was conservative. Some exposure of the foam was produced by the worst-case sequence of free drop and puncture tests. The final configuration of the impact limiter shell and of the exposed foam was included in the HAC fire event thermal model as described in Section 3.5.3.7, *Description of Thermal Model for HAC Conditions*. The impact limiter attachments, subsequent to a redesign and retest under the worst-case free drop and

puncture conditions, successfully retained the impact limiters on the cask. Therefore the impact limiters satisfy their design criteria established in Section 2.1.2.2, *Other Structures*.

Table 2.7-1 – HAC Free Drop Buckling Evaluation: Geometry and Loads

	Outer shell dimensions, inches	**Applied stress, psi**	
Inner Dia.	34.0	σ_{φ}	7,117
Outer Dia.	38.0	σ_{θ}	0
Length (bounding)	55.0	$\sigma_{\varphi\theta}$	0

Table 2.7-2 – HAC Free Drop: N–284–2 Results

Parameter	Value	Remarks
Capacity Reduction Factors (-1511)		
$\alpha_{\phi L}$ =	0.2279	
$\alpha_{\theta L}$ =	0.8000	
$\alpha_{\phi\theta L}$ =	0.8000	
Plasticity Reduction Factors (-1610)		
η_{ϕ} =	0.0568	
η_{θ} =	0.0850	
$\eta_{\phi\theta}$ =	0.0232	
Theoretical Buckling Values (-1712.1.1)		
C_{ϕ} =	0.6050	
$\sigma_{\phi eL}$ =	1,831,806 psi	
$C_{\theta r}$ =	0.1150	
$\sigma_{\theta eL} = \sigma_{reL}$ =	348,340 psi	
$C_{\theta h}$ =	0.1078	
$\sigma_{\theta eL} = \sigma_{heL}$ =	326,534 psi	
$C_{\phi\theta}$ =	0.2527	
$\sigma_{\phi\theta eL}$ =	765,157 psi	
Elastic Interaction Equations (-1713.1.1)		
σ_{xa} =	311,567 psi	
σ_{ha} =	194,946 psi	
σ_{ra} =	207,964 psi	
$\sigma_{\tau a}$ =	456,810 psi	
Axial + Shear ⇨ Check (c):	0.0228	<1 ∴ OK (see note*)
Hoop + Shear ⇨ Check (d):	0.0000	<1 ∴ OK
Inelastic Interaction Equations (-1714.2.1)		
σ_{xc} =	17,687 psi	
σ_{rc} =	17,687 psi	
$\sigma_{\tau c}$ =	10,612 psi	
Max(Axial,Hoop) ⇨ Check (a):	0.4024	<1 ∴ OK
Axial + Shear ⇨ Check (b):	0.4024	<1 ∴ OK
Hoop + Shear ⇨ Check (c):	0.0000	<1 ∴ OK

*Note: Elastic interaction checks (a), (b), (e), and (f) are not applicable.

Table 2.7-3 – Cask Shell Force and Stress Comparison

Case	Impact Limiter Force, lb	Axial Force, R, lb	Shear Force, V, lb	Bending Moment, M, in–lb	Relative Stress Intensity, psi
Side Drop	$1.920(10^6)$	0	$1.920(10^6)$	$33.600(10^6)$	164,077*
15°, Primary	$1.049(10^6)$	271,501	$1.013(10^6)$	$10.508(10^6)$	59,940*
15°, Secondary	$1.220(10^6)$	0	$1.220(10^6)$	$12.652(10^6)$	66,647*

*Stress for comparison purposes only; not actual inner shell stress.

Table 2.7-4 – Fuel Basket Stress Analysis Results

Analysis Description	Reference Section[1]	Margin of Safety
MURR Basket		
Fuel Support Plate Bending		+8.32
Outer Shell Slot Welds		+3.00
Buckling of Lower Shell		Pass[2]
MITR–II Basket		
Buckling of Lower Shell		Pass[2]
ATR Basket		
Fuel Support Plate Bending		+10.2
Outer Shell Slot Welds		+1.02
Side Drop Bending		+4.16
TRIGA Basket		
Fuel Support Plate Bending		+0.65
Shear Load on Spacer Screw		+0.12
Bucking of Fuel Tubes		Pass[2]
Side Drop Bending		+1.81
Square Fuel Basket		
Fuel Support Plate Bending		+0.23
Lower Shell Buckling		Pass[2]
Side Drop Bending		+9.82
Loose Plate Box and Pedestals		
Floor Plate Slot Weld		+1.08
Pedestal Tube		+18.3
Fuel Impact Integrity		
Plate Fuel Lateral Bending Deformation		+2.33
PULSTAR Fuel Lateral Bending		+2.44
PULSTAR Fuel Buckling		+12.4

Notes:
1. Calculational details are presented in Appendix 2.12.8, *Fuel Basket Stress Analysis*.
2. Interaction equation checks are less than unity, as required by [13].

Table 2.7-5 – Fuel Impact Deformation Results

Fuel Type	W, lb	L_{FB} ①	A_{xc}, in^2	W/A_{xc}, lb/in^2	GAP	L, in
MURR	15	0.63	4.584	3.27	1.18	0.035
MITR–II	10	0.61	3.814	2.62	1.17	0.028
ATR	25	1.13	3.961	6.31	1.68	0.096
TRIGA	10	0.99	1.720②	5.81	1.54	0.081
Square③	14	0.50	2.520	5.56	1.05	0.053

Notes:

1. L_{FB} is equal to the basket cavity length minus the minimum fuel length. Minimum fuel length is equal to the maximum length stated in Section 1.2.2, *Contents*, less the irradiation growth of 0.25 inches (0.75 inches for ATR).
2. TRIGA fuel has 0.03–inch thick cladding for aluminum clad and 0.02–inch thick cladding for stainless steel clad fuel. Since the entire fuel cross–section is made of a strong material (fuel pellet of UZrH), the area used is that of the entire pellet cross–section of 1.48 inches.
3. Missouri S&T represents bounding Square fuel case.

Table 2.7-6 – Impact Limiter Attachment Comparisons

Feature Description	Refurbished Test article (Full-scale Equiv.)	Final Production Design (per Appendix 1.3.3)	Remarks
Blade and receptacle material	ASTM Type 304	ASTM Type 304	Same
Blade thickness, in.	3/4	3/4	Same
Blade width, in.	3.0	3.3	Improved
Hole diameter in blade, in.	1.13	1.13	Same
Hole-to-blade edge, in.	0.94	1.06	Improved
Blade weld to limiter inner shell structure	3/8-in. fillet on both sides	3/8-in. fillet on both sides	Same
Receptacle plate thickness, in.	3/8	1/2	Improved
Ball lock pin diameter, in.	1.0	1.0	Same
Pin material	Carbon steel	Stainless steel	Improved
Pin rated double shear strength, lb	65,600	73,500	Improved
Attachment quantity per limiter	6	8	Improved

Table 2.7-7 – Deep Immersion Test: Geometry and Loads

	Inner shell dimensions, inches	Applied stress, psi	
Inner Dia.	16.0	σ_φ	6,289
Outer Dia.	18.0	σ_θ	9,155
Length (bounding)	62.0	$\sigma_{\varphi\theta}$	1,433

Table 2.7-8 – Deep Immersion Test: N–284–2 Results

Parameter	Value	Remarks
Capacity Reduction Factors (-1511)		
$\alpha_{\phi L}$ =	0.2850	
$\alpha_{\theta L}$ =	0.8000	
$\alpha_{\phi\theta L}$ =	0.8000	
Plasticity Reduction Factors (-1610)		
η_{ϕ} =	0.0523	
η_{θ} =	0.2856	
$\eta_{\phi\theta}$ =	0.0417	
Theoretical Buckling Values (-1712.1.1)		
C_{ϕ} =	0.6050	
$\sigma_{\phi eL}$ =	2,014,294 psi	
$C_{\theta r}$ =	0.0387	
$\sigma_{\theta eL} = \sigma_{reL}$ =	128,711 psi	
$C_{\theta h}$ =	0.0387	
$\sigma_{\theta eL} = \sigma_{heL}$ =	128,711 psi	
$C_{\phi\theta}$ =	0.1619	
$\sigma_{\phi\theta eL}$ =	539,157 psi	
Elastic Interaction Equations (-1713.1.1)		
σ_{xa} =	428,445 psi	
σ_{ha} =	76,843 psi	
σ_{ra} =	76,843 psi	
$\sigma_{\tau a}$ =	321,885 psi	
Axial + Shear ⇨ Check (c):	0.0147	<1 ∴ OK (see note*)
Hoop + Shear ⇨ Check (d):	0.1192	<1 ∴ OK
Inelastic Interaction Equations (-1714.2.1)		
σ_{xc} =	22,388 psi	
σ_{rc} =	21,943 psi	
$\sigma_{\tau c}$ =	13,433 psi	
Max(Axial,Hoop) ⇨ Check (a):	0.4172	<1 ∴ OK
Axial + Shear ⇨ Check (b):	0.2923	<1 ∴ OK
Hoop + Shear ⇨ Check (c):	0.4286	<1 ∴ OK

*Note: Elastic interaction checks (a), (b), (e), and (f) are not applicable.

Table 2.7-9 – Minimum Margins of Safety from HAC Evaluations

Component	Loading Condition	Minimum Margin of Safety
	Free Drop	
Cask body (FEA)	End drop, bottom down, membrane stress	+0.98
	End drop, bottom down, membrane + bending	+0.49
	End drop, top down, membrane stress	+0.97
	End drop, top down, membrane + bending stress	+0.92
	Side drop, membrane stress	+1.75
	Side drop, membrane + bending stress	+0.23
Lower closure plate	End drop, bottom down, membrane + bending	+0.40
Closure bolts	End drop, top down	+0.83
Closure lid	End drop, top down	+1.65
Shield plug shell lower plate	End drop, bottom down, assuming simple support, stress at center	+0.46
	End drop, bottom down, assuming fixed edge support, stress at edge (weld)	+0.91
Cask outer shell	End drop, buckling (Code Case N-284-2)	0.4024*
	Puncture	
Cask outer shell	Nelms' Equation	+2.28
	Thermal	
Containment boundary	Internal pressure, fire conditions	+58.0
Closure bolts	Internal pressure, fire conditions	+1.76
Cask	Range of stress	+1.06

*Maximum check value must be less than unity.

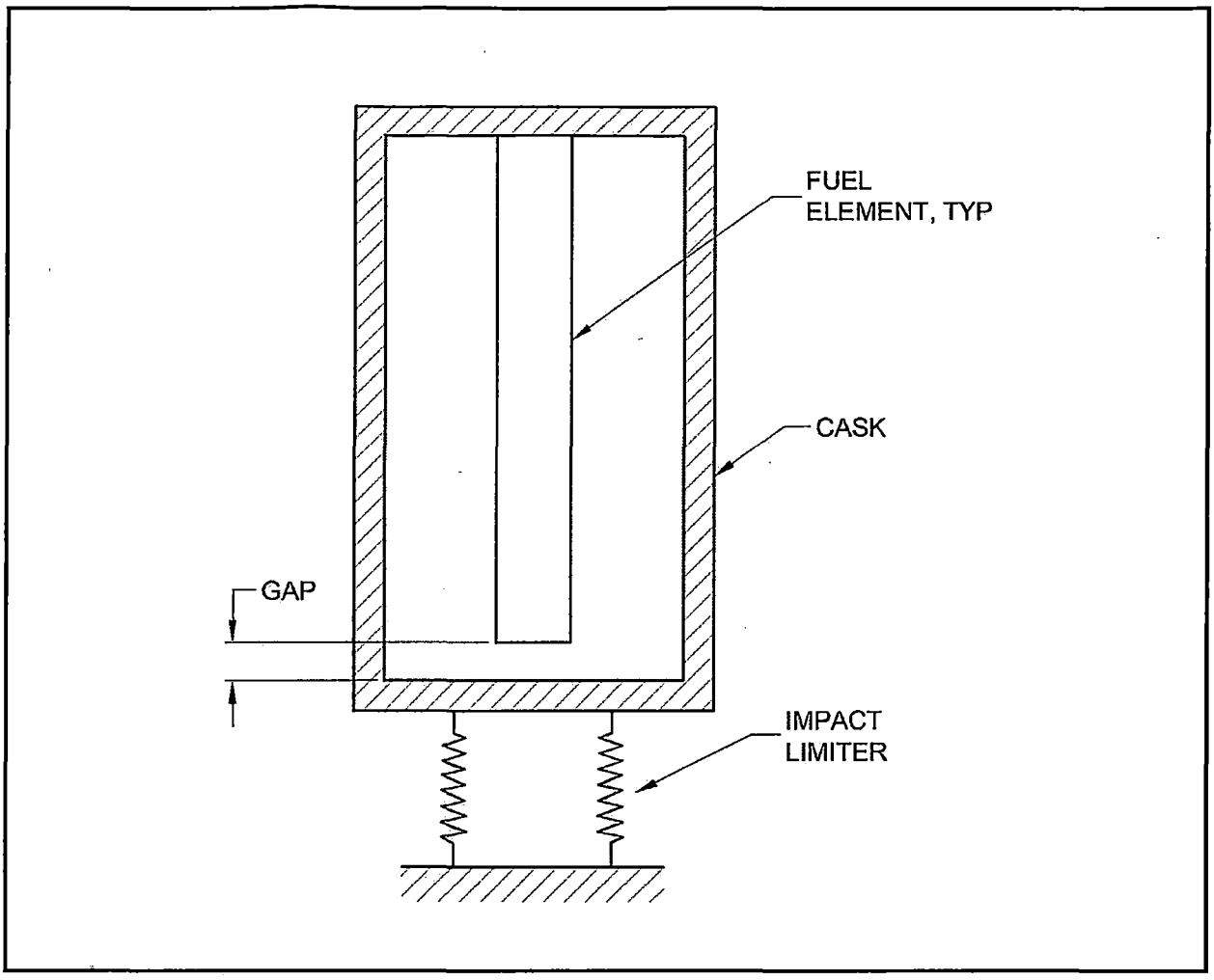

Figure 2.7-1 – Cask Cavity and Fuel During Free End Drop

6.0 CRITICALITY EVALUATION

The Battelle Energy Alliance (BEA) Research Reactor (BRR) package is used to transport spent fuel from a variety of research reactors, including the University of Missouri Research Reactor (MURR), Massachusetts Institute of Technology Research Reactor (MITR-II), Advanced Test Reactor (ATR), PULSTAR, and various types of Training, Research, Isotope General Atomics (TRIGA) reactors. Square plate fuel (plate-type fuel in assemblies that are approximately square in cross-section) used by the Rhode Island Nuclear Science Center (RINSC), University of Massachusetts at Lowell (U-Mass), Ohio State University (Ohio State), Missouri University of Science and Technology (Missouri S&T), University of Florida (U-Florida), and Purdue University (Purdue) may also be transported. The following analyses demonstrate that the BRR package complies with the requirements of 10 CFR §71.55 and §71.59. Based on the analysis, the Criticality Safety Index (CSI), per 10 CFR §71.59, is 0.

6.1 Description of Criticality Design

6.1.1 Design Features

Five basket types are used to properly position the fuel within the cask cavity. These baskets limit the number of fuel elements that may be shipped at a given time, and also control the spacing between the fuel elements. No poisons are utilized in the package. The separation provided by the packaging is sufficient to maintain criticality safety.

6.1.2 Summary Table of Criticality Evaluation

The upper subcritical limit (USL) for ensuring that the package is acceptably subcritical, as determined in Section 6.8, *Benchmark Evaluations*, is:

$$USL = 0.9209$$

The package is considered to be acceptably subcritical if the computed k_{safe} (k_s), which is defined as $k_{effective}$ (k_{eff}) plus twice the statistical uncertainty (σ), is less than or equal to the USL, or:

$$k_s = k_{eff} + 2\sigma \leq USL$$

The USL is determined on the basis of a benchmark analysis and incorporates the combined effects of code computational bias, the uncertainty in the bias based on both benchmark-model and computational uncertainties, and an administrative margin. The results of the benchmark analysis indicate that the USL is adequate to ensure subcriticality of the package.

The packaging design is shown to meet the requirements of 10 CFR 71.55(b). No credit is taken for fuel element burnup in any models. In the single package normal conditions of transport (NCT) models, credit is taken for the leaktight performance of the cask, while in the single package hypothetical accident condition (HAC) models, water is modeled in all cavities at the density in which reactivity is maximized. For the aluminum plate fuel elements, the most reactive credible configuration is utilized by maximizing the gap between the fuel plates. Maximizing this gap maximizes the moderation and hence the reactivity because the fuel elements are undermoderated. In all single package models, 12-in of water reflection is utilized.

Infinite reflection is utilized in both NCT and HAC array models. In the HAC array cases, internal and external water moderation is selected to maximize the reactivity.

The maximum results of the criticality calculations for each of the fuel element types are summarized in Table 6.1-1. The maximum calculated k_s is 0.827, which occurs for the HAC array case for the MURR payload. The maximum reactivity is less than the USL of 0.9209. The most reactive MITR-II, ATR, TRIGA, and Square fuel basket (SFB) cases are well below the USL.

Note that PULSTAR, the Loose Plate Box (LPB), and the Square plate-fuels are transported in the SFB. PULSTAR bounds the LPB and Square plate-fuels. The LPB is used to transport U-Florida, U-Mass(Al), or Purdue fuel plates. Up to eight LPBs may be loaded per package, and the limit on the number of plates per LPB is ≤ 31 for the three plate types authorized:

- Limit on U-Florida plates: ≤ 31 plates per LPB
- Limit on U-Mass(Al) plates: ≤ 31 plates per LPB
- Limit on Purdue plates: ≤ 31 plates per LPB

The LPB is most reactive when filled with the maximum allowed number of fuel plates, although the maximally loaded system is undermoderated. Reactivity is reduced when fewer than 31 fuel plates are loaded, and the analysis bounds loading/unloading operations. Transporting PULSTAR, Square plate fuels, and the LPB within the same basket is authorized, as this payload is bounded by a payload of eight PULSTAR fuel elements.

Note that the TRIGA fuel is significantly more reactive than the plate fuel types and PULSTAR under NCT. This is because hydrogen is included in the TRIGA fuel matrix, providing some moderation. However, the reactivity of the NCT TRIGA cases is still very low.

6.1.3 Criticality Safety Index

An infinite number of packages is used in the array calculations for both NCT and HAC. Therefore, the criticality safety index per 10 CFR 71.59 is 0.

Table 6.1-1 – Summary of Criticality Evaluation

Normal Conditions of Transport (NCT)							
Basket	**MURR**	**MITR-II**	**ATR**	**TRIGA**	**SFB**		
Fuel	**MURR**	**MITR-II**	**ATR**	**TRIGA**	**PULSTAR**	**LPB**	**Square Plate**
Case	k_s	k_s	k_s	k_s	k_s	k_s	k_s
Single Unit Maximum	0.085	0.058	0.088	**0.417**	0.147	0.052	0.036
Infinite Array Maximum	0.197	0.144	0.234	**0.539**	0.229	0.121	0.094
Hypothetical Accident Conditions (HAC)							
Basket	**MURR**	**MITR-II**	**ATR**	**TRIGA**	**SFB**		
Fuel	**MURR**	**MITR-II**	**ATR**	**TRIGA**	**PULSTAR**	**LPB**	**Square Plate**
Case	k_s	k_s	k_s	k_s	k_s	k_s	k_s
Single Unit Maximum	0.784	0.574	0.704	0.709	**0.812**	0.641	0.741
Infinite Array Maximum	**0.827**	0.609	0.721	0.720	0.822	0.647	0.746
USL = 0.9209							

6.2 Fissile Material Contents

Allowed spent fuel contents are MURR, MITR-II, ATR, TRIGA, PULSTAR, and the Square plate-fuels RINSC, U-Mass (silicide or aluminide), Ohio State, Missouri S&T, U-Florida, and Purdue. Up to 31 U-Mass (aluminide), U-Florida, and Purdue plates may also be transported in a Loose Plate Box (LPB). For criticality control purposes, all fuel is modeled as fresh, and the information provided in this section pertains to fresh fuel.

6.2.1 MURR Fuel Element

The package can accommodate up to eight MURR fuel elements. Each MURR element contains up to 782.8 g U-235, with an enrichment of 93 ± 1 wt.%. This fuel loading and enrichment is bounded by modeling 785 g U-235 and 94% enrichment. The weight percents of the remaining uranium isotopes are 1.2 wt.% U-234, 0.7 wt.% U-236, and 5.0-7.0 wt.% U-238. Each fuel element contains 24 curved fuel plates. Fuel plate 1 has the smallest radius, while fuel plate 24 has the largest radius, as shown in Figure 6.2-1. The fuel "meat" is a mixture of uranium metal and aluminum, while the cladding and structural materials are an aluminum alloy.

The relevant fuel element information is summarized in Figure 6.2-2. Each fuel plate is nominally 0.05-in thick, with a thickness tolerance of ±0.002-in. The fuel meat is nominally 0.02-in thick, and the cladding is nominally 0.015-in thick. The minimum cladding thickness is 0.008-in. The plate cladding material is aluminum. Fuel element side plates are fabricated of ASTM B 209, aluminum alloy 6061-T6 or 6061-T651. These fuel element side plates have a minimum thickness of 0.145-in. The average measured channel spacing between fuel plates, over the entire fuel element, is less than or equal to 0.088-in. The maximum local channel spacing is 0.090-in.

The midpoint radii of the fuel plates are treated as fixed quantities, and are computed based on nominal dimensions. Therefore, due to the modeling technique employed, the pitch is fixed at 0.130-in, and the cladding thickness and channel spacing are linked. If the fuel plates are modeled at the maximum average channel spacing of 0.088-in, the as-modeled cladding thickness is 0.011-in. However, if the cladding is modeled at the minimum value of 0.008-in, the as-modeled channel spacing is 0.094-in. Modeling a minimum cladding thickness of 0.008-in and channel spacing of 0.094-in between each fuel plate is conservative, although an actual fuel element would not be constructed in this manner. In the NCT models, a channel spacing of 0.088-in is modeled, and in the most reactive HAC models, the more conservative 0.094-in channel spacing is modeled. The relationship between cladding thickness and channel spacing for the various scenarios is illustrated in Figure 6.2-1.

The arc length of the fuel meat changes from plate to plate. Reference minimum fuel meat arc length and inner radius dimensions for each plate are provided on Figure 6.2-2. The active fuel length ranges from 23.25-in to 24.75-in.

It is necessary to determine the number densities of the fuel meat, which are the same for all fuel plates. To determine the number densities of the fuel meat, it is first necessary to compute the volume of the fuel meat. The volume of the fuel meat for each plate is the maximum arc length of the meat (nominal + 0.065-in) multiplied by the nominal active fuel length (24.0-in) and meat thickness (0.02-in). The active fuel length and meat thickness are modeled at nominal values in all final (i.e., non-parametric) fuel element models, and the use of these dimensions is justified in

Section 6.9.2, *Parametric Evaluations to Determine the Most Reactive Fuel Geometries.* It is demonstrated in Section 6.9.2.2, *MURR Fuel Parametric Evaluation*, that reactivity increases with increasing meat arc length. The results of the fuel meat volume computations for all 24 plates are provided in Table 6.2-1 for maximum fuel arc length.

The U-235 gram density for each fuel plate is computed by dividing the U-235 mass by the total volume, or 785 g/556.4 cm^3 = 1.41 g/cm^3. The fuel itself is a mixture of UAl_x and aluminum. An equation that relates the U-235 density to the overall fuel meat density for ATR fuel is presented in Table 6.2-5. Because ATR and MURR fuel are of the same type, the fuel density equation shown in Table 6.2-5 is also used to develop the MURR fuel matrix density. Using this equation, the total density of the fuel matrix is computed to be approximately 3.77 g/cm^3.

From the fuel volumes, U-235 gram densities, and total mixture densities provided, the number densities for the fuel region may be computed. These number densities are provided in Table 6.2-2. The U-235 weight percent is modeled at 94%. Representative weight percents of 0.6% and 0.35% are utilized for U-234 and U-236, respectively, and the balance (5.05%) is modeled as U-238.

6.2.2 MITR-II Fuel Element

The package can accommodate up to eight MITR-II fuel elements. Each MITR-II element contains up to 513 g U-235, with an enrichment of 93 ± 1 wt.%. This fuel loading and enrichment is bounded by modeling 515 g U-235 and 94% enrichment. The weight percents of the remaining uranium isotopes are 1.2 wt.% U-234, 0.7 wt.% U-236, and 5.0-7.0 wt.% U-238. Each fuel element contains 15 flat fuel plates, as shown in Figure 6.2-3. The fuel "meat" is a mixture of uranium metal and aluminum, while the cladding and structural materials are an aluminum alloy.

The relevant fuel element information is summarized in Figure 6.2-4. Each fuel plate is nominally 0.08-in thick, with a thickness tolerance of ±0.003-in. The fuel meat is nominally 0.03-in thick, and the cladding is nominally 0.025-in thick. The minimum cladding thickness, including the thermal groove, is 0.008-in. The plate cladding material is aluminum. Fuel element side plates are fabricated of ASTM B 209, aluminum alloy 6061-T6. These fuel element side plates have a nominal thickness of 0.188-in. The channel spacing between the plates is 0.078 ± 0.004-in (excluding the thermal grooves). These tolerances represent average and not localized channel spacing. For an actual fuel element, the channel spacing may exceed these tolerances in localized areas. The maximum local channel spacing is 0.090-in (excluding the thermal grooves).

The maximum and minimum active fuel lengths and maximum and minimum active fuel widths may be computed based the dimensions on Figure 6.2-4:

- Maximum active fuel length = (23.0+0.01)-2(0.125) = 22.76-in
- Minimum active fuel length = (23.0-0.01)-2(0.5) = 21.99-in
- Maximum active fuel width = 2.531 – 2(0.18) = 2.171-in
- Minimum active fuel width = 2.521 – 2(0.27) = 1.981-in.

The nominal active fuel length may be estimated as the average of the maximum and minimum values, or 22.375-in.

It is necessary to determine the number densities of the fuel meat, which are the same for all fuel plates. To determine the number densities of the fuel meat, it is first necessary to compute the volume of the fuel meat. The volume of the fuel meat for each plate is the maximum width of the meat (2.171-in) multiplied by the active fuel length (22.375-in) and meat thickness (0.03-in). The active fuel length and meat thickness are modeled at nominal values in all final (i.e., non-parametric) fuel element models, and the use of these dimensions is justified in Section 6.9.2, *Parametric Evaluations to Determine the Most Reactive Fuel Geometries*. It is demonstrated in Section 6.9.2.3, *MITR-II Fuel Parametric Evaluation*, that reactivity increases with increasing meat width. The total meat volume is therefore $(15)(0.03)(22.375)(2.171)(2.54^3) = 358.2$ cm^3.

The centerlines of the fuel plates are treated as fixed quantities, and are computed based on nominal dimensions. Therefore, due to the modeling technique employed, the pitch is fixed at 0.158-in, and the cladding thickness and channel spacing are linked. The average measured channel spacing between fuel plates, over the entire fuel element, is less than or equal to 0.082-in (excluding the thermal grooves). The fuel plates also have grooves a maximum of 0.012-in deep cut into the surface of the fuel plates to increase heat transfer. Because the grooves cover approximately half the surface area of the cladding, half of the groove depth (i.e., 0.006-in) is removed from each cladding plate in the NCT models, increasing the effective channel spacing to 0.094-in. A channel spacing of 0.094-in is modeled in all NCT cases. To achieve this channel spacing between all fuel plates, the cladding is artificially reduced to a thickness of 0.017-in, or a total plate thickness of 0.064-in. However, if the as-modeled cladding thickness is 0.006-in for each plate, the as-modeled channel spacing is 0.116-in. This cladding thickness is conservatively lower than the 0.008-in minimum cladding thickness. The most reactive HAC models utilize a channel spacing of 0.116-in. The relationship between cladding thickness and channel spacing for the various scenarios is illustrated in Figure 6.2-3.

The U-235 gram density for each fuel plate is computed by dividing the U-235 mass by the total volume, or 515 g/358.2 cm^3 = 1.44 g/cm^3. The fuel itself is a mixture of UAl_x and aluminum. An equation that relates the U-235 density to the overall fuel meat density for ATR fuel is presented in Table 6.2-5. Because ATR and MITR-II fuel are of the same type, the fuel density equation shown in Table 6.2-5 is also used to develop the MITR-II fuel matrix density. Therefore, using this equation, the total density of the fuel matrix is computed to be approximately 3.79 g/cm^3.

From the fuel volumes, U-235 gram densities, and total mixture densities provided, the number densities for the fuel region may be computed. These number densities are provided in Table 6.2-3. The U-235 weight percent is modeled at 94%. Representative weight percents of 0.6% and 0.35% are utilized for U-234 and U-236, respectively, and the balance (5.05%) is modeled as U-238.

6.2.3 ATR Fuel Element

The package can accommodate up to eight ATR fuel elements. Each element contains up to 1085 g U-235, with an enrichment of 93 ± 1 wt.%. This fuel loading and enrichment is bounded by modeling 1200 g U-235 and 94% enrichment. The weight percents of the remaining uranium isotopes are 1.2 wt.% U-234 (max), 0.7 wt.% U-236 (max), and 5.0-7.0 wt.% U-238. Each fuel element contains 19 curved fuel plates. Fuel plate 1 has the smallest radius, while fuel plate 19 has the largest radius, as shown in Figure 6.2-5. The fuel "meat" is a mixture of uranium metal and aluminum, while the cladding and structural material are an aluminum alloy.

The relevant fuel element details are summarized on Figure 6.2-6. Fuel plate 1 is nominally 0.080-in thick, fuel plates 2 through 18 are nominally 0.050-in thick, and fuel plate 19 is nominally 0.100-in thick. The plate thickness tolerance is +0.000/-0.002-in for all plates. The fuel meat is nominally 0.02-in thick for all 19 plates. The minimum cladding thickness is 0.018-in for plates 1 and 19, and 0.008-in for plates 2 through 18. The plate cladding material is aluminum ASTM B 209, 6061-0. Fuel element side plates are fabricated of ASTM B 209, aluminum alloy 6061-T6 or 6061-T651. These fuel element side plates have a minimum thickness of 0.182-in. Channels 2 through 10 have an average spacing of 0.078 ± 0.007-in, while channels 11 through 19 have an average spacing of 0.077 +0.008/-0.006-in. The average measured channel spacing between fuel plates, over the entire fuel element, is less than or equal to 0.085-in. The maximum local channel spacing is 0.087-in.

The midpoint radii of the fuel plates are treated as fixed quantities, and are computed based on nominal dimensions. Therefore, due to the modeling technique employed, the pitch is fixed at 0.128-in (plates 2 through 18), and the cladding thickness and channel spacing are linked. If the fuel plates are modeled at the maximum average channel spacing of 0.085-in, the as-modeled cladding thickness is 0.0265-in for plate 1, 0.0115-in for plates 2 through 18, and 0.0365-in for plate 19. However, if the cladding is modeled at the minimum values, the as-modeled channel spacing is 0.097-in between plates 1 and 2, 0.107-in between plates 18 and 19, and 0.092-in between the remaining plates. Modeling the minimum cladding thicknesses for each fuel plate is conservative, although an actual fuel element would not be constructed in this manner. In the NCT models, a channel spacing of 0.085-in is modeled between each plate, and in the most reactive HAC models, the more conservative channel spacing is modeled based on minimum cladding thicknesses, as provided above. The relationship between cladding thickness and channel spacing for the various scenarios is illustrated in Figure 6.2-5.

The arc length of the fuel meat changes from plate to plate. This arc length varies based on the distance from the edge of the fuel meat to the fuel element side plate, as defined for each plate on Figure 6.2-6. This dimension is 0.245-in (max)/0.145-in (min) for fuel plates 1 and 19, 0.145-in (max)/0.045-in (min) for fuel plates 2 through 17, and 0.165-in (max)/0.065-in (min) for fuel plate 18. The smaller this dimension, the larger the arc length of the fuel meat.

The active fuel length varies between a minimum of 47.245-in (= 49.485 – 2*1.12) and a maximum of 48.775-in (= 49.515 – 2*0.37) for all fuel plates.

It is demonstrated in Section 6.9.2.1, *ATR Fuel Parametric Evaluation*, that reactivity increases with increasing meat arc length. Therefore, the arc length is modeled at the maximum value. To determine the number densities of the fuel meat, it is first necessary to compute the volume of the fuel meat. The volume of the fuel meat for each plate is the maximum arc length of the meat multiplied by the fuel length (48-in) and meat thickness (0.02-in). The fuel length and meat thickness are treated as fixed quantities in all fuel element models, and the use of these dimensions is justified in Section 6.9.2.1.

The fuel meat volume for each of the 19 fuel plates is provided in Table 6.2-4. The mass of U-235 per plate utilized in the analysis is also provided in Table 6.2-4. The U-235 gram density for each fuel plate is also computed. Note that the U-235 gram density is higher in the inner plates compared to the outer plates.

The fuel itself is a mixture of UAl_x and aluminum. The density of this mixture is proportional to the U-235 gram density, as shown in Table 6.2-5. These data are perfectly linear, and a linear fit

of the data is $\rho_2 = 0.8733\rho_1 + 2.5357$, where ρ_2 is the total gram density of the mixture, and ρ_1 is the gram density of the U-235 in the mixture. This equation is used to compute the total mixture gram density provided as the last column in Table 6.2-4.

From the fuel volumes, U-235 gram densities, and total mixture densities provided, the number densities for the fuel region of each fuel plate may be computed. These number densities are provided in Table 6.2-6. The U-235 weight percent is modeled at 94%. Representative weight percents of 0.6% and 0.35% are utilized for U-234 and U-236, respectively, and the balance (5.05%) is modeled as U-238.

6.2.4 TRIGA Fuel Element

The package can accommodate up to 19 TRIGA fuel elements. While many different types of TRIGA fuel elements have been fabricated over the past 50 years, only 26 specific TRIGA fuel element types are considered in this analysis. Data for these element types are summarized in Table 6.2-7. Of these 26, two types that bound the other designs are selected for explicit analysis:

1. 8.5 wt.% uranium in the fuel matrix, 70 wt.% U-235 in uranium (136 g U-235), stainless steel clad (General Atomics catalog number 109)
2. 30 wt.% uranium in the fuel matrix, 20 wt.% U-235 in uranium (163 g U-235), stainless steel clad (General Atomics catalog number 119)

The two bounding rod types are selected based on enrichment and total U-235 loading. Rod Type 109 is enriched to 70 wt.% U-235 (U-235/U), which significantly bounds the enrichment of all the other rods, which are enriched to 20 wt.% U-235. Rod Type 119 has a total U-235 loading of 163 grams and bounds the U-235 loading of all the other rod types by a minimum of 22 grams per rod. Note that rod Type 219 is an instrumented version of rod Type 119 and has no differences that are significant to criticality.

The fuel matrix of a TRIGA fuel element consists of a mixture of uranium and zirconium hydride. Therefore, the TRIGA elements contain hydrogen moderator material. A schematic of a typical stainless steel clad fuel element is shown in Figure 6.2-8.

TRIGA fuel elements consist of a central active fuel region with graphite axial reflectors above and below the active fuel. Standard TRIGA fuel elements manufactured prior to 1964 utilize thin samarium trioxide discs between the active fuel and graphite reflectors. Later designs utilize a thin molybdenum disc between the active fuel and lower reflector rather than samarium trioxide. The samarium trioxide discs act a as a burnable poison and are conservatively omitted from the models. The molybdenum disc is only 0.031-in thick and has essentially no effect on the reactivity. For this reason, the molybdenum disc is also omitted from the models.

For all TRIGA fuel elements with the exception of Type 101, a solid zirconium rod with an outer diameter of 0.225-in is placed along the active fuel length in the center of the fuel pellet. It is assumed that the inner diameter of the fuel pellet is 0.25-in to allow a small clearance between the rod and the fuel.

The fuel elements are modeled in detail from the bottom of the bottom reflector to the top of the top reflector. The end cap regions are neglected for simplicity. The graphite reflectors are modeled at the same diameter as the fuel pellets for simplicity, although the actual graphite

reflectors have a slightly smaller diameter, as shown in Table 6.2-7. Fuel elements with high U-235 loadings may contain erbium poison, although this poison is conservatively ignored in the criticality models.

The material densities within the evaluated TRIGA fuel elements are computed based upon the information in Table 6.2-7. Because the masses of U-235 and uranium are provided, the uranium densities in the fuel may be computed based on the known volumes. The uranium is treated as a mix of only U-235 and U-238 for simplicity. The fuel densities for the two evaluated fuel types are summarized in Table 6.2-8.

6.2.5 PULSTAR Fuel Element

The PULSTAR fuel element comes in one of two subtypes that are differentiated by the U-235 enrichment of the uranium in their fuel material. Up to eight elements of either subtype are permitted for transport in the BRR package using the SFB. The nominal enrichments of fuel in the two element subtypes are 4 and 6 wt.% U-235. These enrichments correspond to element-total U-235 mass loadings of 504 and 770 grams (nominal), respectively. All other aspects of the element designs are shared by the two subtypes and are identical. Those features are described below. The bounding higher enrichment is used for all analysis.

Detailed design information for PULSTAR fuel is summarized in Table 6.2-9. Each element contains 25 fuel rods in a regular, rectangular arrangement with a pitch of 0.524-in x 0.606-in. The rod lattice is centered within a zirconium box that extends beyond the ends of the 26.2-in long fuel rods. The surrounding box has a nominal thickness of 0.06-in and outer dimensions of 2.740-in x 3.150-in. Each of the 25 fuel rods in the element contains a stack of UO_2 pellets with a density range of 10.4 to 10.7 g/cm^3 and a height of 24.0-in (max 24.1-in). The maximum diameter of the fuel pellets is 0.423-in. A zirconium alloy is used as cladding for the pellets. The cladding has a minimum thickness of 0.0185-in and an outer diameter ranging from 0.471-in to 0.474-in. Solid zirconium alloy plugs cap each end of the fuel stack.

The modeled density is the density that yields the exact nominal U-235 loading (10.494 g/cm^3). As discussed above, the enrichment of U-235 in the uranium component of the UO_2 is 4 or 6 wt.% depending on the subtype, but all rods in a given element subtype have the same enrichment. An enrichment of 6 wt.% is modeled in all cases and uncertainty in the enrichment (less than 0.1 %) is safely ignored. Each dimension is modeled at its maximum except for cladding thickness, which is modeled at the minimum acceptable value.

The material composition used for PULSTAR fuel is given in Table 6.2-10. The general geometry is shown in Figure 6.2-9.

6.2.6 Square Plate Fuels

Fuel Elements

The plate fuels include elements for RINSC, U-Mass with UAl_x fuel matrix (U-Mass (Al)), U-Mass with U_3Si_2-Al fuel matrix (U-Mass (Si)), Ohio State, Missouri S&T, U-Florida, and Purdue. The UAl_x fuel matrix is referred to as "aluminide" and the U_3Si_2-Al fuel matrix is referred to as "silicide". With the exception of U-Mass (Al), all Square plate fuels have a silicide fuel matrix. U-Mass (Al) fuel originally was manufactured for the Worcester Polytechnic Institute (WPI) reactor; however, the fuel will be used at U-Mass Lowell.

Uranium in the flat plate fuels is 19.75 ± 0.2 % enriched, by weight, in U-235. The design of the elements varies between facilities, but has the same general arrangement of 14 to 22 plates, flat or with mild curvature, arranged in a regular array with 0.099-in to 0.175-in channel spacing. Except for U-Mass (Al) and Purdue, which both contain 9.3 g U-235 per plate, plates of each element contain 12.5 g U-235 per plate. The uranium foils that constitute the meat in each plate are 0.020-in thick except in the aluminide fuel of the U-Mass (Al) element, which is slightly thicker at 0.030-in. The maximum width and length of the foils are 2.5-in and 24.0-in. Aluminum cladding encases the fuel foils. The aluminum cladding has a minimum thickness of 0.005-in.

A summary of the plate and element characteristics that are significant to criticality is given in Table 6.2-11. Plate pitch for each element is adjusted to maintain the channel spacing and plate dimensions. Mass densities for the fuel materials are provided in Table 6.2-12. Note that all silicide fuels have matching composition except Purdue. Material densities are determined assuming U-235 loadings at the maximum of reported ranges.

Loose Plate Box (LPB)

The LPB is used to transport loose plates from three of the elements discussed in the preceding paragraphs. Each LPB can carry up to 31 loose plates per box and occupies 1 of the 8 compartments of the SFB. A payload of 8 LPBs may be transported in the SFB. Loose plates are limited to those from U-Mass (Al), U-Florida, and Purdue fuel. A U-Florida plate with 12.5 grams U-235 per plate is used in the analysis to bound U-Mass (Al) and Purdue plates, which both carry 9.3 grams U-235 per plate.

Table 6.2-1 – MURR Fuel Volume Computation (maximum arc length)

Plate	Midpoint Radius (cm)	Fuel Arc (cm)	Volume① (cm^3)
1	7.0993	4.5034	13.9460
2	7.4295	4.7625	14.7484
3	7.7597	5.0216	15.5507
4	8.0899	5.2832	16.3608
5	8.4201	5.5423	17.1632
6	8.7503	5.8014	17.9655
7	9.0805	6.0604	18.7678
8	9.4107	6.3195	19.5701
9	9.7409	6.5786	20.3724
10	10.0711	6.8377	21.1747
11	10.4013	7.0968	21.9770
12	10.7315	7.3558	22.7793
13	11.0617	7.6149	23.5816
14	11.3919	7.8765	24.3918
15	11.7221	8.1356	25.1941
16	12.0523	8.3947	25.9964
17	12.3825	8.6538	26.7987
18	12.7127	8.9129	27.6011
19	13.0429	9.1719	28.4034
20	13.3731	9.4310	29.2057
21	13.7033	9.6901	30.0080
22	14.0335	9.9492	30.8103
23	14.3637	10.2083	31.6126
24	14.6939	10.4699	32.4228
Total			556.4024

① Volume is computed as Fuel Arc*Active Fuel Height*Fuel Thickness, where Active Fuel Height = 24-in (60.96 cm) and Fuel Thickness = 0.02-in (0.0508 cm).

Table 6.2-2 – MURR Fuel Number Densities (maximum arc length)

Isotope	Number Density (atom/b-cm)
U-234	2.3171E-05
U-235	3.6147E-03
U-236	1.3402E-05
U-238	1.9174E-04
Al	5.0596E-02
Total	5.4439E-02

Table 6.2-3 – MITR-II Fuel Number Densities (maximum meat width)

Isotope	Number Density (atom/b-cm)
U-234	2.3613E-05
U-235	3.6835E-03
U-236	1.3657E-05
U-238	1.9539E-04
Al	5.0481E-02
Total	5.4398E-02

Table 6.2-4 – ATR Fuel Element Volume and Gram Densities (maximum arc length)

Plate	Fuel Meat Arc Length (cm)	Fuel Meat Volume (cm^3)	U-235 Mass Per Plate (g)	U-235 density, ρ_1 (g/cm^3)	Total UAl_x + Al Density, ρ_2 (g/cm^3)
1	4.2247	26.2	27.1	1.04	3.44
2	5.0209	31.1	32.5	1.04	3.45
3	5.2764	32.7	43.2	1.32	3.69
4	5.5319	34.3	45.1	1.32	3.69
5	5.7873	35.8	58.2	1.62	3.95
6	6.0427	37.4	60.9	1.63	3.96
7	6.2982	39.0	63.6	1.63	3.96
8	6.5536	40.6	66.3	1.63	3.96
9	6.8090	42.2	69.0	1.64	3.96
10	7.0644	43.8	71.7	1.64	3.97
11	7.3198	45.3	74.3	1.64	3.97
12	7.5752	46.9	77.0	1.64	3.97
13	7.8306	48.5	79.7	1.64	3.97
14	8.0860	50.1	82.4	1.64	3.97
15	8.3414	51.7	85.2	1.65	3.98
16	8.5968	53.2	71.4	1.34	3.71
17	8.8521	54.8	73.6	1.34	3.71
18	9.0058	55.8	60.1	1.08	3.48
19	8.9039	55.1	58.7	1.06	3.47
Total	--	824.5	1200.0	--	--

Table 6.2-5 – ATR Fuel Density Equation

U-235 Density (g/cm^3) ρ_1	Total Fuel Density (g/cm^3) ρ_2
1.00	3.409
1.30	3.671
1.60	3.933
Linear Fit: $\rho_2 = 0.8733\rho_1 + 2.5357$	

Table 6.2-6 – ATR Fuel Number Densities (maximum arc length)

Plate	U-234 (atom/b-cm)	U-235 (atom/b-cm)	U-236 (atom/b-cm)	U-238 (atom/b-cm)	Aluminum (atom/b-cm)	Total (atom/b-cm)
1	1.7026E-05	2.6560E-03	9.8475E-06	1.4089E-04	5.2187E-02	5.5010E-02
2	1.7156E-05	2.6763E-03	9.9226E-06	1.4196E-04	5.2153E-02	5.4998E-02
3	2.1711E-05	3.3869E-03	1.2557E-05	1.7966E-04	5.0974E-02	5.4574E-02
4	2.1618E-05	3.3724E-03	1.2503E-05	1.7889E-04	5.0998E-02	5.4583E-02
5	2.6648E-05	4.1571E-03	1.5413E-05	2.2051E-04	4.9696E-02	5.4115E-02
6	2.6746E-05	4.1724E-03	1.5470E-05	2.2132E-04	4.9670E-02	5.4106E-02
7	2.6790E-05	4.1791E-03	1.5495E-05	2.2168E-04	4.9659E-02	5.4102E-02
8	2.6830E-05	4.1854E-03	1.5518E-05	2.2201E-04	4.9649E-02	5.4098E-02
9	2.6867E-05	4.1911E-03	1.5539E-05	2.2232E-04	4.9639E-02	5.4095E-02
10	2.6901E-05	4.1965E-03	1.5559E-05	2.2260E-04	4.9630E-02	5.4092E-02
11	2.6933E-05	4.2015E-03	1.5577E-05	2.2287E-04	4.9622E-02	5.4089E-02
12	2.6963E-05	4.2061E-03	1.5595E-05	2.2311E-04	4.9614E-02	5.4086E-02
13	2.6990E-05	4.2105E-03	1.5611E-05	2.2334E-04	4.9607E-02	5.4083E-02
14	2.7017E-05	4.2145E-03	1.5626E-05	2.2356E-04	4.9600E-02	5.4081E-02
15	2.7077E-05	4.2239E-03	1.5661E-05	2.2406E-04	4.9585E-02	5.4075E-02
16	2.2037E-05	3.4377E-03	1.2746E-05	1.8235E-04	5.0889E-02	5.4544E-02
17	2.2037E-05	3.4377E-03	1.2745E-05	1.8235E-04	5.0889E-02	5.4544E-02
18	1.7683E-05	2.7586E-03	1.0228E-05	1.4633E-04	5.2016E-02	5.4949E-02
19	1.7487E-05	2.7279E-03	1.0114E-05	1.4470E-04	5.2067E-02	5.4967E-02

Table 6.2-7 – TRIGA Fuel Characteristics

Catalog Number	Element Type	Cladding Type	Fuel Length (in)	Fuel OD (in)	U (wt% fuel)	U (grams)	U-235 (wt% U)	U-235 (grams)	H/Zr Ratio	Zirconium Rod (in)	Reflector Top / Bot. (in)	Reflector OD (in)
101	Standard	Al	14	1.41	8.0	166	20	32	1.0	N/A	4.0 /4.0	1.4
	Standard	Al	15	1.41	8.5	189	20	37	1.6	15	3.53 / 3.53	1.4
103	Standard	SS	15	1.44	8.5	197	20	39	1.6	15	2.6 / 3.7	1.4
105	Standard	SS	15	1.44	12	285	20	56	1.6	15	2.6 / 3.7	1.4
107	Standard	SS	15	1.40	12	271	20	53	1.6	15	2.6 / 3.7	1.4
109	**Standard**	**SS**	**15**	**1.44**	**8.5**	**194**	**70**	**136**	**1.6**	**15**	**2.6 / 3.7**	**1.4**
117	Standard	SS	15	1.44	20	503	20	99	1.6	15	2.6 / 3.7	1.4
119	**Standard**	**SS**	**15**	**1.44**	**30**	**825**	**20**	**163**	**1.6**	**15**	**2.6 / 3.7**	**1.4**
201	Instrumented	Al	15	1.41	8.5	189	20	37	1.6	15	3.53 / 3.53	1.3
203	Instrumented	SS	15	1.44	8.5	197	20	39	1.6	15	3.1 / 3.4	1.4
205	Instrumented	SS	15	1.44	12	285	20	56	1.6	15	3.1 / 3.4	1.4
207	Instrumented	SS	15	1.40	12	271	20	53	1.6	15	3.1 / 3.4	1.4
217	Instrumented	SS	15	1.44	20	503	20	99	1.6	15	3.1 / 3.4	1.4
219	Instrumented	SS	15	1.44	30	825	20	163	1.6	15	3.1 / 3.4	1.4
303	FFCR	SS	15	1.31	8.5	163	20	32	1.6	15	n/a	n/a
305	FFCR	SS	15	1.31	12	237	20	47	1.6	15	n/a	n/a
317	FFCR	SS	15	1.31	20	418	20	82	1.6	15	n/a	n/a
319	FFCR	SS	15	1.31	30	685	20	135	1.6	15	n/a	n/a
403	Cluster	SS	15	1.37	8.5	166	20	33	1.6	15	3.42 / 3.42	1.3
405	Cluster	SS	15	1.37	12	243	20	48	1.6	15	3.42 / 3.42	1.3
417	Cluster	SS	15	1.37	20	427	20	85	1.6	15	2.6 / 3.4	1.3
419	Cluster	SS	15	1.37	30	710	20	141	1.6	15	2.6 / 3.4	1.3
503	Ins. Cluster	SS	15	1.34	8.5	166	20	33	1.6	15	3.42 / 3.42	1.3
505	Ins. Cluster	SS	15	1.34	12	243	20	48	1.6	15	3.42 / 3.42	1.3
517	Ins. Cluster	SS	15	1.34	20	427	20	85	1.6	15	2.6 / 3.4	1.3
519	Ins. Cluster	SS	15	1.34	30	710	20	141	1.6	15	2.6 / 3.4	1.3

Note: The "Catalog Numbers" do not necessarily uniquely identify fuel. See full specification for identification.

Table 6.2-8 – TRIGA Fuel Pellet Mass Densities

Isotope	Type 109 (g/cm^3)	Type 119 (g/cm^3)
H	0.094	0.086
Zr	5.306	4.872
U-235	0.353	0.420
U-238	0.152	1.705
Total	5.904	7.083

Table 6.2-9 – PULSTAR Fuel Characteristics

Parameter	4% U-235	6% U-235
Fuel Meat Material	Uranium Oxide (UO_2)	Uranium Oxide (UO_2)
Cladding Material	Zirconium Alloy	Zirconium Alloy
Shape	25 fuel rods loaded in a 5 by 5 matrix in a rectangular can	25 fuel rods loaded in a 5 by 5 matrix in a rectangular can
Fuel Rod		
Maximum fuel pellet diameter	0.423"	0.423"
Minimum cladding thickness	0.0185"	0.0185"
Outer diameter	0.474" – 0.471"	0.474" – 0.471"
Active fuel height	24.0" Nom, 24.1" Max	24.0" Nom, 24.1" Max
Length	26.2 ± 0.005"	26.2 ± 0.005"
Rod Pitch	0.524 x 0.606 ± 0.002"	0.524 x 0.606 ± 0.002"
Fuel Assembly		
Length	37.98" (Nom)	37.98" (Nom)
Outside Width	2.740" x 3.150" ± 0.020"	2.740" x 3.150" ± 0.020"
Box wall thickness	0.06" (Nom)	0.06" (Nom)
Fuel Rod Weight	1.45 pounds (Nom)	1.45 pounds (Nom)
Fuel Assembly Weight	44 pounds (Nom)	44 pounds (Nom)
Enrichment (wt% U_{235})	4% ± 0.056%	6% (Nom)
U_{235} content per fuel rod	20.17 g ± 2%	30.8 g (Nom)
Percent theoretical density	10.4 – 10.7 g/cc	10.4 – 10.7 g/cc
U Weight (kg/fuel rod)	0.504 kg ± 2%	0.514 kg (Nom)
U Weight (kg/fuel assembly)	12.6 kg ± 2%	12.8 kg (Nom)
UO_2 Weight (kg/fuel assembly)	14.3 kg ± 2%	14.3 kg ± 2%

Table 6.2-10 – PULSTAR Fuel Pellet Mass Densities

Isotope	Mass Density (g/cm^3)
O	1.244
U-235	0.555
U-238	8.694
Total	10.494

Table 6.2-11 – Square Plate Fuel Characteristics

Element	Fuel Form	U-235 Mass per Element (g)	U-235 Mass Uncertainty (± g)	Plates per Element	U-235 Mass per Plate (nom.) (g)	Plate Geometry	Fuel Meat Thickness (nom.) (in)	Max Fuel Meat Width (in)	Max Fuel Meat Length (in)	Min Cladding Thickness (in)	Max Channel Spacing (in)
RINSC	U_3Si_2-Al	275.0	7.7	22	12.5	flat	0.020	2.47	24.0	0.005	0.099
Missouri S&T	U_3Si_2-Al	225.0	6.3	18	12.5	curved	0.020	2.47	24.0	0.005	0.139
U-Mass (Si)	U_3Si_2-Al	200.0	5.6	16	12.5	flat	0.020	2.47	24.0	0.005	0.122
U-Mass (Al)	UAl_X	167.0	3.3	18	9.3	flat	0.030	2.50	24.0	0.005	0.119
Ohio State	U_3Si_2-Al	200.0	5.6	16	12.5	flat	0.020	2.47	24.0	0.005	0.127
U-Florida	U_3Si_2-Al	175.0	4.9	14	12.5	flat	0.020	2.47	24.0	0.005	0.117
Purdue	U_3Si_2-Al	129.92	2.52	14	9.3	flat	0.020	2.47	24.0	0.005	0.175

Table 6.2-12 – Square Plate Fuel Meat Mass Densities

Isotope	RINSC, Missouri S&T, U-Mass (Si), Ohio State, U-Florida (g/cm^3)	Purdue (g/cm^3)	U-Mass (Al) (g/cm^3)
Al	1.908	2.117	2.472
Si	0.261	0.192	-
U-235	0.661	0.487	0.321
U-238	2.654	1.954	1.287
Total	5.485	4.750	4.079

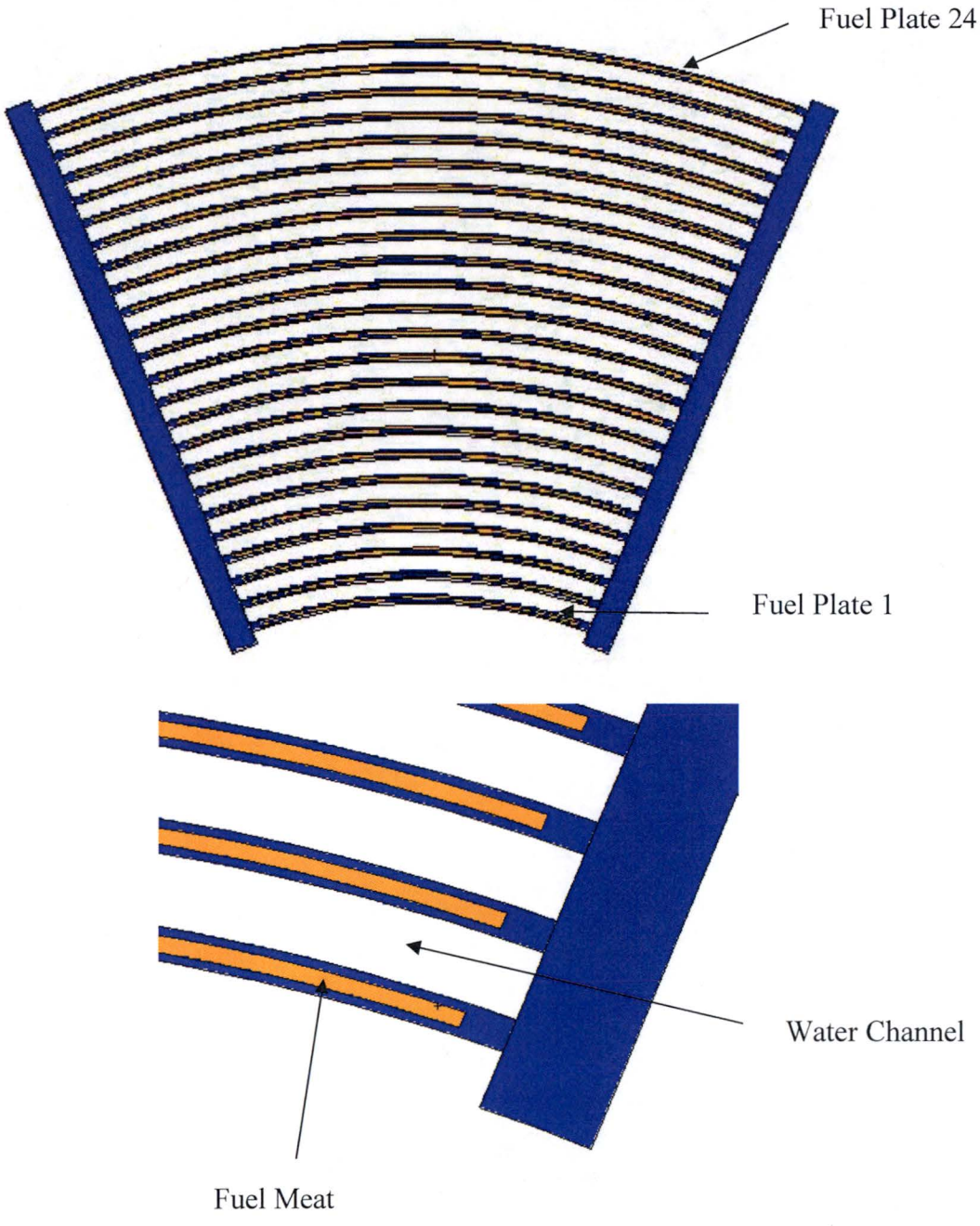

Figure 6.2-1 – MURR Fuel Element Model

(continued)

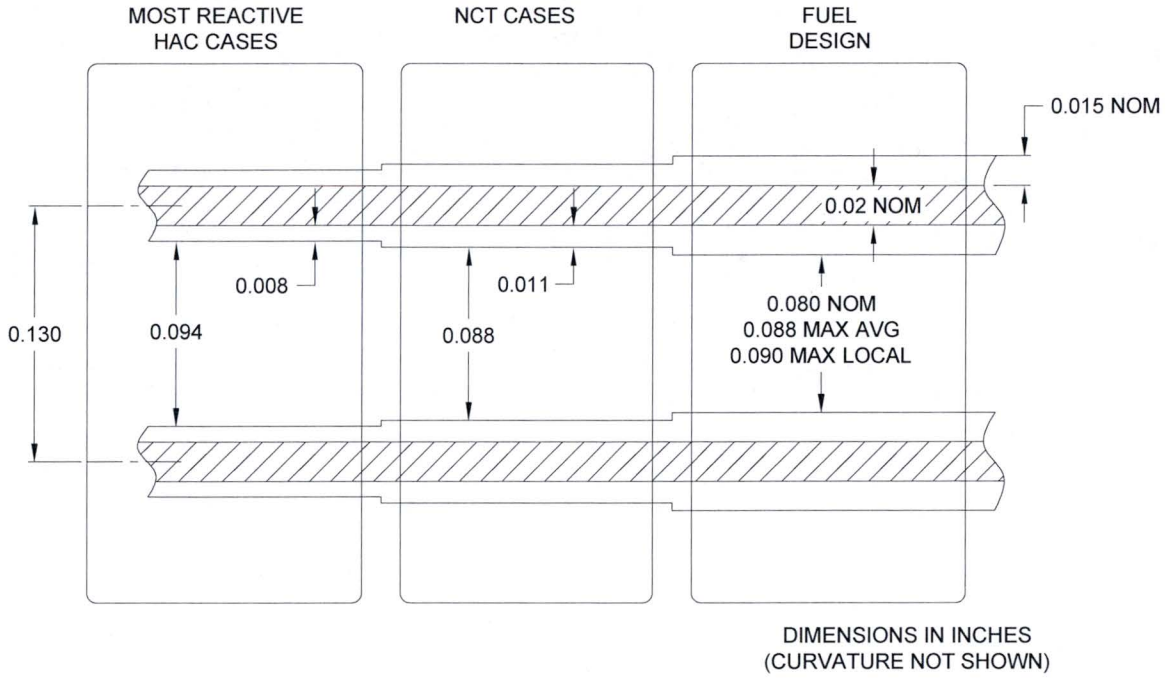

Figure 6.2-1 – MURR Fuel Element Model (concluded)

Security-Related Information Figure Withheld Under 10 CFR 2.390.

Figure 6.2-2 – MURR Fuel Element Details

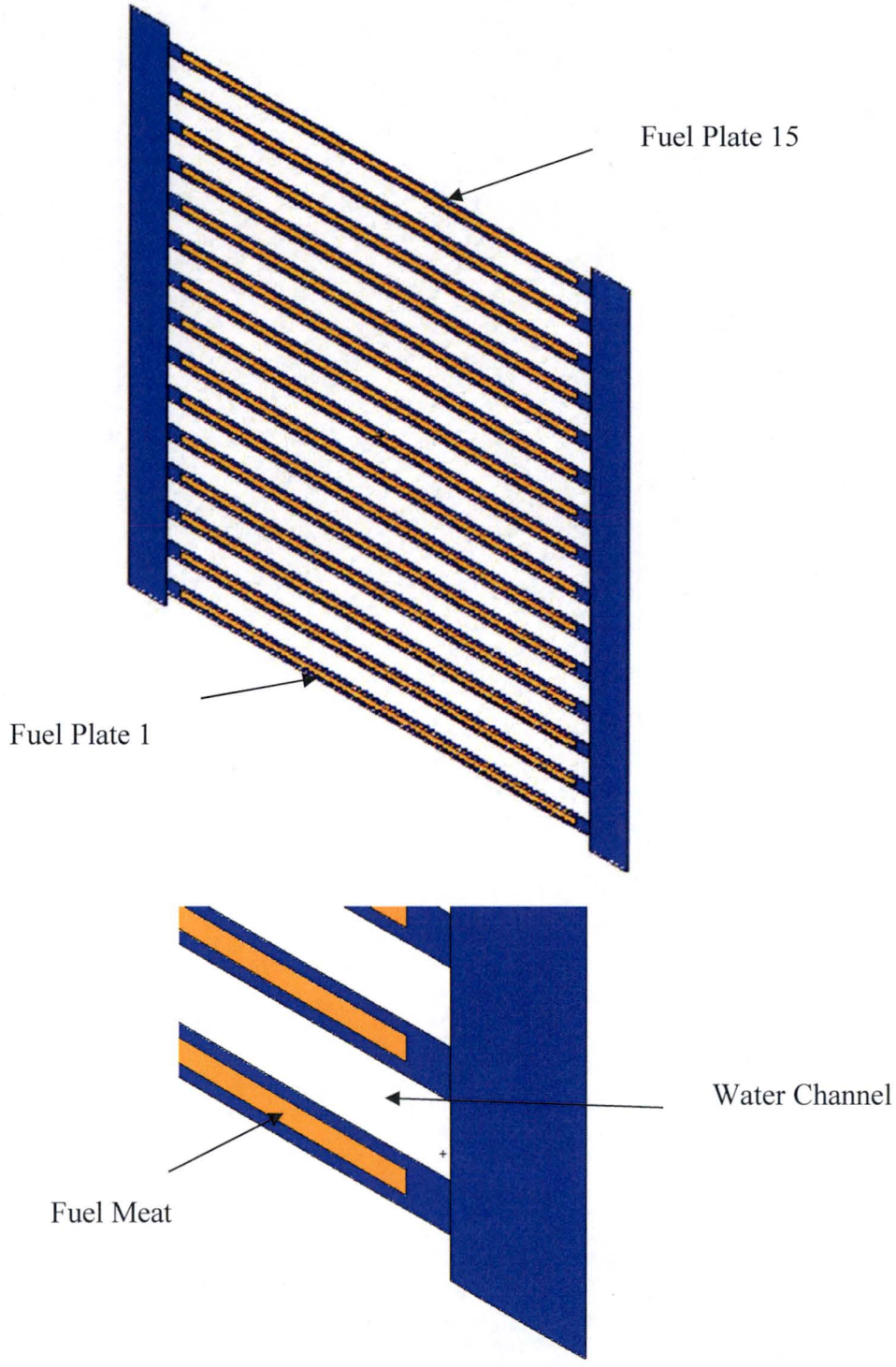

Figure 6.2-3 – MITR-II Fuel Element Model

(continued)

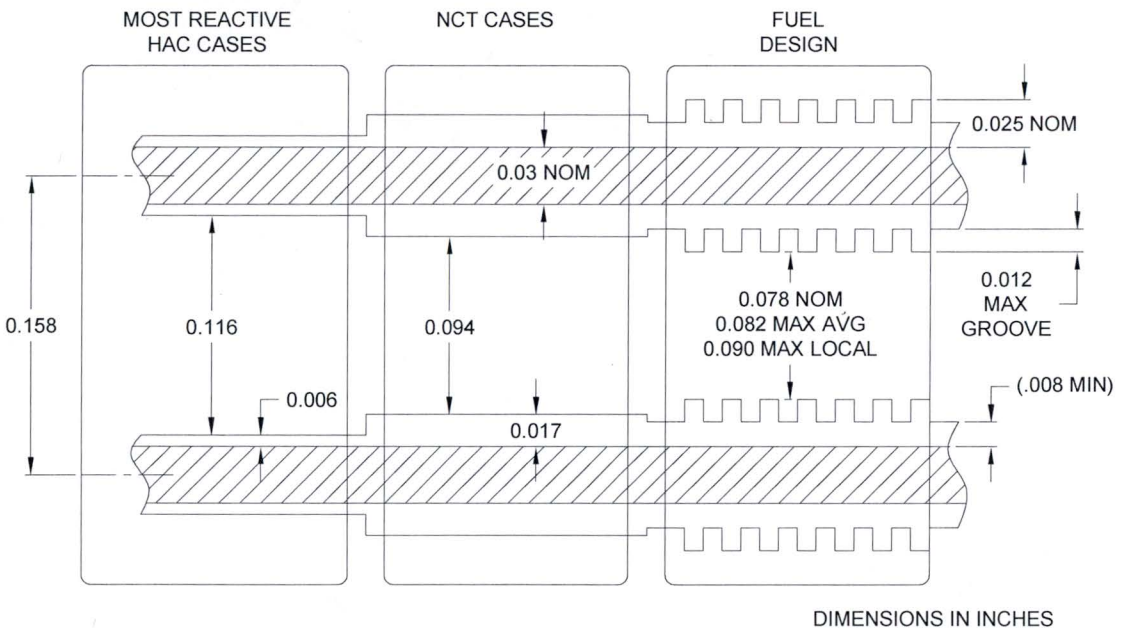

Figure 6.2-3 – MITR-II Fuel Element Model (concluded)

Security-Related Information Figure Withheld Under 10 CFR 2.390.

Figure 6.2-4 – MITR-II Fuel Element Details

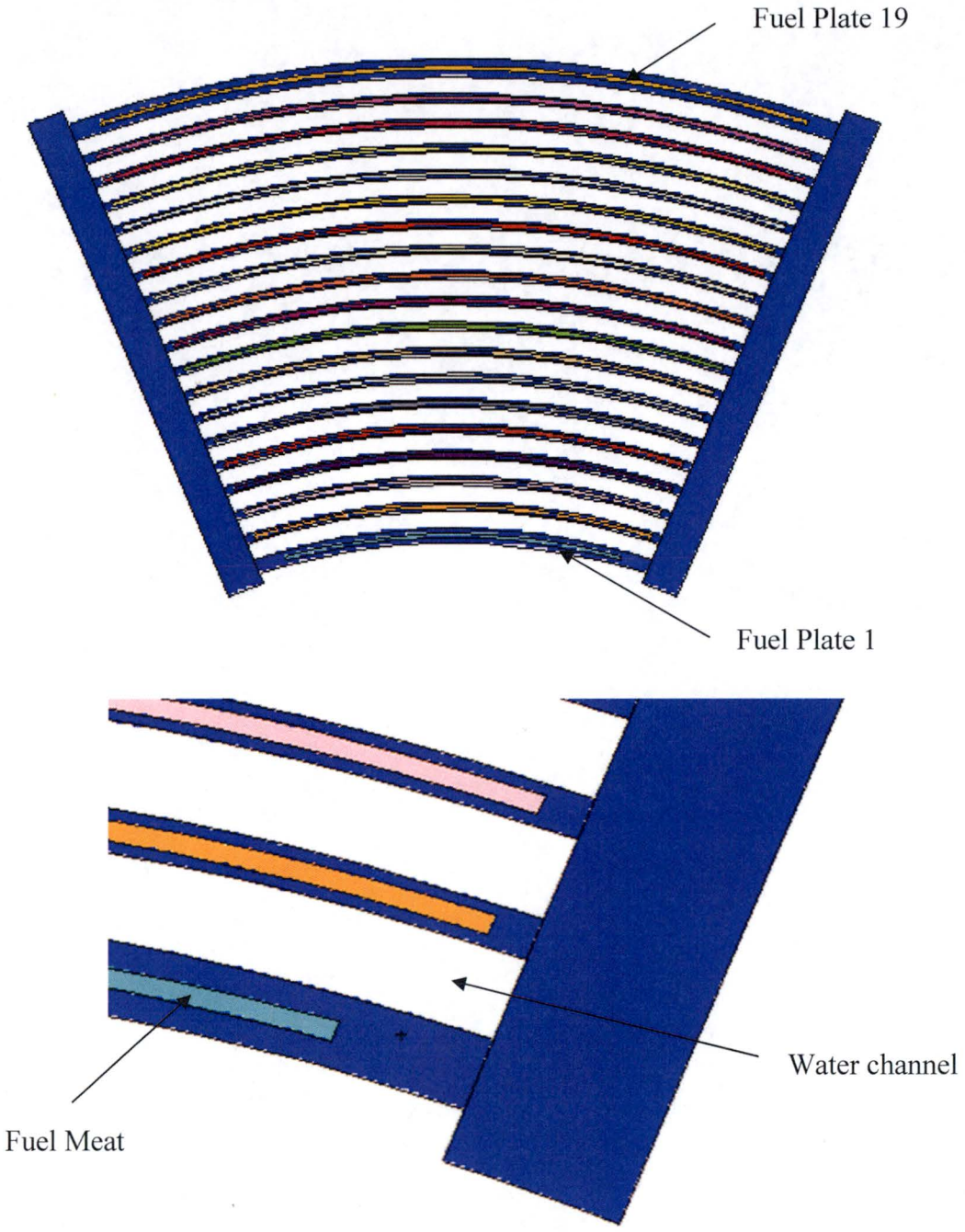

Figure 6.2-5 – ATR Fuel Element Model

(continued)

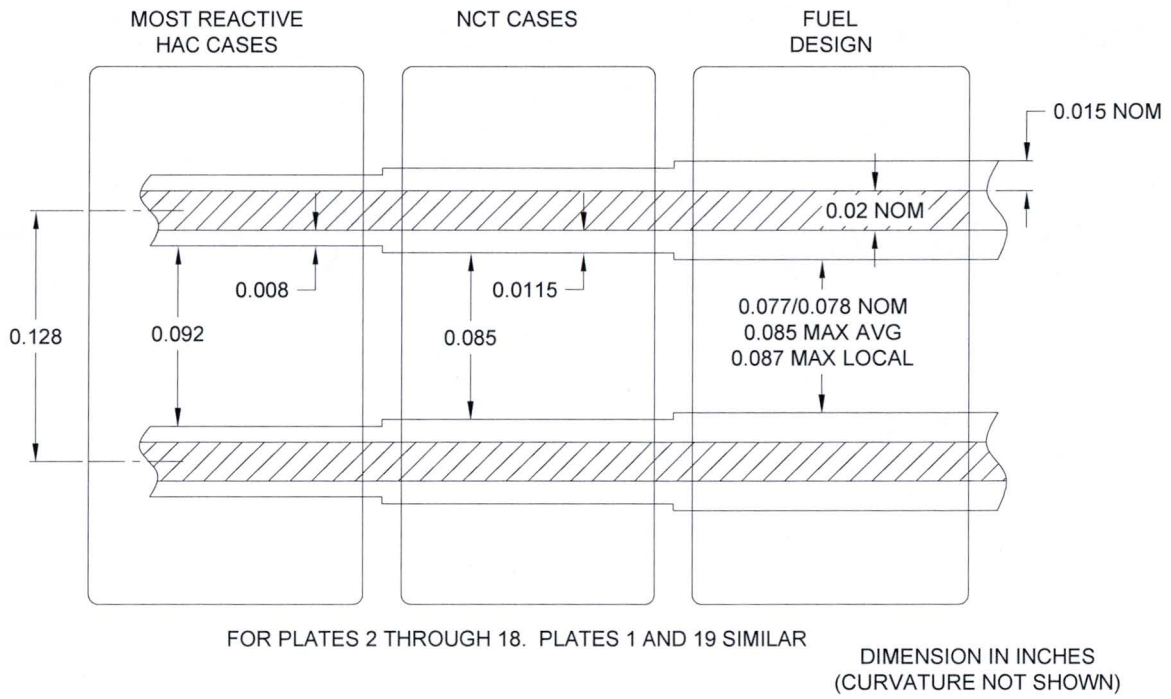

Figure 6.2-5 – ATR Fuel Element Model (concluded)

Security-Related Information Figure Withheld Under 10 CFR 2.390.

Figure 6.2-6 – ATR Fuel Element Details

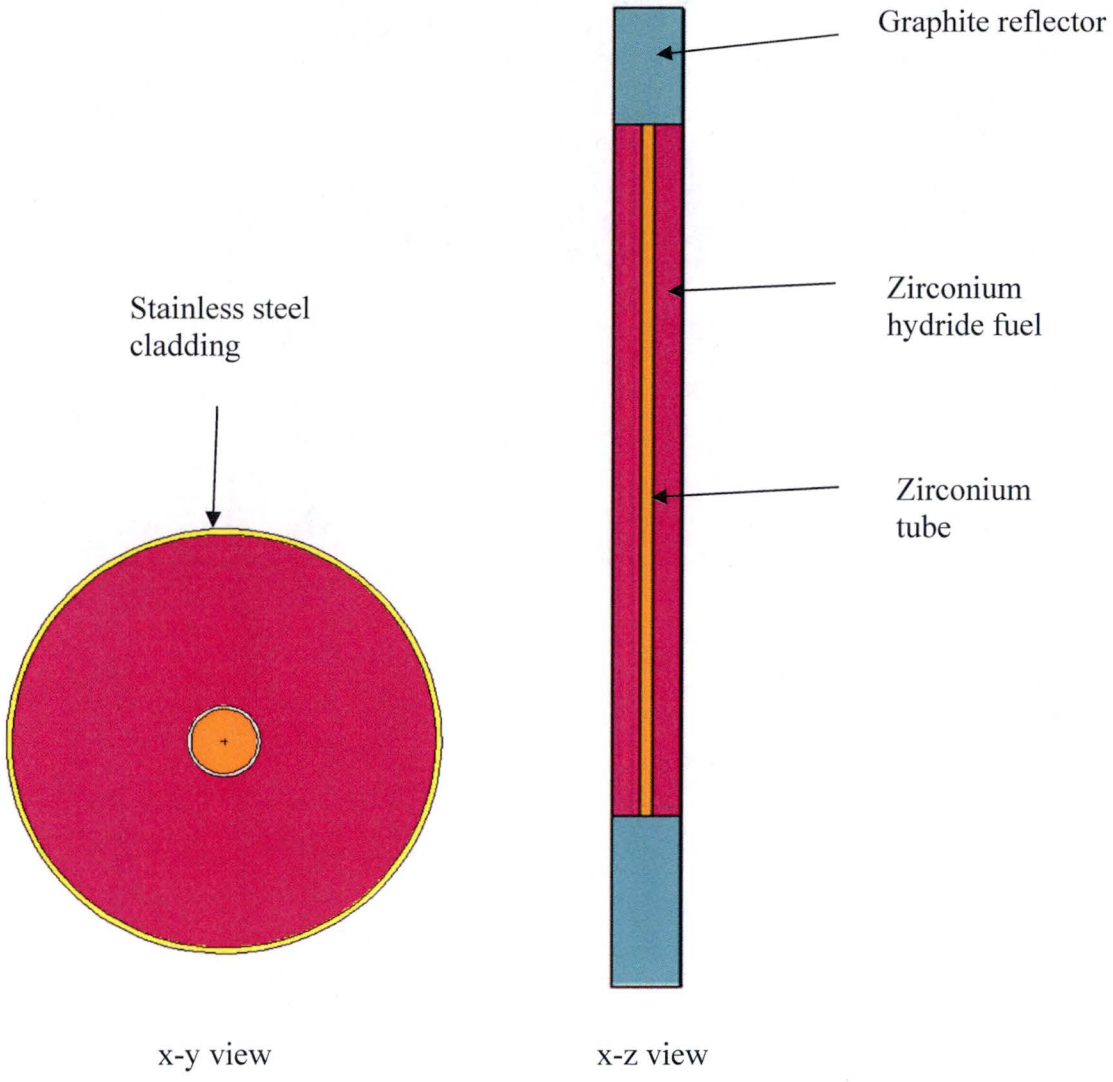

Figure 6.2-7 – Stainless Steel Clad TRIGA Fuel Element (Type 109)

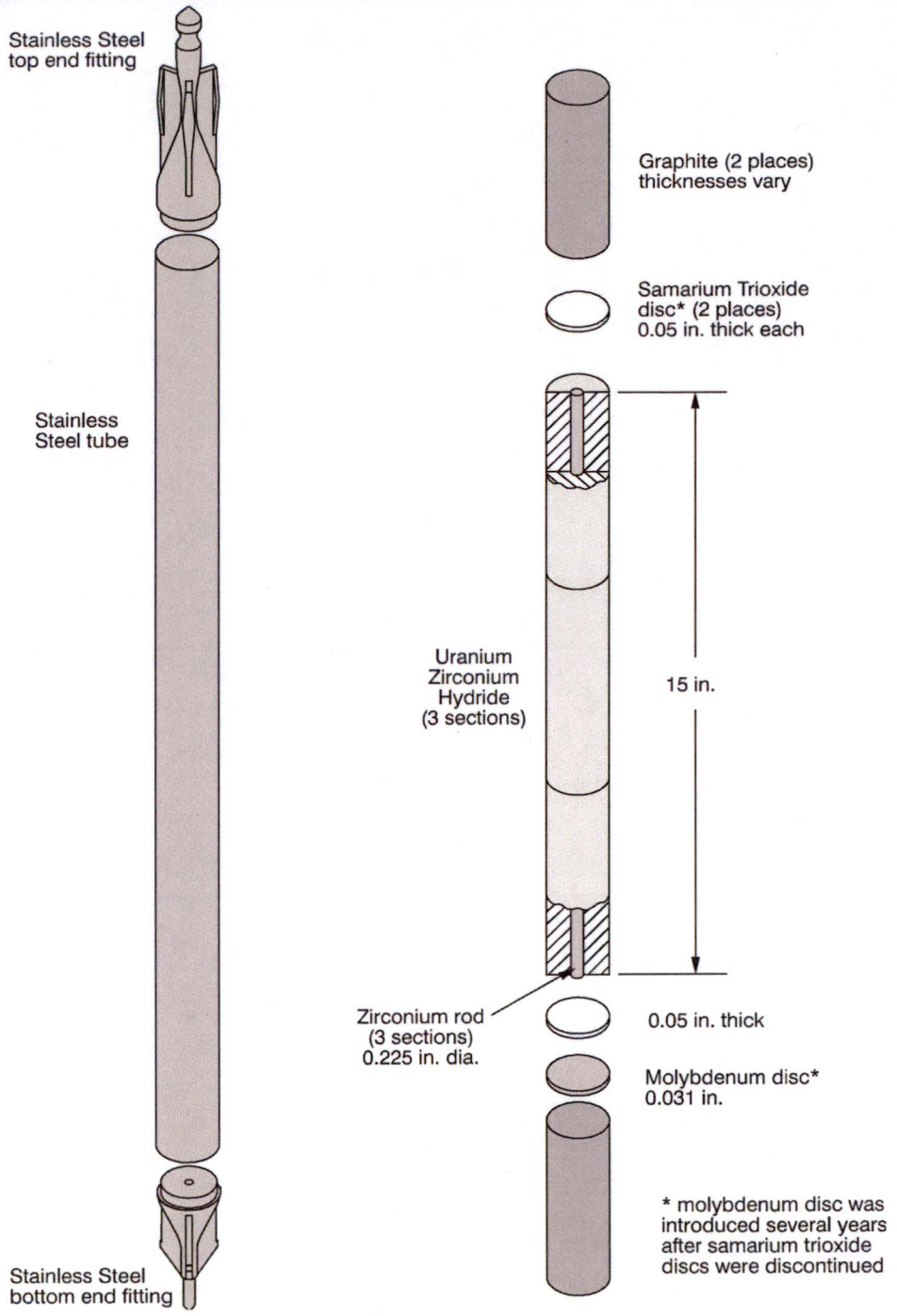

Figure 6.2-8 – Typical Stainless Steel Clad TRIGA Fuel Element

Security-Related Information Figure Withheld Under 10 CFR 2.390.

Dimensions in inches

Figure 6.2-9 – PULSTAR Fuel Element

6.3 General Considerations

6.3.1 Model Configuration

The BRR cask is modeled using conservative simplifying assumptions. The impact limiters are not modeled, and in the single package cases the cask is reflected with 12-in of water. In the array cases, removing the impact limiters conservatively minimizes the separation between the packages and increases the reactivity. The cask body itself is simply modeled as cylinders of steel-lead-steel without modeling the minor cask details, as these minor details have a negligible effect on the system reactivity.

The modeled cask geometry is shown in Figure 6.3-1, and the key model dimensions are provided in Table 6.3-1. Cask dimensions are based on the drawings in Section 1.3.3, *Packaging General Arrangement Drawings*. Note that the cask model in the upper region is simply representative of the shield plug thicknesses and that the 2-in thick steel lid is not included in the model, thereby bringing the casks closer together in the array configuration.

Five baskets are available to accommodate the different fuel geometries. The baskets are modeled in sufficient detail to capture the relevant criticality effects, which are primarily of interest near the active fuel region. The key basket dimensions are included in Table 6.3-2, and x-y and x-z views of the five basket designs are provided in Figure 6.3-2 and Figure 6.3-3, respectively. Basket dimensions are based on the drawings in Section 1.3.3, *Packaging General Arrangement Drawings*. Note that the axial and radial fuel positions shown in these figures do not reflect the most reactive configurations, which is determined in Section 6.4, *Single Package Evaluation.*

Minor differences exist between the as-modeled and packaging general arrangement drawing dimensions, as shown in Table 6.3-1 and Table 6.3-2. These differences are small and are within the uncertainty of the Monte Carlo method and may therefore be neglected.

The baskets are modeled as undamaged in all NCT and HAC models. The baskets have been shown to be elastic in all accident scenarios and maintain their geometry (see Section 2.7.1.5, *Fuel Basket Stress Analysis*). The fuel is modeled in the most reactive axial location and the spacer pedestals are ignored. The LPB has also been shown to maintain its structural integrity in an accident and is credited in the analysis.

With the exception of U-Florida, all fuels transported in the BRR are shown to maintain their structural integrity in an accident (see Section 2.7.1.6, *Fuel Impact Deformation*). Because structural integrity under HAC for U-Florida has not been demonstrated, conservative fuel damage is modeled for U-Florida in which the plates reconfigure within the basket compartment at the most reactive uniform or non-uniform pitch. While PULSTAR fuel is shown to maintain its structural integrity in an accident, damage to PULSTAR fuel under HAC is conservatively modeled. Under HAC, PULSTAR rods are repositioned at the maximum pitch possible within the confines of the fuel element box.

In the NCT cases, credit is taken for the leaktight nature of the package, and the cask cavity is modeled as dry (void). Although the package has been shown to be leaktight under accident conditions, in the HAC cases, water is conservatively modeled in the cask cavity at the density that maximizes reactivity. If it is assumed that water is free to flow throughout the cask cavity and fuel elements (as the baskets are designed to drain freely), the moderator water density

between the fuel plates may be modeled at the same value as the water density between the fuel elements. This assumption is utilized in all MCNP criticality models. However, it has been shown that when an ATR fuel element is removed from a spent fuel pool and allowed to drip dry, a small volume of water remains between the fuel plates due to the surface tension in the thin channels between the fuel plates. Because the quantity of residual water is relatively small, any minor surface tension effects have been neglected in the MCNP modeling. In addition, no models are developed in which the cask is partially filled with water with some fuel elements uncovered (such as might be the case if the cask were on its side in an accident), because this scenario would be less reactive due to lack of moderation in the uncovered fuel elements.

In the array cases, a close-packed hexagonal array is modeled by adding a hexagonal reflective boundary condition. The water density between the casks in the array is adjusted to determine the most reactive condition.

6.3.2 Material Properties

The fuel meat compositions are provided in Table 6.2-2, Table 6.2-3, Table 6.2-6, and Table 6.2-8 for MURR, MITR-II, ATR, and TRIGA fuel, respectively. Fuel meat compositions for PULSTAR and Square plate fuels are provided in Table 6.2-10 and Table 6.2-12, respectively. For all fuels, aluminum structural material is modeled as pure aluminum with a density of 2.7 g/cm^3. Similarly, all zirconium alloy is modeled as pure zirconium with a density of 6.5 g/cm^3.

The TRIGA fuel contains materials not found in the aluminum plate fuels, such as stainless steel, graphite, and zirconium. For the stainless steel clad TRIGA fuel, the composition of stainless steel utilized is the standard composition provided in the SCALE material library [4] and is provided in Table 6.3-3. For the TRIGA fuels that contain a zirconium rod in the center of the fuel element, the zirconium is modeled as pure with a density of 6.5 g/cm^3. The graphite reflectors in the TRIGA fuel elements is modeled as pure graphite with a density of 1.6 g/cm^3. The density is obtained from the TRIGA benchmark experiments (IEU-COMP-THERM-003) listed in the *International Handbook of Evaluated Criticality Benchmark Experiments* [3]. The material properties of the remaining packaging and moderating materials are described as follows.

The inner and outer shells of the package are constructed from stainless steel 304. The baskets and LPB are also constructed of stainless steel 304. The standard compositions for stainless steel 304 are obtained from the SCALE material library [4], which is a standard set accepted for use in criticality analyses. The stainless steel composition and density utilized in the MCNP models are provided in Table 6.3-3. Lead is modeled as pure with a density of 11.35 g/cm^3.

Water is modeled with a density ranging up to 1.0 g/cm^3 and the chemical formula H_2O.

6.3.3 Computer Codes and Cross-Section Libraries

MCNP5 v1.30 is used for the criticality analysis [1]. All cross sections utilized are at room temperature (293.6 K). The uranium isotopes utilize preliminary ENDF/B-VII cross section data that are considered by Los Alamos National Laboratory to be more accurate than ENDF/B-VI cross sections. ENDF/B-V cross sections are utilized for chromium, nickel, iron, and lead because natural composition ENDF/B-VI cross sections are not available for these elements. The remaining isotopes utilize ENDF/B-VI cross sections. Titles of the cross sections utilized in

the models have been extracted from the MCNP output (when available) and provided in Table 6.3-4. The S(α,β) card LWTR.60T is used to simulate hydrogen bound to water in all models. For the TRIGA models only, the S(α,β) cards H/ZR.60T and ZR/H.60T are used to simulate hydrogen and zirconium in zirconium hydride, respectively.

All moderated ATR, MITR-II, MURR, and TRIGA cases are run with at least 2500 neutrons per generation for 250 generations, skipping the first 50. All moderated PULSTAR and Square fuel basket intact fuel element cases are run with at least 5000 neutrons per generation for 250 generations, skipping the first 50 (some cases use 15,000 neutrons per generation for 200 generations, skipping the first 25, which is a larger number of total neutrons run). All moderated loose plate box and damaged U-Florida cases are run with 5000 neutrons per generation for 1050 generations, skipping the first 50. The 1-sigma uncertainty is approximately 0.001 or less for the HAC cases, and somewhat less for the NCT cases.

6.3.4 Demonstration of Maximum Reactivity

The reactivities of the NCT single package and array cases are small (<0.6) because the package is leaktight and no water is present in the package cavity. The TRIGA fuel is the most reactive under NCT because hydrogen moderator is included in the zirconium hydride fuel matrix, although the reactivity is still relatively low.

Under HAC, water is allowed to enter the package cavity at the density that maximizes reactivity. For the intact plate fuels, the system is always the most reactive when full-density water is utilized because the system is undermoderated. Because the intact plate fuel is undermoderated, modeling the minimum cladding thickness and hence maximum channel spacing results in the most reactive condition. For the TRIGA fuel, optimum reactivity is achieved for a reduced water density (0.6 or 0.7 g/cm^3).

It is demonstrated that reactivity increases when the fuel is axially shifted to the top of the cavity, as this configuration maximizes reflection from the lead in the shield plug. It is also demonstrated that reactivity increases when the fuel elements are moved to the radial center of the package. For the MITR-II fuel, which has an inner and outer row of fuel elements, reactivity is maximized by moving the inner row outward and the outer row inward, which decreases the distance between the fuel elements.

For the array cases, a hexagonal reflective boundary condition is placed around the cask, simulating a hexagonal lattice. The water density between the packages is varied between 0 and 1.0 g/cm^3, and the array reactivities (both NCT and HAC) are maximized with no water between the packages.

It has been demonstrated in the structural analysis that the baskets and LPB maintain their structural integrity during an accident condition. With the exception of U-Florida, all fuels transported in the BRR are shown to maintain their structural integrity in an accident. Because structural integrity under HAC for U-Florida has not been demonstrated, conservative fuel damage is modeled for U-Florida in which the plates reconfigure within the basket compartment at the most reactive uniform or non-uniform pitch. While PULSTAR fuel is shown to maintain its structural integrity in an accident, damage to PULSTAR fuel under HAC is conservatively modeled. Under HAC, PULSTAR rods are repositioned at the maximum pitch possible within the confines of the fuel element box.

The MURR payload is the most reactive, with $k_s = 0.827$ (Case D8), which is below the USL of 0.9209. This most reactive case occurs under HAC-array conditions, with full density water flooding the basket and no water between packages.

Table 6.3-1 – Key Cask Model Dimensions

Item	Dimension (in)
Cask Radial	
Cask inner diameter	16.0
Cask inner steel thickness	1.0
Cask lead thickness	8.0
Cask outer steel thickness	2.0
Cask outer diameter (w/o heat shield)	38.00
Cask Axial Top	
Shield plug bottom plate thickness	1.0
Shield plug lead thickness	9.7, modeled as 9.58
Shield plug top plate thickness	0.5
Shield plug overall height	11.2, modeled as 11.08
Cask Axial Bottom	
Bottom outer plate thickness	1.0
Bottom lead thickness at centerline	7.7, modeled as 7.72
Bottom casting inner thickness (after machining)	1.1, modeled as 1.22

Table 6.3-2 – Key Basket Model Dimensions

Item	Dimension (in)
MURR Basket	
Compartment separator width	1.0
Shell outer diameter	15.63
Shell thickness	0.25
Inner tube outer diameter	7.9, modeled as 7.938
Inner tube inner diameter	7.0
MITR-II Basket	
Compartment perpendicular width	2.7
Inner Diameter	Complex, modeled as 9.45
Outer Diameter	15.63
Distance, cutout to center	4.8
ATR Basket	
Compartment separator width	0.375
Shell outer diameter	13.5
Shell thickness	0.25
Inner tube outer diameter	7.2
Inner tube inner diameter	6.5
TRIGA Basket	
Tube outer diameter	2.0
Tube wall thickness	0.12, modeled as 0.11
Inner row position diameter	6.5
Outer row position diameter	11.5
Square Fuel Basket	
Compartment Width (Square)	3.40
Wall thickness	0.1054
Centerline radius, outer compartments	5.42
Loose Plate Box	
Inner lateral dimensions	3.0 x 2.5
Plate thickness	0.125

Table 6.3-3 – SS304 Composition

Component	Wt.%
C	0.08
Si	1.0
P	0.045
Cr	19.0
Mn	2.0
Fe	68.375
Ni	9.5
Density (g/cm^3)	7.94

Table 6.3-4 – Cross Section Libraries Utilized

Isotope/Element	Cross Section Label (from MCNP output)
1001.62c	1-h-1 at 293.6K from endf-vi.8 njoy99.50
6000.66c	6-c-0 at 293.6K from endf-vi.6 njoy99.50
8016.62c	8-o-16 at 293.6K from endf-vi.8 njoy99.50
13027.62c	13-al-27 at 293.6K from endf-vi.8 njoy99.50
14000.60c	14-si-nat from endf/b-vi
15031.66c	15-p-31 at 293.6K from endf-vi.6 njoy99.50
17000.66c	17-cl-0 at 293.6K from endf-vi.0 njoy99.50
24000.50c	njoy
25055.62c	25-mn-55 at 293.6K from endf/b-vi.8 njoy99.50
26000.55c	njoy
28000.50c	njoy
40000.66c	40-zr-0 at 293.6K from endf-vi.1 njoy99.50
82000.50c	njoy
92234.69c	92-u-234 at 293.6K from t16 u234la4 njoy99.50
92235.69c	92-u-235 at 293.6K from t16 u235la9d njoy99.50
92236.69c	92-u-236 at 293.6K from t16 u236la2d njoy99.50
92238.69c	92-u-238 at 293.6K from t16 u238la8h njoy99.50

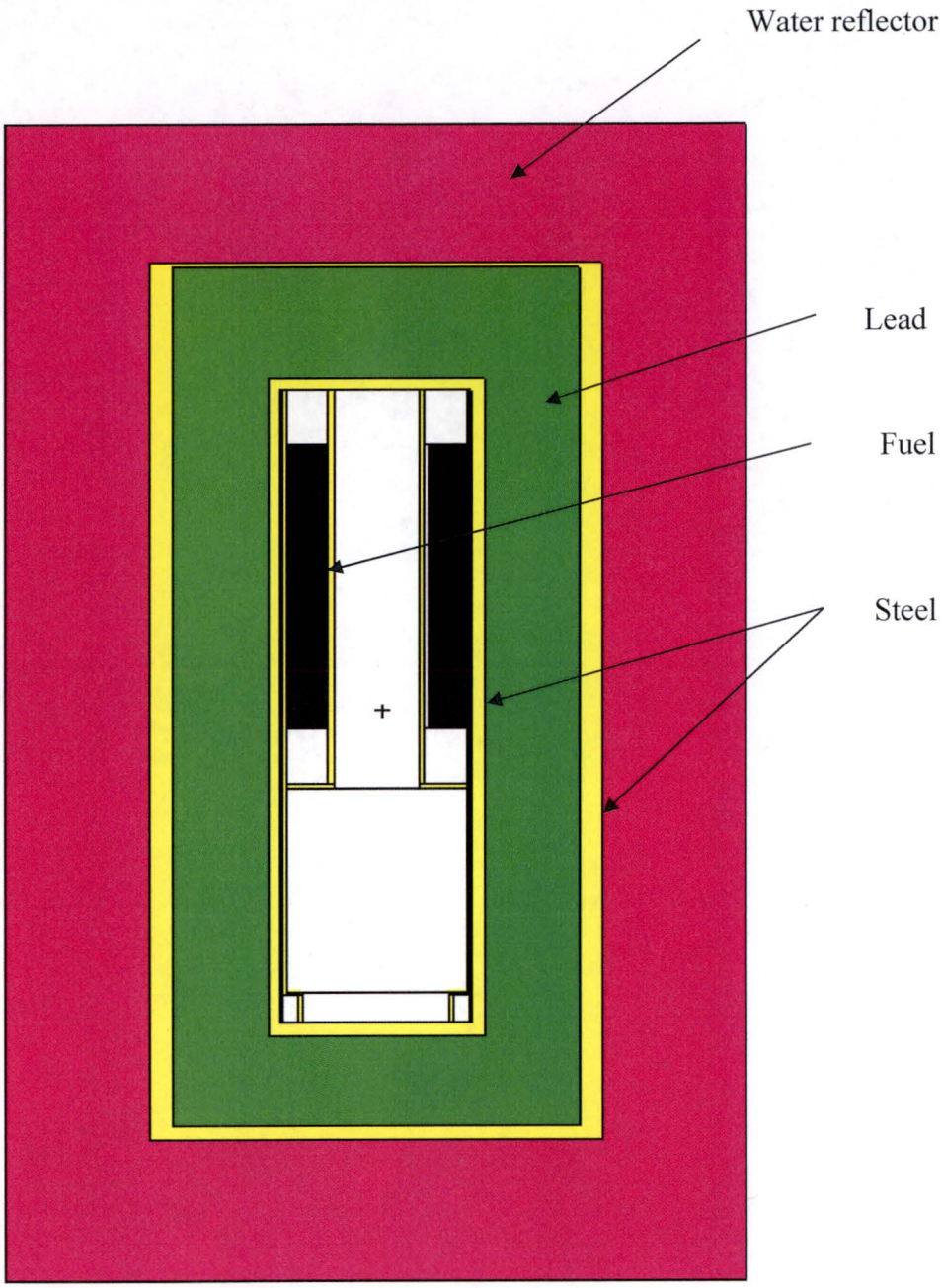

Figure 6.3-1 – NCT Single Package Model (x-z view)

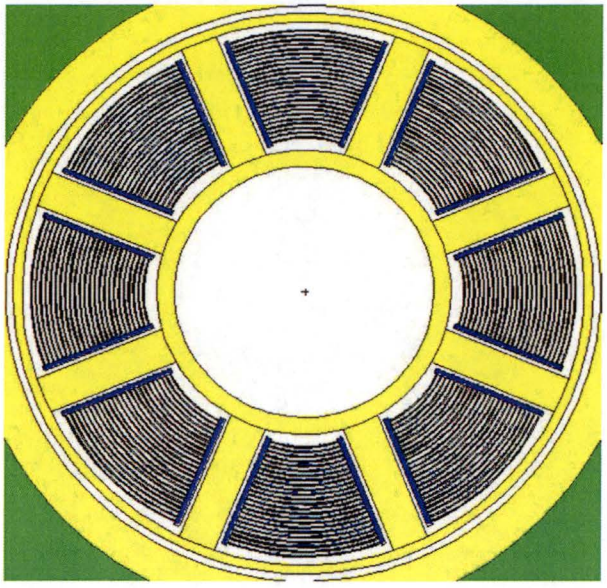

MURR

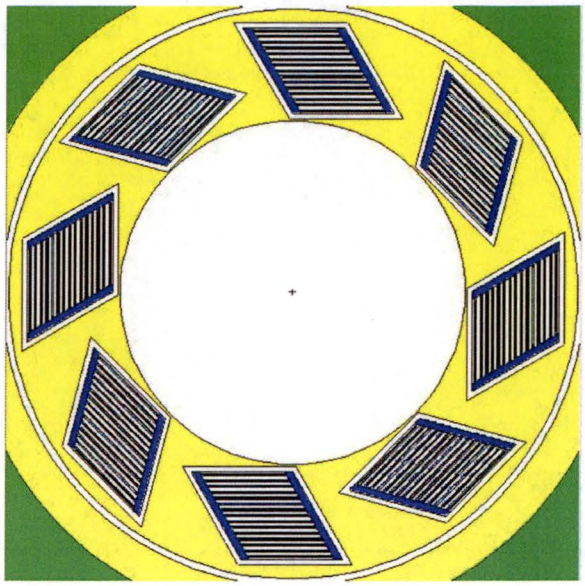

MITR-II

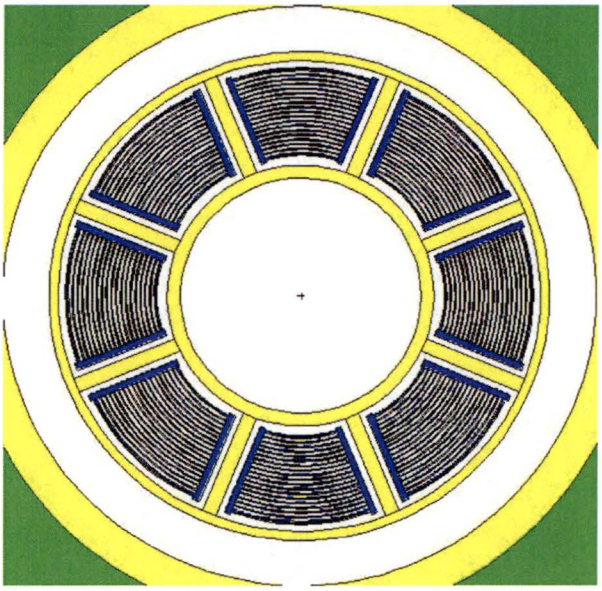

ATR

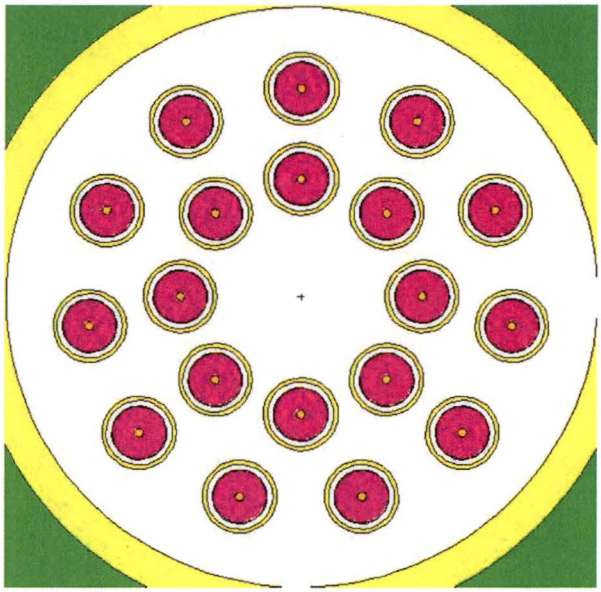

TRIGA

Figure 6.3-2 – Basket Models (x-y view)

(continued)

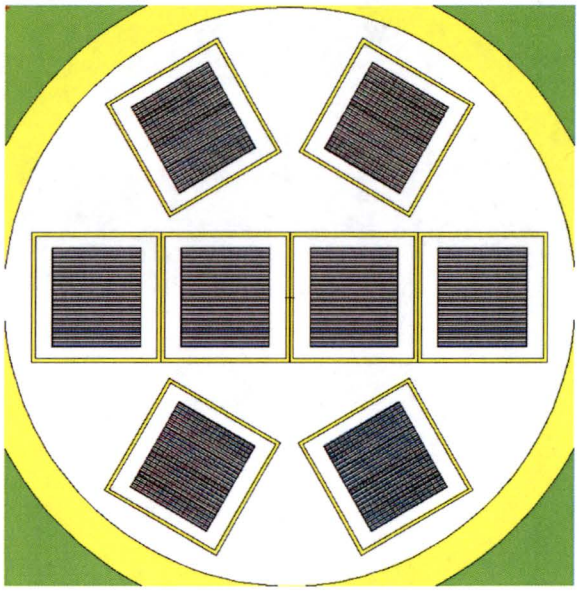

Square Fuel Basket

Figure 6.3-2 – Basket Models (x-y view) (concluded)

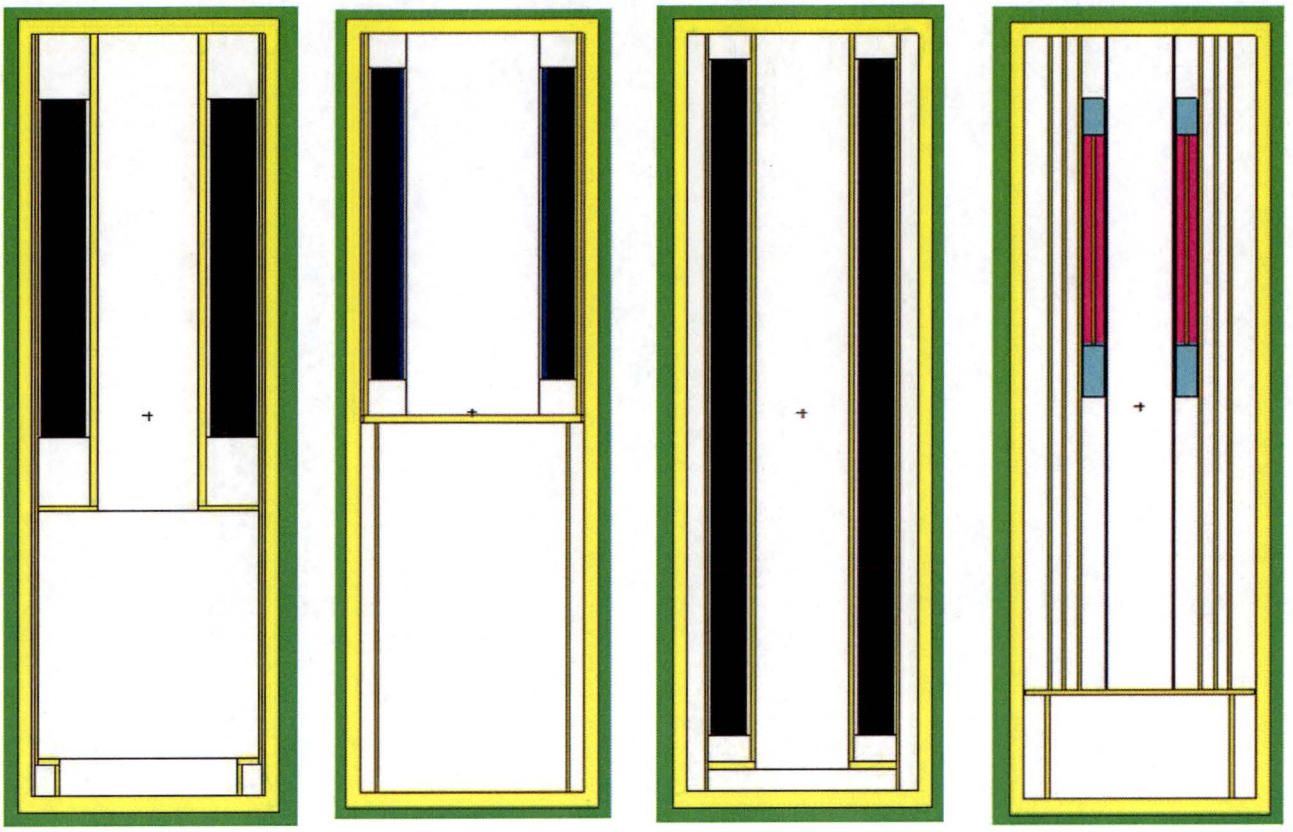

Figure 6.3-3 – Basket Models (x-z view)
(continued)

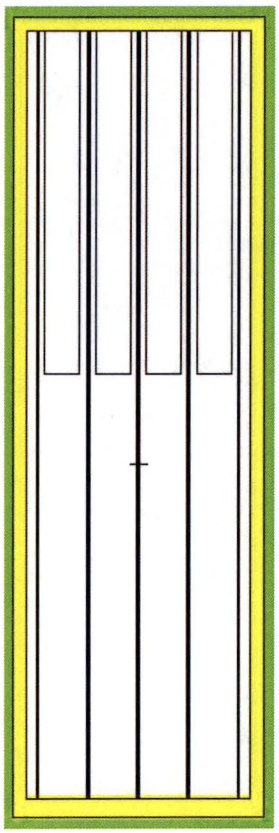

Square Fuel Basket

Figure 6.3-3 – Basket Models (x-z view) (concluded)

6.4 Single Package Evaluation

6.4.1 Configuration

6.4.1.1 NCT Single Package Configuration

The geometry of the NCT single package configuration is discussed in Section 6.3.1, *Model Configuration.* For MURR, MITR-II, and ATR, the fuel element geometry is consistent with the most reactive fuel element models, including tolerances, as determined in Section 6.9.2, *Parametric Evaluations to Determine the Most Reactive Fuel Geometries.*

TRIGA models are developed for a bounding subset of the allowable rod types. The bounding rods (catalog numbers 109 and 119) contain the highest enrichment fuel (136 g U-235 at 70 wt.%) and the highest U-235 loading (163 g U-235 at 20 wt. %), respectively. Other permissible rods are all enriched to 20 wt.% U-235. Given no other significant differences in the design of other permissible rods, Type 109 and 119 are justifiably treated as bounding. Molybdenum discs, a mild neutron absorber, are conservatively ignored.

PULSTAR fuel is modeled with the maximum U-235 enrichment of 6%. The Square plate-fuels are modeled with minimum cladding thickness and maximum possible channel spacing, as the analysis for MURR, MITR-II, and ATR indicated this is the most reactive configuration for plate-type fuel.

MURR

The MURR results are listed in Table 6.4-1 as Cases A1 through A3. In Case A1, the active fuel region is centered both axially and laterally within the basket compartments. In Case A2, all fuel elements are moved within the basket compartments towards the radial center. In Case A3, the fuel elements are moved radially inward (like Case A2) and shifted axially to the top of the package. In actual practice, it would not be possible to shift the active fuel all the way to the top due to the presence of the end fittings. This configuration is the most reactive, as reflection from the package shield plug is maximized. Therefore, Case A3 is the most reactive, with k_s = 0.08545. Clearly, the reactivity of unmoderated MURR fuel is very low.

MITR-II

The MITR-II results are listed in Table 6.4-1 as Cases A10 through A13. In Case A10, the active fuel region is centered both axially and laterally within the basket compartments. In Case A11, the fuel elements are moved within the basket compartments towards the radial center. In Case A12, the fuel elements are pushed to the radial center of the package and shifted axially to the top of the package. In actual practice, it would not be possible to shift the active fuel all the way to the top due to the presence of the end fittings. Case A13 is the same as Case A12 except the fuel elements are shifted radially outward rather than radially inward. The reactivity of all four cases is rather similar. Case A12 is the most reactive, with k_s = 0.05836. Clearly, the reactivity of unmoderated MITR-II fuel is very low.

ATR

The ATR results are listed in Table 6.4-1 as Cases A20 through A22. In Case A20, the active fuel region is centered both axially and laterally within the basket compartments. In Case A21, all fuel elements are moved within the basket compartments towards the radial center. In Case

A22, the fuel elements are moved radially inward (like Case A21) and shifted axially to the top of the package. All three configurations have similar reactivities, although Case A22 is the most reactive, with $k_s = 0.08849$. Clearly, the reactivity of unmoderated ATR fuel is very low.

TRIGA

The TRIGA results for Type 109 rods are listed in Table 6.4-2 as Cases A30 through A33. In Case A30, the fuel elements are laterally centered in the basket compartments, and the fuel elements are offset from the package lid. In Case A31, the fuel elements are moved within the basket tubes towards the radial center. In Case A32, the outer row of elements are moved radially inward, and the inner row is moved radially outward. Comparing Cases A30 through A32, Case A31 is the most reactive. In Case A33, the fuel elements are moved radially inward (like Case A31) and shifted axially to the top of the package. In actual practice, it would not be possible to shift the active fuel all the way to the top due to the end fittings. This configuration is the most reactive, as reflection from the package shield plug is maximized. Therefore, Case A33 is the most reactive, with $k_s = 0.41671$. In Case TL1A1, the most reactive configuration for Type 109 is repeated for Type 119, and the reactivity decreases.

Clearly, the reactivity of unmoderated TRIGA fuel is very low and is significantly less than the USL, although the unmoderated TRIGA fuel results in the highest reactivity compared to the other fuel types.

Square Fuel Basket Fuels

In the absence of internal moderation, the reactivity of SFB fuels is low. Therefore, the most reactive moderated cases from Section 6.4.1.2, *HAC Single Package Configuration*, are modeled with no water in the package cavity. A more detailed description of the model geometry for these cases may be found in Section 6.4.1.2. Other configurations are not investigated because the dry system has a remarkably low k_s value and is not significantly sensitive to changes anticipated under NCT conditions.

Results for SFB fuels are provided in Table 6.4-3. The reactivity of the LPB is maximized with the maximum fuel loading (31 plates), and the bounding plate fuel has the largest fissile mass (RINSC). The results are:

- $k_s = 0.14683$ for PULSTAR
- $k_s = 0.05214$ for the LPB, and
- $k_s = 0.03647$ for plate fuels (RINSC)

6.4.1.2 HAC Single Package Configuration

The HAC single package configurations are similar to the NCT single package configurations except that water is allowed inside the package at the most reactive density. PULSTAR, U-Florida, and LPB payloads are further evaluated to account for changed to the geometric configuration of the fuel under HAC.

MURR

The MURR results are summarized in Table 6.4-4 as Cases B1 through B6. In Cases B1 through B5, the cladding thickness and channel spacing are modeled consistent with the NCT analysis. In Cases B1 through B3, the package cavity is flooded with full-density water. In Case B1, the active fuel is centered both laterally and axially within the basket compartments. In Case B2, the

active fuel is moved within the basket compartments towards the radial center. In Case B3, the radial configuration from Case B2 is maintained, and the fuel elements are shifted upward to the maximum possible extent, maximizing reflection from the shield plug. Case B3 is the most reactive of the three configurations examined.

In Cases B4 and B5, the configuration of Case B3 is modified so that the basket/fuel element water density is reduced to 0.8 and 0.9 g/cm^3, respectively. Because the MURR fuel is undermoderated, reducing the water density will reduce the reactivity. As expected, the reactivity for Case B4 and B5 drops rapidly as the water density is reduced.

In Case B6, Case B3 is rerun using the minimum cladding thickness of 0.008-in and channel spacing of 0.094-in. Case B6 is the most reactive, with $k_s = 0.78432$.

MITR-II

The MITR-II results are summarized in Table 6.4-4 as Cases B20 through B28. In Cases B20 through B27, the cladding thickness and channel spacing are modeled consistent with the NCT analysis. In Cases B20 through B25, the package cavity is flooded with full-density water. In Case B20, the active fuel is centered both laterally and axially within the basket compartments. In Case B21, the active fuel is pushed to the radial center of the package, and the reactivity increases. In Case B22, the radial configuration from Case B21 is maintained, and the fuel elements are pushed upward to the maximum possible extent, maximizing reflection from the lid. In Case B23, the fuel is pushed radially outward but shifted upward as in Case B22. Case B22 is the most reactive of the four configurations examined, although the reactivity effect of the axial shifting is small.

In Cases B25 and B26, the reactivity effect of the basket inner cavity radius is examined. The inner cavity of the basket has an irregular shape that is approximated as a cylinder with a radius of 12.0 cm, which is the largest radius that does not interfere with the fuel element cavity cell descriptions. Cases B25 and B26 are the same as Case B20 except this radius is modeled as 11.0 and 11.5 cm, respectively. Reactivity decreases as the radius decreases, indicating that modeling with the largest possible radius of 12.0 cm is conservative.

In Cases B26 and B27, the configuration of Case B22 is modified so that the basket water density is reduced to 0.8 and 0.9 g/cm^3, respectively. Because the fuel elements and basket are free to drain, reducing the water density in the basket also reduces the water density between the fuel plates. Because the MITR-II fuel is undermoderated, reducing the water density will reduce the reactivity. As expected, the reactivity for Case B26 and B27 drops rapidly as the water density is reduced.

In Case B28, Case B22 is rerun using a cladding thickness of 0.006-in and channel spacing of 0.116-in. Case B28 is the most reactive, with $k_s = 0.57382$.

ATR

The ATR results are summarized in Table 6.4-4 as Cases B40 through B45. In Cases B40 through B44, the cladding thickness and channel spacing are modeled consistent with the NCT analysis. In Cases B40 through B42, the package cavity is fully flooded with full-density water. In Case B40, the fuel elements are centered both axially and laterally within the basket compartments. In Case B41, the fuel elements are moved within the basket compartments towards the radial center. In Case B42, the fuel is also shifted axially to the top of the package in

addition to be moved toward the radial center. Comparing these three cases, Case B42 is the most reactive, although the reactivities are somewhat similar.

In Cases B43 and B44, the configuration of Case B42 is modified so that the basket/fuel element water density is reduced to 0.8 and 0.9 g/cm^3, respectively. Because the ATR fuel is undermoderated, reducing the water density will reduce the reactivity. As expected, the reactivity for Case B43 and B44 drops rapidly as the water density is reduced.

In Case B45, Case B42 is rerun using a cladding thickness of 0.018-in for plates 1 and 19, and 0.008-in for plates 2 through 18. The resulting channel spacing is 0.097-in between plates 1 and 2, 0.107-in between plates 18 and 19, and 0.092-in between the remaining plates. Case B45 is the most reactive, with $k_s = 0.70409$.

TRIGA

The TRIGA results for element Type 109 are summarized in Table 6.4-5 as Cases B60 through B70. In Cases B60 through B64, the package cavity is fully flooded with full-density water. In Case B60, the fuel elements are laterally centered within the basket tubes, at an arbitrary distance away from the package lid. In Case B61, the fuel elements are moved within the basket tubes towards the radial center, and the reactivity increases. In Case B62, the outer row is moved radially inward and the inner row is moved radially outward. Cases B63 and B64 are essentially repeats of Cases B60 and B61, respectively, except that the fuel elements are shifted upward until the top of the graphite reflector touches the bottom of the shield plug. Comparing these five cases, Case B64 is the most reactive. Therefore, the remaining HAC single package cases utilize this configuration (i.e., fuel elements moved to the radial center, shifted up to the maximum extent.)

In Cases B65 through B70, the configuration of Case B64 is modified so that the water density inside of the basket is allowed to vary between 0.4 and 0.9 g/cm^3. The reactivity peaks at a density of 0.7 g/cm^3 and then decreases with decreasing density. The maximum reactivity occurs for Case B68, with $k_s = 0.70869$.

The TRIGA results for element Type 119 are summarized in Table 6.4-5 as Cases TL2A1 through TL2A6. Because of the difference in composition between rod Types 109 and 119, the effect of moderator density is re-evaluated for the payload. The highest k_s observed for the Type 119 payload is 0.70703 and occurs with a moderator density of 0.8 g/cm^3. The Type 119 rods are therefore slightly less reactive than the HEU-bearing Type 109 rods. Peak reactivity for the Type 119 rod occurs at a somewhat higher moderator density (0.8 g/cm^3 vs. 0.7 g/cm^3), which is attributable to the reduced enrichment and the corresponding increased role of U-238.

PULSTAR

The results of the PULSTAR analysis are provided in Table 6.4-6. Three series are used to find maximum reactivity for this condition. The first series, P2A, shows the effect of varied moderator density and demonstrates that maximum reactivity is achieved when full density water floods the basket. The associated k_s value is 0.77926.

The next series, P2B, is based on the most reactive case from P2A (P2A06) and varies the horizontal placement of elements within the two outer SFB compartments in the central horizontal row (dimension R2 in Table 6.4-6 and Figure 6.4-1). The other four outer elements are held fixed at their inner-most position. Series P2B demonstrates that the most reactive placement of the two elements is at their inner-most position.

Next, series P2C, using the most reactive case in Series P2A and P2B (P2A06) as a basis, is used to show the most reactive position of fuel elements in the inner SFB compartments (dimension R1 in Table 6.4-6 and Figure 6.4-1). Series P2C starts with the two inner elements at their most inward position (R1 = 3.76 cm). Nine cases are used to show the change in reactivity as the elements are moved to their most radially-outward position (R1 = 5.42 cm). A peak in reactivity occurs for R1 = 4.17 cm. The k_s value in that position is 0.78274.

It is demonstrated that PULSTAR fuel maintains its structural integrity during HAC. However, as an additional conservatism, it is postulated under HAC that the pitch expands until constrained by the Zircaloy fuel element box. The expanded pitch geometry is illustrated in Figure 6.4-2. A final case, P2D01, models the most reactive case from Series P2B and P2C with the maximum pitch. The maximum reactivity occurs for Case P2D01, with k_s = 0.81215.

Loose Plate Box

The LPB may contain up to 31 loose plates and are limited to U-Florida, U-Mass(Al), and Purdue. Void volume within the LPB is filled with aluminum dunnage so that the void space is small. For U-Mass(Al) and Purdue fuel plates, the plates are in close contact due to the dunnage and the pitch will be small. For U-Florida fuel plates, spacers 0.112-in thick are welded to the fuel plates so that the channel spacing must be at least 0.112-in. The pitch is the sum of the channel spacing and plate thickness, and the minimum pitch for U-Florida plates is 0.112-in + 0.03-in = 0.142-in (0.3607 cm), where 0.03-in is the fuel plate thickness from Table 6.2-11. Because the LPB is 2.5-in wide, the maximum number of U-Florida plates that would fit in the LPB is 2.5/0.142 ~ 17. However, it is demonstrated that loading ≤ 31 plates per LPB in each of the eight LPBs in a package is acceptable.

In the loose plate box analysis, no credit is taken for the aluminum dunnage, which reduces the plate pitch. The analysis is performed for both uniform and non-uniform plate pitches in order to determine the most reactive configuration. The U-Florida plate is modeled to bound the U-Mass(Al) and Purdue plates because the U-Florida plate has more U-235 per plate (12.5 g) than either U-Mass(Al) or Purdue (9.3 g), as shown in Table 6.2-11. Modeling all plates as U-Florida also bounds mixtures of the three different plate types.

Any number of plates, up to the maximum of 31 plates, may be present in each of the eight LPBs in a package. As each LPB is loaded, the LPB may be overmoderated for a small number of plates, optimally moderated for a medium number of plates, and undermoderated for a large number of plates. For a system in which the number of plates is fixed, a reactivity curve may be developed by plotting k_{eff} as a function of plate pitch. This is illustrated in a simple sensitivity study consisting of only fuel plates and water. In this sensitivity study, the LPB, basket, and package are not modeled because the intent is to allow the plate pitch to increase without restriction. The system of plates is reflected by at least 12-in of water in all directions.

Four representative plate systems are examined (31 plates, 19 plates, 15 plates, and 7 plates), and the pitch is adjusted between 0.1 and 1.2 cm to determine the optimum moderation for each system, as shown on Figure 6.4-3. Based on Figure 6.4-3, the optimum pitch for each of the systems examined is shown in following table.

Number of Plates in System	Optimum Pitch (cm)
31	0.7
19	0.8
15	0.9
7	1.2

Based on this study, it is observed that the optimum pitch increases as the number of plates decreases. It is also observed for all cases that the optimum pitch is relatively large in relation to the width of the LPB (6.35 cm). Therefore, optimum moderation is achieved in the LPB for approximately 7 plates (pitch ~1.1 cm). For more than approximately 7 plates, the system will be undermoderated.

It is also observed from Figure 6.4-3 that an undermoderated system with a large number of plates may be more reactive than an optimally moderated system with fewer plates. For 31 plates in the LPB, the pitch ~ 0.2 cm. From Figure 6.4-3, 31 undermoderated plates at a pitch of 0.2 cm ($k \sim 0.4$) is significantly more reactive than an optimally moderated system with 7 plates ($k \sim 0.3$).

In the subsequent cases, the LPB is modeled in the Square fuel basket within the BRR package. In the first series of cases (Series L2A), only uniform plate pitches are examined with the plates centered in the LPB. An example model geometry for 31 plates is shown in the upper half of Figure 6.4-4. Results for the LPB payload pitch studies are provided in Table 6.4-7. In the first four cases (Cases L2A01 through L2A04), 31 plates are modeled from a small pitch (0.12 cm) to the maximum pitch (0.2092 cm). Consistent with the plate pitch study, reactivity increases with increasing plate pitch, reaching a maximum value of $k_s = 0.59880$ for Case L2A04. Because further pitch expansion is limited by the LPB, the system remains undermoderated.

In Cases L2A05 through L2A16, the number of plates in the LPB is varied from 29 to 7 plates. Based on Figure 6.4-3, the system will remain undermoderated if the number of plates per LPB is greater than approximately 7 plates. Because the system is undermoderated, the plates are modeled with the largest uniform pitch that fills the LPB. The pitch ranges from 0.2240 cm (29 plates, Case L2A05) to 1.0456 cm (7 plates, Case L2A16). However, while moderation is increased by removing plates and expanding the pitch, the reactivity steadily decreases as the plates are removed. It may be concluded that the reactivity of an undermoderated system with a large fissile mass is more reactive than a more moderated system with less fissile mass. The case with 7 plates, which is the closest to optimum moderation, has the lowest reactivity.

In Series L2A, uniform pitches are investigated. In Series L2B, the effect of a non-uniform pitch is investigated. While non-uniform pitches may form an infinite number of combinations, the approach is to model some plates in close-contact so that the pitch for the remaining plates may continue to expand. Based on Series L2A, it is expected that 31 plates with a non-uniform pitch would bound a fewer number of plates with a non-uniform pitch. A non-uniform pitch analysis is performed for 31 plates, 25 plates, and 19 plates to confirm the non-uniform pitch system is most reactive for 31 plates. This approach maximizes the fissile mass while allowing greater moderation for most of the plates. A non-uniform pitch configuration is illustrated in the lower half of Figure 6.4-4.

Results for the non-uniform pitch cases are provided in Table 6.4-8. Reactivity increases compared to the uniform pitch cases, but the increase is not significant. The maximum reactivity

occurs with 31 total plates (Case L2B06, $k_s = 0.61048$, 25 plates in an expanded pitch and the remaining plates in close-contact). The most reactive 31 plate non-uniform pitch case is ~12 milli-k larger than the corresponding 31 plate uniform pitch case.

Reactivity for the non-uniform pitch cases with 25 total plates and 19 total plates are bounded by the 31 plate model. Compared to the uniform pitch cases, a non-uniform pitch results in a ~9 milli-k increase for 25 total plates and ~6 milli-k increase for 19 total plates. It is observed that as the total number of plates decreases, the uniform and non-uniform pitch cases become closer in reactivity. Because 31 plates in a uniform pitch bounds a lesser number of plates in a uniform pitch (Series L2A), and 31 plates results in the largest reactivity gain when non-uniform pitches are considered (Series L2B), it is concluded that 31 plates in a non-uniform pitch bounds a lesser number of plates in a non-uniform pitch. Therefore, in subsequent cases, only 31 plates are modeled.

The 31 plate system is undermoderated and in fact has less moderation than the cases with fewer plates. However, for the LPB in the Square fuel basket, undermoderated cases with higher fissile mass are more reactive than higher moderated cases with lower fissile mass. Optimum moderation can be achieved for only a low number of plates (~7 plates per LPB), and the reactivity for an optimally moderated system is low due to the low fissile mass.

The results for the following three series are provided in Table 6.4-9. In Series L2C, the 31 plates are horizontally fanned (offset) in an alternating pattern. Non-uniform pitch Case L2B06 is used as the base case. The geometry for the fanned cases is shown in Figure 6.4-5. This horizontal fanning further increases moderation and increases the reactivity. Note that in the actual configuration the horizontal fanning would be much smaller because the aluminum cladding on the side is not modeled for simplicity. Vertical fanning is neglected because the amount of space for vertical fanning is negligible compared to the length of the fuel plates.

In Series L2D, the eight LPBs are radially shifted to the centerline of the package. This is a more compact configuration and causes the reactivity to increase. Two different configurations are considered, with and without plate fanning. The geometry for the two configurations cases is shown in Figure 6.4-6. Case L2D01 is based on plate geometry without fanning but with the plates and LPBs shifted to the centerline. Case L2D02 is based on the plates with fanning shifted to the centerline. Both cases in Series L2D have essentially the same reactivity, although the case without fanning is slightly larger, with $k_s = 0.64061$.

In Series L2E, the effect of water density is considered. In Series L2A through L2D, the maximum water density of 1.0 g/cm^3 is modeled within the package cavity. The most reactive Case L2D02 is modeled with uniformly reduced water densities within the package cavity to demonstrate that the system is most reactive with full density water.

In Series L2A through L2E, all eight LPBs are modeled with the same number of plates per LPB. It is demonstrated that modeling 31 plates per LPB is the most reactive condition. During a loading or unloading operation, the total number of fuel plates in the basket may vary between one (i.e., one plate in one LPB) to 248 (i.e., 31 plates in eight LPBs). Based on the results in Series L2A through L2E, it may be inferred that reactivity increases as each fuel plate is added to the basket, reaching the maximum reactivity for a fully loaded basket (i.e., 248 fuel plates). Transporting less than 248 fuel plates is less reactive and acceptable. While it is not practical to evaluate every scenario between one and 248 plates, in Series L2F, the number of plates in the basket is varied from 217 to 248 plates by loading seven LPBs with 31 plates and one LPB with

a reduced number of plates. For simplicity, Case L2A04 is used as the base case, in which the fuel plates are centered in the LPBs and spaced uniformly within the compartment. The LPB with the reduced number of plates is an inner LPB, as indicated in Figure 6.4-7, to maximize the reactivity changes. Results are provided in Table 6.4-10. As expected, the reactivity decreases as plates are removed from the LPB. Therefore, the criticality analysis bounds the loading and unloading operations of 10 CFR 71.55(b).

The maximum reactivity occurs for Case L2D01, with $k_s = 0.64061$. This case features 31 plates arranged in a non-uniform pitch (25 plates in an expanded pitch), and the LPBs and fuel plates shifted to the radial centerline. This value is significantly below the USL of 0.9209.

Conclusions from the LPB analysis are:

- Limit on U-Florida plates: ≤ 31 plates per LPB
- Limit on U-Mass(Al) plates: ≤ 31 plates per LPB
- Limit on Purdue plates: ≤ 31 plates per LPB
- The system with 31 plates is undermoderated but has the highest fissile mass. For this system, 31 undermoderated plates are more reactive than fewer plates with greater moderation. Optimal moderation is achieved with ~7 plates, although the reactivity of the optimally moderated system is low due to the low fissile mass.
- Due to geometrical constraints, it is not possible to transport 31 U-Florida plates in an LPB. As noted above, transporting fewer than 31 plates is less reactive and therefore acceptable.
- The LPB criticality analysis bounds the requirements of 71.55(b) for loading and unloading operations because 31 plates are more reactive than a lesser number plates that could be present during loading/unloading operations.

SFB Plate Fuel

Seven intact plate-fuel types may be transported in the SFB. To determine the most reactive element type, each element is modeled in its nominal condition, flooded with water, and centered in the SFB compartment openings. All fuel designs with the exception of U-Florida feature structural side combs along the entire length of the fuel element. These side combs are conservatively ignored in the MCNP models. Results for the SFB plate-fuel-element payloads are provided in Table 6.4-11 in Series PF2A. The maximum k_s of all of the plate fuel payloads is 0.69500 and corresponds to the RINSC fuel payload. RINSC fuel also has the largest U-235 loading of the seven fuel designs. Therefore, RINSC bounds all SFB plate fuel types that remain intact under HAC.

The fuel elements are free to move laterally within a fuel compartment. This effect is exaggerated in the MCNP models because the aluminum combs are not modeled, which allows more space for lateral shifting. In Series PF2B, several different radial locations of the RINSC fuel element are investigated. The outer six and inner two fuel elements are allowed to shift independently of one another. The radial offset is measured from the centerline of the fuel element to the centerline of the package (positive offset is toward the centerline and negative offset is away from the centerline). Two different examples of the radial offset models are illustrated in Figure 6.4-8, Cases PF2B4 and PF2B9. Case PF2B4 is the most reactive, with the outer fuel elements shifted as close as possible to the package centerline and the inner fuel elements shifted near the centerline of the package. The reactivity of this case is $k_s = 0.74099$.

While RINSC bounds all plate fuels that remain intact under HAC, it is postulated that U-Florida fuel may be damaged in an accident. Therefore, an analysis of U-Florida fuel is performed with postulated fuel damage. However, it is demonstrated that a damaged U-Florida fuel element is bounded by the RINSC fuel element.

U-Florida fuel elements are significantly smaller than RINSC fuel elements, resulting in significant void space within the compartments. If the plate pitch is allowed to expand into the free space, the reactivity increases. Results for the U-Florida analysis are provided in Table 6.4-12. The effect of both uniform and non-uniform pitch expansion for U-Florida fuel is investigated in Series PF2C. To mitigate the effects of potential fuel damage due to pitch expansion, U-Florida fuel elements are transported using aluminum dunnage in each compartment. This dunnage has nominal dimensions of 27-in long, 3-in wide, and 0.8-in thick. It is modeled with a thickness of 0.8-in, although the length and width are modeled to match the plate fuel dimensions for convenience. The width of the compartment is 3.4-in, so the space available for pitch expansion is 3.4-in – 0.8-in = 2.6-in (6.604 cm). Based on the allowable space and 14 fuel plates, the maximum regular pitch is limited to 0.50 cm. Several different increased pitches are investigated with the fuel element centered in the compartment (Cases PF2C01 through PF2C03), and reactivity is maximized for the maximum pitch. In these initial cases, the aluminum spacer block is not explicitly modeled.

In Case PF2C04, the 0.8-in thick aluminum spacer block is modeled explicitly, see Figure 6.4-9. The reactivity is essentially the same when the aluminum spacer is added to the model. As the spacer is required to be present, it is modeled explicitly in subsequent cases.

In Cases PF2C05 through PF2C08, the effect of a non-uniform pitch is investigated. While non-uniform pitches may form an infinite number of combinations, the approach is to model some plates in close-contact so that the pitch for the remaining plates may continue to expand. This approach conserves the fissile mass while allowing greater moderation for most of the plates. Various non-uniform pitch configurations are illustrated in Figure 6.4-10. Case PF2C06 is the most reactive, with 12 plates at the maximum uniform pitch. However, the k_s of this case (k_s = 0.61869) is only slightly larger than the k_s of the maximum case with a uniform pitch (Case PF2C04, k_s = 0.61454), indicating there is not a large increase in reactivity for non-uniform pitches.

In Series PF2D, horizontal fanning of the fuel plates is investigated, similar to the approach used in the LPB analysis. Non-uniform pitch Case PF2C06 is used as the base case. In the horizontal fanning models, the fuel element is centered in the compartment while the plates are alternately shifted in the x-direction, see Figure 6.4-11. Fanning the fuel plates in this manner increases the moderation. Three different fanning configurations are investigated (0.39 cm, 0.78 cm, and 1.17 cm), and reactivity is maximized for the maximum fanning (Case PF2D03, k_s = 0.64312). Vertical fanning is neglected because the amount of space for vertical fanning is negligible compared to the length of the fuel plates.

In Series PF2E, radial placement of the fuel elements within the SFB is investigated, similar to the RINSC analysis. Non-uniform pitch Case PF2C06 is used as the base case. Horizontal fanning is not included in the radial placement models because the fuel cannot be shifted radially for maximum fanning (i.e., maximum fanning fills the entire compartment). The outer six and inner two fuel elements are allowed to shift independently of one another. The radial offset is measured from the centerline of the fuel element to the centerline of the package (positive offset

is toward the centerline and negative offset is away from the centerline). Two different examples of the radial offset models are illustrated in Figure 6.4-12, Cases PF2E04 and PF2E08. Case PF2E04 is the most reactive, with the outer fuel elements shifted as close as possible to the package centerline and the inner fuel elements shifted near the centerline of the package. The reactivity of this case is $k_s = 0.66094$. Note that this case is more reactive than the case with maximum fanning due to the more compact arrangement of the eight fuel elements.

The relative location of the aluminum spacer in each compartment is random in the actual loading configuration and is not required to follow the pattern shown in Figure 6.4-9. In Series PF2F, two additional orientations of the aluminum spacers are investigated, as illustrated in Figure 6.4-13. The reactivity of Case PF2F01 increases slightly to $k_s = 0.66336$. While many other orientations are possible, the effect on the reactivity would be low and the overall system reactivity for U-Florida is bounded by RINSC fuel. Therefore, sufficient configurations of U-Florida fuel have been investigated.

In Case PF203, most reactive Case PF201 is run with a wide aluminum spacer that spans the 3.4-in width of the cavity, bounding the nominal spacer width of 3-in. In the previous models, the spacer is modeled to match the width of the fuel for convenience, or 2.47-in (see Figure 6.4-9). Reactivity decreases slightly for Case PF203, indicating that modeling the spacer with a width < 3-in is acceptable.

Comparing the SFB plate fuels, RINSC is bounding, with $k_s = 0.74099$ (Case PF2B4). The reactivity of RINSC also bounds damaged U-Florida fuel by a large margin, as $k_s = 0.66336$ for the most reactive U-Florida configuration.

Combinations of SFB Contents

The most reactive SFB contents are:

- $k_s = 0.81215$ for PULSTAR
- $k_s = 0.64061$ for the LPB, and
- $k_s = 0.74099$ for plate fuels (RINSC)

Therefore, the reactivity for any combination of SFB contents will not exceed the reactivity of the PULSTAR payload.

6.4.2 Results

Following are the tabulated results for the single package cases. The most reactive configuration within each series is listed in boldface.

Table 6.4-1 – NCT Single Package Results, MURR, MITR-II, ATR

Case ID	Filename	k_{eff}	σ	k_s (k+2σ)
MURR				
A1	NS_MURR	0.08167	0.00023	0.08213
A2	NS_MURR_IN	0.08152	0.00022	0.08196
A3	**NS_MURR_INUP**	**0.08499**	**0.00023**	**0.08545**
MITR-II				
A10	NS_MIT2	0.05655	0.00015	0.05685
A11	NS_MIT2_IN	0.05709	0.00016	0.05741
A12	**NS_MIT2_INUP**	**0.05808**	**0.00014**	**0.05836**
A13	NS_MIT2_OUTUP	0.05762	0.00016	0.05794
ATR				
A20	NS_ATR	0.08689	0.00024	0.08737
A21	NS_ATR_IN	0.08759	0.00025	0.08809
A22	**NS_ATR_INUP**	**0.08797**	**0.00026**	**0.08849**

Table 6.4-2 – NCT Single Package Results, TRIGA

Case ID	Filename	k_{eff}	σ	k_s (k+2σ)
Type 109				
A30	NS_TRIGA	0.39557	0.00089	0.39735
A31	NS_TRIGA_IN	0.40299	0.00092	0.40483
A32	NS_TRIGA_INOUT	0.40078	0.00092	0.40262
A33	**NS_TRIGA_INUP**	**0.41493**	**0.00089**	**0.41671**
Type 119				
TL1A1	TR_NCT_SGL_A_01	0.38203	0.00034	0.38271

Table 6.4-3 – NCT Single Package Results, Square Fuel Basket

Case ID	Filename	k_{eff}	σ	k_s (k+2σ)
PULSTAR				
P1A1	NS_PULSTAR	0.14653	0.00015	0.14683
Loose Plate Box				
L1A1	NS_LOOSE_EXP25SH	0.05196	0.00009	0.05214
Plate Fuels (RINSC)				
PF1A1	NS_RINSC_SH3A	0.03633	0.00007	0.03647

Table 6.4-4 – HAC Single Package Results, MURR, MITR-II, ATR

Case ID	Filename	Water Density (g/cm^3)	k_{eff}	σ	k_s (k+2σ)
MURR					
B1	HS_MURR	1.0	0.75395	0.00115	0.75625
B2	HS_MURR_IN	1.0	0.75287	0.00123	0.75533
B3	HS_MURR_INUP	1.0	0.75898	0.00113	0.76124
B4	HS_MURR_C080INUP	0.8	0.69306	0.00108	0.69522
B5	HS_MURR_C090INUP	0.9	0.72871	0.00118	0.73107
B6	**HS_MURR_INUPC**	**1.0**	**0.78186**	**0.00123**	**0.78432**
MITR-II					
B20	HS_MIT2_W100	1.0	0.50737	0.00107	0.50951
B21	HS_MIT2_W100IN	1.0	0.52143	0.00111	0.52365
B22	HS_MIT2_W100INUP	1.0	0.52284	0.00103	0.52490
B23	HS_MIT2_W100OUTUP	1.0	0.49263	0.00103	0.49469
B24	HS_MIT2_W100INUP_R11	1.0	0.48905	0.00107	0.49119
B25	HS_MIT2_W100INUP_R11P5	1.0	0.49907	0.00095	0.50097
B26	HS_MIT2_W080INUP	0.8	0.48751	0.00096	0.48943
B27	HS_MIT2_W090INUP	0.9	0.50573	0.00102	0.50777
B28	**HS_MIT2_W100INUPC**	**1.0**	**0.57166**	**0.00108**	**0.57382**
ATR					
B40	HS_ATR	1.0	0.67992	0.00113	0.68218
B41	HS_ATR_IN	1.0	0.68013	0.00110	0.68233
B42	HS_ATR_INUP	1.0	0.68279	0.00123	0.68525
B43	HS_ATR_C080INUP	0.8	0.64718	0.00105	0.64928
B44	HS_ATR_C090INUP	0.9	0.66179	0.00106	0.66391
B45	**HS_ATR_INUPC**	**1.0**	**0.70183**	**0.00113**	**0.70409**

Table 6.4-5 – HAC Single Package Results, TRIGA

Case ID	Filename	Water Density (g/cm^3)	k_{eff}	σ	k_s (k+2σ)
Type 109					
B60	HS_TRIGA_W100	1.0	0.66788	0.00108	0.67004
B61	HS_TRIGA_W100IN	1.0	0.69115	0.00097	0.69309
B62	HS_TRIGA_W100INOUT	1.0	0.67398	0.00098	0.67594
B63	HS_TRIGA_W100UP	1.0	0.66998	0.00112	0.67222
B64	HS_TRIGA_W100INUP	1.0	0.69348	0.00106	0.69560
B65	HS_TRIGA_W040INUP	0.4	0.67497	0.00119	0.67735
B66	HS_TRIGA_W050INUP	0.5	0.69534	0.00124	0.69782
B67	HS_TRIGA_W060INUP	0.6	0.70552	0.00104	0.70760
B68	**HS_TRIGA_W070INUP**	**0.7**	**0.70661**	**0.00104**	**0.70869**
B69	HS_TRIGA_W080INUP	0.8	0.70510	0.00099	0.70708
B70	HS_TRIGA_W090INUP	0.9	0.70164	0.00106	0.70376
Type 119					
TL2A1	TR_HAC_SGL_A_01	0.4	0.66703	0.00049	0.66801
TL2A2	TR_HAC_SGL_A_02	0.5	0.68848	0.00048	0.68944
TL2A3	TR_HAC_SGL_A_03	0.6	0.70051	0.00049	0.70149
TL2A4	TR_HAC_SGL_A_04	0.7	0.70596	0.00043	0.70682
TL2A5	**TR_HAC_SGL_A_05**	**0.8**	**0.70605**	**0.00049**	**0.70703**
TL2A6	TR_HAC_SGL_A_06	0.9	0.70302	0.00046	0.70394

Table 6.4-6 – HAC Single Package Results, PULSTAR

Case ID	Filename	Water Density (g/cm^3)	R1 (cm)	R2 (cm)	k_{eff}	σ	k_s (k+2σ)
P2A, Water Density							
P2A01	PS_SNGL_HAC_2A_01	0.5	4.59	12.93	0.68160	0.00106	0.68372
P2A02	PS_SNGL_HAC_2A_02	0.6	4.59	12.93	0.71530	0.00097	0.71724
P2A03	PS_SNGL_HAC_2A_03	0.7	4.59	12.93	0.73743	0.00101	0.73945
P2A04	PS_SNGL_HAC_2A_04	0.8	4.59	12.93	0.75614	0.00099	0.75812
P2A05	PS_SNGL_HAC_2A_05	0.9	4.59	12.93	0.76771	0.00101	0.76973
P2A06	**PS_SNGL_HAC_2A_06**	**1.0**	**4.59**	**12.93**	**0.77708**	**0.00109**	**0.77926**
P2B, Outer Horizontal Compartments, Horizontal Element Placement							
P2A06	***PS_SNGL_HAC_2A_06***	***1.0***	***4.59***	***12.93***	***0.77708***	***0.00109***	***0.77926***
P2B01	PS_SNGL_HAC_2B_01	1.0	4.59	13.35	0.77768	0.00115	0.77998
P2B02	PS_SNGL_HAC_2B_02	1.0	4.59	13.76	0.77754	0.00101	0.77956
P2B03	PS_SNGL_HAC_2B_03	1.0	4.59	14.18	0.77600	0.00106	0.77812
P2B04	PS_SNGL_HAC_2B_04	1.0	4.59	14.59	0.77034	0.00113	0.77260
P2C, Inner Horizontal Compartments, Horizontal Element Placement							
P2C01	PS_SNGL_HAC_2C_01	1.0	3.76	12.93	0.78011	0.00049	0.78109
P2C02	PS_SNGL_HAC_2C_02	1.0	3.96	12.93	0.78075	0.00047	0.78169
P2C03	**PS_SNGL_HAC_2C_03**	**1.0**	**4.17**	**12.93**	**0.78182**	**0.00046**	**0.78274**
P2C04	PS_SNGL_HAC_2C_04	1.0	4.38	12.93	0.78018	0.00046	0.78110
P2A06	*PS_SNGL_HAC_2A_06*	*1.0*	*4.59*	*12.93*	*0.77710*	*0.00112*	*0.77934*
P2C05	PS_SNGL_HAC_2C_05	1.0	4.79	12.93	0.77471	0.00047	0.77565
P2C06	PS_SNGL_HAC_2C_06	1.0	5.00	12.93	0.77096	0.00049	0.77194
P2C07	PS_SNGL_HAC_2C_07	1.0	5.21	12.93	0.76548	0.00044	0.76636
P2C08	PS_SNGL_HAC_2C_08	1.0	5.42	12.93	0.75993	0.00044	0.76081
P2D, Rod Pitch Maximized in Element Box							
P2D01	**PS_SINGLE_HAC_2D_01**	**1.0**	**4.17**	**12.93**	**0.81125**	**0.00045**	**0.81215**

Table 6.4-7 – HAC Single Package Results, Loose Plate Box, Uniform Pitch Study

Case ID	Filename	Number of Plates in LPB	Uniform Pitch (cm)	k_{eff}	σ	k_s (k+2σ)
L2A, Uniform Pitch						
L2A01	HS_LOOSE_P06	31	0.1200	0.45998	0.00030	0.46058
L2A02	HS_LOOSE_P08	31	0.1600	0.52275	0.00034	0.52343
L2A03	HS_LOOSE_P10	31	0.2000	0.58386	0.00034	0.58454
L2A04	HS_LOOSE_P1046	31	0.2092	0.59814	0.00033	**0.59880**
L2A05	HS_LOOSE_N29	29	0.2240	0.59503	0.00033	0.59569
L2A06	HS_LOOSE_N27	27	0.2414	0.59062	0.00032	0.59126
L2A07	HS_LOOSE_N25	25	0.2614	0.58505	0.00032	0.58569
L2A08	HS_LOOSE_N23	23	0.2852	0.57812	0.00033	0.57878
L2A09	HS_LOOSE_N21	21	0.3136	0.56841	0.00033	0.56907
L2A10	HS_LOOSE_N19	19	0.3486	0.55708	0.00030	0.55768
L2A11	HS_LOOSE_N17	17	0.3922	0.54219	0.00030	0.54279
L2A12	HS_LOOSE_N15	15	0.4482	0.52419	0.00030	0.52479
L2A13	HS_LOOSE_N13	13	0.5228	0.50018	0.00028	0.50074
L2A14	HS_LOOSE_N11	11	0.6274	0.46927	0.00026	0.46979
L2A15	HS_LOOSE_N9	9	0.7842	0.42976	0.00025	0.43026
L2A16	HS_LOOSE_N7	7	1.0456	0.37615	0.00023	0.37661

Table 6.4-8 – HAC Single Package Results, Loose Plate Box, Non-Uniform Pitch Study

Case ID	Filename	Number of Plates in LPB	Number of Plates with Expanded Pitch	Expanded Pitch (cm)	k_{eff}	σ	k_s (k+2σ)
L2B, Non-Uniform Pitch, 31 plates per LPB							
L2B01	HS_LOOSE_EXP30	31	30	0.2138	0.60221	0.00032	0.60285
L2B02	HS_LOOSE_EXP29	31	29	0.2186	0.60525	0.00032	0.60589
L2B03	HS_LOOSE_EXP28	31	28	0.2238	0.60766	0.00034	0.60834
L2B04	HS_LOOSE_EXP27	31	27	0.2296	0.60852	0.00032	0.60916
L2B05	HS_LOOSE_EXP26	31	26	0.2358	0.60919	0.00033	0.60985
L2B06	HS_LOOSE_EXP25	31	25	0.2424	0.60984	0.00032	**0.61048**
L2B07	HS_LOOSE_EXP24	31	24	0.2496	0.60974	0.00032	0.61038
L2B08	HS_LOOSE_EXP23	31	23	0.2574	0.60885	0.00032	0.60949
L2B09	HS_LOOSE_EXP22	31	22	0.2660	0.60756	0.00034	0.60824
L2B10	HS_LOOSE_EXP21	31	21	0.2756	0.60647	0.00033	0.60713
L2B11	HS_LOOSE_EXP20	31	20	0.2860	0.60473	0.00033	0.60539
L2B, Non-Uniform Pitch, 25 plates per LPB							
L2B21	HS_N25_E24	25	24	0.2694	0.58946	0.00032	0.59010
L2B22	HS_N25_E23	25	23	0.2782	0.59255	0.00032	0.59319
L2B23	HS_N25_E22	25	22	0.2878	0.59433	0.00033	0.59499
L2B24	HS_N25_E21	25	21	0.2984	0.59428	0.00033	0.59494
L2B25	HS_N25_E20	25	20	0.3102	0.59442	0.00030	**0.59502**
L2B26	HS_N25_E19	25	19	0.3232	0.59292	0.00031	0.59354
L2B27	HS_N25_E18	25	18	0.3376	0.59151	0.00032	0.59215
L2B28	HS_N25_E17	25	17	0.3540	0.58910	0.00033	0.58976
L2B29	HS_N25_E16	25	16	0.3726	0.58632	0.00031	0.58694
L2B30	HS_N25_E15	25	15	0.3938	0.58186	0.00031	0.58248
L2B31	HS_N25_E14	25	14	0.4182	0.57752	0.00031	0.57814

(1/2)

Table 6.4-8 – HAC Single Package Results, Loose Plate Box, Non-Uniform Pitch Study

Case ID	Filename	Number of Plates in LPB	Number of Plates with Expanded Pitch	Expanded Pitch (cm)	k_{eff}	σ	k_s (k+2σ)
L2B, Non-Uniform Pitch, 19 plates per LPB							
L2B41	HS_N19_E18	19	18	0.3646	0.56133	0.00031	0.56195
L2B42	HS_N19_E17	19	17	0.3826	0.56356	0.00030	**0.56416**
L2B43	HS_N19_E16	19	16	0.4030	0.56291	0.00031	0.56353
L2B44	HS_N19_E15	19	15	0.4264	0.56147	0.00030	0.56207
L2B45	HS_N19_E14	19	14	0.4532	0.55848	0.00031	0.55910
L2B46	HS_N19_E13	19	13	0.4848	0.55491	0.00030	0.55551
L2B47	HS_N19_E12	19	12	0.5218	0.54916	0.00029	0.54974
L2B48	HS_N19_E11	19	11	0.5664	0.54289	0.00030	0.54349
L2B49	HS_N19_E10	19	10	0.6208	0.53426	0.00029	0.53484
L2B50	HS_N19_E9	19	9	0.6890	0.52443	0.00029	0.52501
L2B51	HS_N19_E8	19	8	0.7766	0.51260	0.00028	0.51316
L2B52	HS_N19_E7	19	7	0.8932	0.49927	0.00028	0.49983

(2/2)

Table 6.4-9 – HAC Single Package Results, Loose Plate Box, Additional Cases

Case ID	Filename	Horizontal Fanning (cm)	Water Density (g/cm^3)	k_{eff}	σ	k_s ($k+2\sigma$)
L2C, Horizontal Fanning						
L2C01	HS_LOOSE_EXP25H1	0.3285	1.0	0.61655	0.00032	0.61719
L2C02	HS_LOOSE_EXP25H2	0.6470	1.0	0.63063	0.00034	0.63131
L2D, Radial Shifting of LPB to Centerline						
L2D01	HS_LOOSE_EXP25SH	0.0000	1.0	0.64001	0.00030	**0.64061**
L2D02	HS_LOOSE_EXP25H2SH	0.6470	1.0	0.63936	0.00031	0.63998
L2E, Reduced Moderator Density						
L2E01	HS_LOOSE_EXP25SH_W090	0.0000	0.9	0.62555	0.00032	0.62619
L2E02	HS_LOOSE_EXP25SH_W080	0.0000	0.8	0.60948	0.00032	0.61012
L2E03	HS_LOOSE_EXP25SH_W070	0.0000	0.7	0.59170	0.00032	0.59234
L2E04	HS_LOOSE_EXP25SH_W060	0.0000	0.6	0.56848	0.00032	0.56912
L2E05	HS_LOOSE_EXP25SH_W050	0.0000	0.5	0.53896	0.00030	0.53956

Note: All cases in this table feature 31 plates in a non-uniform lattice, with 25 plates in an expanded pitch of 0.2424 cm.

Table 6.4-10 – HAC Single Package Results, Loose Plate Box, Loading/Unloading

Case ID	Filename	Number of Plates per LPB, 7 LPBs	Number of Plates in Inner LPB	Total Number of Plates in Basket	k_{eff}	σ	k_s (k+2σ)
L2F, 7 LPBs with 31 plates per LPB, one inner LPB with a reduced number of plates							
L2A04	HS_LOOSE_P1046	31	31	248	0.59814	0.00033	**0.59880**
L2F01	HS_LOOSE_P1046_IP29	31	29	246	0.59765	0.00031	0.59827
L2F02	HS_LOOSE_P1046_IP27	31	27	244	0.59720	0.00033	0.59786
L2F03	HS_LOOSE_P1046_IP25	31	25	242	0.59584	0.00033	0.59650
L2F04	HS_LOOSE_P1046_IP23	31	23	240	0.59495	0.00032	0.59559
L2F05	HS_LOOSE_P1046_IP21	31	21	238	0.59289	0.00032	0.59353
L2F06	HS_LOOSE_P1046_IP19	31	19	236	0.58972	0.00032	0.59036
L2F07	HS_LOOSE_P1046_IP17	31	17	234	0.58702	0.00032	0.58766
L2F08	HS_LOOSE_P1046_IP15	31	15	232	0.58382	0.00032	0.58446
L2F09	HS_LOOSE_P1046_IP13	31	13	230	0.57860	0.00032	0.57924
L2F10	HS_LOOSE_P1046_IP11	31	11	228	0.57260	0.00031	0.57322
L2F11	HS_LOOSE_P1046_IP09	31	9	226	0.56535	0.00031	0.56597
L2F12	HS_LOOSE_P1046_IP07	31	7	224	0.55781	0.00032	0.55845
L2F13	HS_LOOSE_P1046_IP0	31	0	217	0.52322	0.00031	0.52384

Table 6.4-11 – HAC Single Package Results, SFB Plate Fuel

Case ID	Filename	Element	Inner Offset (cm)①	Outer Offset (cm)①	k_{eff}	σ	k_s (k+2σ)
PF2A, Determination of Bounding Plate Fuel Type							
PF2A1	PF_SINGLE_HAC_2A_01	U-Florida	0	0	0.55832	0.00046	0.55924
PF2A2	PF_SINGLE_HAC_2A_02	OSU	0	0	0.61832	0.00046	0.61924
PF2A3	PF_SINGLE_HAC_2A_03	U-Mass (Si)	0	0	0.61116	0.00041	0.61198
PF2A4	PF_SINGLE_HAC_2A_04	Missouri S&T	0	0	0.68039	0.00045	0.68129
PF2A5	PF_SINGLE_HAC_2A_05	RINSC	0	0	0.69400	0.00050	**0.69500**
PF2A6	PF_SINGLE_HAC_2A_06	Purdue	0	0	0.55388	0.00037	0.55462
PF2A7	PF_SINGLE_HAC_2A_07	U-Mass (Al)	0	0	0.58884	0.00041	0.58966
PF2B, Location Study for RINSC							
PF2B1	HS_RINSC_SH1	RINSC	0.39	0.39	0.70976	0.00077	0.71130
PF2B2	HS_RINSC_SH2	RINSC	0.78	0.78	0.72122	0.00080	0.72282
PF2B3	HS_RINSC_SH3	RINSC	1.17	1.17	0.73677	0.00070	0.73817
PF2B4	HS_RINSC_SH3A	RINSC	0.78	1.17	0.73961	0.00069	**0.74099**
PF2B5	HS_RINSC_SH3B	RINSC	0.39	1.17	0.73875	0.00079	0.74033
PF2B6	HS_RINSC_SH3C	RINSC	0	1.17	0.73575	0.00076	0.73727
PF2B7	HS_RINSC_SH3D	RINSC	-0.39	1.17	0.72848	0.00076	0.73000
PF2B8	HS_RINSC_SH3E	RINSC	-0.78	1.17	0.71899	0.00074	0.72047
PF2B9	HS_RINSC_SH3F	RINSC	-1.17	1.17	0.71142	0.00075	0.71292

①Offset is measured radially from the center of the fuel element to the centerline of the package. "Inner" refers to the two inner fuel elements, and "outer" refers to the outer six fuel elements.

Table 6.4-12 – HAC Single Package Results, U-Florida

Case ID	Filename	Pitch (cm)	Plates at Expanded Pitch	Horizontal Fanning (cm)	Inner Offset (cm)①	Outer Offset (cm)①	k_{eff}	σ	k_s (k+2σ)
PF2C, Pitch Variation									
PF2C01	HS_FLORIDA_P20	0.4000	14	0	0	0	0.57413	0.00032	0.57477
PF2C02	HS_FLORIDA_P22	0.4400	14	0	0	0	0.59002	0.00032	0.59066
PF2C03	HS_FLORIDA_P25	0.5021	14	0	0	0	0.61349	0.00031	0.61411
PF2C04	HS_FLORIDA_AL_14EXP	0.5021	14	0	0	0	0.61396	0.00029	0.61454
PF2C05	HS_FLORIDA_AL_13EXP	0.5376	13	0	0	0	0.61731	0.00030	0.61791
PF2C06	HS_FLORIDA_AL_12EXP	0.5796	12	0	0	0	0.61809	0.00030	**0.61869**
PF2C07	HS_FLORIDA_AL_11EXP	0.6299	11	0	0	0	0.61556	0.00029	0.61614
PF2C08	HS_FLORIDA_AL_10EXP	0.6914	10	0	0	0	0.60880	0.00030	0.60940
PF2D, Horizontal Plate Fanning									
PF2D01	HS_FLORIDA_AL_12EXP_H1	0.5796	12	0.39	0	0	0.62317	0.00030	0.62377
PF2D02	HS_FLORIDA_AL_12EXP_H2	0.5796	12	0.78	0	0	0.63293	0.00028	0.63349
PF2D03	HS_FLORIDA_AL_12EXP_H3	0.5796	12	1.17	0	0	0.64252	0.00030	**0.64312**
PF2E, Location Study									
PF2E01	HS_FLORIDA_AL_12EXP_SH1	0.5796	12	0	0.39	0.39	0.63321	0.00028	0.63377
PF2E02	HS_FLORIDA_AL_12EXP_SH2	0.5796	12	0	0.78	0.78	0.64695	0.00028	0.64751
PF2E03	HS_FLORIDA_AL_12EXP_SH3	0.5796	12	0	1.17	1.17	0.65836	0.00029	0.65894
PF2E04	HS_FLORIDA_AL_12EXP_SH3A	0.5796	12	0	0.78	1.17	0.66032	0.00031	**0.66094**
PF2E05	HS_FLORIDA_AL_12EXP_SH3B	0.5796	12	0	0.39	1.17	0.65881	0.00030	0.65941
PF2E06	HS_FLORIDA_AL_12EXP_SH3C	0.5796	12	0	0.00	1.17	0.65474	0.00029	0.65532
PF2E07	HS_FLORIDA_AL_12EXP_SH3D	0.5796	12	0	-0.39	1.17	0.64867	0.00029	0.64925
PF2E08	HS_FLORIDA_AL_12EXP_SH3E	0.5796	12	0	-0.78	1.17	0.64175	0.00029	0.64233
PF2E09	HS_FLORIDA_AL_12EXP_SH3F	0.5796	12	0	-1.17	1.17	0.63367	0.00029	0.63425

①Offset is measured radially from the center of the fuel element to the centerline of the package. "Inner" refers to the two inner fuel elements, and "outer" refers to the outer six fuel elements.

(continued)

Table 6.4-12 – HAC Single Package Results, U-Florida (concluded)

Case ID	Filename	Pitch (cm)	Plates at Expanded Pitch	Horizontal Fanning (cm)	Inner Offset (cm)①	Outer Offset (cm)①	k_{eff}	σ	k_s (k+2σ)
PF2F, Alternate Configurations of Aluminum Spacer									
PF2F01	HS_FLORIDA_AL2_12EXP_SH3A	0.5796	12	0	0.78	1.17	0.66276	0.0003	**0.66336**
PF2F02	HS_FLORIDA_AL3_12EXP_SH3A	0.5796	12	0	0.78	1.17	0.66007	0.0003	0.66067
PF2F03	HS_FLORIDA_AL4_12EXP_SH3A	0.5796	12	0	0.78	1.17	0.65973	0.0003	0.66033

①Offset is measured radially from the center of the fuel element to the centerline of the package. "Inner" refers to the two inner fuel elements, and "outer" refers to the outer six fuel elements.

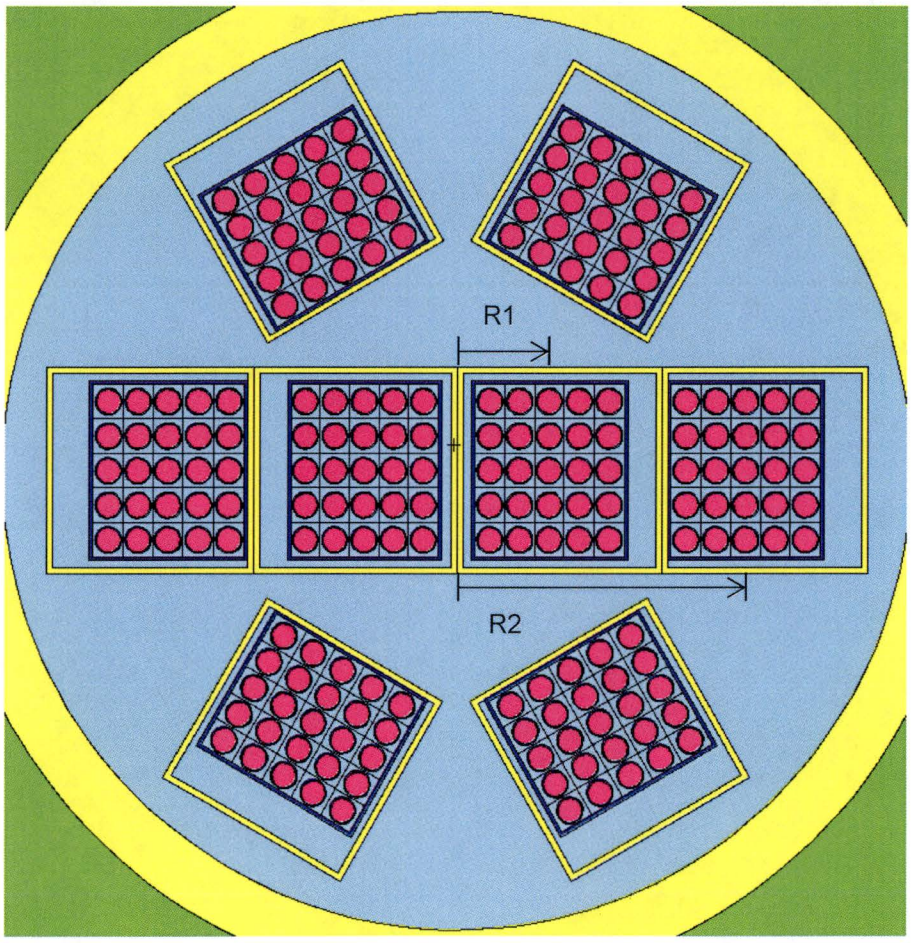

Orientation shown is for Case P2C03 (R1 = 4.17 cm, R2 = 12.93 cm)

Figure 6.4-1 – PULSTAR Element Positions

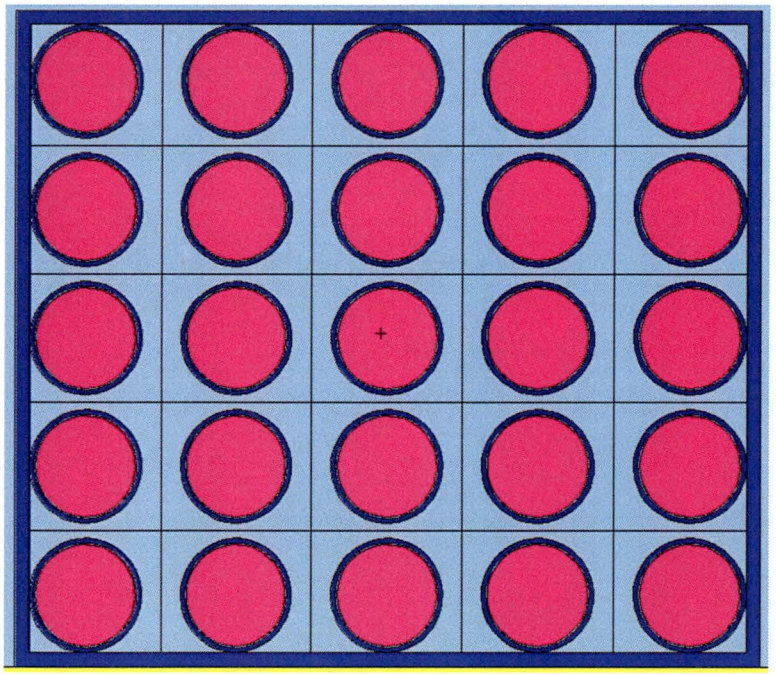

Figure 6.4-2 – PULSTAR Damaged Fuel Element Model

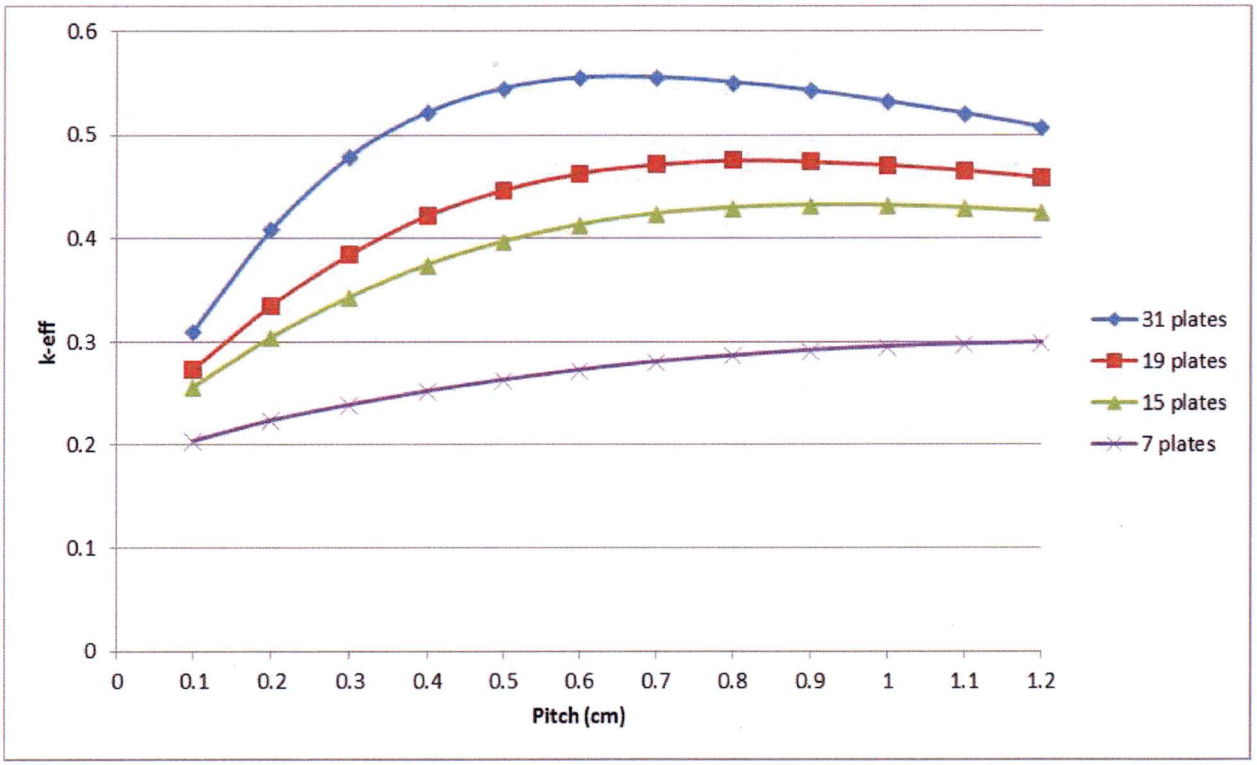

Figure 6.4-3 – Plate Optimization Study

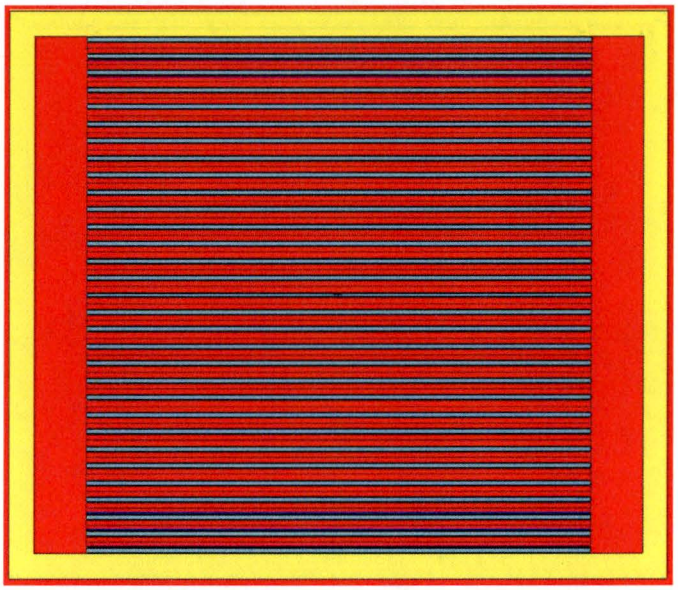

31 plates with uniform pitch (Case L2A04)

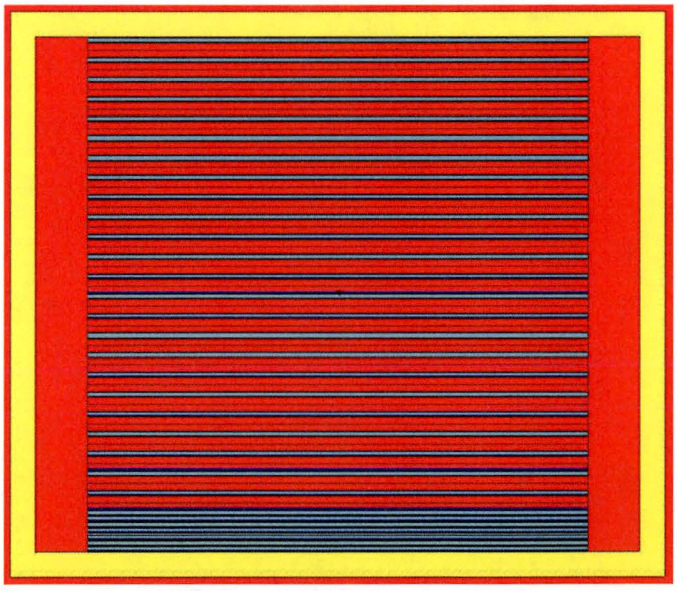

31 plates with non-uniform pitch (25 expanded) (Case L2B06)

Figure 6.4-4 – LPB Pitch Configurations

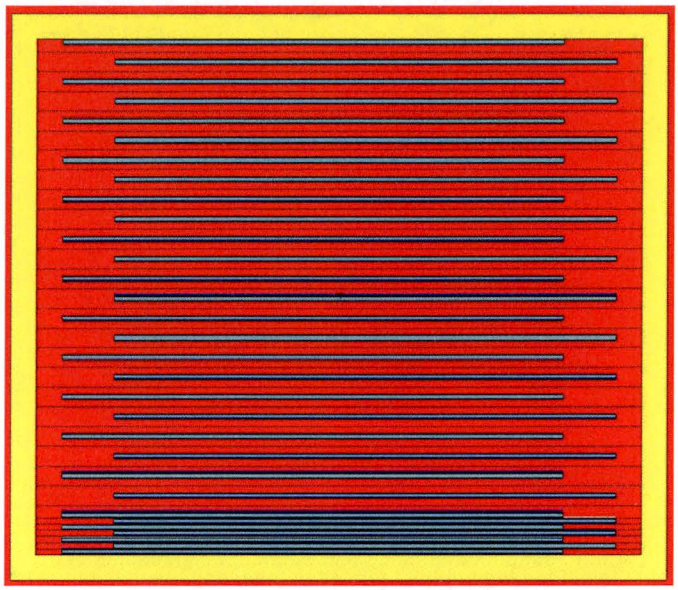

Horizontal Fanning (0.3285 cm) (Case L2C01)

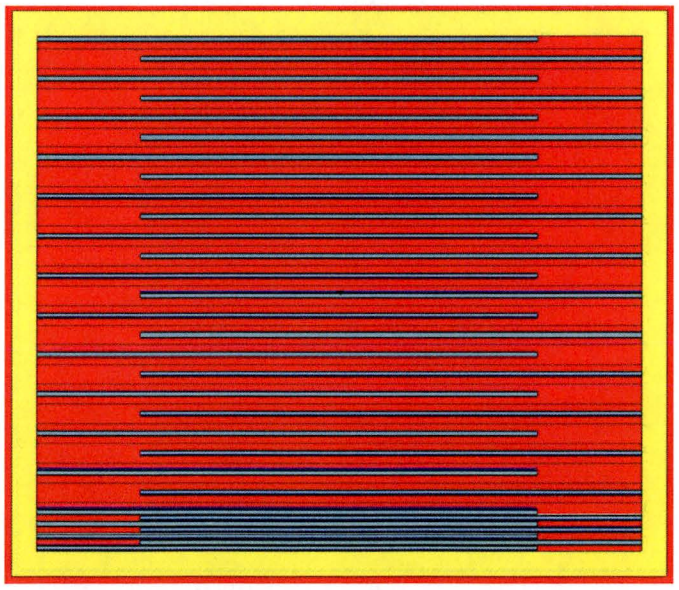

Horizontal Fanning (0.6470 cm) (Case L2C02)

Figure 6.4-5 – LPB Horizontal Fanning Configurations

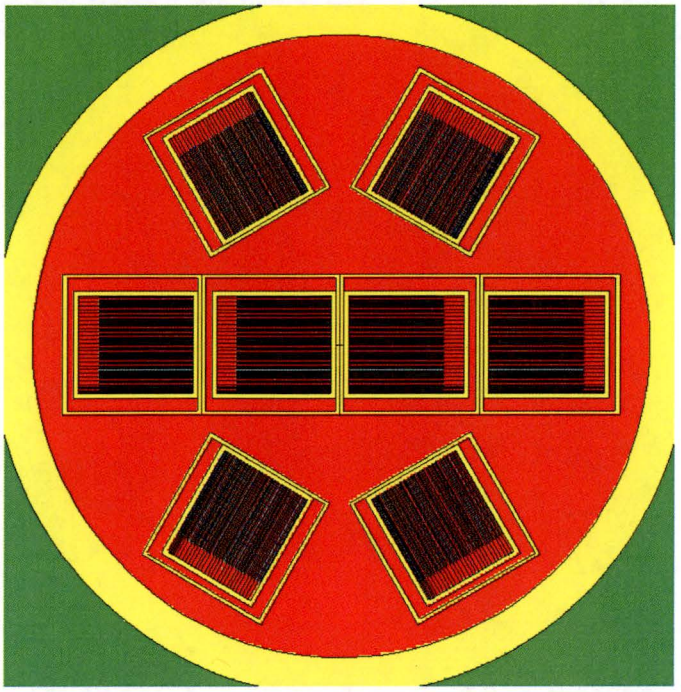

LPBs Shifted to Centerline, Without Fanning (Case L2D01)

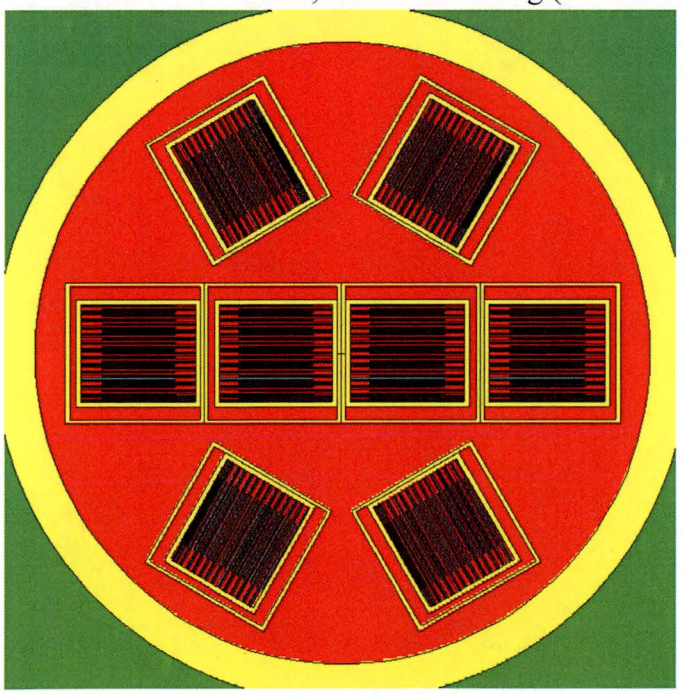

LPBs Shifted to Centerline, With Fanning (Case L2D02)

Figure 6.4-6 – LPB Radial Arrangement

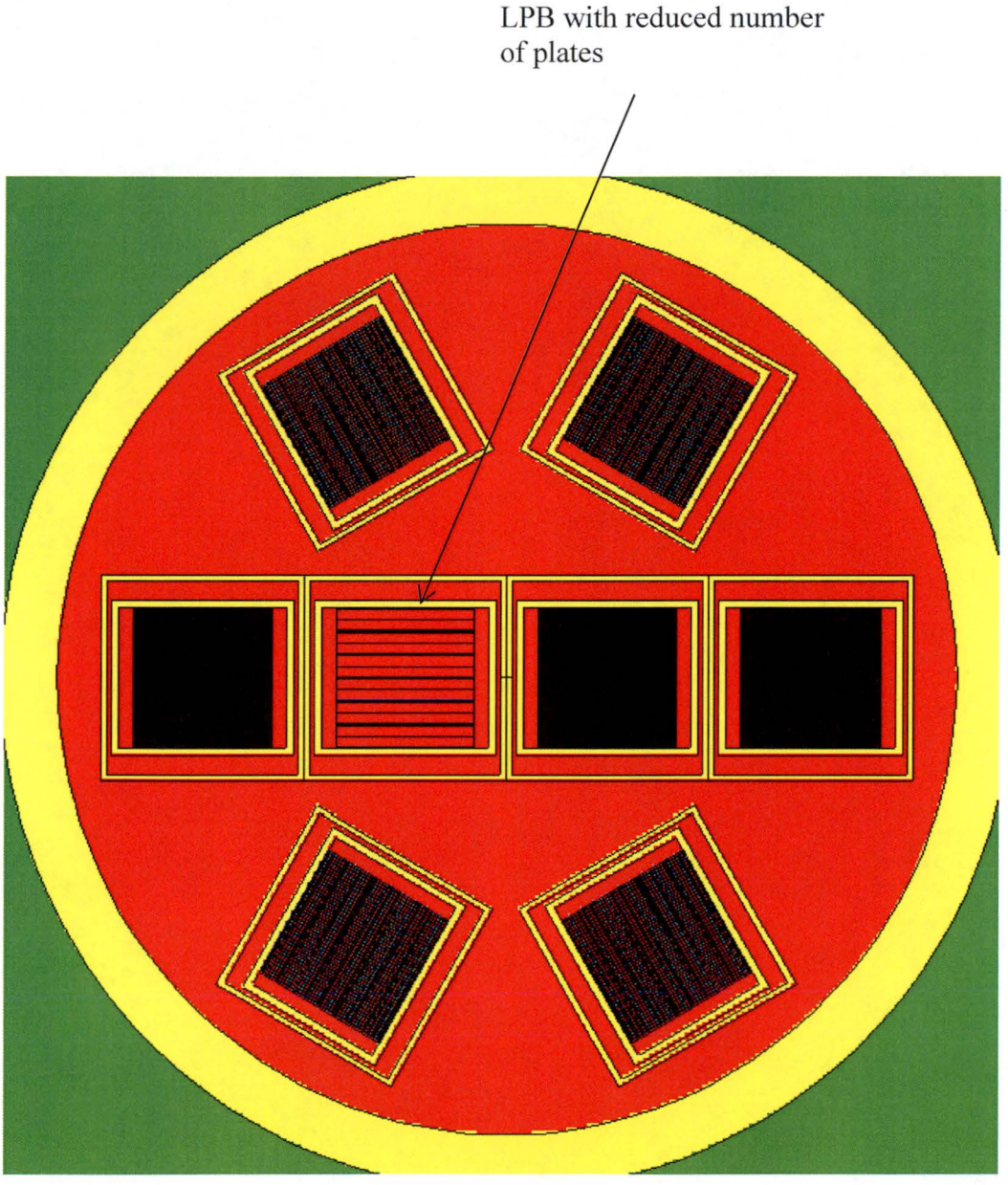

Figure 6.4-7 – LPB Loading/Unloading

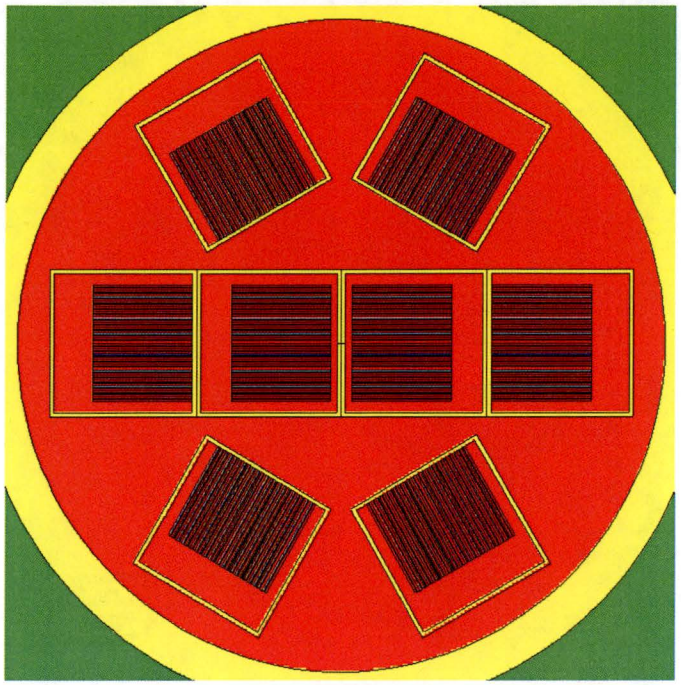

Inner offset = 0.78 cm, Outer offset = 1.17 cm (Case PF2B4)

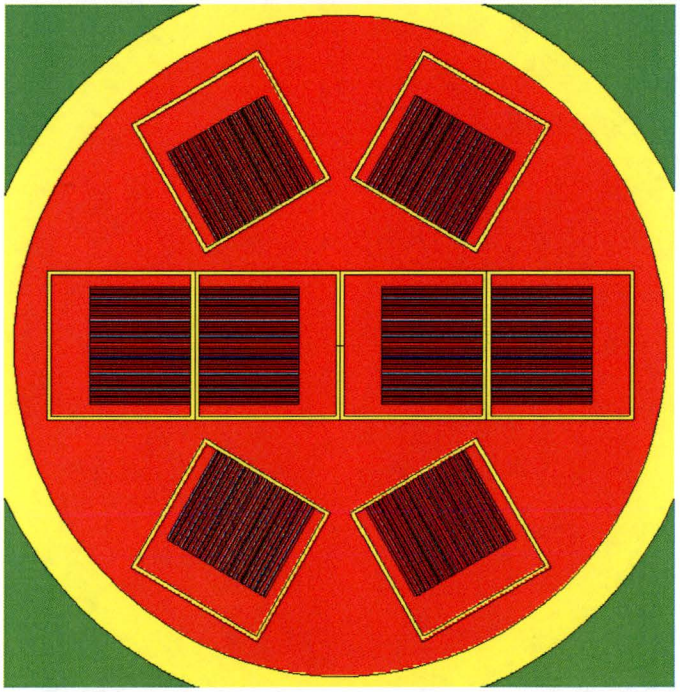

Inner offset = -1.17 cm, Outer offset = 1.17 cm (Case PF2B9)

Figure 6.4-8 – RINSC Radial Arrangement

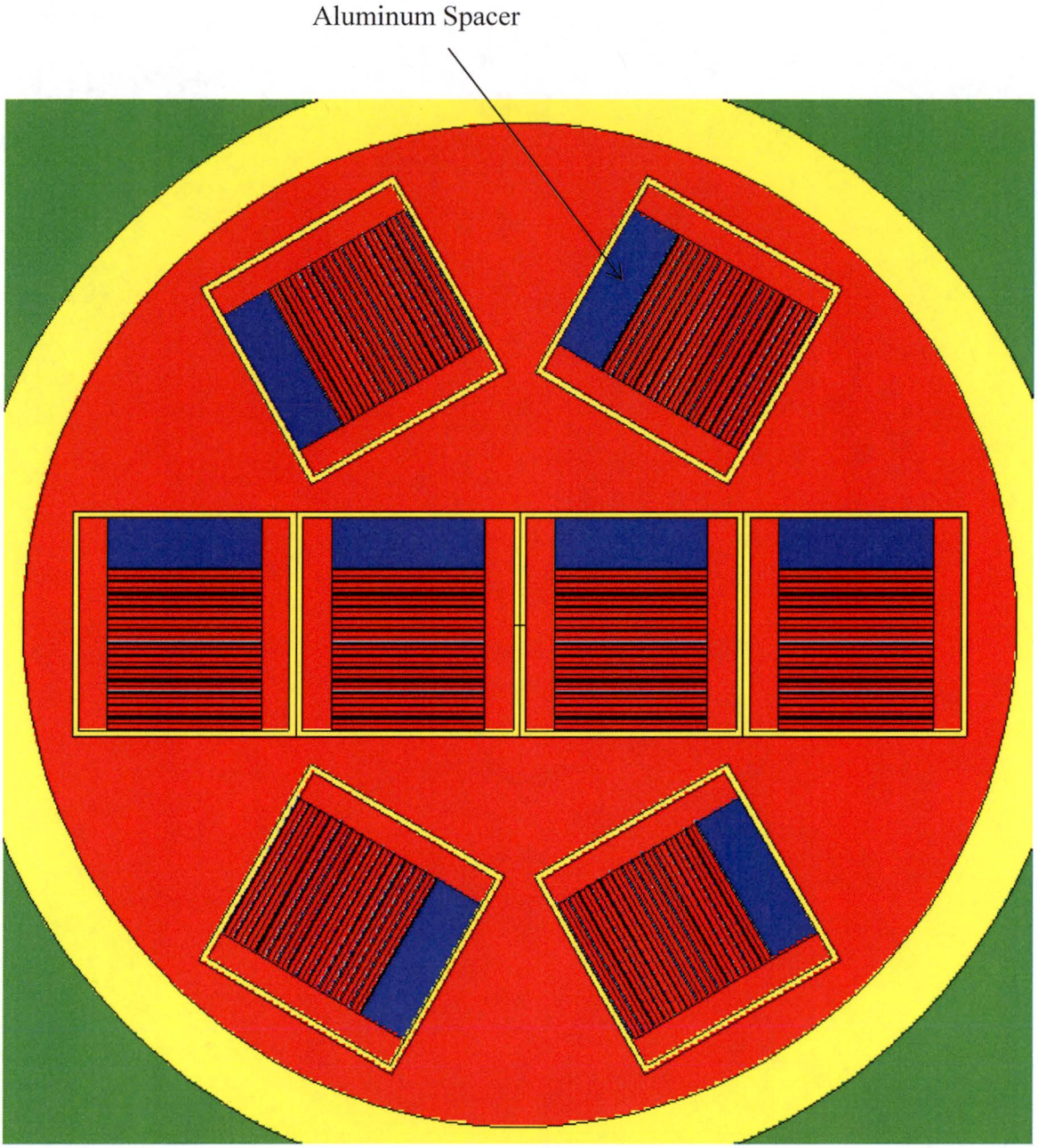

Figure 6.4-9 – Damaged U-Florida Element with Aluminum Spacer

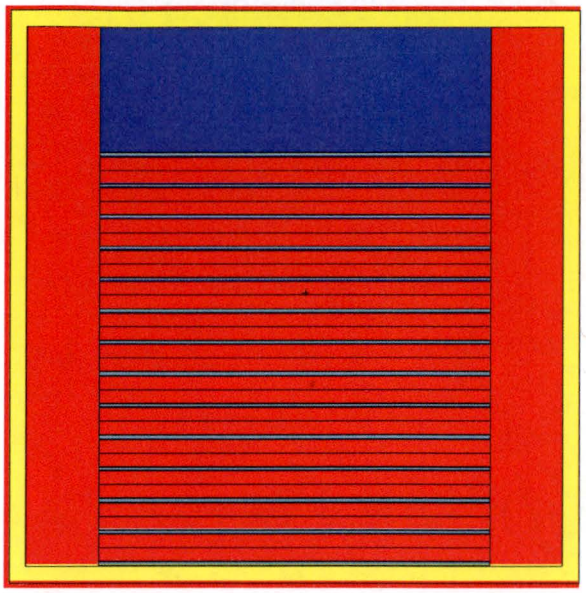

14 plates expanded pitch (Case PF2C04)

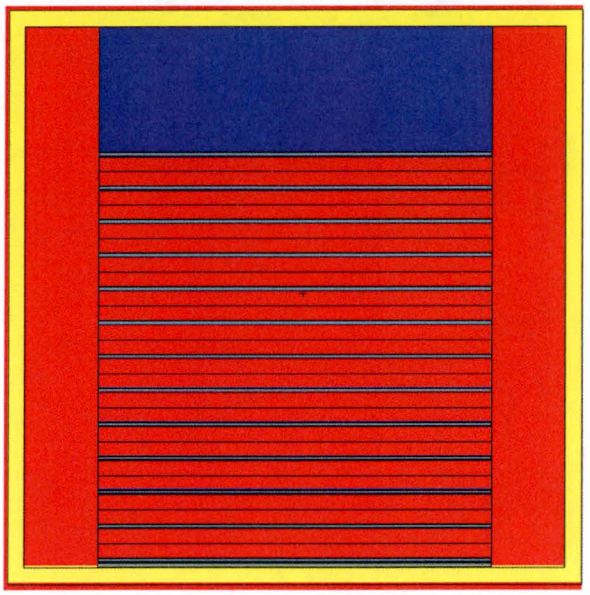

13 plates expanded pitch (Case PF2C05)

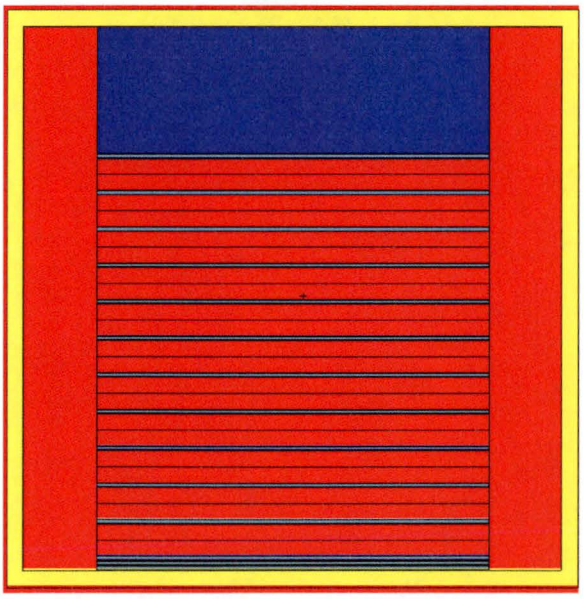

12 plates expanded pitch (Case PF2C06)

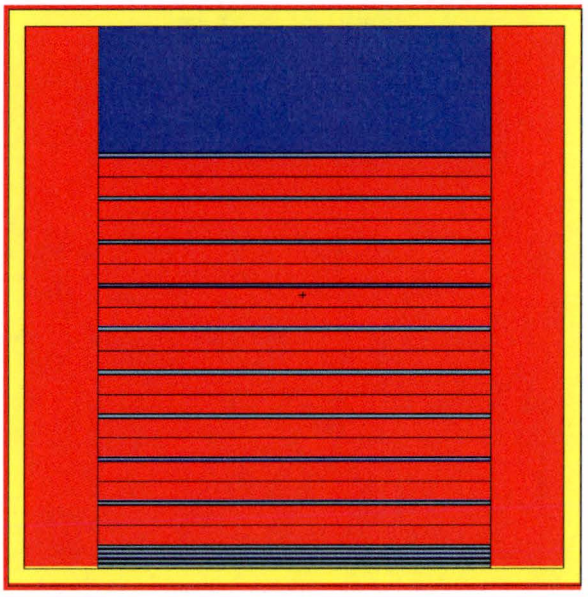

10 plates expanded pitch (Case PF2C08)

Note: All configurations feature 14 fuel plates.

Figure 6.4-10 – Damaged U-Florida Element, Pitch Configurations

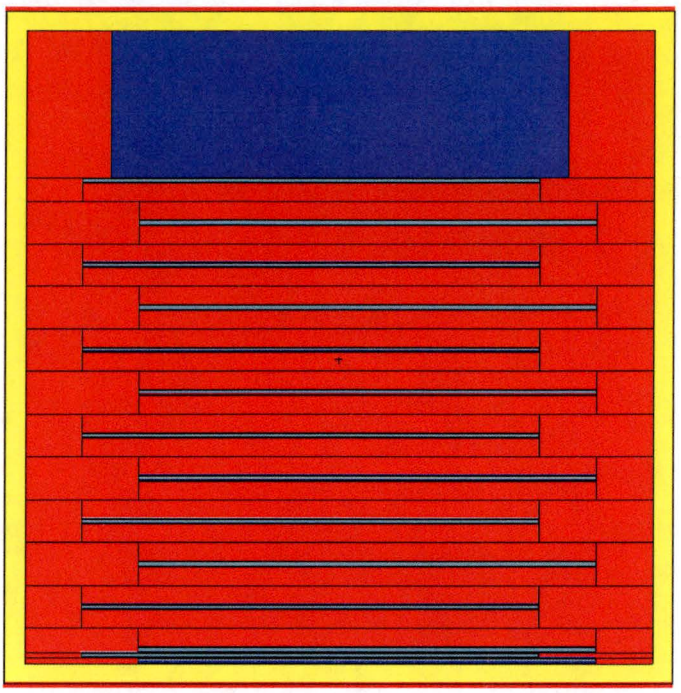

Horizontal Fanning 0.39 cm (Case PF2D01)

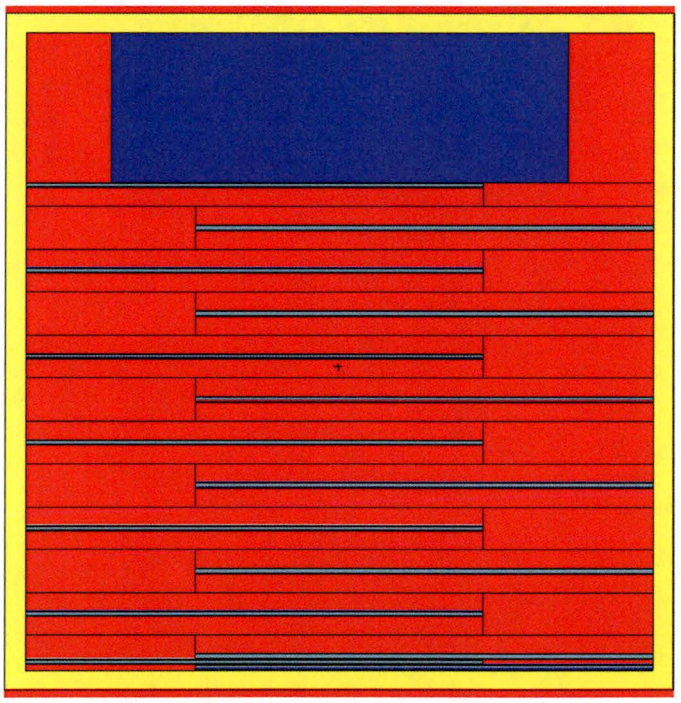

Horizontal Fanning 1.17 cm (Case PF2D03)

Figure 6.4-11 – Damaged U-Florida Element, Fanning Configurations

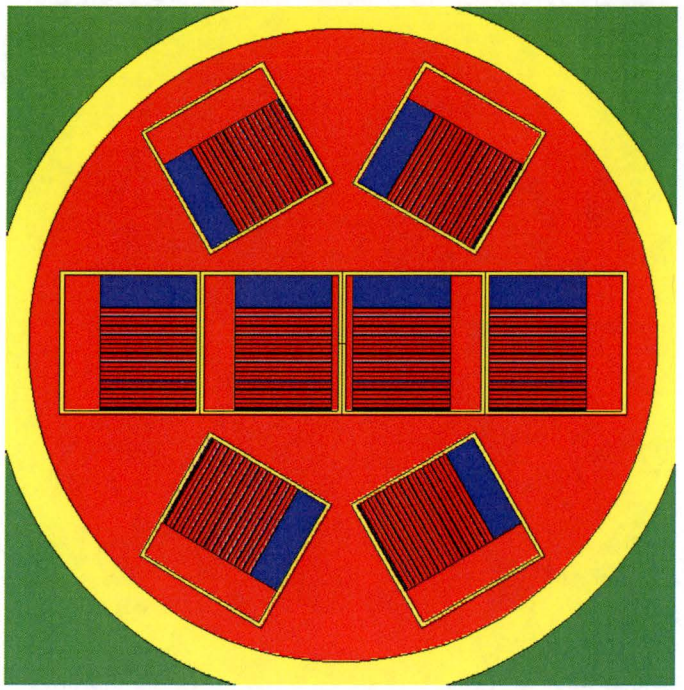

Case PF2E04 (inner offset = 0.78 cm, outer offset = 1.17 cm)

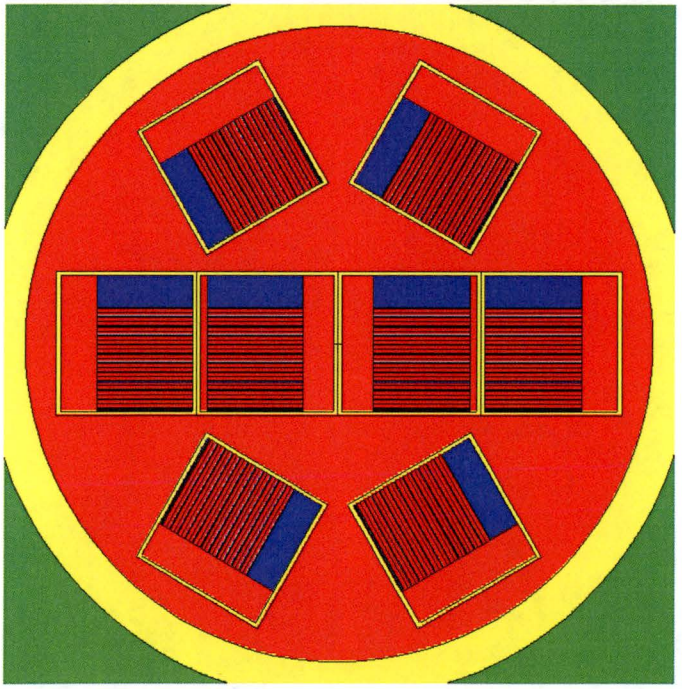

Case PF2E08 (inner offset = -0.78 cm, outer offset = 1.17 cm)

Figure 6.4-12 – Damaged U-Florida Element, Radial Arrangement

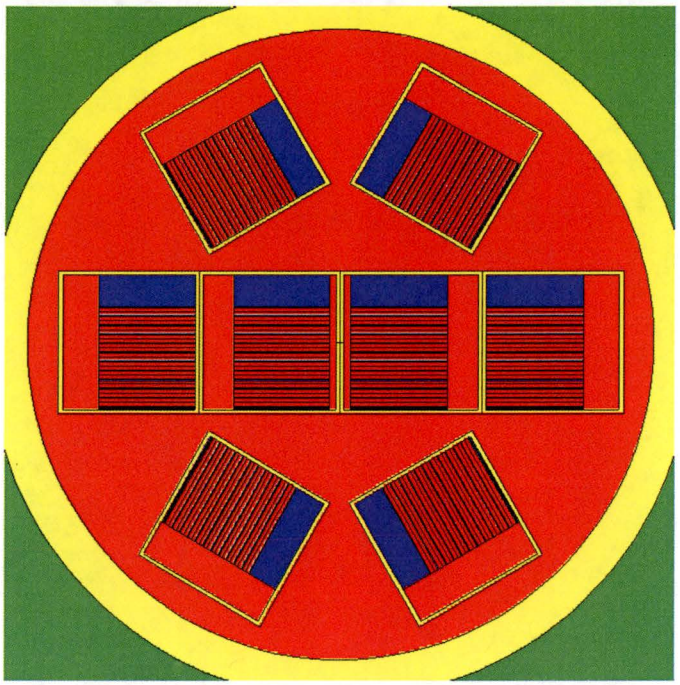

Alternate Configuration 1 (Case PF2F01)

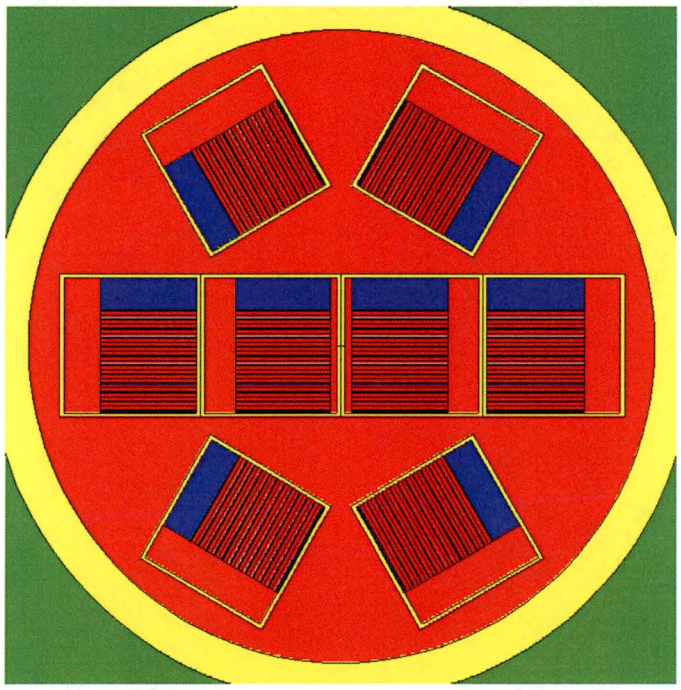

Alternate Configuration 2 (Case PF2F02)

Figure 6.4-13 – Damaged U-Florida Element, Alternate Configurations

6.5 Evaluation of Package Arrays under Normal Conditions of Transport

6.5.1 Configuration

In the NCT array configurations, the most reactive NCT single package configuration for each fuel type determined in Section 6.4.1.1, *NCT Single Package Configuration*, is utilized. A hexagonal reflective surface is added around the package, as shown in Figure 6.5-1. The SFB model is not shown in this figure but the boundary conditions are the same. This simulates a close-packed infinite hexagonal array of packages. The reflective boundary is also present on the top and bottom surfaces.

Five cases are run for MURR, MITR-II, ATR, and TRIGA. The initial case is simply the most reactive NCT single package case with reflective boundary conditions and no water between the packages. In the remaining four cases, the water density between the packages is varied between 0.25 and 1.0 g/cm^3. In each case, the reactivity is maximized with no water between the packages. This conclusion is applied to the subsequent SFB models. Also, each SFB payload is evaluated in a nominal configuration and centered in the SFB compartment.

MURR, MITR-II, and ATR results are summarized in Table 6.5-1. Cases C1 through C5 are for MURR, Cases C10 through C14 are for MITR-II, and Cases C20 through C24 are for ATR. TRIGA results are summarized in Table 6.5-2. Cases C30 through C34 are for TRIGA Type 109 and Case TL3A1 is for TRIGA Type 119. The SFB payload results are provided in Table 6.5-3.

TRIGA fuel Case C30 with no water between the packages is the most reactive, with k_s = 0.53939. Consistent with the single package results, TRIGA Type 109 bounds Type 119. TRIGA fuel is significantly more reactive than the other fuels because hydrogen is present in the fuel matrix and the package cavity is modeled as dry for NCT.

6.5.2 Results

The results for the NCT array cases are provided in Table 6.5-1 through Table 6.5-3. The most reactive configuration for each fuel type is listed in boldface.

Table 6.5-1 – NCT Array Results, MURR, MITR-II, ATR

Case ID	Filename	External Water Density (g/cm^3)	k_{eff}	σ	k_s ($k+2\sigma$)
MURR					
C1	**NA_MURR_INUP**	**0**	**0.19604**	**0.00037**	**0.19678**
C2	NA_MURR_W025INUP	0.25	0.12467	0.00031	0.12529
C3	NA_MURR_W050INUP	0.50	0.11327	0.00029	0.11385
C4	NA_MURR_W075INUP	0.75	0.10858	0.00026	0.10910
C5	NA_MURR_W100INUP	1.0	0.10606	0.00027	0.10660
MITR-II					
C10	**NA_MIT2_W000**	**0**	**0.14305**	**0.00028**	**0.14361**
C11	NA_MIT2_W025	0.25	0.09091	0.00027	0.09145
C12	NA_MIT2_W050	0.50	0.08283	0.00021	0.08325
C13	NA_MIT2_W075	0.75	0.07970	0.00022	0.08014
C14	NA_MIT2_W100	1.0	0.07704	0.00021	0.07746
ATR					
C20	**NA_ATR_INUP**	**0**	**0.23274**	**0.00041**	**0.23356**
C21	NA_ATR_W025INUP	0.25	0.13567	0.00032	0.13631
C22	NA_ATR_W050INUP	0.50	0.12103	0.00031	0.12165
C23	NA_ATR_W075INUP	0.75	0.11473	0.00029	0.11531
C24	NA_ATR_W100INUP	1.0	0.11116	0.00028	0.11172

Table 6.5-2 – NCT Array Results, TRIGA

Case ID	Filename	External Water Density (g/cm^3)	k_{eff}	σ	k_s ($k+2\sigma$)
Type 109					
C30	**NA_TRIGA_INUP**	**0**	**0.53733**	**0.00103**	**0.53939**
C31	NA_TRIGA_W025INUP	0.25	0.46130	0.00099	0.46328
C32	NA_TRIGA_W050INUP	0.50	0.44977	0.00096	0.45169
C33	NA_TRIGA_W075INUP	0.75	0.44506	0.00096	0.44698
C34	NA_TRIGA_W100INUP	1.0	0.43997	0.00094	0.44185
Type 119					
TL3A1	TR_NCT_ARY_A_01	0	0.49222	0.00038	0.49298

Table 6.5-3 – NCT Array Results, Square Fuel Basket

Case ID	Filename	External Water Density (g/cm^3)	k_{eff}	σ	k_s ($k+2\sigma$)
PULSTAR					
P3A1	NA_PULSTAR	0.0	0.22802	0.00048	0.22898
Loose Plate Box					
L3A1	NA_LOOSE_EXP25SH	0.0	0.12015	0.00018	0.12051
Plate Fuels (RINSC)					
PF3A1	NA_RINSC_SH3A	0.0	0.09325	0.00032	0.09389

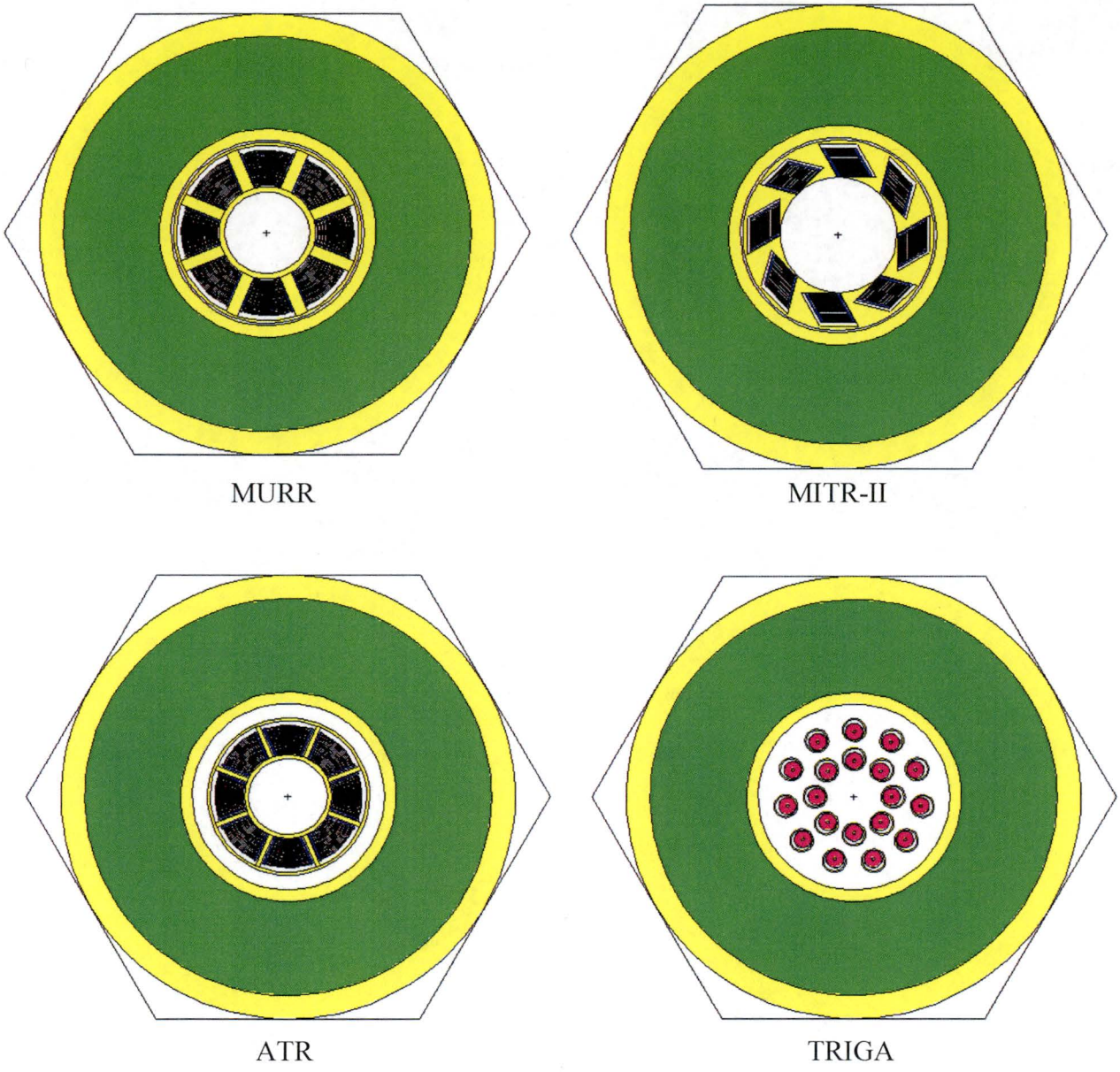

Figure 6.5-1 – NCT Array Geometry

6.6 Package Arrays under Hypothetical Accident Conditions

6.6.1 Configuration

In the HAC array configuration, an infinite hexagonal array of packages is modeled in the same manner as the NCT array. Various internal moderation conditions are examined, as well as various moderation conditions between packages.

MURR

The MURR results are reported in Table 6.6-1 as Cases D1 through D8. In Cases D1 through D7, the cladding thickness and channel spacing are modeled consistent with the NCT analysis. In Case D1, the fuel elements are moved radially inward and shifted to the top of the package, which was determined to be the most reactive single package orientation. The package cavity is flooded with full-density water, and void is modeled between the packages.

In Cases D2 and D3, the configuration of Case D1 is modified so that all water inside the cavity is treated as variable density (0.8 and 0.9 g/cm^3, respectively). Because the water density between the fuel plates is reduced in this configuration, moderation is decreased and the reactivity decreases.

In Cases D4 through D7, the most reactive case (Case D1) is run with variable water density between the packages. The reactivity decreases when water is added to this region.

In Case D8, Case D1 is rerun using the minimum cladding thickness of 0.008-in and channel spacing of 0.094-in. Case D8 is the most reactive, with $k_s = 0.82681$. Note that this is also the most reactive case of all fuel types examined.

MITR-II

The MITR-II results are reported in Table 6.6-2 as Cases D20 through D27. In Cases D20 through D27, the cladding thickness and channel spacing are modeled consistent with the NCT analysis. In Case D20, the fuel elements are pushed radially inward and shifted to the top of the package, which was determined to be the most reactive single package orientation. The package cavity is flooded with full-density water, and void is modeled between the packages.

In Cases D21 and D22, the configuration of Case D20 is modified so that all water inside the cavity is treated as variable density (0.8 and 0.9 g/cm^3, respectively). Because the water density between the fuel plates is reduced in this configuration, moderation is decreased and the reactivity decreases.

In Cases D23 through D26, the most reactive case (Case D20) is run with variable water density between the packages. The reactivity decreases when water is added to this region.

In Case D27, Case D20 is rerun using the minimum cladding thickness of 0.008-in and channel spacing of 0.116-in. Case D27 is the most reactive, with $k_s = 0.60948$.

ATR

The ATR results are reported in Table 6.6-3 as Cases D40 through D47. In Cases D40 through D46, the cladding thickness and channel spacing are modeled consistent with the NCT analysis. In Case D40, the fuel elements are moved radially inward and shifted to the top of the package,

which was determined to be the most reactive single package orientation. The package cavity is flooded with full-density water, and void is modeled between the packages.

In Cases D41 and D42, the configuration of Case D40 is modified so that all water inside the cavity is treated as variable density (0.8 and 0.9 g/cm^3, respectively). Because the water density between the fuel plates is reduced in this configuration, moderation is decreased and the reactivity decreases.

In Cases D43 through D46, the most reactive case (Case D40) is run with variable water density between the packages. The reactivity decreases when water is added to this region.

In Case D47, Case D40 is rerun using a cladding thickness of 0.018-in for plates 1 and 19, and 0.008-in for plates 2 through 18. The resulting channel spacing is 0.097-in between plates 1 and 2, 0.107-in between plates 18 and 19, and 0.092-in between the remaining plates. Therefore, Case D47 is the most reactive, with $k_s = 0.72066$.

TRIGA

The TRIGA results are reported in Table 6.6-4. Type 109 results are provided in Cases D60 to D71, and Type 119 results are provided in Cases TL4A1 through TL4A6. In all models, the fuel elements are moved radially inward and axially shifted to the top of the cask, which was determined to be the most reactive single package orientation. It is expected that the most reactive condition will occur at a reduced internal water density, consistent with the single package TRIGA results.

In Cases D60 through D67, the cavity water density is varied from 0.3 to 1.0 g/cm^3, while void is modeled external to the package. The maximum reactivity occurs for Case D63, which has a water density of 0.6 g/cm^3. In Cases D68 through D71, the internal water density is modeled at 0.6 g/cm^3 (Case D63 configuration) while the external water density is varied between 0.25 and 1.0 g/cm^3. The reactivity decreases when water is modeled between the packages. Therefore, Case D63 is the most reactive, with $k_s = 0.72039$.

Because of the difference in composition between rod Types 109 and 119, the effect of moderator density is revaluated for Type 119. External water (between packages in the array) is demonstrated to reduce reactivity in Type 109 cases D68-D71. This finding is applicable to the Type 119 payload and therefore these cases are evaluated with void between adjacent packages in the array. The highest k_s observed for the Type 119 payload is 0.71738 and occurs with a moderator density of 0.7 g/cm^3. The Type 119 rods are therefore slightly less reactive than the HEU bearing Type 109 rods. Peak reactivity for the Type 119 rods occurs at a somewhat higher moderator density (0.7 g/cm^3 vs. 0.6 g/cm^3), which is attributable to the reduced enrichment and the corresponding increased role of U-238.

Square Fuel Basket

It is observed from the results for MURR, MITR-II, and ATR that reactivity in an infinite array is maximized with full moderation within the cavity and void between adjacent packages. Therefore, only this moderation condition is considered in the SFB HAC array cases. The most reactive SFB single package cases from Section 6.4, *Single Package Evaluation*, are modified to change the boundary condition to a close-packed reflective hexagonal array, which represents an infinite array of packages. Results are provided in Table 6.6-5. The HAC array results are:

- $k_s = 0.82202$ for PULSTAR

- k_s = 0.64661 for the LPB, and
- k_s = 0.74629 for plate fuels (RINSC)

All results are significantly below the USL of 0.9209. The reactivity for any combination of authorized SFB contents will not exceed the reactivity of the PULSTAR payload.

6.6.2 Results

Following are the tabulated results for the HAC array cases. The most reactive configuration in each series is listed in boldface.

Table 6.6-1 – HAC Array Results, MURR

Case ID	Filename	Internal Water Density (g/cm^3)	External Water Density (g/cm^3)	k_{eff}	σ	k_s (k+2σ)
D1	HA_MURR	1.0	0	0.80428	0.00115	0.80658
D2	HA_MURR_C080	0.8	0	0.74913	0.00111	0.75135
D3	HA_MURR_C090	0.9	0	0.77692	0.00116	0.77924
D4	HA_MURR_W025	1.0	0.25	0.77495	0.00125	0.77745
D5	HA_MURR_W050	1.0	0.50	0.77403	0.00106	0.77615
D6	HA_MURR_W075	1.0	0.75	0.77030	0.00115	0.77260
D7	HA_MURR_W100	1.0	1.0	0.76810	0.00131	0.77072
D8	**HA_MURRC**	**1.0**	**0**	**0.82441**	**0.00120**	**0.82681**

Table 6.6-2 – HAC Array Results, MITR-II

Case ID	Filename	Internal Water Density (g/cm^3)	External Water Density (g/cm^3)	k_{eff}	σ	k_s (k+2σ)
D20	HA_MIT2	1.0	0	0.56103	0.00102	0.56307
D21	HA_MIT2_C080	0.8	0	0.53082	0.00099	0.53280
D22	HA_MIT2_C090	0.9	0	0.54724	0.00106	0.54936
D23	HA_MIT2_W025	1.0	0.25	0.54199	0.00096	0.54391
D24	HA_MIT2_W050	1.0	0.50	0.53616	0.00096	0.53808
D25	HA_MIT2_W075	1.0	0.75	0.53278	0.00111	0.53500
D26	HA_MIT2_W100	1.0	1.0	0.53347	0.00105	0.53557
D27	**HA_MIT2C**	**1.0**	**0**	**0.60736**	**0.00106**	**0.60948**

Table 6.6-3 – HAC Array Results, ATR

Case ID	Filename	Internal Water Density (g/cm^3)	External Water Density (g/cm^3)	k_{eff}	σ	k_s (k+2σ)
D40	HA_ATR	1.0	0	0.69505	0.00117	0.69739
D41	HA_ATR_C080	0.8	0	0.66976	0.00104	0.67184
D42	HA_ATR_C090	0.9	0	0.68206	0.00109	0.68424
D43	HA_ATR_W025	1.0	0.25	0.68753	0.00115	0.68983
D44	HA_ATR_W050	1.0	0.50	0.68575	0.00111	0.68797
D45	HA_ATR_W075	1.0	0.75	0.68528	0.00106	0.68740
D46	HA_ATR_W100	1.0	1.0	0.68342	0.00110	0.68562
D47	**HA_ATRC**	**1.0**	**0**	**0.71864**	**0.00101**	**0.72066**

Table 6.6-4 – HAC Array Results, TRIGA

Case ID	Filename	Internal Water Density (g/cm^3)	External Water Density (g/cm^3)	k_{eff}	σ	k_s (k+2σ)
Type 109						
D60	HA_TRIGA_W0C030	0.3	0	0.68281	0.00107	0.68495
D61	HA_TRIGA_W0C040	0.4	0	0.70304	0.00102	0.70508
D62	HA_TRIGA_W0C050	0.5	0	0.71234	0.00113	0.71460
D63	**HA_TRIGA_W0C060**	**0.6**	**0**	**0.71827**	**0.00106**	**0.72039**
D64	HA_TRIGA_W0C070	0.7	0	0.71592	0.00107	0.71806
D65	HA_TRIGA_W0C080	0.8	0	0.71130	0.00109	0.71348
D66	HA_TRIGA_W0C090	0.9	0	0.70455	0.00107	0.70669
D67	HA_TRIGA_W0C100	1.0	0	0.69737	0.00112	0.69961
D68	HA_TRIGA_W025C060	0.6	0.25	0.70793	0.00125	0.71043
D69	HA_TRIGA_W050C060	0.6	0.50	0.70781	0.00097	0.70975
D70	HA_TRIGA_W075C060	0.6	0.75	0.70655	0.00110	0.70875
D71	HA_TRIGA_W100C060	0.6	1.0	0.70660	0.00105	0.70870
Type 119						
TL4A1	TR_HAC_ARY_A_01	0.4	0	0.69599	0.00040	0.69679
TL4A2	TR_HAC_ARY_A_02	0.5	0	0.70854	0.00045	0.70944
TL4A3	TR_HAC_ARY_A_03	0.6	0	0.71531	0.00046	0.71623
TL4A4	**TR_HAC_ARY_A_04**	**0.7**	**0**	**0.71646**	**0.00046**	**0.71738**
TL4A5	TR_HAC_ARY_A_05	0.8	0	0.71293	0.00047	0.71387
TL4A6	TR_HAC_ARY_A_06	0.9	0	0.70827	0.00050	0.70927

Table 6.6-5 – HAC Array Results, Square Fuel Basket

Case ID	Filename	Internal Water Density (g/cm^3)	External Water Density (g/cm^3)	k_{eff}	σ	k_s (k+2σ)
PULSTAR						
P4A1	PS_ARRAY_HAC_4B_01	1.0	0	0.82114	0.00044	0.82202
Loose Plate Box						
L4A1	HA_LOOSE_EXP25SH	1.0	0	0.64597	0.00032	0.64661
Plate Fuels (RINSC)						
PF4A1	HA_RINSC_SH3A	1.0	0	0.74471	0.00079	0.74629

7.0 PACKAGE OPERATIONS

7.1 Procedures for Loading the Package

This section delineates the procedures for loading a payload from the BRR packaging. Hereafter, reference to specific BRR packaging components may be found in Appendix 1.3.3, *Packaging General Arrangement Drawings*.

7.1.1 Preparation for Loading

1. Remove the BRR package tie–down cover from the upper impact limiter.
2. Optionally, remove the cask and transport pallet from the transport trailer using the fork pockets in the pallet. Before lifting the pallet from the trailer, secure the tie–down cover to the pallet using the chains provided. Remove the tiedown cover and chains when pallet movement is complete.
3. Attach rigging to the upper impact limiter using the three (3) 1/2–13 UNC threaded holes marked as impact limiter lift points.
4. Remove the (8) eight ∅1–inch ball lock pins from each upper impact limiter attachment.
5. Using an overhead crane (or equivalent), lift and remove the upper impact limiter from the cask body.
6. Secure the lift adaptor to the cask body using the four (4) 1– 8UNC bolts. If rigging is used, secure the swivel hoist rings in place using swivel hoist ring 1-8UNC fasteners. Tighten the bolts/fasteners to 220 ±20 ft–lb torque.
7. Remove the (8) eight ∅1–inch ball lock pins from each lower impact limiter attachment.
8. Lift the cask body from the lower impact limiter, and place it on the facility transport equipment or in the desired staging location.
9. Secure the cask body to the facility transport equipment or in the staging location, and remove the rigging from the lift adaptor.

7.1.2 Loading of Contents

The BRR package is designed to be loaded either in a pool of water (wet) or in a hot cell (dry), as delineated in the following sections.

7.1.2.1 Wet Loading

1. Remove the twelve (12) 1–8UNC socket head cap screws (SHCSs) that retain the closure lid.
2. Install three (3) hoist rings (or equivalent) into the three (3) 1/2–13 UNC threaded holes in the closure lid.
3. Lift and remove the closure lid from the cask body. Store the closure lid in a manner to minimize potential damage to the O–ring seals and sealing surfaces.
4. Install and secure the sealing surface protector to the cask body.

5. Using the center 1/2–13 UNC threaded hole in the shield plug as a lift point, remove the shield plug from the cask body.
6. If not previously installed, install the appropriate fuel basket into the cask body cavity. Verify that spacer pedestals are installed if required, as specified by Table 7.1-1 for Square fuels and Table 7.1-2 for TRIGA fuels. (Note: spacer pedestals are not used with the MURR, MITR-II, or ATR baskets.)
7. Remove the drain port dust cover and then the drain port plug. Install an appropriate drain fitting to the drain port.
8. Using an overhead crane (or equivalent), and attached to the lift adaptor, lift the cask body with the fuel basket from the facility transport equipment or staging location and position over the spent fuel pool staging area.
9. Slowly lower the cask body into the pool until the cavity is flooded, and the cask body is properly positioned and secured for fuel loading.
10. Verify that fuel to be loaded is intact and undamaged. ATR fuel end boxes may be trimmed.
11. Load fuel elements into the designated fuel basket.
    a. Up to eight (8) fuel elements may be loaded into the MURR, MITR-II, ATR, or Square fuel baskets. Mixing of element types in the Square fuel basket is permitted.
    b. When loading fuel elements from the University of Florida reactor, place an aluminum spacer plate, 27 ±¼ inches long, 3 ±¼ inches wide, and 0.8, -0.0/+0.03 inches thick, into the Square fuel basket opening beside the fuel element, oriented parallel to the fuel plates. The spacer plate is shown on the left side of the drawing in Figure 7.1-1.
    c. Up to nineteen (19) fuel elements may be loaded into the TRIGA basket. Mixing of TRIGA element types in the same basket is permitted.
12. If shipping loose plates:
    a. Load loose plates into the loose plate box. This may be performed before or after placing the loose plate box into the Square fuel basket.
    b. Using aluminum dunnage sheets as necessary, reduce the free space between the flat face of the loose plates and the box opening to a value of ¼ inches or less. The dunnage sheets shall be 25½ ±¼ inches long, 2½ ±¼ inches wide, and a minimum of 1/16 inches thick. A dunnage sheet is shown on the right side of the drawing in Figure 7.1-1.
    c. Up to eight (8) loose plate boxes may be loaded into the Square fuel basket, each box containing up to thirty-one (31) loose plates of the types shown in Table 7.1-1. Mixing of loose plate boxes and elements in the Square fuel basket is permitted.
13. Using the center 1/2–13 UNC threaded hole as a lift point, lower the shield plug into the cask body cavity. Visually verify that the shield plug is properly seated, and reposition if necessary.
14. If required, install the shield plug restraint, or optionally, install the shield plug restraint once the cask body has been raised to the working level.

15. Lift the loaded cask body from the spent fuel pool while rinsing exposed portions with clean demineralized water. Perform a radiological survey of the cask body as it is raised out of the pool.
16. Open the drain fitting to drain the pool water from the cavity. Continue draining the cavity until no appreciable water is noted. Close the drain fitting. Optionally, the cavity may be drained after securing the cask body in the facility work area.
17. Lift the loaded cask body out of the spent fuel pool area and secure it in the facility work area.
18. Connect drain tubing to the drain fitting, and route the drain tubing to an appropriate container. Open the drain fitting.
19. Remove the sealing surface protector and, if installed, the shield plug restraint from the shield plug and cask body.
20. Remove and discard both main O–ring seals (if present), and clean and inspect the sealing surfaces in the closure lid and the mating surfaces on the cask body. If damage is present which is sufficient to impair containment integrity (scratches or dents, etc.), repair the damaged surfaces per Section 8.2.3.2, *Sealing Area Routine Inspection and Repair*.
21. Install two new (unused) O-rings in the appropriate grooves in the closure lid. As an option, sparingly apply vacuum grease to the O–ring seals and/or sealing surfaces.
22. Install the closure lid on the cask body, using the alignment pin to guide the closure lid into position.
23. Visually inspect the closure SHCSs for wear or damage that could impair their function and, if necessary, replace or repair per the requirements of the drawings in Appendix 1.3.3, *Packaging General Arrangement Drawings*.
24. Install the twelve (12) 1–8UNC SHCSs to secure the closure lid to the cask body. Using a star pattern, tighten the closure SHCSs to 220 ±20 ft–lb torque (lubricated).
25. Remove the vent port dust cover, vent port plug, test port dust cover, and test port plug.
26. Install a vent port tool into the vent port, and connect a source of dry pressurized air to the vent port tool.
27. Open the air supply flow control valve to permit dry pressurized air flowing through the cavity, ensuring that the air pressure does not exceed 25 psig. Continue the air supply flow until all apparent free standing water has been removed from the cavity.
28. Remove the drain port fitting and tubing from the drain port.
29. Remove and discard the vent, test, and drain port sealing washers from their respective port plugs (if present), and clean and inspect each sealing surface. If damage is present that is sufficient to impair containment integrity (scratches or dent, etc.), repair the damaged surfaces per Section 8.2.3.2, *Sealing Area Routine Inspection and Repair*.
30. Install the drain port plug and a new (unused) sealing washer in the drain port. Tighten the drain port plug to 20 ±2 ft–lb torque.
31. Using the vent port tool, install the vent port plug with a new (unused) sealing washer. Ensure that the vent port plug is sufficiently loose to allow airflow through the vent port.

32. Install the test port plug and a new (unused) sealing washer in the closure lid approximately finger-tight.
33. Connect a vacuum pump and a shutoff valve to the vent port tool and evacuate the cavity until the internal pressure is 1 – 2 torr. Isolate the vacuum pump from the cask body cavity by closing the shutoff valve and shutting off the vacuum pump, closing the shutoff valve and venting the suction line to atmosphere, or other appropriate means that does not maintain a vacuum on the outlet of the shutoff valve.
34. Monitor the cavity pressure for a minimum of 30 minutes. If the cavity pressure does not exceed 3 torr at the end of the time period, proceed to Step 36. If it appears that cavity pressure will exceed 3 torr, it is not necessary to wait 30 minutes before proceeding to step 35. As an option, repeat Steps 33 and 34 without first performing Step 35.
35. Open the port tool to re–pressurize the cask body cavity to atmospheric pressure and repeat Steps 33 and 34. The cask may be re-pressurized with air, nitrogen, or helium.
36. Disconnect the vacuum pump from the vent port tool and connect a source of helium gas.
37. Provide a helium atmosphere inside the cask payload cavity by backfilling with helium gas to a pressure of slightly greater than atmospheric pressure, i.e., +1, -0 psig.
38. Disconnect the helium gas source from the vent port tool.
39. Using the vent port tool, tighten the vent port plug to 9 ±1 ft–lb torque.
40. Perform leakage rate testing on the containment O-ring seal and the drain and vent port sealing washers per Section 8.2.2.2, *Helium leakage Rate Testing the Main Containment O-ring Seal*, Section 8.2.2.3, *Helium Leakage Rate Testing the Drain Port Sealing Washer*, and Section 8.2.2.4, *Helium Leakage Rate Testing the Vent Port Sealing Washer*.
41. At the conclusion of all leakage rate testing, install the drain port dust cover, the test port dust cover, and vent port dust cover.

7.1.2.2 Dry Loading

Steps 1 – 6 may be performed either inside or outside of the hot cell. A transfer cask may be used in place of the hot cell for this procedure. The cask must remain upright at all times.

1. Remove the twelve (12) 1–8UNC socket head cap screws (SHCSs) that retain the closure lid.
2. Install three (3) hoist rings (or equivalent) into the three (3) 1/2–13 UNC threaded holes in the closure lid.
3. Lift and remove the closure lid from the cask body. Store the closure lid in a manner to minimize potential damage to the O–ring seals and sealing surfaces.
4. Install and secure the sealing surface protector to the cask body.
5. Using the center 1/2–13 UNC threaded hole in the shield plug as a lift point, remove the shield plug from the cask body.
6. If not previously installed, install the appropriate fuel basket into the cask body cavity. Verify that spacer pedestals are installed if required, as specified by Table 7.1-1 for Square fuels and Table 7.1-2 for TRIGA fuels. (Note: spacer pedestals are not used with the MURR, MITR-II, or ATR baskets.)

7. If steps 1 – 6 were performed outside of the hot cell, reinstall shield plug in cask.
8. Mate the cask opening with the hot cell. If necessary, place the cask body inside the hot cell.
9. If required, remove the shield plug.
10. Verify that fuel to be loaded is intact and undamaged. ATR fuel end boxes may be trimmed.
11. Load fuel elements into the designated fuel basket.
    a. Up to eight (8) fuel elements may be loaded into the MURR, MITR-II, ATR, or Square fuel baskets. Mixing of element types in the square fuel basket is permitted.
    b. When loading fuel elements from the University of Florida reactor, place an aluminum spacer plate, 27 ±¼ inches long, 3 ±¼ inches wide, and 0.8, -0.0/+0.03 inches thick, into the Square fuel basket opening beside the fuel element, oriented parallel to the fuel plates. The spacer plate is shown on the left side of the drawing in Figure 7.1-1.
    c. Up to nineteen (19) fuel elements may be loaded into the TRIGA basket. Mixing of TRIGA element types in the same basket is permitted.
12. If shipping loose plates:
    a. Load loose plates into the loose plate box. This may be performed before or after placing the loose plate box into the Square fuel basket.
    b. Using aluminum dunnage sheets as necessary, reduce the free space between the flat face of the loose plates and the box opening to a value of ¼ inches or less. The dunnage sheets shall be 25½ ±¼ inches long, 2½ ±¼ inches wide, and a minimum of 1/16 inches thick. A dunnage sheet is shown on the right side of the drawing in Figure 7.1-1.
    c. Up to eight (8) loose plate boxes may be loaded into the Square fuel basket, each box containing up to thirty-one (31) loose plates of the types shown in Table 7.1-1. Mixing of loose plate boxes and elements in the Square fuel basket is permitted.
13. Using the center 1/2–13 UNC threaded hole as a lift point and a remote lift adapter, lower the shield plug into the cask body cavity. Visually verify that the shield plug is properly seated, and reposition if necessary.
14. Optionally, install the shield plug restraint.
15. If the cask was placed within the hot cell remove the loaded cask body from the hot cell. Perform a radiological survey of the cask body as it is removed.
16. If the cask was mated to the hot cell, disconnect the cask from the hot cell. Perform a radiological survey of the cask body as it is removed.
17. Remove the sealing surface protector and, if installed, the shield plug restraint from the shield plug and cask body.
18. Remove and discard both main O–ring seals (if present), and clean and inspect the sealing surfaces in the closure lid and the mating surfaces on the cask body. If damage is present which is sufficient to impair containment integrity (scratches or dents, etc.), repair the damaged surfaces per Section 8.2.3.2, *Sealing Area Routine Inspection and Repair.*

19. Install two new (unused) O-rings in the appropriate grooves in the closure lid. As an option, sparingly apply vacuum grease to the O–ring seals and/or sealing surfaces.
20. Install the closure lid on the cask body, using the alignment pin to guide the closure lid into position.
21. Visually inspect the closure SHCSs for wear or damage that could impair their function and, if necessary, replace or repair per the requirements of the drawings in Appendix 1.3.3, *Packaging General Arrangement Drawings*.
22. Install the twelve (12) 1–8UNC SHCSs to secure the closure lid to the cask body. Using a star pattern, tighten the closure SHCSs to 220 ±20 ft–lb torque (lubricated).
23. Remove the vent port dust cover, vent port plug, test port dust cover, and test port plug.
24. Remove the drain port dust cover and drain port plug.
25. Remove and discard the vent, test, and drain port sealing washers from their respective port plugs (if present), and clean and inspect each sealing surface. If damage is present that is sufficient to impair containment integrity (scratches or dent, etc.), repair the damaged surfaces per Section 8.2.3.2, *Sealing Area Routine Inspection and Repair*.
26. Install the drain port plug and a new (unused) sealing washer in the drain port. Tighten the drain port plug to 20 ±2 ft–lb torque.
27. Using the vent port tool, install the vent port plug with a new (unused) sealing washer. Ensure that the vent port plug is loose enough to allow airflow through the vent port.
28. Install the test port plug and a new (unused) sealing washer in the closure lid approximately finger-tight.
29. Connect a vacuum pump and a shutoff valve to the vent port tool and evacuate the cavity until the internal pressure is 1 – 2 torr. Isolate the vacuum pump from the cask body cavity by closing the shutoff valve and shutting off the vacuum pump, closing the shutoff valve and venting the suction line to atmosphere, or other appropriate means that does not maintain a vacuum on the outlet of the shutoff valve.
30. Monitor the cavity pressure for a minimum of 30 minutes. If the cavity pressure does not exceed 3 torr at the end of the time period, proceed to Step 32. If it appears that cavity pressure will exceed 3 torr, it is not necessary to wait 30 minutes before proceeding to step 31. As an option, repeat Steps 29 and 30 without first performing Step 31.
31. Open the port tool to re–pressurize the cask body cavity to atmospheric pressure and repeat Steps 29 and 30. The cask may be re-pressurized with air, nitrogen, or helium.
32. Disconnect the vacuum pump from the vent port tool and connect a source of helium gas.
33. Provide a helium atmosphere inside the cask payload cavity by backfilling with helium gas to a pressure of slightly greater than atmospheric pressure, i.e., +1, -0 psig.
34. Disconnect the helium gas source from the vent port tool.
35. Using the vent port tool, tighten the vent port plug to 9 ±1 ft–lb torque.
36. Perform leakage rate testing on the containment O-ring seal and the drain and vent port sealing washers per Section 8.2.2.2, *Helium leakage Rate Testing the Main Containment O-ring Seal*,

Section 8.2.2.3, *Helium Leakage Rate Testing the Drain Port Sealing Washer*, and Section 8.2.2.4, *Helium Leakage Rate Testing the Vent Port Sealing Washer*.

37. At the conclusion of all leakage rate testing, install the drain port dust cover, the test port dust cover, and vent port dust cover.

7.1.3 Preparation for Transport

1. Utilizing the lift adaptor, or optional rigging, lift and lower the cask body into the lower impact limiter that is located on the transport pallet. Ensure that the cask body is aligned with the impact limiter alignment stripe for correct circumferential location.
2. Install the (8) eight ∅1–inch ball lock pins into each lower impact limiter attachment.
3. Remove the (4) four 1 – 8 UNC bolts that attach the lift adaptor to the cask body. Remove the lift adaptor or rigging hardware. The lifting holes may be optionally plugged.
4. Lift and lower the upper impact limiter onto the cask body. Ensure that the upper impact limiter is aligned with the cask body stripe for correct circumferential location.
5. Install the (8) eight ∅1–inch ball lock pins into each upper impact limiter attachment.
6. Install the tamper–indicating device (security seal) in the appropriate upper impact limiter attachment location.
7. Remove the rigging from the upper impact limiter lift points. The lifting holes may be optionally plugged.
8. Place the BRR package tie–down cover over the upper impact limiter.
9. If the transport pallet was removed from the transport trailer, secure the tie–down cover to the pallet using the chains provided. Using the fork pockets in the pallet, place the pallet on the transport trailer and attach to the trailer. Then, remove the chains between the tie–down cover and pallet.
10. Secure the tie–down cover to the transport trailer using the tie–down attachments. Optionally, install a weather seal on the bottom impact limiter.
11. Monitor external radiation for each loaded BRR package per the requirements of 49 CFR §173.441.
12. Determine that surface contamination levels for each loaded BRR package is per the requirements of 10 CFR §71.87(i) and 49 CFR §173.443.
13. Determine the transport index for each loaded BRR package per the requirements of 49 CFR §173.403.
14. Complete all necessary shipping papers in accordance with Subpart C of 49 CFR 172 [3].
15. BRR package marking shall be in accordance with 10 CFR §71.85(c) and Subpart D of 49 CFR 172. Package labeling shall be in accordance with Subpart E of 49 CFR 172. Package placarding shall be in accordance with Subpart F of 49 CFR 172.

Table 7.1-1 – Spacer Pedestal Requirements for Square Fuels

Fuel Payload Type	Spacer Pedestal Height, inches②
RINSC①	None used
U-Mass (aluminide)	None used
U-Mass (silicide)	None used
Ohio State	4.44
Missouri S&T	5.19
Purdue	7.20
PULSTAR	1.46
U-Florida	12.31
Loose plates from: ·U-Mass (aluminide) ·U-Florida ·Purdue	Loose Plate Box②

Notes:

1. Rhode Island Nuclear Science Center.
2. Spacer pedestals and the Loose Plate Box are shown on drawing 1910-01-03-SAR.

Table 7.1-2 – Spacer Pedestal Requirements for TRIGA Fuels

TRIGA Fuel Catalog No.	Spacer Length, in①	Spacer Description
101	19.01	Adjustable, 4th position
201	18.48	Adjustable, 3rd position
103, 105, 109	18.48	Adjustable, 3rd position
117, 119	17.70	Adjustable, 2nd position
107	17.25	Adjustable, 1st position
403, 405, 417, 419	17.25	Adjustable, 1st position
217, 219	7.28	Fixed, long
303, 305, 317, 319	3.63	Fixed, medium
203, 205, 207, 503, 505, 517, 519	2.13	Fixed, short

Notes:

1. Spacer pedestals are shown on drawing 1910-01-03-SAR.

Security-Related Information Figure Withheld Under 10 CFR 2.390.

Figure 7.1-1 - Drawing of U-Florida Spacer Plate and Loose Plate Dunnage Sheet